Metal Mediated Reduction of Borazines for the Regeneration of Boron-Nitrogen Hydrogen Storage Materials

by
Tyler Joseph Carter

A dissertation submitted in partial fulfillment
of the requirements for the degree of
Doctor of Philosophy
(Chemistry)
in the University of Michigan
2014

Doctoral Committee:

Assistant Professor Nathaniel K. Szymczak, Chair
Associate Professor Bart M. Bartlett
Professor Melanie S. Sanford
Assistant Professor Donald J. Siegel

Dedication

To my family for their constant support and encouragement.

Acknowledgements

Graduate school has been one of the most difficult, but simultaneously rewarding, experiences of my life. I have gotten to know some really amazing people during my 5+ years in Ann Arbor, and I am grateful to all of my co-workers, mentors, and friends who have, each in their own way, helped me tremendously on my Ph.D. journey.

I owe a huge thank you to my advisor, Professor Nathaniel Szymczak. I am proud to be his first graduating student, and it has been a unique opportunity being in the lab from the very start. I have always admired Nate's passion for chemistry and dedication to the work that he does. He has always encouraged me to strive for excellence and I know that I am a much better scientist as a result of his mentorship.

I also need to thank all of my current and former Szymczak lab co-workers: Cameron, Oscar, Chengbao, Tim, Qi, Eric, Chelsea, Jacob, Justin, and Lilly. It has been a pleasure working with all of you. I need to thank Justin in particular, for all of his hard work on a very difficult project. I also want to thank Oscar for all of the helpful discussions, scientific and otherwise. I am tremendously grateful to Professor Zachariah Heiden; who was our computational collaborator for the last year of my graduate career. He was a huge help in driving my project forward, and I sincerely appreciate all of his help.

During the fall of 2012, I participated in an internship at the Toyota Research Institute of North America, and I need to thank everyone I worked with there. Tim, Nik, Paul, Ruigang, Fumi, Prem, Michael, Kimber, Torrin, John, and Bobby, I learned so much from all of you, and I am grateful to have had the opportunity to work with you. I also owe a special thanks to Rana, who was my mentor during my time at Toyota. I sincerely appreciate everything you have done for me. Your support and encouragement meant a lot at a time when I really needed it.

During the early years of my graduate career, I was involved in an outreach

program called Science Saturdays. I want to thank all of the Future program students, guest speakers, and graduate student volunteers who worked so hard to make Science Saturdays a huge success. I will always look back fondly on those days (even the ones I was up until 3 a.m. preparing for). I also need to thank Dr. Mary Starr, from the IDEA Institute, who was instrumental in keeping everything on track and teaching me to explain chemistry to non-scientists, a skill that I still use to this day. Mary has also been a big inspiration and a great mentor, and I am really grateful to have had the opportunity to work with her.

As much as graduate students try to pretend they work ALL the time, some of my best memories from my time in Ann Arbor were outside the lab. I have met some of the most generous, caring, and all around awesome people I have ever know since I moved here. Frank, Emily, Dorran, Amanda, Tyler, Joe, Anna, Seryun, Justin, Danielle, Brad, Cheryl, and everyone else, thank you for all of the great memories. I will never forget the game nights, fakesgivings, and all of the outdoor activities that were questionably undertaken during thunderstorms.

I also need to thank my family. I am so grateful to my parents, Bob and Karen, and my sister, Nikki, for all of the love, support, and encouragement they have given me over the years. I would not have made it to where I am today without them, and I am so lucky to have had such a supportive upbringing with so many opportunities available to me.

Finally, I need to acknowledge my wife, and best friend, Kelsey. We met shortly after we had both arrived in Ann Arbor, and she has been the most kind, generous, understanding, and supportive partner anyone could ask for. Her encouragement helped me through some of the most difficult times in graduate school, and I'm not sure I would have made it without her. I'm also grateful that she agreed to adopt our three pets (Marty, Elijah, and Henry), whose adorable antics (and occasional hairballs) provided a much needed diversion on the inevitable days when grad school felt tedious and futile. I can't wait for all of us to start our new life together, and I am so proud of both of us!

Table of Contents

List of Figures

List of Schemes

List of Tables

List of Appendices

Abstract

Boron-nitrogen materials such as ammonia borane and cyclotriborazane are promising candidates for hydrogen storage due to their high gravimetric and volumetric hydrogen capacities. Though many examples of hydrogen release from these materials have been reported in the scientific literature, low-energy regeneration of the spent fuel products (such as borazine and polyborazylene) remains a significant challenge. Therefore, developing reactions that directly convert these spent fuel products back to useful hydrogen storage materials would be a key advance towards realizing practical application of B-N hydrogen storage materials. This thesis explores transition-metal coordination as a promising strategy to mediate indirect hydrogenation of B=N bonds in these materials and establishes proof of concept for metal-mediated B=N bond reduction.

The reactivity of $Cr(CO)_3$ and $Mn(CO)_3^+$ coordination complexes of hexamethylborazine (a model for B-N spent fuel) with respect to hydride and proton addition is examined. Reduction of these complexes by hydride addition is shown to produce stable dearomatized borazine complexes; which is the most energy intensive step in recycling borazine to useful hydrogen storage materials such as cyclotriborazane. Hydride delivery is accomplished through direct addition of chemical hydrides, as well as one and two electron transfer pathways. In each case, the mechanism of these transformations is studied in detail, to provide a basis for adaptation of this methodology to a catalytic scheme for the regeneration of B-N materials. Protonation of a dearomatized borazine complex is also demonstrated resulting in complete B=N bond reduction. By establishing proof-of-concept for metal mediated B=N bond reduction, this work builds a foundation for later studies which will seek to develop a comprehensive, low-energy, B-N spent fuel regeneration pathway.

Chapter 1: Introduction to Boron-Nitrogen Hydrogen Storage Materials

1.1 Hydrogen as an alternative energy source

Due to increasing demands for energy from a rapidly growing world population, as well as environmental concerns over climate change and the release of other pollutants associated with fossil fuel combustion, modern societies face a pressing need to develop renewable and environmentally friendly energy sources. Though the merits of numerous alternative energy platforms are still the subject of vigorous debate, it is clear that no single solution is capable of meeting the demands of 21st century societies.[1] However, all of these proposed energy systems have one thing in common, they ultimately rely on the sun as their primary energy input (with the exception of Nuclear Fission). While impressive advances have been made in technologies for solar energy conversion,[2] the fact remains that solar energy is only effective during daylight hours. However, modern standards of living dictate that energy be available in portable, on-demand, format for transportation, communications, and a variety of other uses. As such, numerous technologies have been proposed which seek to harness the power of the sun, and store it in a form that can be readily accessed to produce electricity and mechanical energy.

Of the many proposed energy storage systems, one of the most promising is the use of sunlight to drive the production of chemical fuels. These fuels can then be stored onboard a vehicle, and converted to electrical energy when used in concert with an appropriate fuel cell. Based on its high energy density (120 MJ kg^{-1}), hydrogen is often proposed as the chemical fuel of choice for such systems. Additionally, assuming a perfectly reversible system, water and oxygen (compounds found on earth in large abundance) would be the sole feedstocks, and by-products, of a hydrogen energy infrastructure. While promising from a theoretical perspective, technical hurdles with regard to hydrogen generation, storage, and utilization, must be overcome before hydrogen can see practical application as a chemical fuel.[3]

1.2 Hydrogen storage

Hydrogen storage is particularly problematic simply due to the fact that hydrogen is a gas at standard temperature and pressure. As a result, storing hydrogen with high energy density continues to be a major challenge. For transportation applications, such a system would need to offer a 300 mile range for a single H_2 filling, and be capable of releasing H_2 with sufficient rates to be compatible with modern fuel cell technologies.[3] To aid in the development of materials that meet such high demands, the U.S. Department of Energy has developed a series of detailed performance targets that a theoretical H_2 storage material would need to meet. Amongst these targets, the two areas where most materials fall short are the gravimetric density target of 7.5 wt.% H_2 and the volumetric density target of 70 kg H_2 m^{-3} (Figure 1-1).[4]

While numerous designs for storing high pressure hydrogen on-board a vehicle have been considered, the additional equipment-weight associated with such systems dramatically decreases the effective gravimetric capacity of the stored hydrogen. Liquid hydrogen has also been considered, however, the utility of these systems is severely limited by the energy cost associated with liquefaction as well as the need for slow, but nearly constant, boil-off of hydrogen as the tank warms. Physisorbtion methods, such as

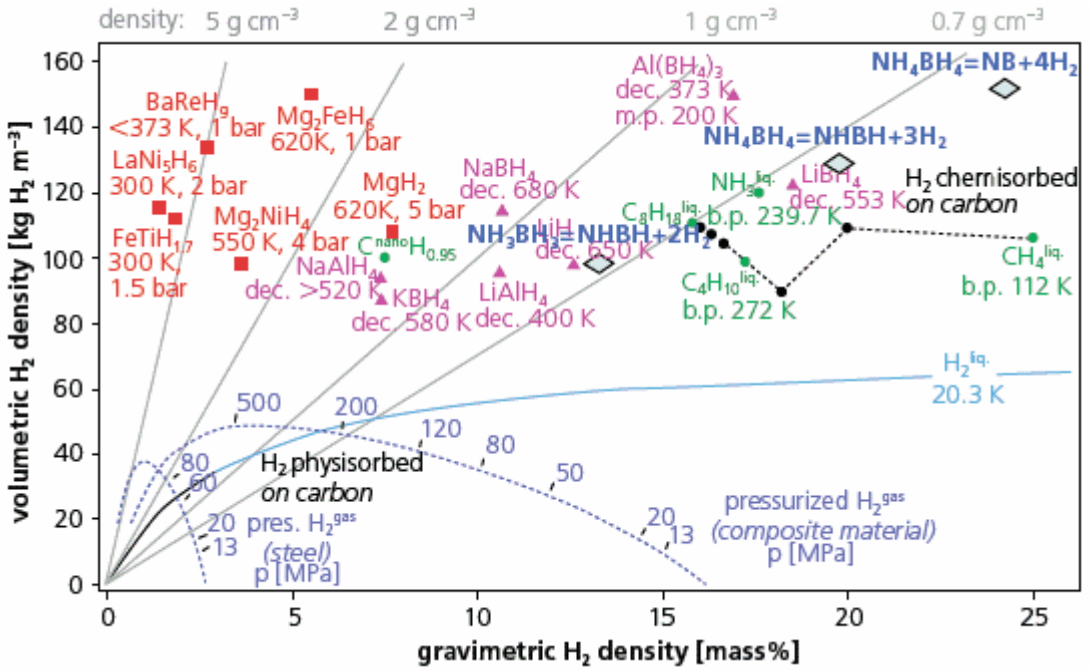

Figure 1-1. Volumetric and gravimetric density of a variety of hydrogen storage methods and materials.[5]

the uptake of hydrogen into porous networks (e.g. metal-organic-frameworks) have also been proposed. However, significant quantities of hydrogen can only be stored in these materials at very low (~77 K) temperatures, imposing many of the same limitations as liquid H_2. An alternative strategy is the storage of hydrogen in the form of chemical bonds wherein the hydrogen is incorporated into solid (or liquid) materials that can be easily dehydrogenated. The main advantage of these condensed phase materials is that they offer much higher volumetric and gravimetric energy densities than methods for storing gaseous hydrogen.[6,7]

A wide variety of chemical hydrogen storage materials have been proposed, however, there are few that offer a satisfactory balance of high capacity and favorable dehydrogenation and regeneration conditions. For instance, many complex metal hydrides have been considered, however, the release of hydrogen from these materials often requires high temperatures (> 200 ºC) and the hydrogen storage capacities of these materials are often much lower (< 5 wt.% H_2) than the DOE targets. A wide variety of simple organic molecules have also been considered, however, slow dehydrogenation kinetics (under reasonable operating conditions) has proven challenging.[7]

1.3 Boron-nitrogen hydrogen storage materials; promise and challenges

One class of condensed phase hydrogen storage materials that offer both gravimetric and volumetric hydrogen densities high enough to meet the U.S. Department of Energy's targets for vehicle based hydrogen storage systems are commonly referred to as Boron-Nitrogen adducts. The simplest of these molecules, ammonia borane (NH_3BH_3, AB), contains 19.8 wt. % H_2, nearly all of which can be easily released depending on the dehydrogenation conditions employed. Additionally, a rich network of dihydrogen bonds results in a dense crystalline material with high (144 kg H_2 m^{-3}) volumetric hydrogen density. This unique combination of high volumetric and gravimetric capacity makes ammonia borane one of the most energy dense hydrogen storage materials under consideration (Figure 1-1).[6,8]

Ammonia borane was first synthesized by Shore and Parry in 1956 although its structure remained a mystery for some time due to its tendency to disproportionate into

Scheme 1-1. Typical ammonia borane dehydrogenation pathways.

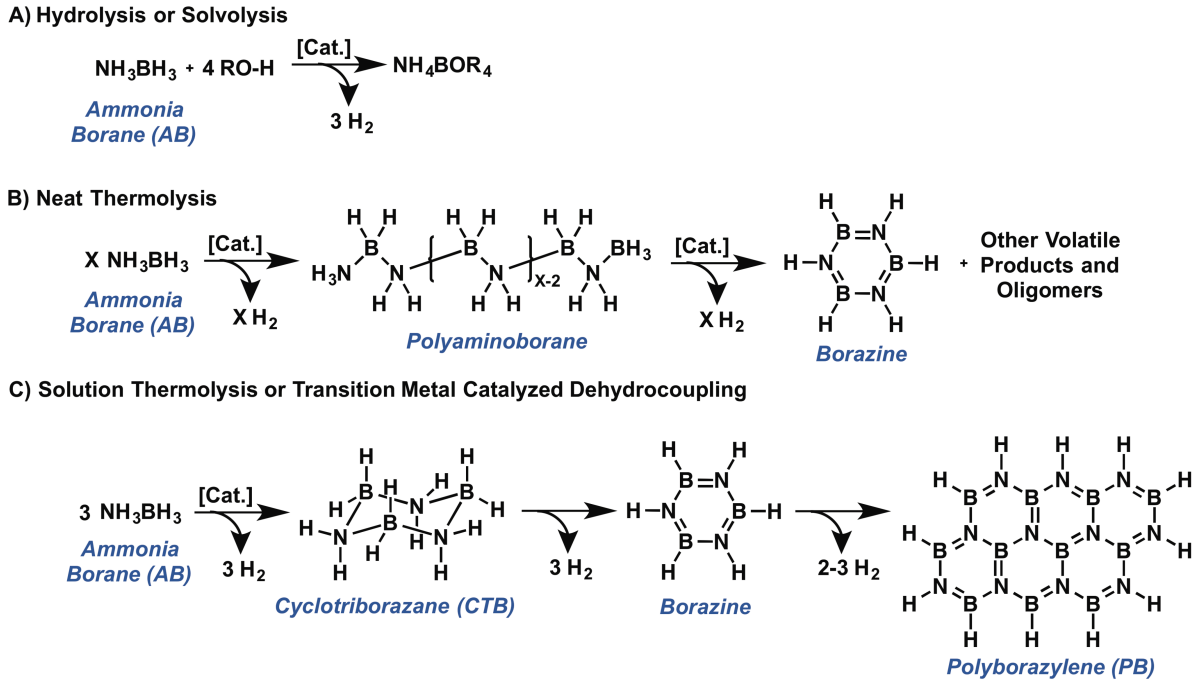

a structural isomer, diamonate of diborane ($[NH_3BH_2NH_3]BH_4$).[9] Early work described the tendency of these compounds to undergo slow decomposition with hydrogen evolution, as well as thermal dehydrogenation when AB was heated.[10] Beginning in the early 2000's, ammonia borane received significant interest as a potential hydrogen storage material, and the number of references dealing with hydrogen release from ammonia borane has significantly expanded in the last decade.[8,11-26]

Dehydrogenation of ammonia borane generally proceeds by hydrolysis, thermolysis, or transition metal catalyzed dehydrocoupling (Scheme 1-1). Each method has been extensively studied and provides a unique set of spent fuel products. Hydrolysis (or solvolysis using an alcohol such as methanol) is one of the most straightforward examples. In a typical hydrolysis reaction, ammonia borane is placed in contact with a protic solvent and vigorous hydrogen evolution results. A full three equivalents of H_2 are released, and very impressive rates (H_2 release complete in < 10 min at RT) have been observed in examples catalyzed by clusters of Fe, Ni, and other earth abundant metals.[24] The spent fuel afforded from hydrolysis is, almost exclusively, borate salts of the formula $B(OR)_4^-$ (R = H or Me). The high rates, extensive dehydrogenation, and well defined nature of the spent fuel make hydrolysis very attractive for single-use hydrogen

storage systems. However, for the idealized reversible systems that are needed for future applications, the formation of B–O bonds in the spent fuel presents a very high energy barrier for recycling. Consequently, a great deal of effort has been devoted to developing ammonia borane dehydrogenation pathways which afford more easily recyclable spent fuel products.

The thermal dehydrogenation of ammonia borane was first studied in 1978[10] as an extension of the observation by Shore and Perry[9] that ammonia borane undergoes slow decomposition in solution. Subsequent studies examined the thermal stability of ammonia borane by thermal gravimetry which revealed strong exotherms at 110 ºC and 130 ºC.[27] The first exotherm is linked to the loss of a single equivalent of hydrogen from ammonia borane to form oligomers referred to as polyaminoboranes (Scheme 1-1B). The structure of these oligomers is not yet fully understood, however, currently available experimental and computational evidence suggest a mixture of short-chain linear and cyclic structures.[17,24] The second release of hydrogen is associated with the formation of iminoboane oligomers. Unlike aminoboranes, these species are primarily cyclic with the trimer borazine being the only well characterized iminoborane. Dehydrogenation can also be driven to favor cyclic oligomers (CTB and Borazine) if the thermolysis is conducted in solution, where dilution presumably suppresses the formation of larger spent fuel products.[24] While this dehydrogenation pathway is operationally quite simple and does not produce spent fuel products containing B–O bonds, phase changes from solid to liquid, and the evolution of trace volatile byproducts (which poison fuel cell catalysts) effectively rule out direct thermolysis as a dehydrogenation route for vehicular H_2 storage.

In an effort to circumvent borate formation, improve the rates of hydrogen release relative to thermolysis, and minimize issues with phase change and volatile by-products during dehydrogenation, homogeneous catalysis has also been widely studied for the dehydrogenation of B–N compounds. In general, a wide variety of transition metal catalysts have been shown to increase the rate and extent of hydrogen release from ammonia borane.[19] Most catalytic systems release 2-3 equivalents of hydrogen and produce cyclic oligomers like borazine and PB as the spent fuel products.[17,19,24] A notable example by Keaton, Blacquiere and Baker showed that a nickel catalyst could

release 2.8 equivlants of H_2 from ammonia borane in just four hours at 60 ºC.[16] Manners and coworkers later showed that iron-carbonyl complexes could be photolytically activated to release H_2 from ammonia borane at room temperature.[28] Both of these examples suggest that catalytic dehydrogenation can also be effectively carried out with earth abundant metals, which will be important for wide-scale implementation of AB fuels. While the catalyzed release of H_2 from ammonia borane is a promising alternative to solvolysis, there are several key challenges that must be overcome before these methods can see practical application. Chief among them is the need to develop efficient means to recycle the spent fuel products.[29] Although catalyzed dehydrocoupling avoids the formation of highly stable B–O bonds, the methods by which borazine and polyborazylene can be recycled to ammonia boane (see section 1.4) are currently limited and energetically costly.

Liu and coworkers proposed an interesting alternative to ammonia borane, the cyclic organic/B-N hybrid 1,2-azaborine and substituted derivatives thereof (Scheme 1-2A). The most attractive feature of this approach is that the calculated reaction thermodymanics favor reversibility with ΔG_{rxn} = 1.9 kcal/mol for release of 3 eq. (7.1 wt.%) H_2 from 1,2-azaborine.[30,31] However, suitable experimental conditions for the dehydrogenation of these molecules have not yet been reported. In addition to azaborines, the Liu group also explored an alkyl bridged analogue of ammonia borane (2,3-B-N-1-methylcyclopentane, Scheme 1-2B) which was shown to dehydrogenate fully to its corresponding borazine by heating at 80 ºC in the presence of $FeCl_2$.[32] In this system, the components remain as condensed phase liquids throughout the dehydrogenation process (assuming the system is kept above the 28-30 ºC melting point of the resultant spent fuel),[33] and the corresponding methylcyclopentyl-B-N-bridged borazine is non-volatile making it compatible with current fuel cell technology.[32] However, the challenge of regenerating the resultant spent fuel still remains unsolved.

Scheme 1-2. A) Azaborine spent fuel regeneration and proposed dehydrogenation pathway. B) Catalytic dehydrogenation of methylcyclopentyl fused ammonia borane

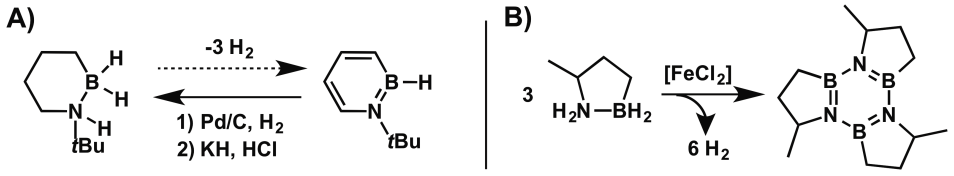

1.4 The "regeneration problem"

It is not surprising that borazine and PB recycling is a major challenge when the thermodynamics of the dehydrogenation reaction (Scheme 1-3) are considered. The direct hydrogenation (reaction with H_2) of both borazine and polyborazylene is non-spontaneous and highly entropically disfavored.[34-36] As a result, hydrogenation cannot be affected without the introduction of an external driving force. In addition to these challenges (or perhaps because of them) the so-called "regeneration problem" has received relatively little attention in comparison to the huge body of work conducted on H_2 release methodologies.[29] Several promising initial examples have been reported, however, all of these rely on digestion of the spent fuel prior to reduction. Digestion creates a stoichiometric waste product whose energy of formation acts as the driving force for the reaction, offseting the energy required for the net transformation of PB (or borazine) back to ammonia borane. The resulting digestatate is then reduced (often with strong hydrides) and treated with ammonia to return ammonia borane.

Scheme 1-3. Free energy of reaction for the dehydrogenation of ammonia borane to borazine.[34]

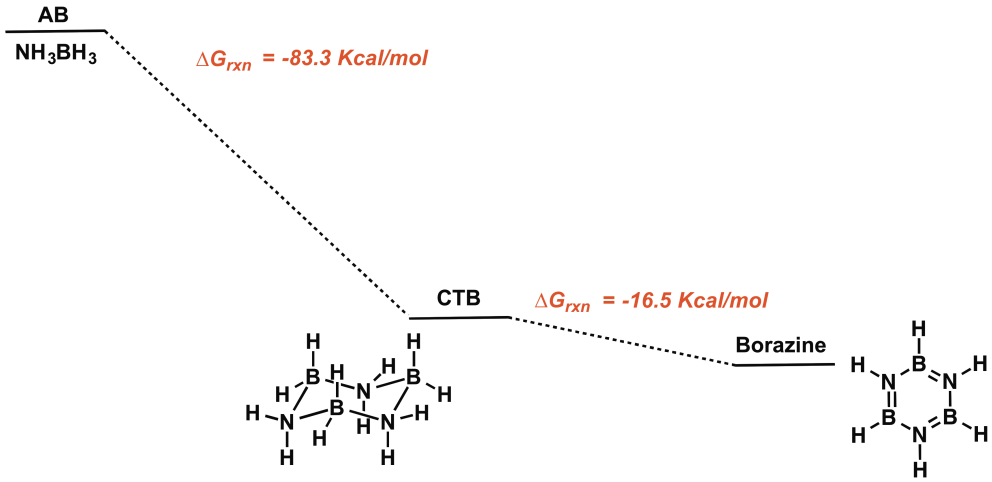

Ramachandran and Gagare observed that borates resulting from AB solvolysis could be converted back to AB in 81% yield by treatment with $LiAlH_4$ and NH_4Cl (Scheme 1-4A).[37] Similar methodologies were developed independently by Sneddon and Mertens wherein cross-linked and oligomerized spent fuel products were digested with strong acids and the resulting halo or oxo borane/borate was then reduced using metal hydrides.[38-39] Mertens further improved his approach by incorporating a catalytic

Scheme 1-4. A) Solvolysis H_2 storage cycle for AB based on regeneration via LAH reduction. B) Digestion and reduction scheme incorporating hydrodechlorination.

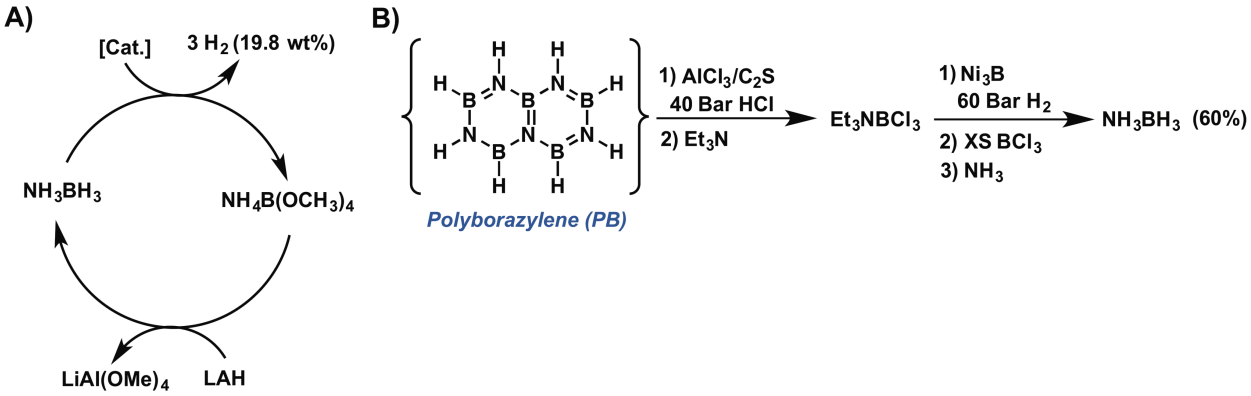

hydrodehalogenation step (Scheme 1-4B) which partially hydrogenated the B-Cl bonds in the BCl_3 digestate. However, the addition of a large excess of BCl_3 was required to drive the reaction.[40] Indeed, for all of these examples, the ultimate utility of these systems is impacted by the need for energetically costly terminal reductants, or stoichiometric waste products produced during the digestion/reduction sequence.

Dixon, Gordon, and coworkers further extended this type of regeneration methodology by using 1,2-benzenedithiol as the digesting agent (Scheme 1-5). The unique chelating effect of the di-thiol drove the digestion reaction, resulting in a digestate with weak (in comparison to B–O or B-Cl bonds) B–S bonds. The resulting digestate was then reduced by treatment with a relatively weak hydride, Bu_3SnH (or Bu_2SnH_2). Ammonia borane was recovered from polyborazylene in 67% yield, and later work established that the tin hydride (Bu_3SnH) could be recycled by chemical conversion to a tin formate which decomposes to the hydrde in-situ eliminating CO_2.[41] Though the use of chelating agents as a means to access digested species which can be more easily reduced is a promising area for future research, the low recovery, and inefficient regeneration mechanisms available for Bu_2SnH_2, rule out commercial viability for this system.

Sutton, Gordon, and coworkers developed a unique one-pot digestion and reduction system in which borazine or polyborazylene is treated with hydrazine in liquid ammonia (Scheme 1-6).[42] In this case, ammonia borane recovery as high as 85% was observed in the crude reaction mixture. Yu and coworkers also demonstrated that ammonia

Scheme 1-5. Digestion and reduction regeneration sequence utilizing 1,2-benzenedithiol.

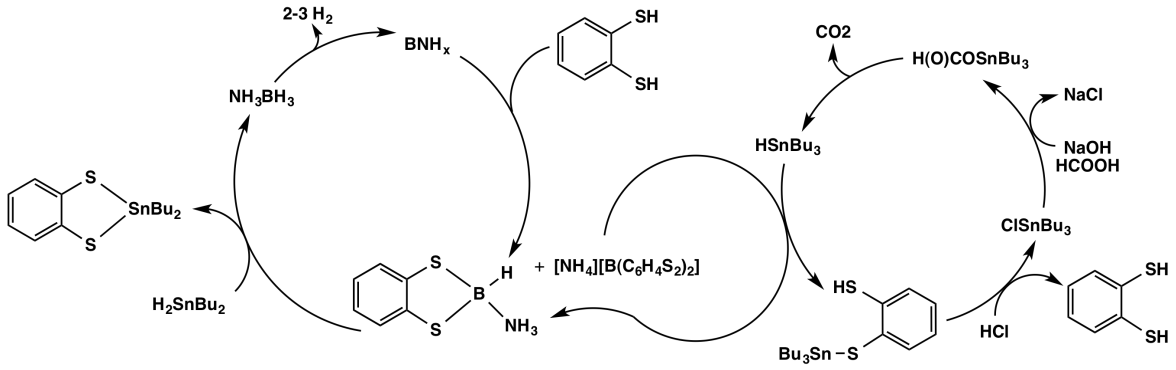

borane supported on mesoporous carbon-nitride can be combined with this regeneration methodology allowing cycling between AB and polyborazylene as many as five times before reversible hydrogen capacity was lost.[43] However, the added weight of the solid support significantly reduces the net gravimetric capacity of the ammonia borane.

Scheme 1-6. Hydrazine in liquid ammonia one-pot regeneration sequence.

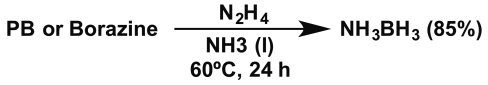

The unmodified system developed by Sutton and Gordon is remarkable in both its novelty and simplicity, and constitutes the current state of the art for regenerating ammonia borane spent fuels. Never the less, further improvements need to be made before ammonia borane can see practical application. Hydrazine production is energetically costly, and the price of hydrazine is currently too high for this system to be implemented on large-scale.[42] Additionally, the mechanism by which this reaction proceeds is not well understood which complicates its extension to the development of other direct methodologies for B–N spent fuel recycling. In order to address these issues, our research seeks to develop a new, low-energy, pathway for the recycling of B-N spent fuels that does not rely on digestion, high energy reductants, or an abundance of stoichiometric waste products.

1.5 Direct regeneration methods

To accomplish this, we hypothesized that indirect hydrogenation reactions would offer a promising alternative regneration route. Indirect hydrogenation relies on the

delivery of hydrides and protons (rather than H_2) to facilitate the hydrogenation of unsaturated bonds. Unlike direct hydrogenation, the reaction thermodynamics can be manipulated by tuning the hydricity, or acidity, of the reagents selected, thereby providing a driving force for the energetically challenging regeneration reaction. Additionally, though the thermodynamic barrier associated with these reactions cannot be modified through catalysis, transition metal activation of the spent fuel molecules could lower the activation barriers associated with these transformations, allowing the regeneration scheme to operate with as little additional energy input as possible (in excess of the thermodynamic barrier). Indirect hydrogenation would also be a major advance as it would eliminate the need for a digestion step, greatly reducing the complexity and energetic cost of regeneration. Finally, transition metal hydrides can be readily formed by protonation of a reduced species,[44] potentially allowing for B=N bond reduction solely from protons and electrons, at an overpotential that can be tuned by selection of an appropriate electocatalyst.

In order to address whether this strategy was feasible, we first needed to select an appropriate metal scaffold to determine how B-N waste products are affected by metal coordination. To do this, we drew inspiration from the fact that borazine (a prototypical B-N spent fuel) is isoelectronic and isostructural with benzene.[45] This is significant, as a wealth of previous studies have determined that arenes, when coordinated to metal centers, become activated towards a wide variety of interesting transformations.[46] Of

Scheme 1-7. A) Metal-mediated arene C=C bond hydrogenation. B) Proposed reversible hydrogen storage system based on CTB and borazine.

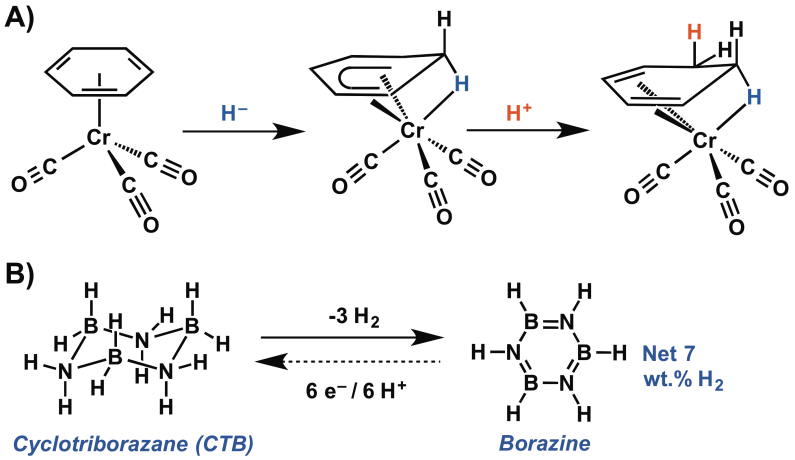

particular note are studies that show coordination to $Cr(CO)_3$ and $Mn(CO)_3^+$ fragments facilitates dearomatization of a variety of arenes via stepwise addition of hydride and proton equivalents (Scheme 1-7A).[47-50] We hypothesized that if borazines were coordinated to these metal fragments, they will be activated towards similar transformations. As such, or initial goal was to reduce borazine to cyclotriborazane (CTB, an inorganic analogue of cyclohexane) by metal-mediated indirect hydrogenation (Scheme 1-7B). Demonstrating reversible cycling between borazine and CTB would also constitute a system with 7 wt. % net H_2 capacity, which is close to the DOE's ultimate target.[4]

1.6 Unique structure, bonding, and reactivity of borazines

While comparing borazine to benzene is suitable to a first approximation, we were also aware of some significant differences between borazines and arenes. Like benzene, borazine has a planar structure with completely symmetric B=N bond lengths, suggesting at least partial aromatic character.[51] However, computational findings have suggested that the highly polar nature of the borazine B=N bonds, a result of the significant electronegativity difference between nitrogen (3.066) and boron (2.051),[52] causes the π-system in borazines to be only partially delocalized (Scheme 1-8A) resulting in a much smaller aromatic stabilization energy (11.1 kcal mol^{-1}) as compared to benzene (22.1 kcal mol^{-1}).[53,54] Borazines also undergo a variety of unique reactions which are not observed for arenes. For example, strong acids (such as HCl) undergo concerted additions across the B=N bonds of borazines to yield the substituted cyclotriborazane $Cl_3H_3B_3N_3H_6$ (Scheme 1-8B). A variety of other polar molecules, such as MeOH, MeI, and halogens, are also reported to react with borazine; although the resulting adducts have not been subjected to full structural characterization.[45,55] Borazines also readily undergo nucleophilic substitution reactions at the boron centers. For instance, $H_3B_3N_3H_3$ and $H_3B_3N_3Me_3$ can be converted to their corresponding B–R (R = Me or Et) analogues by treatment with 3 equivalents of the corresponding Grignard or alkyl lithium reagent via substitution of the hydride (Scheme 1-8B). B-Cl bonds can also be substituted in this way,[56] and B-R substituents can be exchanged by the addition of excess R'–Li or R'–Mg–X.[57,58]

Scheme 1-8. A) Calculated electron density of borazine vs. benzene highlighting the polarized nature of the B=N bonds. B) Unique reactivity of borazines. C) Dearomatization of borazines by nucleophillic addition.

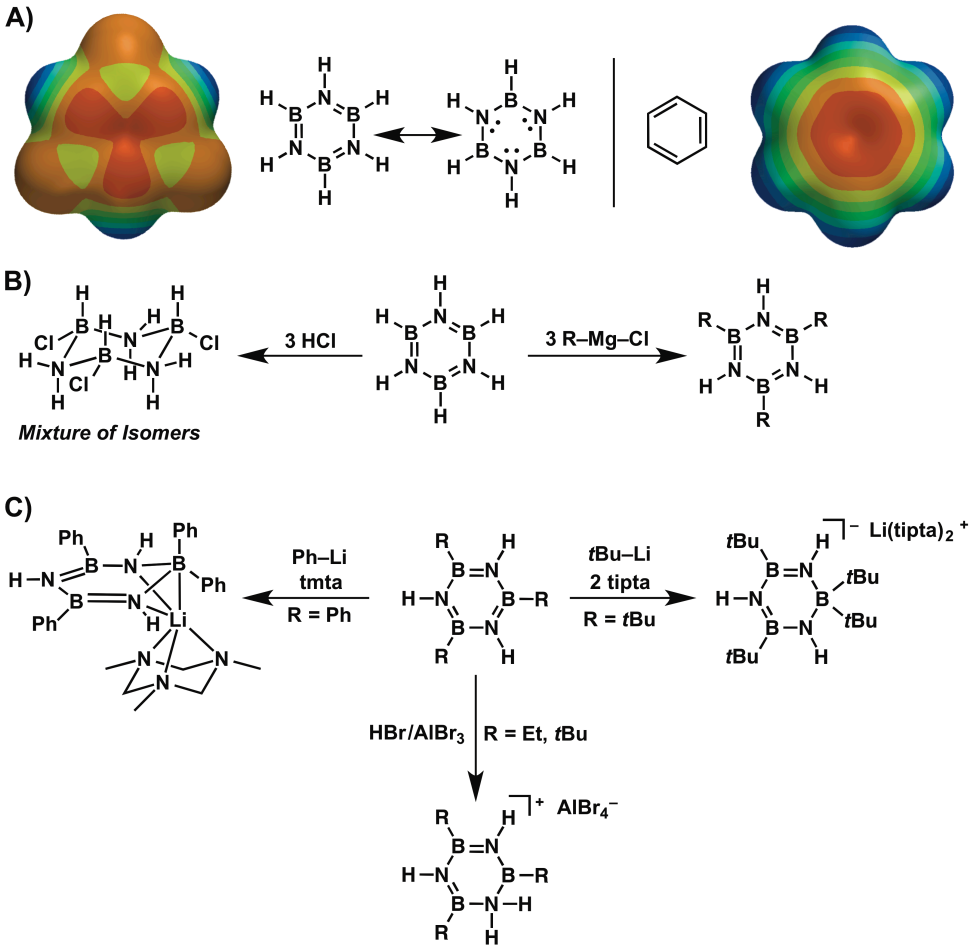

Presumably, these reactions proceed through a dearomatized intermediate featuring a four coordinate tetrahedral boron atom which disrupts the π-conjugation of the aromatic system. Not surprisingly, isolation of this type of intermediate is somewhat rare. However, work by Nöth and co-workers, exploring the reaction of borazines with a variety of alkyl lithium reagents (Scheme 1-8C), established that addition of Ph or *t-butyl* nucleophile to a substituted borazine resulted in stable dearomatized adducts which were crystallographically characterized.[59,60] In a later study, a substituted borazine was reacted with the super acid HBr:$AlBr_3$ to isolate a borazine dearomatized by N-protonation.[61] Lewis acids and bases have also been shown to interact with the borazine N atom lone pairs or B-atom empty p-orbitals respectively,[61,62] an observation which further supports bond polarization reducing aromatic character in borazines. This

strategy has also been explored computationally as a means to lower the activation barrier associated with the direct hydrogenation of borazines.[36]

The use of Lewis acids as mediators for direct hydrogenation has not been explored experimentally, however, as direct hydrogenation of borazine is both enthalpically and entropically disfavored. This is in further contrast with arene reactivity, where hydrogenation to cyclohexenes or cyclohexane is exergonic.[63] As a result, while cyclohexenes and cyclohexadienes are relatively stable molecules, partially hydrogenated borazines have not been previously observed. The thermodynamic favorability of borazines is also reflected in their electrochemistry, where the parent borazine ($H_3B_3N_3H_3$) has not been polaragraphically reduced or oxidized within the available potential window of common non-aqueous electrolyte systems. The derivative $Ph_3B_3N_3H_3$ was reduced at -3.3 V (vs. NHE), however, the phenyl group likely serves as an electron reservoir, suggesting that the reported reduction potential is not an accurate reflection of the energy required to reduce the B-N heterocycle itself.[64]

These important differences in the chemistry of borazines and arenes suggest that while transition metal arene chemistry can be used as an initial guide to understand the metal-mediated chemistry of borazines, significant differences should be expected. For instance, the uniquely polar bonds present in borazines will likely serve to facilitate ionic hydrogenation reactions as the boron is a better acceptor for hydrides and the nitrogen a better acceptor for protons than an arene C=C bond. However, the limited stability of partially hydrogenated borazines will likely present a significant challenge. The competing influences of these two important factors can likely be influenced by the selection of a suitable metal center for borazine activation. Indeed, the work of Nöth and coworkers has demonstrated that stable dearomatized borazines are accessible if highly specific reagents are selected.[59-61] If metal coordination can be used to further stabilize such intermediates (by drawing electron density from the borazine N-aotms via σ-donation) the addition of hydrides and protons to borazine could likely be realized.

1.7 Borazine coordination chemistry

While arene adducts of most (26) transition metals have been previously described,[65] the chemical literature includes only a small handful of transition metal

borazine complexes (Cr, Mo, and Rh) which feature π-type bonding.[66,67] Amongst these, only the chromium complexes of alkyl borazines (reported by Werner and coworkers) were isolated and fully characterized (including by X-ray diffraction).[68-72] The Werner lab (in 1967) initially attempted to adapt methods used in the synthesis of Tm-Arene complexes to borazines, but were unsuccessful, likely due to the weak binding affinity of borazines (see below). Despite these challenges, they were able to discover a unique synthetic methodology, referred to as the entrainment method (Figure 1-2), whereby coordinated MeCN ligands are continuously removed from the metal center by the application of vacuum.[68] This had the effect of manipulating the reaction equilibrium, and allowing for the isolation of the complex (η^6-$Et_3B_3N_3Et_3$)$Cr(CO)_3$, and a variety of other analogues with various substituents on the borazine ring.[70] Unfortunately, this synthesis was not compatible with the parent borazine $H_3B_3N_3H_3$ due to its high vapor pressure.

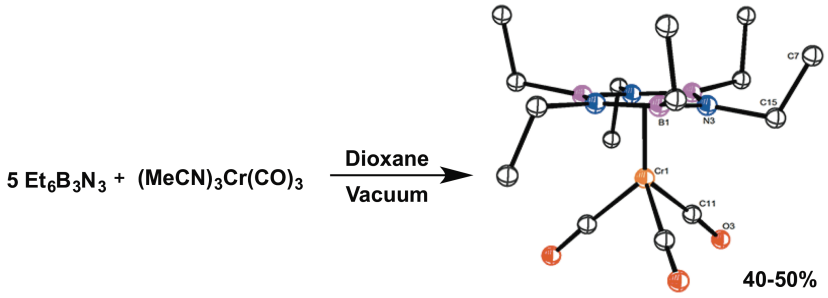

Figure 1-2. Synthesis and X-ray crystal structure of (η^6-$Et_3B_3N_3Et_3$)$Cr(CO)_3$.

The nature of the metal borazine bond was debated early on with two competing theories proposed. Both acknowledged that the metal-borazine bond is distinct from that observed in M-arene complexes, however, they varied considerably in their account of the key binding interactions. The first, postulated by Werner and coworkers, proposed that borazine binding was a cooperative interaction where the ring nitrogen atoms were primarily σ-donors, and the boron atoms participated by accepting π-electron density into their empty p-orbitals.[72] The second theory, proposed by Lagowski, suggested that borazine was essentially a cyclic tri-amine ligand with N-σ-donation being the only significant binding interaction.[73] Both theories were based primarily on interpretation of the X-ray structure of (η^6-$Et_3B_3N_3Et_3$)$Cr(CO)_3$, in which the ring N-atoms are trans disposed to the carbonyl ligands.[69] This is in contrast to transition metal π-arene

complexes where the carbonyl ligands are trans to the center of the C=C bonds.[74] Also noteworthy is the slight (15º) distortion from planarity that the borazine ring undergoes following coordination; a feature not observed in arene complexes. Decades later, computational findings reported by Bridgeman,[75] and Kang,[76] suggested a significant π-backbonding contribution from the metal into the empty p-orbitals of the borazine B-atoms consistent with Werner's proposal. Bridgeman further highlighted the unique nature of the M-borazine bond by observing a dramatic decrease in M–N and carbonyl C–O bond order when the borazine ligand was rotated 60º adopting the confirmation observed in the analogous complex (η^6-Arene)$Cr(CO)_3$.[75]

Scheme 1-9. Metal arene and metal borazine bond enthalpy.

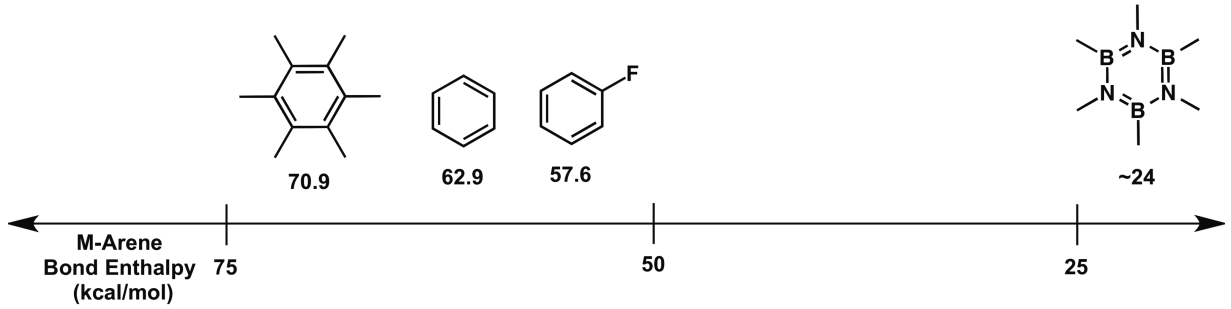

In addition to developing the only known synthetic methodology for coordinating borazines to transition metals, the Werner group conducted a series of kinetic experiments examining the rate of borazine displacement from the metal center. This allowed them to determine a borazine binding enthalpy of 16-34 kcal/mol,[77-79] which is approximately half that observed for analogous arene complexes (Scheme 1-9).[80] These observations also provided a reasonable explanation for the difficulty in synthesizing these complexes, as well as their incompatibility with many common coordinating solvents (e.g. THF, MeCN, dioxane, etc.). Surprisingly, this work was the only examination of the reactivity of coordinated borazines to appear in the 57 year period since Werner's original report.

1.8 Strategy to accomplish metal-mediated B=N bond reduction

Although very little is known about the reactivity of Werner's complexes, they are ideally suited for establishing the feasibility of the metal-mediated stepwise hydrogenation of B=N bonds. As described in section 1.5, half-sandwich complexes of

Cr(0) are among the most widely studied for arene activation chemistry and several examples of C=C bond hydrogenation via the addition of H^- and H^+ have been reported.[46,47,81] Isoelectronic and isostructural arene complexes of Mn(I) were also developed and extensively studied.[49,50,82-84] Being slightly more electrophillic, these complexes can be reduced to cyclohexenes, and reports of their electrochemical reduction are also ubiquitous allowing access to such intermediates from protons and electrons in addition to the use of strong chemical hydrides. As such, we utilized (η^6-$Me_3B_3N_3Me_3$)$Cr(CO)_3$ for our initial studies to establish proof-of-concept for metal mediated indirect hydrogenation of B=N bonds and later sought to extend this work to develop an analogous Mn(I) borazine adduct.

Scheme 1-10. Proposed metal-mediated regeneration route for spent B-N hydrogen storage materials.

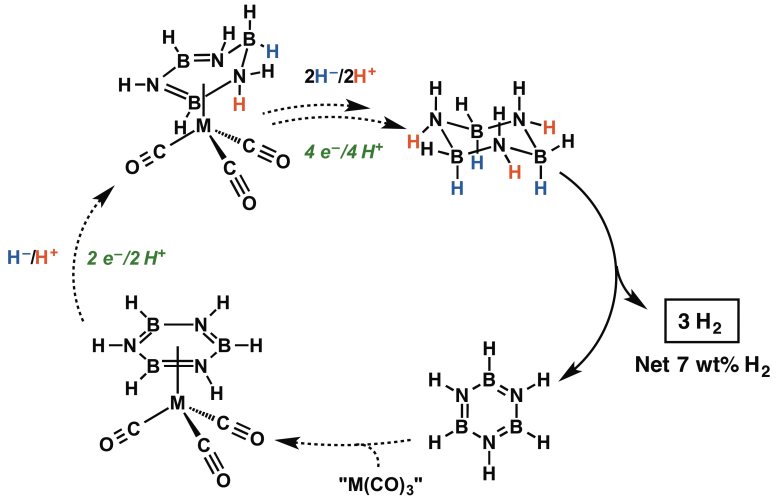

While the long-term aim of this project is to develop a metal mediated system for the indirect hydrogenation of borazine (or polyborazylene) from protons and electrons (Scheme 1-10), the work outlined in this thesis describes a series of more fundamental studies carried out on the $Me_3B_3N_3Me_3$ complexes discussed in section 1.7. This work was necessary in order to establish the feasibility of key steps in our proposed regeneration sequence. Specifically, computational studies have suggested that dearomatization via hydride delivery is the highest energy step for borazine hydrogenation,[34-36] and this reaction has not been demonstrated to proceed directly. Thus, studying hydride delivery to metal-borazine complexes has been a key goal of the work described here. Studying these reactions stoichiometrically contributes to a

fundamental understanding of metal-mediated borazine reduction and is an important proof of concept for developing a low energy pathway back to CTB. For these reasons, this work will provide an important foundation for continuing studies that will seek to apply this strategy to the electro-catalytic reduction of B–N heterocycles.

1.9 References

1) Pirrong, C.; Rapier, R.; Martén, I.; Taylor, J.; Levi, M.; Thurber, M.; Gordon, K.; Ball, J.; Cohen, A.; Skaf, M.; Myers, T. *The Wall Street Journal* **2013**, in The Experts: What Renewable Energy Source Has the Most Promise?, Accessed: Septermber 20, 2014.

2) In *Solar Energy Conversion Systems*; Brownson, J. R. S.; Academic Press: Boston, **2014**.

3) www.hydrogen.energy.gov/pdfs/program_plan2011.pdf.

4) www1.eere.energy.gov/vehiclesandfuels/pdfs/program/hstt_roadmap_june2013.pdf.

5) Used with permission from reference 24.

6) Karkamkar, A.; Aardahl, C.; Autrey, T. *Material Matters*, **2007**, *2*, 6.

7) Satyapal, S.; Petrovic, J.; Read, C.; Thomas, G.; Ordaz, G. *Catal. Today* **2007**, *120*, 246.

8) Huang, Z.; Autrey, T. *Energy Environ. Sci.* **2012**, *5*, 9257.

9) Shore, S. G.; Parry, R. W. *J. Am. Chem. Soc.* **1958**, *80*, 8.

10) Hu, M. G.; Geanangel, R. A.; Wendlandt, W. W. *Thermochim. Acta* **1978**, *23*, 249.

11) Jaska, C. A.; Temple, K.; Lough, A. J.; Manners, I. *J. Am. Chem. Soc.* **2003**, *125*, 9424.

12) Gutowska, A.; Li, L.; Shin, Y.; Wang, C. M.; Li, X. S.; Linehan, J. C.; Smith, R. S.; Kay, B. D.; Schmid, B.; Shaw, W.; Gutowski, M.; Autrey, T. *Angew. Chem. Int. ed.* **2005**, *44*, 3578.

13) Mohajeri, N.; In *Materials Research Society Symposium* 2005, p 844E.

14) Bluhm, M. E.; Bradley, M. G.; Butterick, R.; Kusari, U.; Sneddon, L. G. *J. Am. Chem. Soc.* **2006**, *128*, 7748.

15) Denney, M. C.; Pons, V.; Hebden, T. J.; Heinekey, D. M.; Goldberg, K. I. *J. Am. Chem. Soc.* **2006**, *128*, 12048.

16) Keaton, R. J.; Blacquiere, J. M.; Baker, R. T. *J. Am. Chem. Soc.* **2007**, *129*, 1844.

17) Stephens, F. H.; Pons, V.; Tom Baker, R. *Dalton Transactions* **2007**, 2613.

18) Yan, J. M.; Zhang, X. B.; Han, S.; Shioyama, H.; Xu, Q. *Angew. Chem. Int. ed.* **2008**, *47*, 2287.

19) Hamilton, C. W.; Baker, R. T.; Staubitz, A.; Manners, I. *Chem. Soc. Rev.* **2009**, *38*, 279.

20) Himmelberger, D. W.; Yoon, C. W.; Bluhm, M. E.; Carroll, P. J.; Sneddon, L. G. *J. Am. Chem. Soc.* **2009**, *131*, 14101.

21) Shrestha, R. P.; Diyabalanage, H. V. K.; Semelsberger, T. A.; Ott, K. C.; Burrell, A. K. *Int. J. Hydrogen Energy* **2009**, *34*, 2616.

22) Conley, B. L.; Williams, T. J. *Chem. Commun.* **2010**, *46*, 4815.

23) Smythe, N. C.; Gordon, J. C. *Eur. J. Inorg. Chem.* **2010**, *2010*, 509.

24) Staubitz, A.; Robertson, A. P. M.; Manners, I. *Chem. Rev.* **2010**, *110*, 4079.

25) Kostka, J. F.; Schellenberg, R.; Baitalow, F.; Smolinka, T.; Mertens, F. *Eur. J. Inorg. Chem.* **2012**, *2012*, 49.

26) Müller, K.; Stark, K.; Müller, B.; Arlt, W. *Energy Fuels* **2012**, *26*, 3691.

27) Frueh, S.; Kellett, R.; Mallery, C.; Molter, T.; Willis, W. S.; King'ondu, C.; Suib, S. L. *Inorg. Chem.* **2010**, *50*, 783.

28) Vance, J. R.; Robertson, A. P. M.; Lee, K.; Manners, I. *Chem. Eur. J.* **2011**, *17*, 4099.

29) Summerscales, O. T.; Gordon, J. C. *Dalton Trans.* **2013**, *42*, 10075.

30) Marwitz, A. J. V.; Matus, M. H.; Zakharov, L. N.; Dixon, D. A.; Liu, S. Y. *Angew. Chem. Int. ed.* **2009**, *48*, 973.

31) Campbell, P. G.; Zakharov, L. N.; Grant, D. J.; Dixon, D. A.; Liu, S. Y. *J. Am. Chem. Soc.* **2010**, *132*, 3289.

32) Luo, W.; Campbell, P. G.; Zakharov, L. N.; Liu, S. Y. *J. Am. Chem. Soc.* **2011**, *133*, 19326.

33) Luo, W.; Campbell, P. G.; Zakharov, L. N.; Liu, S. Y. *J. Am. Chem. Soc.* **2013**, *135*, 8760.

34) Matus, M. H.; Anderson, K. D.; Camaioni, D. M.; Autrey, S. T.; Dixon, D. A. *J. Phys. Chem. A* **2007**, *111*, 4411.

35) Nutt, W. R.; McKee, M. L. *Inorg. Chem.* **2007**, *46*, 7633.

36) Lisovenko, A. S.; Timoshkin, A. Y. *Inorg. Chem.* **2010**, *49*, 10357.

37) Ramachandran, P. V.; Gagare, P. D. *Inorg. Chem.* **2007**, *46*, 7810.

38) Hausdorf, S.; Baitalow, F.; Wolf, G.; Mertens, F. O. R. L. *Int. J. Hydrogen Energy* **2008**, *33*, 608.

39) www.hydrogen.energy.gov/pdfs/progress07/iv_b_5e_sneddon.pdf.

40) Reller, C.; Mertens, F. O. R. L. *Angew. Chem. Int. ed.* **2012**, *51*, 11731.

41) Sutton, A. D.; Davis, B. L.; Bhattacharyya, K. X.; Ellis, B. D.; Gordon, J. C.; Power, P. P. *Chem. Commun.* **2010**, *46*, 148.

42) Sutton, A. D.; Burrell, A. K.; Dixon, D. A.; Garner, E. B.; Gordon, J. C.; Nakagawa, T.; Ott, K. C.; Robinson, J. P.; Vasiliu, M. *Science* **2011**, *331*, 1426.

43) Tang, Z.; Chen, X.; Chen, H.; Wu, L.; Yu, X. *Angew. Chem. Int. ed.* **2013**, *52*, 5832.

44) Crabtree, R. H. *The organometallic chemistry of the transition metals*; Wiley-Interscience: Hoboken, N.J., 2005.

45) Mellon, E. K.; Lagowski, J. J. *Advances in inorganic chemistry and radiochemistry*; Academic Press.: New York, 1959; Vol. 5.

46) Kündig, E. P. *Transition metal arene [pi]-complexes in organic synthesis and catalysis*; Springer-Verlag: Berlin, 2004.

47) Djukic, J. P.; Rose-Munch, F.; Rose, E.; Dromzee, Y. *J. Am. Chem. Soc.* **1993**, *115*, 6434.

48) Kuendig, E. P.; Amurrio, D.; Bernardinelli, G.; Chowdhury, R. *Organometallics* **1993**, *12*, 4275.

49) Lamanna, W.; Brookhart, M. *J. Am. Chem. Soc.* **1981**, *103*, 989.

50) Brookhart, M.; Lamanna, W.; Pinhas, A. R. *Organometallics* **1983**, *2*, 638.

51) Boese, R.; Maulitz, A. H.; Stellberg, P. *Chem. Ber.* **1994**, *127*, 1887.

52) Miessler, G. L.; Tarr, D. A. *Inorganic chemistry*; Pearson/Prentice Hall: Upper Saddle River, N.J., 2004.

53) Islas, R.; Chamorro, E.; Robles, J.; Heine, T.; Santos, J.; Merino, G. *Structural Chemistry* **2007**, *18*, 833.

54) The term aromaticity, and dearomatization are used throughout this document to describe borazines and their transformations. However, it should be noted that the extent to which borazines can be considered aromatic is an ongoing subject of debate.

55) Muetterties, E. L. *Boron hydride chemistry*; Academic Press: New York, 1975.

56) Powell, P.; Semlyen, J. A.; Blofeld, R. E.; Phillips, C. S. G. *J. Chem. Soc.* **1964**, 280.

57) Adcock, J. L.; Lagowski, J. J. *Inorg. Nuc. Chem. Lett.* **1971**, *7*, 473.

58) Melcher, L. A.; Adcock, J. L.; Lagowski, J. J. *Inorg. Chem.* **1972**, *11*, 1247.

59) Nöth, H.; Rojas-Lima, S.; Troll, A. *Eur. J. Inorg. Chem.* **2005**, *2005*, 1895.

60) Nöth, H.; Troll, A. *Eur. J. Inorg. Chem.* **2005**, *2005*, 3524.

61) Gemünd, B.; Günther, B.; Nöth, H. *ARKIVOC* **2008**, 136.

62) Anton, K.; Fußstetter, H.; Nöth, H. *Chem. Ber.* **1981**, *114*, 2723.

63) Engel, T.; Reid, P. *Thermodynamics, statistical thermodynamics, and kinetics*; Pearson Benjamin Cummings: San Francisco, 2006.

64) Shriver, D. F.; Smith, D. E.; Smith, P. *J. Am. Chem. Soc.* **1964**, *86*, 5153.

65) Cambridge Structural Database, version 5.34, November 2013; Cambridge Crystallographic Data Centre, 12 Union Road, Cambridge CB2 1EZ, U.K.

66) Deckelmann, K.; Werner, H. *Helv. Chim. Acta* **1971**, *54*, 2189.

67) Scotti, M.; Valderrama, M.; Ganz, R.; Werner, H. *J. Organomet. Chem.* **1985**, *286*,

399.

68) Prinz, R.; Werner, H. *Angew. Chem. Int. ed.* **1967**, *6*, 91.

69) Huttner, G.; Krieg, B. *Angew. Chem. Int. ed.* **1971**, *10*, 512.

70) Werner, H.; Prinz, R.; Deckelmann, E. *Chem. Ber.* **1969**, *102*, 95.

71) Deckelmann, K.; Werner, H. *Helv. Chim. Acta* **1970**, *53*, 139.

72) Scotti, M.; Werner, H. *Helv. Chim. Acta* **1974**, *57*, 1234.

73) Lagowski, J. J. *Coord. Chem. Rev.* **1977**, *22*, 185.

74) Bailey, M. F.; Dahl, L. F. *Inorg. Chem.* **1965**, *4*, 1298.

75) Bridgeman, A. J. *Polyhedron* **1998**, *17*, 2279.

76) Kang, H. S. *J. Phys. Chem. A* **2005**, *109*, 1458.

77) Scotti, M.; Werner, H. *J. Organomet. Chem.* **1974**, *81*, C17.

78) Scotti, M.; Werner, H.; Brown, D. L. S.; Cavell, S.; Connor, J. A.; Skinner, H. A. *Inorg. Chim. Acta* **1977**, *25*, 261.

79) Deckelmann, E.; Werner, H. *Helv. Chim. Acta* **1969**, *52*, 892.

80) Adedeji, F. A.; Lalage, D.; Brown, S.; Connor, J. A.; Leung, M. L.; Paz-Andrade, I. M.; Skinner, H. A. *J. Organomet. Chem.* **1975**, *97*, 221.

81) Sneeden, R. P. A. *Organochromium compounds*; Academic Press: New York, 1975.

82) Neto, C. C.; Baer, C. D.; Chung, Y. K.; Sweigart, D. A. *J. Chem. Soc. Chem. Commun.* **1993**, *0*, 816.

83) Watson, E. J.; Virkaitis, K. L.; Li, H.; Nowak, A. J.; D'Acchioli, J. S.; Yu, K.; Carpenter, G. B.; Chung, Y. K.; Sweigart, D. A. *Chem. Commun.* **2001**, *0*, 457.

84) Dai, W.; Kim, S. B.; Pike, R. D.; Cahill, C. L.; Sweigart, D. A. *Organometallics* **2010**, *29*, 5173.

Chapter 2: Reduction of Borazines Mediated by Low-Valent Chromium[1]

2.1 Introduction

As described in chapter 1, the recycling of B–N spent fuels is a major hurdle to the practical application of ammonia borane for chemical hydrogen storage. Methods that permit regeneration with minimal energy cost (above the associated thermodynamic barrier) are of particular interest. Specifically, the hydrogenation of borazine with a reductant derived from H_2, or discrete H^+/e^- equivalents, is highly desirable. Along these lines, this chapter describes our initial studies into the delivery of hydrides and proton donors to a coordinated borazine. We demonstrate that stepwise metal-mediated reduction of B=N bonds is achievable, illustrating a key step of spent B-N fuel regeneration (Scheme 2-1). Because hydride equivalents can be generated using H_2 and/or protonation of reduced metal fragments, these reactions demonstrate the feasibility of a low-energy reduction strategy which remains a challenge for the regeneration of B-N hydrogen storage materials.

While studying the reactivity of natural borazine ($H_3B_3N_3H_3$) would be ideal, the Werner complexes of hexamethyl borazine ($Me_3B_3N_3Me_3$), discussed in chapter 1, are the only well characterized borazine π-complexes reported in the literature. It was also clear from Werner's reports that developing synthetic conditions which favor borazine coordination is a significant challenge. Additionally, alkyl borazines are less susceptible

Scheme 2-1. Dehydrogenation of cycylotriborazane, and the subsequent rehydrogenation strategy under investigation.

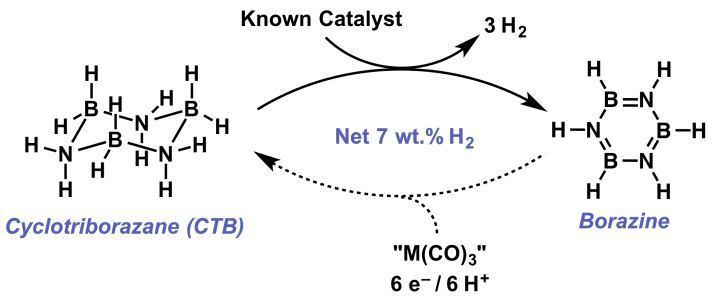

to B-N cross-linking, and exhibit low volatility, which allows for greater ease of handling. For this reason, we elected to study one of Werner's complexes, η^6-[$(Me_3B_3N_3Me_3)Cr(CO)_3$] (**1**), in an effort to establish initial proof-of-concept for metal mediated B=N bond hydrogenation before proceeding to develop natural borazine coordination complexes. We initially explored the hydrogenation thermodynamics of both substrates computationally,[2] however, to verify that our experimental studies conducted on $Me_3B_3N_3Me_3$ would translate to natural borazine.

2.2 Results and Discussion

We first sought to benchmark our computational model by calculating the free energy of hydrogenation for both borazine and benzene using the B3LYP and M06-2X functionals (see experimental section for details). While the M06-2X functional generally provided more accurate estimates of hydrogenation free energy values (Table A-1), the B3LYP functional was superior for calculating the vibrational frequencies and redox potentials of the metal complexes (See Section 4.2.2) so it was implemented in all subsequent computational analysis. The calculated free energies of hydrogenation for benzene (-13.0 kcal/mol) were lower than the experimental value (-23 kcal/mol at 298 K) but within 10 kcal/mol.[3] The predicted free energy (Scheme 2-2) of hydrogenation for taking borazine ($H_6B_3N_3$) to cyclotriborazine ($H_{12}B_3N_3$) (27.8 kcal/mol) was also low when compared with the calculated values reported by Matus et. al. (43.3 kcal/mol) and Miranda and Ceder (~48 kcal/mol).[4-5] However, our calculated reaction enthalpy (1.4 kcal/mol) is in good agreement with the experimental value (1 kcal/mol) reported by Schellenberg, Kriehme, and Wolf,[6] suggesting that our calculated values provide a reasonable estimate of borazine reaction thermodynamics.

Having established that our computational methods were yielding satisfactory free energy values, we next sought to compare the hydrogenation free energies of borazine and hexamethylborazine ($Me_3B_3N_3Me_3$). As discussed in chapters 1-3, the only known transition metal complexes of borazines are those of alkyl substituted variants.[7] Understanding the thermodynamics of hydrogenation for both substrates is therefore essential to establish whether the reactivity of alkyl borazines discussed in chapters 2 and 3 can be used to inform the design of strategies for metal-mediated borazine

Scheme 2-2. Calculated free energy of $H_3B_3N_3H_3$ and $Me_3B_3N_3Me_3$ hydrogenation

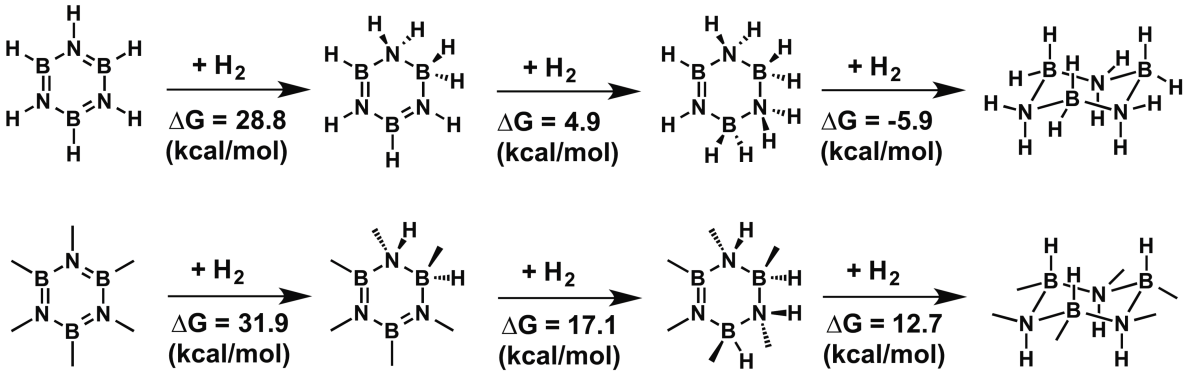

reduction. In support of this, we noted that the addition of a single equivalent of H_2 to form a 1,2-H_2-borazine was predicted to have a nearly identical reaction free energy (ΔG = 31.9 vs. 28.8 kcal/mol) for both substrates. We were also able to predict, in agreement with other computational studies, that the first hydrogenation step is indeed the most difficult, likely due to the conjugation stabilization energy of the borazine ring. Interestingly, the subsequent two hydrogenation steps required to transform borazine back to cyclotriborazane ($H_6B_3N_3H_6$) are essentially thermo-neutral (ΔG = -1 kcal/mol), suggesting that achieving the ionic hydrogenation of the first B=N bond in the borazine unit is the crucial step in a regeneration scheme which relies on the stepwise reduction and protonation. In contrast, the remaining hydrogenation steps for $Me_3B_3N_3Me_3$ (ΔG = 30 kcal/mol) are predicted to be substantially higher in energy than those for $H_6B_3N_3$. This is likely a product of the increased hydricity of the N-B(H)Me-N unit, compared with that of the N-BH_2-N unit for regular borazine, favoring H_2 loss. Despite these differences, the fact that that ΔG for both reactions is comparable for the first, and most difficult, hydrogenation step suggests that $Me_3B_3N_3Me_3$ is indeed a suitable model for our studies aimed at uncovering a general route to reduce B=N bonds via metal-mediated ionic hydrogenation.

Confident that $Me_3B_3N_3Me_3$ is a suitable model substrate for studying metal mediated borazine reactivity, **1** was prepared in 69 % yield following a modification of the previously reported procedure.[8] Although previously described,[8-9] no structural characterization of **1** has been reported. Accordingly, orange needles of **1** were grown from Et_2O solution and analyzed by X-ray diffraction. The structure of **1** is similar to that of η^6-[($Et_6B_3N_3$)Cr($CO)_3$], the only reported structure of a transition-metal η^6-borazine

complex.[10] The ring nitrogen atoms are *trans*-disposed to the carbonyl ligands, and the boron atoms are slightly puckered away from the metal center (Figure 2-1A, Figure A-26). As a result of this distortion from planarity, the N-B-N angles are slightly smaller (ca. 115°) than the B-N-B bond angles (ca. 125°), and the B–N bond distances vary slightly (B1–N1 1.462(5), B2–N2 1.458(5), B3–N3 1.447(5) Å).

Although the synthesis of metal–borazine adducts was reported more than forty years ago, to the best of our knowledge, subsequent reactivity studies of these complexes have not been disclosed, with the exception of ligand-displacement reactions.[11-12] Accordingly, we sought to explore the reactivity of **1** to assess whether it can mediate reductive transformations of the coordinated borazine. Direct reduction of borazine with hydride reagents has not been reported,[13,] and in line with the lack of

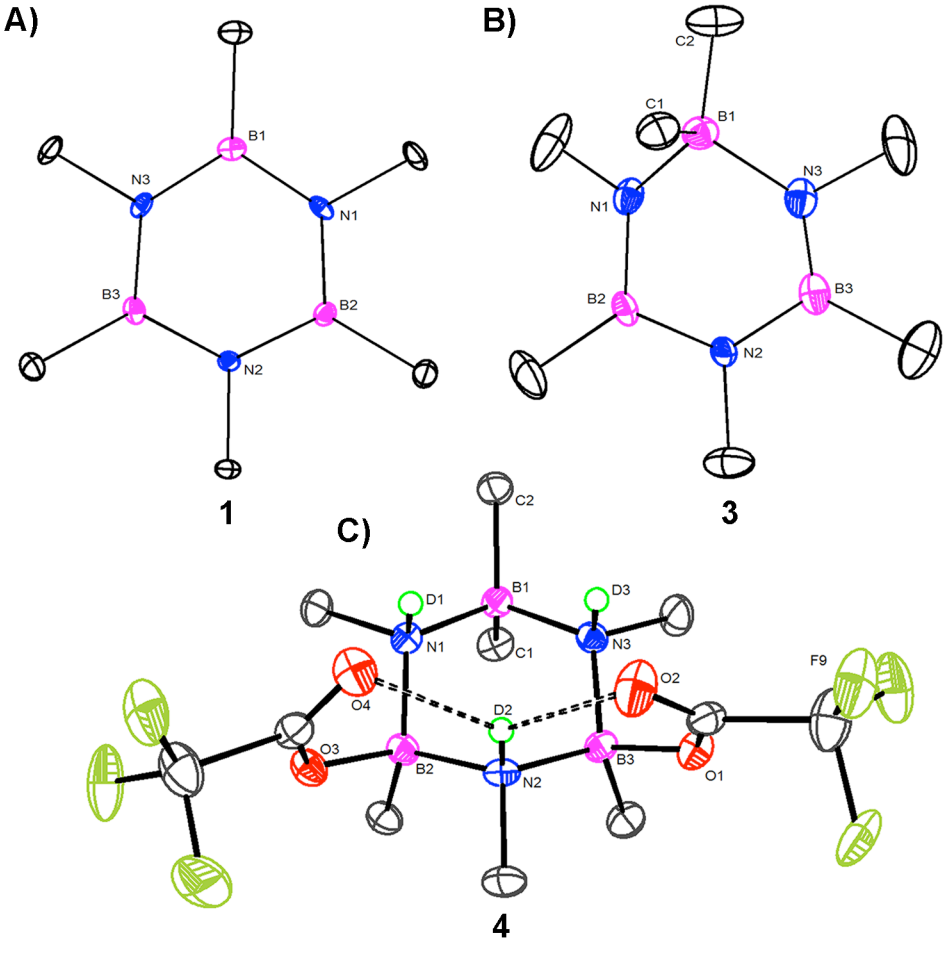

Figure 2-1. ORTEP of the B_3N_3 units of **1** (A), **3** (B), and **4** (C). $Cr(CO)_3$, countercations, solvents of crystallization, and hydrogen atoms removed for clarity; ellipsoids are set at 35 % probability.

literature precedent, when $Me_3B_3N_3Me_3$ was treated with $LiEt_3BH$ or LiH in ethereal solvents, no reaction occurred (<1 % conversion) over the course of 12 days, as monitored by ^{11}B NMR spectroscopy. In contrast, when **1** was treated with 3 equiv. $LiEt_3BH$ in diethyl ether at −35 °C, a reaction occurred, as assessed by ^{11}B NMR spectroscopic analysis at −20 °C. ^1H NMR spectra obtained at −20 °C confirmed that a new compound (**2**) formed, with loss of threefold symmetry as indicated by the inequivalence of the N–CH_3 and B–CH_3 groups. Additionally, a new high-field resonance at −2.92 ppm was observed, consistent with a Cr–H unit.

Complex **2** (Figure 2-2) crystallizes as a lithium etherate bridged dimer, and contains a dearomatized borazine unit coordinated to a $Cr(CO)_3$ fragment. The hydride ligand was located from the difference map and was found to exist as a B–H–Cr bridging unit. Notably, the B–N bond distances are asymmetric around the ring, with the B1–N1 and B1–N3 distances significantly elongated compared to **1**, increasing from 1.462(5) and 1.455(6) to 1.532(3) and 1.533(3) Å, respectively, whereas the B3–N2 distance is shorter, decreasing from 1.460(5) to 1.444(4) Å; the former B–N bond distances are consistent with reduction of the B–N bond order. Additionally, the N1-B1-N3 angle is reduced from 114.5(3)° to 105.9(2)°, confirming tetrahedral geometry about B1. These distortions imply that the aromaticity of $Me_3B_3N_3Me_3$ is effectively disrupted, and represents successful delivery of a hydride unit to a borazine fragment. Attempts to establish further reactivity from **2** were hampered by significant thermal instability.[14]

In contrast to the thermal instability of products obtained from the reaction of **1** with hydride nucleophiles, similar reactions with anionic alkyl sources afforded thermally robust products that were amenable to subsequent reactivity studies. For example, when solutions containing **1** were treated with one equiv MeMgBr, a new, thermally stable, compound (**3**) was generated in quantitative yield. Similar to **2**, ^1H NMR spectroscopic analysis confirmed the loss of threefold symmetry, and the introduction of new N-CH_3 resonances at 2.85 and 2.42 ppm, (integrating 2:1), as well as three new B–CH_3 resonances at −0.83, −0.07, and 0.55 ppm (integrating to 1:1:2). The ^{11}B NMR spectrum revealed two new resonances at 3.90 and 31.0 ppm, concomitant with loss of the resonance at 27.2 ppm for **1**. IR spectroscopy further aided the analysis, with new ν_{CO} bands observable at 1925, 1763, and 1694 cm^{-1} (shifted from 1947 and 1845 cm^{-1}

in **1**), which are consistent with enhanced nucleophillic character at chromium. In contrast to the hydride addition product (**2**), **3** is readily isolable and stable at room temperature, if stored under inert atmosphere, for periods exceeding two months.

Crystals suitable for X-ray diffraction were obtained by slow diffusion of pentane into a THF solution of **3**. The solid-state structure is geometrically similar to **2** about the borazine unit, however the metal binding mode is distinct. In contrast to the κ^2-*N*,*N*′-(μ-H) mode observed in **2**, the borazine unit of **3** is bound η^5 with no bridging CH_3 unit and a significant out-of-plane distortion of B1. The B–N bond distances and angles are similar to the isolated hydride addition product (Figure 2-2), which confirms that this species is a suitable surrogate for further reactivity studies.

Following isolation of a stable, anionic, dearomatized borazine unit, we sought to

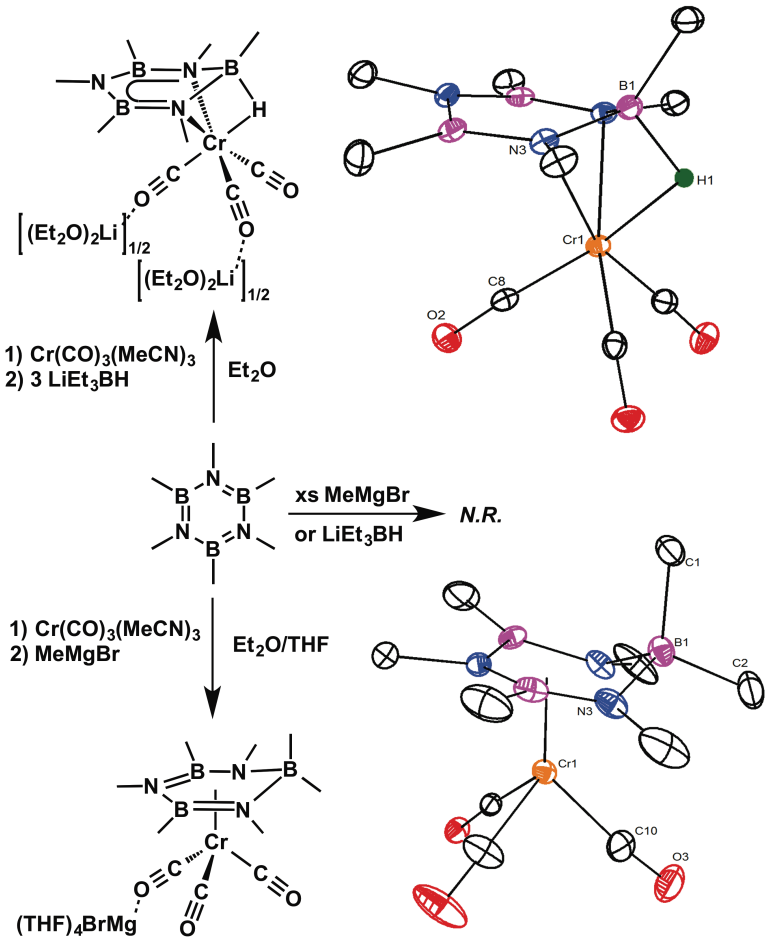

Figure 2-2. Reactivity of $Me_3B_3N_3Me_3$ with hydride and alkyl nucleophiles in the presence (top and bottom path) and absence (middle path) of $[Cr(CO)_3(MeCN)_3]$, as well as solid-state structures of **2** and **3**. Ellipsoids are set at 35 % probability.

complete a single B–N bond reduction cycle by the addition of a suitable proton donor. The reaction of **3** with a single equivalent of HCl or 2-methoxy-6-methylpyridinium chloride yielded mixtures of products, the distribution of which was dependent on the acid strength, reaction temperature, and solvent used.[15] The addition of excess TMS-OTf (trimethylsilyltriflate) gave rise to a new species in the crude ^{11}B NMR (Figure A-17) with resonances at 41 and -2 ppm, which was potentially consistent with a 1,2-addition product. However, attempts to isolate this complex afforded only free $Me_3B_3N_3Me_3$. Note that 1,2-addition products obtained by single H^+ addition are predicted to have limited thermodynamic stability relative to the corresponding borazine or monoene species.[16,17] As an alternative, we targeted a quench/trap method to capture unstable and reactive diene intermediates by derivatization. Because H–X additions to borazine (X = Cl, Br) were previously reported,[18,19] we examined acids that feature coordinating anions as trapping reagents, and initiated our studies with H^+ donors featuring attenuated acidity relative to HCl.

To confirm the efficacy of this approach with non-hydrohalic acids, $Me_3B_3N_3Me_3$ was treated with excess $DOAc^F$ ([D_1]trifluoroacetic acid)[20] in frozen dimethoxyethane solvent, which was then allowed to thaw to room temperature. Consistent with prior reports on triple H–X addition to borazine, a new B-N product formed that was identified as the 3:1 $DOAc^F$–borazine adduct, $OAc^F{}_3Me_3B_3N_3Me_3D_3$. Confirmation of the empirical formula was provided by elemental analyses, and the solution structure was interrogated by a suite of multinuclear NMR spectroscopic (^{1}H, ^{11}B, ^{2}H, ^{19}F, ^{13}C) experiments. The NMR spectra revealed a mixture of isomers, noted by ^{1}H and ^{19}F resonances that appeared at similar chemical shifts, all of which had an identical ^{11}B resonance (5.87 ppm). Furthermore, the IR spectrum showed ν_{ND} bands at 2407 cm^{-1}. and 2380 cm^{-1}.[21] The collection of spectroscopic data provided evidence consistent with the proposed structure. Unfortunately, the presence of multiple isomeric species hindered crystallization, and thus precluded analysis by X-ray crystallography.

Complementary to the addition of $DOAc^F$ to $Me_3B_3N_3Me_3$ noted above, the addition of excess (5 equiv) $DOAc^F$ to **3** afforded $OAc^F{}_2Me_4B_3N_3Me_3D_3$ (**4**) in 40 % yield (Scheme 2-3). Following crystallization from a saturated pentane solution, a dominant

Scheme 2-3. Reaction of $Me_3B_3N_3Me_3$ with $DOAc^F$ (top path) and reduction of $Me_3B_3N_3Me_3$ mediated by $Cr(CO)_3$ using a quench/trap process.

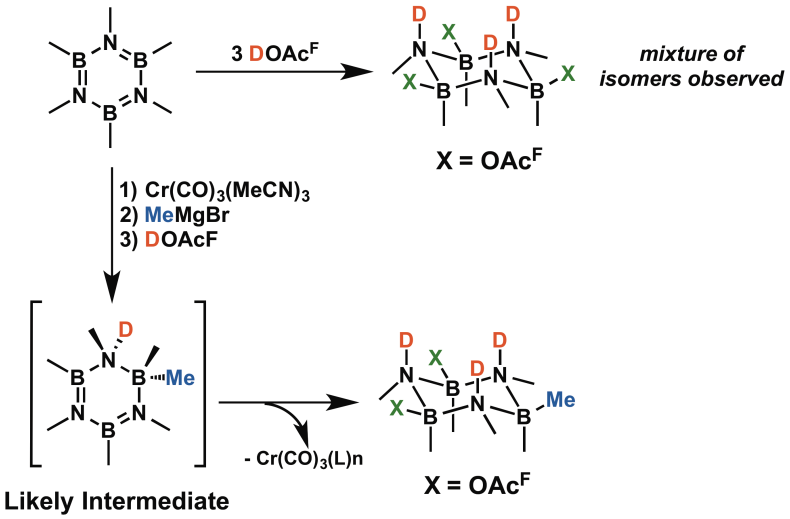

isomer was obtained (75 %) in which all three deuterium atoms are axial and the installed OAc^F groups are equatorial. The solution structure was deduced by multinuclear NMR spectroscopy, and visualized by three distinct B–CH_3 resonances in the ^{1}H NMR appearing at −0.10 (s, 6 H), −0.28 (s, 3 H), and −0.31 ppm (s, 3 H) and two resonances present in the ^{11}B NMR spectrum at 0.94 and 6.31 ppm. The spectral data was further supported by the solid-state structure (Figure 2-1C), featuring a chair conformation in which all ring atoms exhibit tetrahedral geometry and the installed deuteride atoms and OAc^F groups are all axial. The B–N bonds neighboring the methylated boron atom are slightly longer (1.634(4), and 1.637(4) Å) than those neighboring OAc^F substituted atoms (between 1.573–1.584 Å) and consistent with the enhanced donor ability of the methyl group compared to OAc^F. Close-contact interactions exist between the oxygen atoms of OAc^F (O2 and O4) and the ND unit of N2 (ca. 2.9 Å), consistent with a bifurcated hydrogen bond. This intramolecular interaction most likely provides sufficient stabilization to favor the isomer that exhibits several unfavorable $CH_3\cdots CH_3$ 1,3-diaxial interactions. Unfortunately, attempts to repeat the quench/trap strategy using **2** did not proceed cleanly and were complicated by the competitive protolytic release of H_2.

Crystallographic characterization of these B_3N_3 reduction products provides a snapshot of how B-N materials can be reduced by stepwise addition, lending insight

toward the design of B-N spent-fuel-regeneration systems. As noted by Werner and others,[6,10,22,23] coordination of borazine to $Cr(CO)_3$ induces subtle structural changes, most clearly illustrated by the slight out-of-plane distortions of the B-N atoms (deviation from planarity in **1** = 8.2–9.1°).[24] However, the consistent B–N bond lengths (ca. 1.45 Å) suggest that the partial electron delocalization observed for free borazines is maintained upon coordination. Addition of a hydride or methyl anion disrupts the ring conjugation by the introduction of an sp^3-hybridized boron atom (N3-B1-N1 angles of 105.9 and 97.5° for **2** and **3**, respectively), and asymmetry is introduced into the B_3N_3 bonding manifold. Bond distances similar to cyclotriborazane ($H_6B_3N_3H_6$; CTB) (1.53 in **2** and 1.59/1.62 Å in **3**) and free borazines (1.43–1.48 Å for both **2** and **3**) are both present, which suggests that the independent reduction of each B=N bond may be possible. Quenching/trapping the proposed diene product with $DOAc^F$ affords a substituted CTB (**4**) with irregular bond lengths that retains the installed methyl group. The structural changes associated with the reduction of the B-N unit clearly illustrate a successful initial reduction cycle of borazine and the feasibility of a metal-mediated reduction strategy.

2.3 Conclusions

In summary, this chapter demonstrates the successful stepwise reduction of a B=N bond in $Me_3B_3N_3Me_3$, mediated by low-valent chromium. The alkyl borazine was activated by coordination to a $Cr(CO)_3$, which facilitated methyl and hydride transfer to the borazine ring. The methylated dearomatized borazine complex was then successfully quenched with $DOAc^F$ to give a substituted CTB, effectively establishing a metal-mediated B=N reduction pathway. These reactions represent the first well-defined examples of the metal-mediated reduction of an alkyl borazine, which, because of its similarity to B–N spent fuel products, establishes proof-of-principle for a new B–N regeneration strategy.

2.4 Experimental Details

Computational Details: All structures were fully optimized without symmetry constraints using either the M06-2X[25] or the B3LYP[26-29] functional as implemented in Gaussian 09,[30] using the 6-31G** basis set.[31,32] The ultrafine integration grid was

employed in all calculations, which ensured the stability of the optimization procedure for the investigated molecules. Each stationary point was confirmed by a frequency calculation at the same level of theory to be a real local minimum on the potential energy surface without imaginary frequency. More accurate electronic energies were computed for the optimized geometries using the larger 6-311++G(d,p) basis set.[33,34] All reported free energies are for Et_2O solution at the standard state (T = 298 K, P = 1 atm, 1 mol/L concentration of all species in Et_2O) as modeled by a polarized continuum model.[35] The energy values given in the paper correspond to solvent-corrected Gibbs free energies that are based on B3LYP/6-311++G(d,p) electronic energies and all corrections calculated at the B3LYP/6-31G(d) level. Initial optimizations employed the M06-2X functional as the included dispersion corrections have been shown to provide better estimation of main-group systems.[25,36,37] Although computations employing the M06-2X functional better modeled the thermochemistry of borazine and hexamethylborazine, all computations reported within made use of the B3LYP functional, which was found to model the manganese and chromium complexes better than the M06-2X functional.

General Experimental Procedures: All experiments were conducted using standard Schlenk techniques or in a nitrogen filled glovebox. NMR spectra were recorded on Varian MR400, vnmrs 500, Inova 500, or vnmrs 700 MHz spectrometers. ^{1}H NMR, and Wet1D ^{1}H NMR spectra were referenced relative to the protio solvent resonance, and ^{11}B, ^{13}C, and ^{19}F spectra are referenced indirectly based on the ^{1}H spectrum.[38] As previously reported,[39] the carbon atoms directly bound to boron were difficult to observe and/or unambiguously assign by ^{13}C NMR due to quadrapolar coupling. IR Spectra were recorded on a Nicolet iS-10 spectrometer from Thermo Scientific as either KBr pellets or on a diamond attenuated total reflectance (ATR) accessory. Cyclic voltammetry experiments were collected on a Pine Research Instrumentation WaveNow potentiostat. Experiments were conducted in a 0.05 M solution of tetrabutylammonium tetrakis[3,5-bis(trifluoromethyl)phenyl]borate ($^{n}Bu_4NBAr'$) in either diethyl ether or 1,2-dimethoxyethane solvent. A glassy carbon working electrode and a platinum disk counter electrode were used and voltammograms referenced relative to ferrocene ($Fc^{0/+}$) using a silver wire pseudo reference electrode. Potentials are reported as $E_{1/2}$

values where a return wave is present and as E_{Pa} or E_{Pc} values where a return wave is absent or very weak. Scan rate was 0.1 V/s unless otherwise specified. $^{n}Bu_4NBAr'$ was synthesized using a modified version of the procedure reported by Kobayashi and coworkers[40] for the synthesis of tetraethylammonium tetrakis[3,5-bis(trifluoromethyl)phenyl]borate. Tetrabutylammonium chloride was used in place of tetraethylammonium iodide, and extraction with ether followed by drying over $MgSO_4$ was used in-lieu of column chromatography. Sodium tetrakis[3,5-bis(trifluoromethyl)phenyl]borate, hexamethylborazine ($Me_3B_3N_3Me_3$), and $Cr(CO)_3(CH_3CN)_3$ were synthesized by previously reported routes.[41-43] Diethyl ether, pentane, tetrahydrofuran, and 1,2-dimethoxyethane were ordered from Fisher Scientific and passed through an S.G. Waters solvent purification system. 1,4-dioxane was distilled from sodium and degassed prior to use. Deuterated NMR solvents were either obtained as sealed ampoules and used as received, or degassed and dried by standard methods.[44] All other chemicals were purchased from commercial vendors and used as received.

Synthesis of 1 (η^6-$(Me_3B_3N_3Me_3)Cr(CO)_3$): A simplified version of the procedure reported by Werner and co-workers[9] was used. A solution of $Cr(CO)_3(CH_3CN)_3$ (1.5 g, 5.8 mmol) and hexamethylborazine ($Me_3B_3N_3Me_3$; 4.8 g, 29.0 mmol) was prepared in 1,4-dioxane (50 mL). The orange solution was stirred at 25 ºC under dynamic vacuum until the solvent evaporated. Reaction progress was monitored by IR spectroscopy and solvent addition and removal was repeated 5 times. Complete conversion to η^6-$(Me_3B_3N_3Me_3)Cr(CO)_3$ was confirmed by the disappearance of $Cr(CO)_3(CH_3CN)_3$ in the IR spectrum (bands at 1912 and 1772 cm^{-1}). The resulting yellow solid was then dissolved in Et_2O (200 mL), filtered through a medium porosity sintered glass frit, and the solvent was removed *in vacuo*. Solid was then washed 5 times with cold pentane (10 mL) and dried under vacuum. Yield: 1.2 g, (69%). The product obtained is spectroscopically identical to that previously reported in C_6D_6, however, because borazine is slowly displaced by this solvent, we report characterization in substitutionally-inert solvent (CD_2Cl_2). ^1H NMR (399.54 MHz, CD_2Cl_2): δ 2.94 (s, 9H; N–*CH_3*), 0.79 (s, 9H; B–*CH_3*); ^{11}B NMR (128.19 MHz, CD_2Cl_2): δ 27.20 (s); Cyclic voltammetry (0.05 M $^{n}Bu_4NBAr'$ in Et_2O): E_{Pa} (*V* vs. $Fc^{0/+}$), –2.92, –3.57, Crystals

suitable for X-ray diffraction were obtained from diethyl ether/pentane (1:1) at –35 ºC.

Synthesis of 2 ([η^3-($Me_3B_3N_3Me_3$)(μ-H)$Cr(CO)_3$]$Li(Et_2O)_2$): To a frozen solution of **1** (21.0 mg, 0.070 mmol) in 10 mL Et_2O was added a solution (obtained by reducing a 1.0 M solution from Sigma Aldrich under vacuum to 1:1.5 mol/mol as determined by ^{1}H NMR integration) of $LiEt_3BH$ in THF (44.3 mg, 0.210 mmol). The mixture was allowed to thaw in a –35 ºC freezer and further react for 18 h. **2** is thermally sensitive and decomposes readily at room temperature, however, it can be observed in solutions of the reaction mixture by low temperature (–20 °C) ^{11}B and ^{1}H NMR spectroscopy. Wet1D ^{1}H NMR (500.10 MHz, Et_2O): δ 2.57 (s, 3H; N–*CH*$_3$), 2.24 (s, 6H; N–*CH*$_3$), 0.33 (s, 6H; B–*CH*$_3$), 0.17 (s, 3H; B–*CH*$_3$), –2.92 (br, 1H; B–*H*–Cr); ^{11}B NMR (160.45 MHz, Et_2O): δ –0.82 (s). Note: while two 11B resonances are expected, only one could be conclusively identified. Enhanced quadrapolar relaxation, introduced through asymmetry of the electric field gradient surrounding the B=N bonding scaffold, likely broadens the resulting ^{11}B resonance into the baseline.[45] Similar observations have been reported previously.[46] Crystals suitable for X-ray diffraction were obtained by performing the reaction in Et_2O/pentane (5:1) at –35 ºC.

Synthesis of 3 ([η^5-($Me_4B_3N_3Me_3$)$Cr(CO)_3$]$Mg(THF)_4Br$): To a frozen solution of **1** (60.0 mg, 0.2 mmol) in 5 mL Et_2O, was added a solution of MeMgBr (3.0 M in Et_2O from Sigma Aldrich; 66.0 µL, 0.22 mmol). The solution was allowed to thaw and the resulting yellow precipitate was collected on a glass microfiber filter pad, washed with pentane (3 x 1mL), and passed through the filter with THF. The solvent was removed under vacuum to afford a yellow powder (77.4 mg; 95%). ^{1}H NMR (500.10 MHz, [D_8]THF): δ 2.85 (s, 3H; N–*CH*$_3$), 2.42 (s, 6H; N–*CH*$_3$), 0.55 (s, 6H; B–*CH*$_3$), –0.07 (s, 3H; B–*CH*$_3$), –0.83 (s, 3H; B–*CH*$_3$); ^{11}B NMR (128.19 MHz, [D_8]THF): δ 30.98 (s), 3.90 (s); ^{13}C NMR (125.71 MHz, [D_8]THF): δ 251.69 (s), 203.90 (s), 39.13(s), 38.04 (s); IR (KBr): ν_{CO} 1925, 1763, 1694 cm^{-1}, ν_{BN} 1468, 1456, 1400, 1384, 1350 cm^{-1}. Cyclic voltammetry (0.05 M ^{n}Bu_4NBAr' in 1,2-dimethoxyethane): $E_{1/2}$ (V vs. $Fc^{0/+}$) –0.77, E_{Pa} (V vs. $Fc^{0/+}$) –0.13, 0.22. Crystals suitable for X-ray diffraction were obtained by slow diffusion of pentane into a THF solution of **3** at –35 ºC.

Treatment of 3 with TMSOTf: To a frozen solution of **3** (5.0 mg, 0.007 mmol) in 0.7 mL

DME was added TMSOTf (63.0 µL, 0.35 mmol). The solution was allowed to thaw and warm to room temperature over 10 minutes. The sample was then taken for NMR analysis. New resonances were observed at 41 and -2 ppm in addition to unreacted **3** and compound **1** (Figure A-17).

Synthesis of 4 ($OAc^F_2Me_4B_3N_3Me_3D_3$): To a frozen solution of **3** (20.9 mg, 0.030 mmol) in 2 mL DME was added $DOAc^F$ (11.4 µL, 0.149 mmol). The solution was allowed to thaw and warm to room temperature over 10 minutes. The solvent was removed. Solid was washed with pentane (1 x 3 mL) and the pentane solution was decanted and retained. The solvent was removed to afford 4.5 mg (40.2% yield) of a white solid. **4** is obtained as a mixture of isomers. The most abundant isomer (ca. 75% of the mixture) is consistent with the solid-state structure and can be obtained in good purity by recrystalization from a saturated pentane solution stored at –35 ºC. **4** decomposes slowly at room temperature, but is stable over periods of at least 2 weeks when stored at –35 ºC. ^{1}H NMR (399.54 MHz, C_6D_6): *δ* 1.80 (s, 6H; N–*CH*$_3$), 1.73 (s, 3H; N–*CH*$_3$), –0.10 (s, 6H; B–*CH*$_3$), –0.28 (s, 3H; B–*CH*$_3$), –0.31 (s, 3H; B–*CH*$_3$); ^{2}H NMR (61.33 MHz, C_6H_6): *δ* 4.79 (s; N–D), 2.99 (s; N–D); ^{11}B NMR (128.19 MHz, C_6D_6): *δ* 6.31 (s), 0.94 (s); ^{19}F NMR (375.91 MHz, C_6D_6): *δ* –76.14 (s); IR (KBr): $\nu_{N\text{-}D}$ 2386, , $\nu_{CO\text{-}OAcF}$ 1716, ν_{BN} 1426, 1335, 1318 cm^{-1}. Crystals suitable for X-ray diffraction were obtained from a cooling a saturated pentane solution of **5** to –35 ºC.

Synthesis of 5 ($OAc^F_3Me_3B_3N_3Me_3D_3$): To a frozen solution of hexamethylborazine (76.4 mg, 0.46 mmol) in 10 mL pentane was added $DOAc^F$ (180 µL, 2.30 mmol). The solution was allowed to thaw and warm to room temperature over 10 minutes with stirring. Following the formation of a white precipitate, the solution was decanted and the solid was rinsed with Et_2O (2 x 2 mL). The solid was dried in-vacuo to give 178.9 mg (76.3 % yield) of the title compound. **5** is obtained as a mixture of isomers with distinct ^{1}H and ^{19}F resonances but with an identical ^{11}B resonance. This, in combination with elemental analysis is taken as evidence that all species present share the same empirical formula. NMR data is presented for the most abundant isomer. **5** decomposes slowly at room temperature, but is stable over periods of at least 2 weeks when stored at –35 ºC. ^{1}H NMR (500.09 MHz, $CDCl_3$): *δ* 2.37 (s, 9H; N–*CH*$_3$), 0.11 (s, 9H; B–*CH*$_3$); ^{2}H NMR (61.33 MHz, $CHCl_3$): *δ* 4.89 (s; N–D); ^{11}B NMR (160.45 MHz, $CDCl_3$): *δ* 5.87.;

^{19}F NMR (470.52 MHz, $CDCl_3$): δ –75.90 (s); ^{13}C NMR (125.71 MHz, $CDCl_3$): δ 160.16 (s, OAc^F–CO), δ 114.40 (q, CF_3, ^2J(C,F)=287.43 Hz), δ 29.97 (s, N–CH_3); IR (KBr): $\nu_{N\text{-}D}$ 2407, 2380 cm^{-1}, $\nu_{CO\text{-}OAcF}$ 1767, 1721 cm^{-1}, ν_{BN} 1421, 1396, 1334 cm^{-1}. Elemental analysis calculated (corrected for deuterium) for $C_{12}H_{18}B_3D_3F_9N_3O_6$: C 28.27, H 4.18, N 8.24; found: C 28.40, H 4.11, N 8.11. Note that when $HOAc^F$ is used a product which is identical to the deuterate is obtained with the exception of the N–H bonds as visualized by IR spectroscopy: $\nu_{N\text{-}H}$ 3233, 3207 cm^{-1} (See Figures SI-18 and SI-19).

2.5 References

1) Reproduced with permission from: Carter, T. J.; Kampf, J. W.; Szymczak, N. K. *Angew. Chem. Int. ed.* **2012**, *51*, 13168.

2) All computational studies were conducted by Dr. Zachariah M. Heiden from Washington State University.

3) Engel, T.; Reid, P. *Thermodynamics, statistical thermodynamics, and kinetics*; Pearson Benjamin Cummings: San Francisco, 2006.

4) Werner and co-workers have characterized a $Cr(CO)_3$ complex of $H_3B_3N_3Me_3$ through ring metathesis, however, no structural data or reactivity studies for this complex have been reported.

5) Matus, M. H.; Anderson, K. D.; Camaioni, D. M.; Autrey, S. T.; Dixon, D. A. *J. Phys. Chem. A*, **2007**, *111*, 4411.

6) Miranda, C. R.; Ceder, G. *J. Chem. Phys.*, **2007**, *126*.

7) Schellenberg, R.; Kriehme, J.; Wolf, G. *Thermochim. Acta*, **2007**, *457*, 103.

8) Prinz, R.; Werner, H. *Angew. Chem. Int. ed.* **1967**, *6*, 91.

9) Werner, H.; Prinz, R.; Deckelmann, E. *Chem. Ber.* **1969**, *102*, 95.

10) Huttner, G.; Krieg, B. *Angew. Chem. Int. ed.* **1971**, *10*, 512.

11) Deckelmann, E.; Werner, H. *Helv. Chim. Acta* **1969**, *52*, 892.

12) Scotti, M.; Werner, H.; Brown, D. L. S.; Cavell, S.; Connor, J. A.; Skinner, H. A. *Inorg. Chim. Acta* **1977**, *25*, 261.

13) Direct reduction of a derivative of an alternative H_2-storage material related to 1,2-dihydro-1,2-azaborine was recently reported to occur with both KH/HCl and H_2 with Pd/C. See Ref. [4e] for more details.

14) Compound **2** is thermally sensitive and decomposes rapidly at room temperature; however, the reaction mixture may be stored in the freezer for up to five days without significant decomposition. Species **2** can be observed in solutions of the reaction mixture by low-temperature (-20 ºC) NMR spectroscopy.

15) Free $Me_3B_3N_3Me_3$ was typically one of the reaction products, and most likely results from protolytic attach of the B–CH_3 unit, leading to the release of methane.

16) Lisovenko, A. S.; Timoshkin, A. Y. *Inorg. Chem.* **2010**, *49*, 10357.

17) Matus, M. H.; Anderson, K. D.; Camaioni, D. M.; Autrey, S. T.; Dixon, D. A. *The J. Phys. Chem. A* **2007**, *111*, 4411.

18) Shore, S. G.; Hickam, C. W. *Inorg. Chem.* **1963**, *2*, 638.

19) Dahl, G. H.; Schaeffer, R. *J. Am. Chem. Soc.* **1961**, *83*, 3032.

20) Studies used $DOAc^F$ to aid spectroscopic analyses. Note that control reactions using $HOAc^F$ proceeded identically.

21) Assigned by comparison to the reaction with $HOAc^F$, which has bands at 3233 and 3207 cm^{-1}.

22) Adcock, J. L.; Lagowski, J. J. *Inorg. Chem.* **1973**, *12*, 2533.

23) Lagowski, J. J. *Coord. Chem. Rev.* **1977**, *22*, 185.

24) Measured as the angle between the N1-N2-N3 plane and a plane defined to contain each of the boron atoms and its two adjacent nitrogen atoms.

25) Zhao, Y.; Truhlar, D. G. *J. Chem. Theory Comput.* **2008**, *4*, 1849.

26) Becke, A. D. *J. Chem. Phys.* **1993**, *98*, 5648.

27) Lee, C.; Yang, W.; Parr, R. G. *Phys. Rev. B* **1988**, *37*, 785.

28) Vosko, S. H.; Wilk, L.; Nusair, M. *Canadian J. Phys.* **1980**, *58*, 1200.

29) Stephens, P. J.; Devlin, F. J.; Chabalowski, C. F.; Frisch, M. J. *J. Phys. Chem.* **1994**, *98*, 11623.

30) Gaussian 09, Revision D.01, M. J. Frisch, G. W. Trucks, H. B. Schlegel, G. E. Scuseria, M. A. Robb, J. R. Cheeseman, G. Scalmani, V. Barone, B. Mennucci, G. A. Petersson, H. Nakatsuji, M. Caricato, X. Li, H. P. Hratchian, A. F. Izmaylov, J. Bloino, G. Zheng, J. L. Sonnenberg, M. Hada, M. Ehara, K. Toyota, R. Fukuda, J. Hasegawa, M. Ishida, T. Nakajima, Y. Honda, O. Kitao, H. Nakai, T. Vreven, J. A. Montgomery, Jr., J. E. Peralta, F. Ogliaro, M. Bearpark, J. J. Heyd, E. Brothers, K. N. Kudin, V. N. Staroverov, T. Keith, R. Kobayashi, J. Normand, K. Raghavachari, A. Rendell, J. C. Burant, S. S. Iyengar, J. Tomasi, M. Cossi, N. Rega, J. M. Millam, M. Klene, J. E. Knox, J. B. Cross, V. Bakken, C. Adamo, J. Jaramillo, R. Gomperts, R. E. Stratmann, O. Yazyev, A. J. Austin, R. Cammi, C. Pomelli, J. W. Ochterski, R. L. Martin, K. Morokuma, V. G. Zakrzewski, G. A. Voth, P. Salvador, J. J. Dannenberg, S. Dapprich, A. D. Daniels, O. Farkas, J. B. Foresman, J. V. Ortiz, J. Cioslowski, and D. J. Fox, Gaussian, Inc., Wallingford CT, 2013.

31) Dill, J. D.; Pople, J. A. *J. Chem. Phys.* **1975**, *62*, 2921.

32) Hehre, W. J.; Ditchfield, R.; Pople, J. A. *J. Chem. Phys.* **1972**, *56*, 2257.

33) Krishnan, R.; Binkley, J. S.; Seeger, R.; Pople, J. A. *J. Chem. Phys.* **1980**, *72*, 650.

34) Francl, M. M.; Pietro, W. J.; Hehre, W. J.; Binkley, J. S.; Gordon, M. S.; DeFrees, D. J.; Pople, J. A. *J. Chem. Phys.* **1982**, *77*, 3654.

35) Cossi, M.; Rega, N.; Scalmani, G.; Barone, V. *J. Comp. Chem.* **2003**, *24*, 669.

36) Zhao, Y.; Truhlar, D. G. *Theor. Chem. Accounts* **2008**, *120*, 215.

37) Goerigk, L.; Grimme, S. *Phys. Chem. Chem. Phys.* **2011**, *13*, 6670.

38) Harris, R. K.; Becker, E. D.; Menezes, S. M. C.; Goodfellow, R.; Granger, P. *Pure Applied Chem.* **2001**, *73*, 1795.

39) Daini, M.; Suginome, M. *Chem. Commun.* **2008**, 5224.

40) Nishida, H.; Takada, N.; Yoshimura, M.; Sonoda, T.; Kobayashi, H. *Bull. Chem. Soc. Japan* **1984**, *57*, 2600.

41) Bonham, J.; Drago, R. S.; Spielvogel, B. F.; Phillips, J. A.; Payet, C. R. In *Inorganic Syntheses*; John Wiley & Sons, Inc.: 2007, p 8.

42) Brookhart, M.; Grant, B.; Volpe, A. F. *Organometallics* **1992**, *11*, 3920.

43) Ross, B. L.; Grasselli, J. G.; Ritchey, W. M.; Kaesz, H. D. *Inorg. Chem.* **1963**, *2*, 1023.

44) Armarego, W. L. F.; Chai, C. L. L.; Knovel; ScienceDirect *Purification of laboratory chemicals*; Elsevier/Butterworth-Heinemann: Amsterdam ; Boston, 2009.

45) Bacon, J.; Gillespie, R. J.; Quail, J. W. *Can. J. Chem.* **1963**, *41*, 3063.

46) Salentine, C. G. *Inorg. Chem.*, *22*, 3920.

Chapter 3: Mn-Mediated Hydride Delivery to a Borazine by Stepwise Reduction and Protonation[1]

3.1 Introduction

The work presented in chapter 2 demonstrated that hexamethylborazine ($Me_3B_3N_3Me_3$), a convenient model for spent B–N fuels due to its low volatility and inability to participate in B–N cross-linking, was activated for subsequent reduction by coordination to a $Cr(CO)_3$ center.[2] Reduction was achieved by addition of a methyl nucleophile to afford a reduced species that was trapped with 3 equiv of $HOAc^F$, which demonstrated that metal-mediated pathways may indeed be a viable strategy to achieve B=N bond hydrogenation. However, hydride addition afforded a complex with low thermal stability (decomposition above −20 °C), which was too unstable for extensive characterization/reactivity studies (Scheme 3-1). Development of new hydride delivery mechanisms is crucial as boron hydrides are often introduced using high-energy hydride sources or by complicated digestion processes. Also, the first hydride addition to borazines is predicted to be the thermodynamically most demanding step of the reduction sequence.[3,4] As such, the generation of boron hydrides *without* using chemical hydride reagents (Scheme 3-1) is an attractive application of metal-mediated B=N bond reduction. To accomplish this, we targeted a system capable of promoting hydride addition from exogenous sources of electrons and protons as the next crucial step to establish the viability of a metal-mediated borazine reduction pathway.

Scheme 3-1. Metal-mediated routes for hydride delivery to borazine.

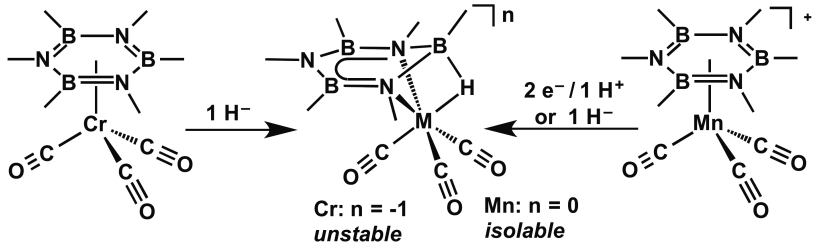

3.2 Results and Discussion

The reduction potentials for (η^6-$Me_3B_3N_3Me_3$)$Cr(CO)_3$ were highly negative (< −2.5 V; vs $Fc^{0/+}$) and irreversible, suggesting that the corresponding reduced adducts were not tractable.[2] This was confirmed experimentally as attempts to chemically reduce **1** with $Na/C_{10}H_8$ resulted in immediate decomposition, even when conducted at the thawing point of diethyl ether. To attain a less cathodic reduction potential for a metal–borazine unit whose protonation would afford an active hydride, we targeted the cationic, and isoelectronic, manganese(I) tricarbonyl fragment. Mn(I)–arene adducts are reduced at ca. −1.5 V (vs $Fc^{0/+}$),[5-7] and we hypothesized that a similar shift would be observed with analogous borazine adducts, allowing reductive reactivity to be effected at less anodic redox potentials.

In contrast to the multitude of η^6 metal–arene adducts that are structurally characterized for most (26) transition metals,[8] the only structurally characterized transition-metal π complexes of borazine share the formula [(η^6-$R_6B_3N_3$)$Cr(CO)_3$].[9-11] This likely stems from reaction incompatibilities, as the known synthetic methods to promote η^6 coordination are not readily translated from established metal–arene syntheses. For example, the direct syntheses of Mn–arene complexes is typically conducted in neat arene at reflux with $Mn(CO)_5Br$ in the presence of Ag(I) or $AlCl_3$ or, alternatively, from $Mn_2(CO)_{10}$ in the presence of $HOAc^F$ and $(CF_3CO)_2O$.[12,13] Borazines react with most acids, including $HOAc^F$ and $AlCl_3$,[2,14,15] and in our hands, reactions of $Mn(CO)_5Br$ with assorted Ag(I) salts in the presence of $Me_3B_3N_3Me_3$ did not afford the desired product. The poor reactivity is likely due to borazine's weaker binding affinity in comparison to that of arenes, which decreases the associated driving force for the necessary ligand exchange reaction,[16,17] due to competitive binding with many solvents and counteranions. These limitations were overcome by careful selection of reaction conditions; when $Me_3B_3N_3Me_3$ and $Mn(CO)_5Br$ were heated to 90 °C in di-*n*-butyl ether in the presence of the halide abstracting agent TlBAr′, (BAr′ = tetrakis(3,5-bis(trifluoromethyl)phenyl)borate) featuring a weakly coordinating anion, the target compound [(η^6-$Me_3B_3N_3Me_3$)$Mn(CO)_3$]BAr′ (**1**) was obtained in 65% yield.

Coordination of $Me_3B_3N_3Me_3$ was confirmed by ^{11}B NMR spectroscopy, which

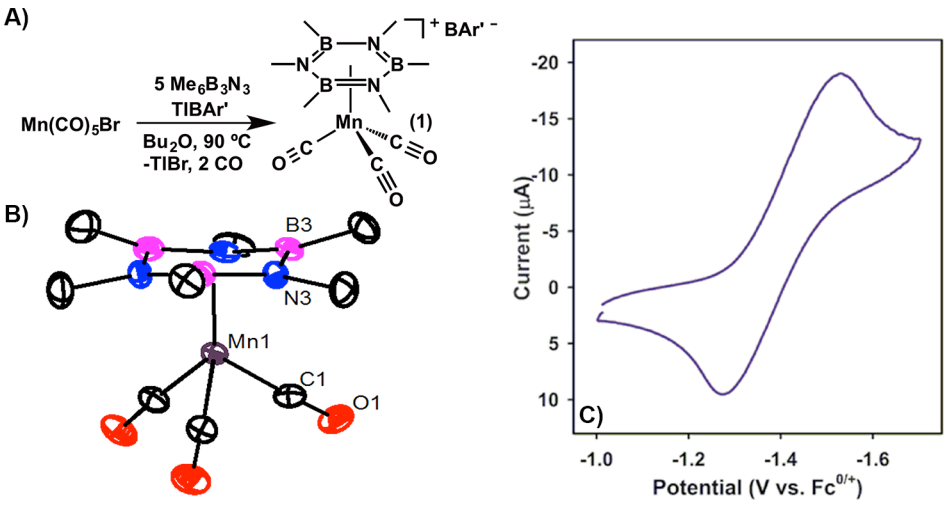

Figure 3-1. A) Synthesis of **1**. B) X-ray crystal structure of **1**. Thermal ellipsoids are shown at 35% probability. Hydrogen atoms and the BAr′ counteranion are omitted for clarity. C) Cyclic voltammogram of **1** in 0.1 M [^{n}Bu$_4$N]PF$_6$/CH$_2$Cl$_2$ (scan rate 100 mV s^{-1}).

revealed a new resonance at 32.0 ppm, shifted 6 ppm upfield from the signal for free $Me_3B_3N_3Me_3$. Further structural data were obtained from the IR spectrum, which displayed new ν_{CO} bands at 2072 and 1999 cm^{-1}, consistent with the predicted C_{3v} symmetry. Single crystals were obtained by cooling a solution of **1** in CH_2Cl_2, Et_2O, and pentane to −35 °C and analyzed by X-ray diffraction. The solid-state structure (Figure 3-1B) confirmed the η^6 coordination of $Me_3B_3N_3Me_3$ to the $Mn(CO)_3^+$ fragment.

Given that the only structurally characterized π complexes of borazine contain Cr(0), the salient structural features of **1** were examined and compared to those of (η^6-$Me_3B_3N_3Me_3$)$Cr(CO)_3$. Both complexes display similar structural metrics. The slight deviation from planarity observed in (η^6-$Me_3B_3N_3Me_3$)$Cr(CO)_3$ (9.11°, measured as the angle between the B1, N1, N3 and N1, N2, N3 planes) is more pronounced in the structure of **1** (12.08°). The average B–N bond distance of 1.459 Å for **1** and 1.455 Å for (η^6-$Me_3B_3N_3Me_3$)$Cr(CO)_3$ are consistent with little change in B=N bond order upon coordination. One of the few differences is the shorter M–N1 bond distance (2.142(3) vs 2.217(3) Å) observed for **1** in comparison to (η^6-$Me_3B_3N_3Me_3$)$Cr(CO)_3$,[2] which may be attributed to the smaller ionic radius of Mn(I) versus Cr(0).

Although they are structurally similar, borazine adducts of $Cr(CO)_3$ and $Mn(CO)_3^+$ were found to exhibit large differences in reactivity. For instance, competitive ligand displacement studies were conducted in which (η^6-$Me_3B_3N_3Me_3$)$Cr(CO)_3$ and **1** were

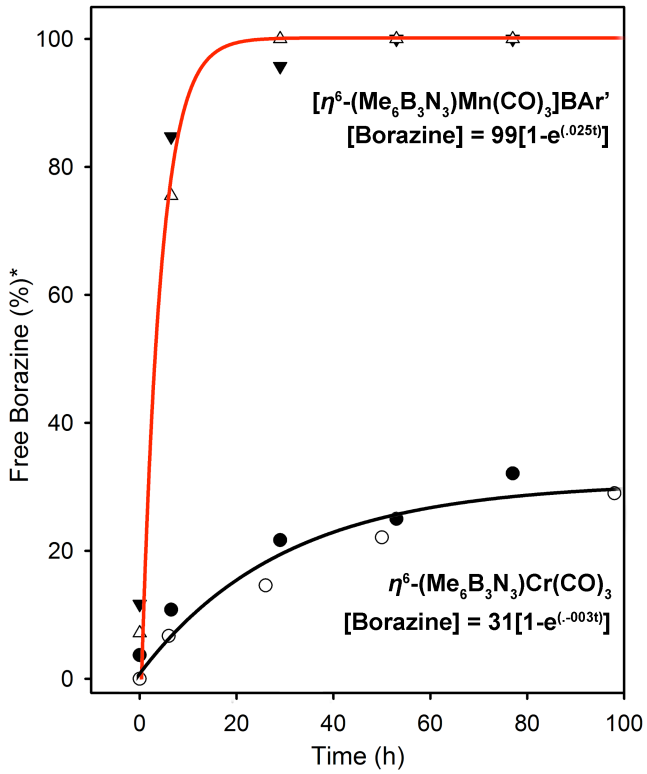

Figure 3-2. Rate of borazine displacement by THF from **1** and (η^6-$Me_3B_3N_3Me_3$)$Cr(CO)_3$**.** Black and white symbols denote replicate trials conducted under identical conditions. Curves were fit as hyperbolic functions using Sigma Plot (t = hours after THF addition).

titrated with THF and the rate of borazine release was measured.[18] The resulting kinetic profiles (Figure 3-2) revealed that the borazine unit of **1** displayed a higher substitutional lability (ca. 3x) than the chromium analogue. These results can be rationalized by considering the bonding interactions of coordinated borazines, wherein cooperative binding via σ donation from the N-atoms and π acceptance by the B-atoms is proposed.[19-21] For the isostructural $Me_3B_3N_3Me_3$ complexes, Mn(I) is less electron rich than Cr(0), as quantified by observed A_1 CO bands (2072 and 1947 cm^{-1} for Mn and Cr, respectively). This likely increases borazine's substitutional lability and is consistent with the observed ligand displacement reactivity (vide supra).

In addition to ligand substitution reactivity, we hypothesized that the electrophilic $Mn(CO)_3^+$ fragment would also facilitate nucleophilic attack at the borazine unit. While uncoordinated $Me_3B_3N_3Me_3$ did not react with excess CH_3MgBr, **1** and 1 equiv of CH_3MgBr were cleanly converted to a new product when a frozen Et_2O solution containing both reactants was warmed to room temperature. The product was isolated

in 59% yield and identified as the dearomatized borazine adduct (η^5-$Me_4B_3N_3Me_3$)$Mn(CO)_3$ (**2**), by heteronuclear NMR and IR spectroscopy. The ^{11}B NMR spectrum contained resonances at 34.2 and 9.3 ppm, the latter of which appears in the region characteristic of B–N derived tetrahedral boron atoms, which typically appear between −10 and +10 ppm.[22-24] ^1H NMR spectroscopy further bolstered the assignment by the identification of three unique B–CH_3 groups, observed in a 2:1:1 ratio at 0.66, 0.05, and −0.69 ppm, as well as two N–CH_3 resonances observed in a 2:1 ratio at 2.90 and 2.47 ppm. Finally, the IR spectrum displayed three CO stretches (2023, 1922, and 1901 cm^{-1}), shifted to lower energy and consistent with the predicted C_s symmetry.

Single crystals suitable for X-ray diffraction were isolated from a concentrated pentane solution at −35 °C, and the solid-state structure of **2** (Figure 3-3A) was confirmed as (η^5- $Me_4B_3N_3Me_3$)$Mn(CO)_3$. The borazine ring is severely distorted by the introduction of a tetrahedral boron atom (B1), as evidenced by the elongation of the B1–N1 bond (1.599(6) Å) as well as the out-of-plane distortion of B1 (44°) relative to the ring nitrogen atoms. These structural distortions are in good agreement with those

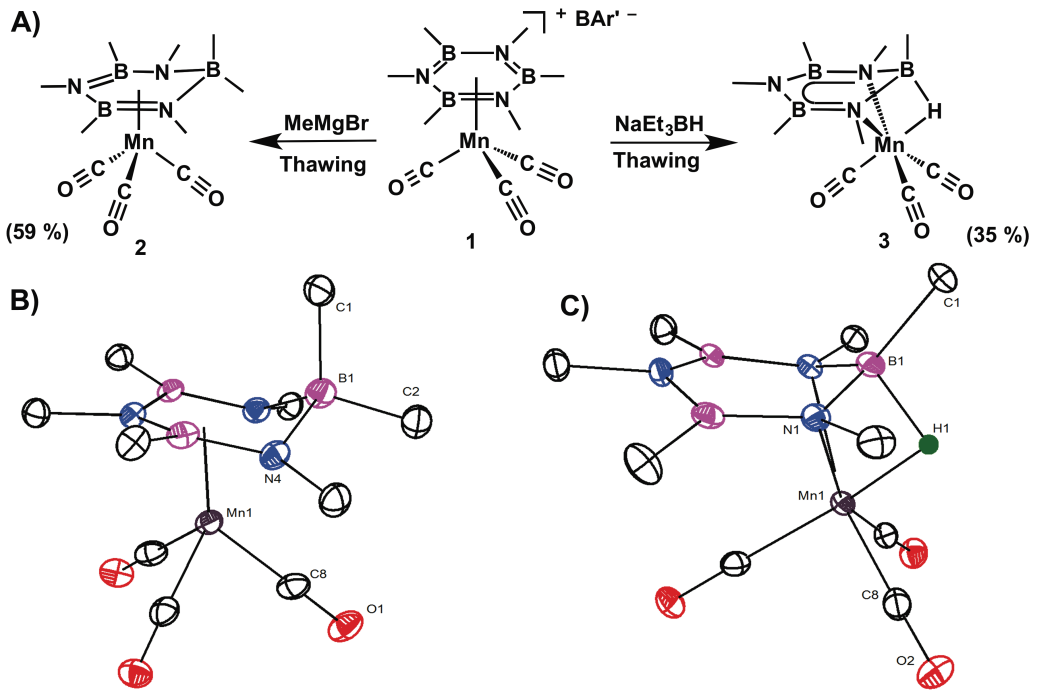

Figure 3-3. Direct synthesis (A) and X-ray crystal structures of complexes (B) **2** and (C) **3**. Thermal ellipsoids are shown at the 35% probability level. Hydrogen atoms, with the exception of the bridging hydride (H1), were omitted for clarity.

previously observed for [(η^5-$Me_4B_3N_3Me_3$)$Cr(CO)_3$]MgBr and collectively illustrate a general approach for the isolation of dearomatized borazine fragments.[2]

Following isolation, we sought to quench compound **2** by the addition of excess $DOAc^F$ to obtain the substituted cyclotriborazne (CTB), $OAc^F{}_2Me_4B_3N_3Me_3D_3$, that was observed when [(η^5- $Me_4B_3N_3Me_3$)$Cr(CO)_3$]MgBr was reacted under identical conditions. Interestingly, **2** was inert with respect to proton addition at low (-30 ºC) temperature. Warming to 30 ºC afforded only free $Me_3B_3N_3Me_3$ and $OAc^F{}_3Me_3B_3N_3Me_3D_3$ in which the installed B–Me unit had been hydrolyzed. This is not surprising, as hydrolysis of the Me^- nucleophile is expected to be the thermodynamic product of this reaction. However, ineffective trapping at -30 ºC is likely a result of the more electrophillic Mn center decreasing the bascicity of the ring nitrogen atoms (relative to [(η^5-$Me_7B_3N_3$)$Cr(CO)_3$]MgBr) which represents a significant reactivity difference between **1** and its isostructural Cr analogue.

In addition to attack by carbon nucleophiles, reactivity with hydride donors was pursued. Key reactivity differences between analogous arene and borazine $Mn(CO)_3$ compounds were noted. For instance, in contrast to reports of Mn(arene)$(CO)_3^+$, where two hydride additions to the arene complete C–C bond reduction,[25] analogous double hydride addition was not observed for **1**. Instead, the reaction of **1** with 1–2 equiv of $LiAlH_4$, in Et_2O at −35 °C, afforded the monohydride Mn(μ-H)$(Me_3B_3N_3Me_3)(CO)_3$ (**3**) with a κ^2-*N*,*N*′-(μ-H) binding mode, as visualized by solution cell IR spectroscopy (Figure B-17). Removal of solvent followed by extraction with pentane allowed for the isolation of **3**, and the structural assignment was confirmed by ^{11}B NMR spectroscopy which featured two resonances in a 2:1 ratio at 40.6 and 5.9 ppm, similar to the shifts of **2**.[26] A hydride resonance in the ^{1}H spectrum was also noted at −3.7 ppm, consistent with a bridging hydride unit.[27,28] This species exhibited solvent-dependent behavior, and analysis of Et_2O solutions containing **3** showed ^{11}B NMR resonances at 31.1 and 5.9 ppm (Figure 3). The IR spectrum of **3** revealed three CO stretches (2023, 1935, and 1906 cm^{-1}) at energies similar to those observed for **2.** Further structural confirmation was made possible from single crystals of **3**.

The X-ray structure (Figure 3-3B) reveals a hydride, located from the difference

map, that bridges the borazine and $Mn(CO)_3$ fragments. As observed for **2**, the B1–N1 bond is significantly elongated (1.508(4) Å) and B1 is distorted out of the N1–N2–N3 plane (32°). Notably, **3** also exhibits an elongation of the Mn–C bond trans to H1 (0.016 Å), consistent with the large trans influence of the hydride ligand. Although the structural metrics indicate similarities between the Mn and Cr structures, their solution behaviors were distinct. While the Cr hydride ($[Cr(\mu\text{-}H)(Me_3B_3N_3Me_3)(CO)_3]Li$) decomposed above −20 °C,[2] **3** was moderately stable at room temperature both in the solid state and as a solution in pentane or cyclohexane, which facilitated more complete spectroscopic characterization than was possible with Cr.

The marked stability of **3**, as noted above, suggested that hydride adducts of **1** might also be generated by alternative means. For instance, in addition to direct addition of exogenous hydride donors, metal hydrides can also be generated by protonation of a low-valent metal center.[29] We therefore sought to explore whether such reactivity could be mediated by **1**. As an initial step, the reductive electrochemistry of **1** was interrogated to probe the stability of reduced adducts, as well as the potential at which reduction occurred. A cyclic voltammetry experiment in 0.1 M $[^nBu_4N]PF_6$ in CH_2Cl_2 (Figure 3-1, Figure B-22, and Figure B-23) revealed a quasi-reversible reductive event at −1.38 V in addition to an irreversible reduction at −1.88 V (vs Fc^0/Fc^+). The first reduction event was minimally solvent dependent; voltammetry experiments in Et_2O (Figure B-24) displayed a redox event at −1.34 V, with the second event at −2.00 V (vs $Fc^{0/+}$; 0.05 M $[^nBu_4N]BAr'$ as electrolyte). However, the couple at −1.34 V was irreversible in Et_2O at room temperature and an unrelated return wave at −0.92 V (vs $Fc^{0/+}$) was observed.

The reversible reduction events noted in the voltammetry studies suggested that reduction of **1** should be chemically accessible. We hypothesized that, if sufficiently long-lived, the reduced adduct could be intercepted by a proton donor to furnish a metal hydride capable of transfer to the borazine unit. Addition of 2 equiv of $Na/C_{10}H_8$ to a thawing solution of **1** in Et_2O afforded a new complex, **4**. EPR spectroscopy conducted on frozen solutions of **4** immediately after preparation showed no signals which could be attributed to a d^7 paramagnetic species.[30] **4** was characterized using in situ IR spectroscopy at −30 °C (Figure B-18), where a single new set of CO stretches was visualized immediately after the addition of $Na/C_{10}H_8$, at significantly lower energy (2006

and 1901 cm^{-1}) than for **1**, suggesting that reduction proceeds cleanly through a $2e^-$ pathway. Unfortunately, the reduced adduct was thermally unstable at temperatures greater than −30 °C, which precluded further detailed analyses.

Although the reduction of **1** at low temperature afforded a species with limited stability, the addition of acid immediately following reduction provided a means to effectively capture the reduced adduct. For instance, when an ethereal solution of **4** was treated with 1 equiv of $HOAc^F$, conversion to **3** in 75% yield was observed. The product was confirmed by spectroscopic comparison with Et_2O solutions of the independently prepared sample (vide supra). The ^{11}B NMR spectrum exhibited new resonances at 32.2 and 7.1 ppm (Figure 3-4), and solution-cell IR spectroscopy (Figure B-17) revealed nearly identical CO stretching bands for **3** prepared by both pathways.[31] To the best of our knowledge, the formation/delivery of a boron hydride derived from sequential reduction and protonation is an unprecedented, yet noteworthy, metal-mediated reaction to consider for spent B–N fuel regeneration.

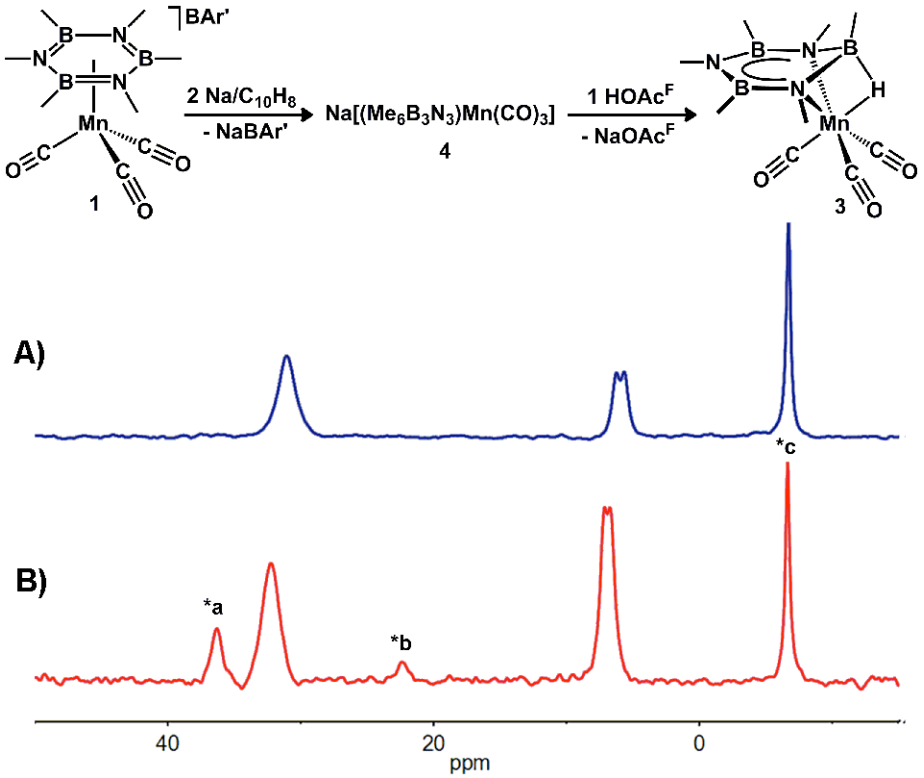

Figure 3-4. (top) Generation of **3** from stepwise reduction and protonation. (bottom) Overlay of ^{11}B NMR (−30 °C) of **3** generated (A) using $LiAlH_4$ and (B) using $Na/C_{10}H_8$ followed by $HOAc^F$. Legend: (*a) free $Me_3B_3N_3Me_3$; (*b) proposed borazine ring coupling product;[32] (*c) Na or LiBAr′ used as internal standard.

With access to a stable reduced hydride complex, we next explored the reactivity of **3** with proton sources. In contrast to attempts to quench **2**, compound **3** reacts with 1 eq. $DOAc^F$ at -30 ºC, in chloroform solution, to produce a probable 1,2-H_2 complex. Unfortunately, the resultant product is highly thermally sensitive, and precipitates completely from solution which prevented characterization by NMR spectroscopy. However, an IR spectrum of the crude reaction mixture (Figure B-19) reveled a new set of M-CO (2039 and 1945 cm^{-1}) bands which were distinct from both compounds **1** and **3**. When this solution is warmed to room temperature complex **1** is obtained as the sole product presumably through release of H_2 from the 1,2-H_2-adduct. If an excess (3 eq.) of $DOAc^F$ is used, only a mixture of $Me_3B_3N_3Me_3$ and $OAc^F{}_3Me_3B_3N_3Me_3D_3$ is obtained after warming to room temperature. This suggests that the B–H bond is readily hydrolyzed by excess acid. However, the promising initial results with respect to the addition of a single equivalent of acid suggest that crucial 1,2-H_2-intermediates are indeed accessible under carefully controlled conditions and may be intercepted to accomplish subsequent reductive reactions.

3.3 Conclusions

In this chapter, we have demonstrated a key transformation relevant to borazine reduction. Although isoelectronic with benzene, the reactivity of metal-coordinated borazines is distinct, and while some parallels exist between redox transformations at both fragments, reactivity differences imposed by the more polar B=N bonds have been largely unexplored. Using carefully selected reaction conditions, the $Mn(CO)_3^+$ fragment was found to coordinate and activate a borazine for nucleophilic addition reactions of H^- and Me^- to give isostructural analogues of the Cr(0) complexes discussed in chapter 2. In addition to direct reaction with a hydride source, utilizing the more electrophillic Mn(I) center gave access to synthetically tractable reductive chemistry allowing us to demonstrate stepwise reduction/protonation reactions to provide a hydride equivalent to the borazine unit, which is the thermodynamically most demanding step of borazine reduction.[3,4] The demonstration of this reaction solely from electrons and protons clearly illustrates how metal coordination may be used to promote reduction reactions of B=N units, which is an important step toward the development of systems that can regenerate useful hydrogen storage materials via low-energy pathways.

3.4 Experimental Details

General Experimental Procedures: All experiments were conducted using standard Schlenk techniques or in a nitrogen filled glovebox. NMR spectra were recorded on Varian MR400, vnmrs 500, or vnmrs 700 MHz spectrometers. ^{1}H and ^{13}C NMR spectra were referenced relative to the solvent resonance, and ^{11}B, and ^{19}F spectra were referenced indirectly based on the ^{1}H spectrum.[33] IR spectra were recorded on a Nicolet iS-10 spectrometer from Thermo Scientific in a KBr plate solution cell or on a diamond attenuated total reflectance (ATR) accessory. In-situ IR spectra of **4** were recorded using a ReactIR istrument from Mettler Toledo equipped with a diamond tipped fiber-optic probe. Mass spectra were collected by electron impact ionization on a VG 70-250-S magnetic sector, double-focusing mass spectrometer. The electron energy was set to 70 eV, and the source temperature was 240 ºC. In all cases, nominal mass spectra were obtained initially, scanning the magnet from m/z 1000 to m/z 35 at 8 seconds per decade, using an external mass calibration. Exact mass measurements were then carried out once a molecular ion peak was identified. A linear voltage scan was preformed across the mass of interest and a reference (perfluorokerosene-H) mass peak above and below the sample mass peak. Cyclic voltammetry experiments were collected on a Pine Research Instrumentation WaveNow potentiostat. Experiments were conducted in a 0.05 M solution of tetrabutylammonium tetrakis[3,5-bis(trifluoromethyl)phenyl]borate ($^{n}Bu_4NBAr'$) in diethyl ether or 0.1 M tetrabutylammonium hexafluorophosphate ($^{n}Bu_4NPF_6$) in CH_2Cl_2. A glassy carbon working electrode and a platinum disk counter electrode were used and voltammograms referenced relative to ferrocene ($Fc^{0/+}$) using a silver wire pseudo reference electrode. Potentials are reported as $E_{1/2}$ values where a return wave is present and as E_{Pa} or E_{Pc} values where a return wave is absent or very weak. Scan rate was 0.1 V/s unless otherwise specified. Sodium tetrakis[3,5-bis(trifluoromethyl)phenyl]borate (BAr'), hexamethylborazine ($Me_3B_3N_3Me_3$), and $(Me_3B_3N_3Me_3)Cr(CO)_3$ were synthesized by previously reported routes.[2,10,34-36] TlBAr' was prepared by a modification of the procedure reported by Hughes, Linder, Rheingold, and Yap.[37] Complete removal of residual EtOH was essential for the synthesis of **1** and this was accomplished by drying at 60 ºC for 48 h. $^{n}Bu_4NBAr'$ was synthesized using a modified version of the procedure

reported by Kobayashi and coworkers for the synthesis of tetraethylammonium tetrakis[3,5-bis(trifluoromethyl)phenyl]borate.[38] Tetrabutylammonium chloride was used in place of tetraethylammonium iodide, and extraction with ether followed by drying over $MgSO_4$ was used in-lieu of column chromatography. Diethyl ether, pentane, tetrahydrofuran, dichloromethane, and 1,2-dimethoxyethane were obtained from Fisher Scientific and passed through an S.G. Waters solvent purification system. MTBE was distilled from sodium and degassed by sparging with N_2 for 30 min prior to use. Deuterated NMR solvents, purchased from Cambridge Isotope Laboratories, were either obtained as sealed ampoules and used as received, or degassed and dried by standard methods.[39] All other chemicals were purchased from commercial vendors and used as received. All filtrations were conducted using a pipet blocked with Whatman glass fiber filter paper.

Synthesis of 1 ([η^6-($Me_3B_3N_3Me_3$)$Mn(CO)_3$]BAr'): $Mn(CO)_5Br$ (56.2 mg, 0.20 mmol), TlBAr' (218.0 mg, 0.20 mmol), and hexamethylborazine ($Me_3B_3N_3Me_3$; 337 mg, 2.0 mmol) were combined in a 20 mL scintillation vial followed by the addition of 2 mL of di-n-butyl ether. The resulting orange/yellow suspension was heated to 90 ºC for 20 minutes without stirring and with a loosened Teflon cap. The mixture was then removed from heat and allowed to cool to room temperature, then 2 mL of dichloromethane (DCM) was added, which resulted in an orange solution with a tan precipitate. The solution was filtered, and the filtrate was again heated to 90 ºC without stirring. The cap was left loose, and the DCM was allowed to evaporate. After heating for an additional 20 minutes, the solution was decanted and allowed to cool. A yellow precipitate resulted upon cooling to room temperature. The solid was isolated by decanting the filtrate and set aside. Heating of the filtrate resumed for an additional 20 minutes and the cooling/decanting process was repeated to yield additional yellow precipitate. This process was repeated until the filtrate appeared yellow, and no additional precipitate was produced upon cooling. At this point, the combined precipitated solids were dissolved in 5 mL Et_2O and filtered. Solvent was removed under vacuum and the solid was washed with pentane (5 X 5 mL). The filtrate was decanted and discarded, and the residual solid was dissolved in (3 mL) DCM and filtered. Solvent was then removed from the filtrate under vacuum to give 151.3 mg (0.13 mmol, 64.8 %) of yellow solid **1**. If

desired, the product can easily be recrystallized by additon of pentane to a concentrated solution of **1** in Et_2O. ^1H NMR (399.5 MHz, [D_1]chloroform): δ 7.71 (s, 8H; Ar–H_{meta}), 7.55 (s, 4H; Ar–H_{para}), 2.98 (s, 9H; N–CH_3), 0.90 (s, 9H; B–CH_3), –0.83; $^{13}C\{^1H\}$ NMR (174.97 MHz, dichloromethane, -30 ºC): δ 213.0 (s, Mn-CO), 161.4 (q, J_{CB} = 49.8 Hz, BAr'), 134.3 (s, BAr'), 128.3 (q, J_{CF} = 31.8 Hz, BAr'), 122.6 (q, J_{CF} = 273.4 Hz, BAr'), 115.7 (s, BAr'), 40.0 (s, N-CH_3), -2.3 (s, B-CH_3); ^{11}B NMR (128.19 MHz, [D_1]chloroform): δ 32.0 (s), -6.6 (s; BAr'); ^{19}F NMR (470.51 MHz, [D_2]DCM): δ -60.9 (s; CF_3); IR (Diamond-ATR): ν_{CO} 2072, 1997 cm^{-1}, ν_{BN} 1493, 1466, 1435 cm^{-1}. Elemental Analysis calculated for $C_{41}H_{30}B_4F_{24}MnN_3O_3$: C 42.20, H 2.59, N 3.60; found: C 42.35, H 2.69, N 3.39. Cyclic voltammetry (0.1 M $^nBu_4NPF_6$ in DCM): $E_{1/2}$ (V vs. $Fc^{0/+}$) –1.38, E_{Pa} (V vs. $Fc^{0/+}$) –1.88. Crystals suitable for X-ray diffraction were obtained from DCM/diethyl ether/pentane (1:1:1) at –35 ºC.

Synthesis of 2 (η^5-($Me_7B_3N_3$)Mn($CO)_3$): To a frozen solution of **1** (40.2 mg, 0.034 mmol) in 1.5 mL Et_2O, was added a solution of MeMgBr (0.1 M in Et_2O; 345.0 µL, 0.35 mmol). The mixture was allowed to thaw with stirring in a -35 ºC freezer for 5 minutes. The sample was then warmed to room temperature and stirred for 5 minutes. The solvent was removed under vacuum and the residue was extracted with 2 mL of pentane. The resulting yellow solution containing **2** was filtered to remove a tan solid, and the solvent was removed under vacuum to give 6.5 mg (59%) of a yellow solid. Isolated **2** was removed from vacuum as soon as the solvent was evaporated (solid **2** can be readily sublimed at room temperature). ^1H NMR (399.54 MHz, [D_{12}]cyclohexane): δ 2.90 (s, 3H; N–CH_3), 2.47 (s, 6H; N-CH_3), 0.66 (s, 6H; B–CH_3), 0.05 (s, 3H; B–CH_3), –0.69 (s, 3H; B–CH_3); $^{13}C\{^1H\}$ NMR (174.97 MHz, dichloromethane, -30 ºC): 222.2 (s, Mn-CO), 215.3 (Mn-CO), 38.8 (s, N-CH_3), 37.2 (s, N-CH_3), 13.3 (s, B-CH_3), 7.7 (s, B-CH_3), -3.0 (s, B-CH_3); ^{11}B NMR (128.20 MHz, [D_{12}]cyclohexane): δ 34.2 (s), 9.3 (s); IR (Diamond-ATR): ν_{CO} 2023, 1922, 1901 cm^{-1}, ν_{BN} 1461, 1427 cm^{-1}. Cyclic voltammetry (0.1 M $^nBu_4NBAr'$ in Et_2O): $E_{1/2}$ (V vs. $Fc^{0/+}$) –2.47, E_{Pa} (V vs. $Fc^{0/+}$) –1.33, -2.82, E_{Pc} (V vs. $Fc^{0/+}$) 1.21. EI-HRMS calculated for $C_9H_{18}B_3MnN_3O_3$ (loss of Me group): 304.1008 Da; found: 304.1020. Crystals suitable for X-ray diffraction were grown from a pentane solution of **2** held at -35 ºC. Crystals were taken from the walls of the vial above the solvent level.

Synthesis of 3 from $LiAlH_4$ (κ^2-N,N'-(μ-H)($Me_3B_3N_3Me_3$)Mn(CO)$_3$): To a frozen solution of **1** (40.0 mg, 0.034 mmol) in 2 mL Et_2O was added a solution of $LiAlH_4$* (0.1 M in Et_2O; 345 µL, 0.035 mmol). The mixture was allowed to thaw in a –35 ºC freezer for 30 min. Pentane (2 mL) was then added and the solution was filtered at room temperature. The solvent was removed from the filtrate under vacuum to give 6.5 mg of a yellow solid. The residue was extracted with 1 mL pentane and solvent was removed under vacuum to afford 4.5 mg of a yellow solid. Isolated **3** was removed from vacuum as soon as solvent was evaporated (solid **3** can be readily sublimed at room temperature when subjected to reduced pressures). This procedure provided **3** which contained 25 mol% $Me_3B_3N_3Me_3$ that was not easily removed due to its similar solubility properties with **3** (yield based on 75 mol% **3** = 35%). Attempts to purify **3** by sublimation led to isolaton of **3** with ~4 equivalents of $Me_3B_3N_3Me_3$ on the sublimation cold-finger. The ^{1}H and ^{11}B NMR spectrum of this mixture is reported. ^{13}C NMR data was collected immediately following solvent removal without sublimation. ^{1}H NMR (500.08 MHz, [D$_8$]toluene): δ 2.34 (s, 3H; N–*CH*$_3$), 2.01 (s, 6H; N–*CH*$_3$), 0.56 (s, 3H; B–*CH*$_3$), 0.19 (s, 6H; B–*CH*$_3$), –3.7 (br, 1H; B–*H*–Cr); ^{13}C{^{1}H} NMR (175.98 MHz, [D$_8$]toluene, -30 ºC): 222.3 (s, Mn-CO), 219.1 (s, Mn-CO), 40.9 (s, N-*CH*$_3$), 37.4 (s, N-*CH*$_3$), 0.0 (s, B-*CH*$_3$), -1.9 (s, B-*CH*$_3$); ^{11}B NMR (160.45 MHz, [D$_8$]toluene): δ 40.7 (s, 2B), 5.9 (s, 1B); IR (Diamond-ATR): ν_{CO} 2023, 1935, 1906 cm^{-1}, ν_{BN} 1465, 1424 cm^{-1}. Cyclic voltammetry (0.1 M ^{n}Bu$_4$NPF$_6$ in DCM): E_{Pa} (V vs. Fc$^{0/+}$) –1.39, E_{Pc} (V vs. Fc$^{0/+}$) 0.60, 1.02. EI-HRMS calculated for $C_8H_{19}B_3MnN_3O_2$ (loss of CO ligand): 277.1137 Da; found: 277.1144. Crystals suitable for X-ray diffraction were obtained from a pentane solution of **3** held at –35 ºC. Crystals were taken from the walls of the vial above the solvent level.

Additional characterization was obtained by studying reaction mixtures of **3** in Et_2O prior to work up. The ^{11}B NMR (SI Figure-13) and IR (SI Figure-17) spectra of **3** were found to be affected by the presence of the BAr' salts formed as a by-product of the reaction, possibly due to an interaction between alkali metal atoms and the metal carbonyl ligands as previously observed for the analogous complex (η^3-($Me_3B_3N_3Me_3$)(μ-H)Cr(CO)$_3$).[2] Additionally, solutions of **3** prepared in this manner afford no new resonances in the ^{11}B NMR spectrum, possibly due to dynamic hydride exchange. However, this process can be arrested by the addition of 2 eq. $LiAlH_4$ which affords a

well resolved ^{11}B NMR spectrum. Solution-cell IR (SI Figure-17) studies confirm that the same product is obtained by treatment with 1 or 2 eq. of $LiAlH_4$. ^{11}B NMR (160.45 MHz, Et_2O): δ 31.1 (s, 2B), 5.9 (s, 1B); IR (Solution-cell; Et_2O): ν_{CO} 2029, 1951, 1939 cm^{-1}.

* A 1.0 M solution of $NaEt_3BH$ in toluene can also be substituted in this procedure.

Synthesis of 3 from Na/$C_{10}H_8$ and HOAc^F (κ^2-N,N'-(μ-H)($Me_3B_3N_3Me_3$)Mn(CO)$_3$): To a frozen solution of **1** (10.6 mg, 0.009 mmol) in 0.7 mL Et_2O was added a solution of Na/$C_{10}H_8$ (1.0 M in THF; 18 µL, 0.018 mmol). The mixture was allowed to thaw until a color change (to brown/orange) was observed. A solution of HOAc^F (0.15 M in Et_2O; 60 µl, 0.009 mmol) was then quickly added. The mixture was transferred to a J-Young NMR tube and refrozen until the time of analysis. In the crude reaction mixture, **3** is thermally sensitive and decomposes at room temperature, thus, in-situ characterization was carried out by low temperature (–30 °C) ^{11}B NMR spectroscopy, as well as solution-cell IR spectroscopy carried out on solutions immediately after thawing. Comparison of ^{11}B NMR (Figure 3) and IR spectra (SI Figure-17) of solutions containing **3** synthesized from $LiAlH_4$ (before work-up) and **3** synthesized from Na/$C_{10}H_8$ and HOAc^F showed only small differences (Δ^{11}B = 1.1 and 1.2 ppm, $\Delta\nu_{CO}$ = 7, 2, and 0 cm^{-1}) likely due the effect of solvent composition or the presence of residual Na^+ or Li^+ salts in solution. The chemical yield was determined to be 75% by integration using the BAr' salt as an internal standard.[4041] ^{11}B NMR (160.45 MHz, Et_2O): δ 32.3 (s, 2B), 7.1 (s, 1B); IR (Solution-cell; Et_2O): ν_{CO} 2036, 1953, 1939 cm^{-1},

Synthesis of 4 [η^6-($Me_3B_3N_3Me_3$)Mn(CO)$_3$]Na: To a frozen solution of **1** (8.1 mg, 0.007 mmol) in 1 mL Et_2O was added a solution of Na/$C_{10}H_8$ (1.0 M in THF; 14 µL, 0.014 mmol). The mixture was allowed to thaw until a color change (to brown/orange) was observed. The mixture was transferred to a J-Young NMR tube and refrozen until the time of analysis. **4** is thermally sensitive and decomposes at room temperature, thus, in-situ characterization was carried out by low temperature (–30 °C) in-situ IR spectroscopy carried out on solutions of **1** treated with 2 eq. Na/$C_{10}H_8$. IR (diamond-tipped fiber-optic probe): ν_{CO} 2006,1901 cm^{-1}.

3.5 References

1) Reproduced with permission from: Carter, T. J.; Wang, J. Y.; Szymczak, N. K.

Organometallics **2014**, *33*, 1540.

2) Carter, T. J.; Kampf, J. W.; Szymczak, N. K. *Angew. Chem. Int. ed.* **2012**, *51*, 13168.

3) Lisovenko, A. S.; Timoshkin, A. Y. *Inorg. Chem.* **2010**, *49*, 10357.

4) Nutt, W. R.; McKee, M. L. *Inorg. Chem.* **2007**, *46*, 7633.

5) Dessy, R. E.; Stary, F. E.; King, R. B.; Waldrop, M. *J. Am. Chem. Soc.* **1966**, *88*, 471.

6) Dai, W.; Kim, S. B.; Pike, R. D.; Cahill, C. L.; Sweigart, D. A. *Organometallics* **2010**, *29*, 5173.

7) Neto, C. C.; Baer, C. D.; Chung, Y. K.; Sweigart, D. A. *J. Chem. Soc. Chem. Commun.* **1993**, *0*, 816.

8) Cambridge Structural Database, version 5.34, November 2013; Cambridge Crystallographic Data Centre, 12 Union Road, Cambridge CB2 1EZ, U.K.

9) Lagowski, J. J. *Coord. Chem. Rev.* **1977**, *22*, 185.

10) Prinz, R.; Werner, H. *Angew. Chem. Int. ed.* **1967**, *6*, 91.

11) Werner, H.; Prinz, R.; Deckelmann, E. *Chem. Ber.* **1969**, *102*, 95.

12) Jackson, J. D.; Villa, S. J.; Bacon, D. S.; Pike, R. D.; Carpenter, G. B. *Organometallics* **1994**, *13*, 3972.

13) Kündig, E. P. *Transition metal arene [pi]-complexes in organic synthesis and catalysis*; Springer-Verlag: Berlin, 2004.

14) Anton, K.; Fußstetter, H.; Nöth, H. *Chem. Ber.* **1981**, *114*, 2723.

15) Gemünd, B.; Günther, B.; Nöth, H. *ARKIVOC* **2008**, 136.

16) Deckelmann, E.; Werner, H. *Helv. Chim. Acta* **1969**, *52*, 892.

17) Scotti, M.; Werner, H.; Brown, D. L. S.; Cavell, S.; Connor, J. A.; Skinner, H. A. *Inorg. Chim. Acta* **1977**, *25*, 261.

18) Decomposition kinetic measurements were conducted by Justin Y. Wang, an undergraduate working under my supervision.

19) Bridgeman, A. J. *Polyhedron* **1998**, *17*, 2279.

20) Kang, H. S. *J. Phys. Chem. A* **2005**, *109*, 1458.

21) Scotti, M.; Werner, H. *Helv. Chim. Acta* **1974**, *57*, 1234.

22) Narula, C. K.; Janik, J. F.; Duesler, E. N.; Paine, R. T.; Schaeffer, R. *Inorg. Chem.* **1986**, *25*, 3346.

23) Lingam, H. K.; Wang, C.; Gallucci, J. C.; Chen, X.; Shore, S. G. *Inorg. Chem.* **2012**, *51*, 13430.

24) Jaska, C. A.; Temple, K.; Lough, A. J.; Manners, I. *J. Am. Chem. Soc.* **2003**, *125*, 9424.

25) Brookhart, M.; Lamanna, W.; Pinhas, A. R. *Organometallics* **1983**, *2*, 638.

26) Partial decomposition of **3**, to release $Me_6B_3N_3$, occurs during the workup

procedure. Due to the nearly identical solubilities that precluded complete separation, **3** was isolated with 25% free $Me_6B_3N_3$.

27) Shimoi, M.; Nagai, S.; Ichikawa, M.; Kawano, Y.; Katoh, K.; Uruichi, M.; Ogino, H. *J. Am. Chem. Soc.* **1999**, *121*, 11704.

28) Kawano, Y.; Yamaguchi, K.; Miyake, S.; Kakizawa, T.; Shimoi, M. *Chem. Eur. J.* **2007**, *13*, 6920.

29) Crabtree, R. H. *The organometallic chemistry of the transition metals*; Wiley-Interscience: Hoboken, N.J., 2005.

30) < 1% unreacted $Na/C_{10}H_8$ was observed.

31) The spectroscopic characteristics of **3** are dependent on solvent and the presence of residual BAr′ salts. When the reaction was monitored in situ in Et_2O, without a workup procedure, negligible differences in the ^{11}B NMR spectrum and ν_{CO} bands were observed between independently generated **3** and the product from reduction/protonation.

32) Arene ring coupling is a common side reaction when Mn–arene complexes are chemically reduced. See: Thompson, R. L.; Geib, S. J.; Cooper, N. J. *J. Am. Chem. Soc.* **1991**, *113*, 8961

33) Harris, R. K.; Becker, E. D.; Menezes, S. M. C.; Goodfellow, R.; Granger, P. *Pure and Applied Chemistry* **2001**, *73*, 1795.

34) Smalley, J. H.; Stafiej, S. F. *J. Am. Chem. Soc.* **1959**, *81*, 582.

35) Brookhart, M.; Grant, B.; Volpe, A. F. *Organometallics* **1992**, *11*, 3920.

36) Bonham, J.; Drago, R. S.; Spielvogel, B. F.; Phillips, J. A.; Payet, C. R. In *Inorganic Syntheses*; John Wiley & Sons, Inc.: 2007, p 8.

37) Hughes, R. P.; Lindner, D. C.; Rheingold, A. L.; Yap, G. P. A. *Inorg. Chem.* **1997**, *36*, 1726.

38) Nishida, H.; Takada, N.; Yoshimura, M.; Sonoda, T.; Kobayashi, H. *Bull. Chem. Soc. Japan* **1984**, *57*, 2600.

39) Armarego, W. L. F.; Chai, C. L. L.; Knovel; ScienceDirect *Purification of laboratory chemicals*; Elsevier/Butterworth-Heinemann: Amsterdam ; Boston, 2009.

40) Control experiments were conducted by adding 2 eq. of $Na/C_{10}H_8$ to a solution containing NaBAr', and the integration of the BAr' anion was unaffected by the presence of paramagnetic species. Additionally, the guidlines developed by Baker and coworkers for quantitative ^{11}B NMR were followed.[41] INVREC experiments indicated that the BAr' salt had the longest relaxation delay (t_1 = 0.7s) of all observed products. Yield determination was therefore conducted with d_1 = 10 s.

41) Davis, B. L.; Rekken, B. D.; Michalczyk, R.; Garner, E. B.; Dixon, D. A.; Kalviri, H.; Baker, R. T.; Thorn, D. L. *Chem. Commun.* **2013**, *49*, 9095.

Chapter 4: Discovery of Low Energy Pathways to B=N Bond Reduction via η^6-Coordination Guided by Computation and Experiment [1]

4.1 Introduction

Chapters 2 and 3 demonstrated that η^6-coordination to a $Cr(CO)_3$ or $Mn(CO)_3^+$ fragment allows for facile dearomatization of the coordinated borazine by nucleophilic addition.[2,3] Furthermore, for the Mn system, we were able to achieve hydride delivery to the coordinated borazine solely from protons and electrons, which is an important step in a theoretical (electro)catalytic regeneration cycle for these materials. Key to further optimizing these systems is to establish an intimate understanding of the extent to which $Me_3B_3N_3Me_3$ can be activated by coordination to $Cr(CO)_3$ or $Mn(CO)_3^+$. It would be quite informative to have a more quantitative measure of this activation in order to minimize the energy input required for reduction by selecting a hydride source (or reductant and acid/H-atom donor) with a thermodynamic hydricity as close as possible to that required.

To accomplish this, we applied a combination of experimental and computational techniques to further develop our hypotheses,[4] as there is currently little data available to describe the extent to which borazines are activated upon transition metal coordination. In this study, we have sought to quantitatively describe the extent of activation in terms directly relevant to metal-mediated ionic hydrogenation of B=N bonds by direct comparison of pK_a values and thermodynamic hydricities (ΔG_{H-}) before and after coordination of the borazine to a transition-metal fragment. These values can then be used as a guide for selection of the lowest energy hydride source (or chemical reductant) that is competent to reduce the aforementioned coordination complexes, which will allow for the targeted discovery of new pathways for B-N bond reduction.

4.2 Results and Discussion

4.2.1 Effect of metal coordination on pK_a and ΔG_{H-} of $Me_3B_3N_3Me_3$

To examine this, we determined the optimized structures for the relevant borazine metal complexes using the B3LYP/31g(d,p) level of theory. The validity of our computational method was then established by comparing with experimental data. With few exceptions, the calculated values matched our experimental data with an error of < 20 cm^{-1} when a suitable correction factor (0.96)[5] was applied (Table C-1). Additionally, redox potentials (Table C-2) were calculated and found to be in good agreement with experimental data (when available).

Following calculation of the optimized structures, the effect of M-coordination was probed by examining the two properties of borazines most relevant to ionic hydrogenation, pK_a (Table C-3) and thermodynamic hydricity (Scheme 4-1). As expected, based on the lack of observed background reactivity with hydride sources and many relatively strong acids,[2,6] the uncoordinated borazine is predicted to be inert with respect to hydride addition and protonation by all but the most aggressive reagents. Following coordination, a significant increase in predicted conjugate acid strength of the coordinated borazine ligand by 13 and 44 pK_a units is observed for Cr and Mn, respectively. More remarkable is the dramatic increase in thermodynamic hydricity observed for the corresponding hydrides $[(Me_3B_3N_3Me_3)(\mu\text{-}H)Cr(CO)_3]Li$ (**3**; ΔG_{H-} = 41.1

Scheme 4-1. Calculated thermodynamic hydricity values of borazines, M-borazine complexes, and common hydride sources.

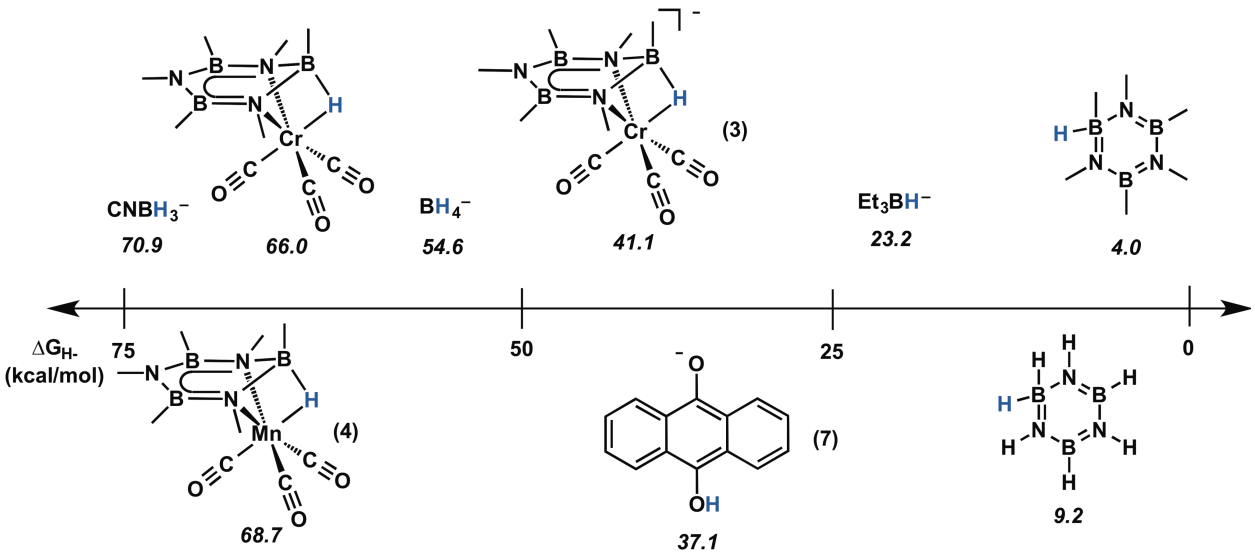

kcal/mol) and $(Me_3B_3N_3Me_3)(\mu\text{-}H)Mn(CO)_3$ (**4;** ΔG_{H-} = 68.7 kcal/mol). This is in agreement with our previous experimental results which showed that Et_3BH^- was competent at reducing both metal complexes, but not free $Me_3B_3N_3Me_3$.[2,3]

Using these values as a guide, we next sought to affect the hydride reduction of **1** using a much milder hydride $HCo(dmpe)_2$,[7] (ΔG_{H-} = 37 kcal/mol) than the $LiEt_3BH$ used in the original report (ΔG_{H-} = 23.2 kcal/mol). In agreement with the calculated thermodynamic hydricities, **1** was reduced readily when treated with 1 eq. of $HCo(dmpe)_2$ at -40 ºC in 2-Me-THF, to produce a hydride adduct (~30 % yield) whose spectral characteristics are in good agreement with the previously reported complex **3**. This is significant, because $HCo(dmpe)_2$ can be synthesized directly from H_2, which is an important step in the development of low-energy regeneration pathways.

4.2.2 Cr(I)-borazine complex by 1 e⁻ oxidation.

We next sought to extend the utility of computationally derived thermodynamic hydricity values to develop an understanding of how redox processes could lower the energy required to affect borazine dearomatization. In addition to comparing the relative hydride affinity and pK_a values, we were interested in exploring how redox processes (changes in metal oxidation state) affect the structure and bonding of coordinated borazine as odd-electron borazine complexes have not been previously studied. For instance, **1** displays a highly reversible 1 e^- oxidation which suggests that a stable Cr(I)-borazine complex may be accessible. Indeed, treatment of **1** with 1 eq. of $AgPF_6$ in thawing DCM results in immediate precipitation of Ag(0) (Figure 4-1A). The resulting solution is then filtered to give a yellow solution of $[(Me_3B_3N_3Me_3)Cr^{I}(CO)_3]PF_6$ (**5**) which was confirmed by the observation of new ν_{CO} bands at 2057 and 1980 cm^{-1} in the solution IR spectrum. The 106 and 136 cm^{-1} blue shift observed for the CO bands is consistent with oxidation of the metal center. Additionally, the observation of only two CO bands is consistent with retention of C_{3V} symmetry in solution, suggesting the borazine ring does not undergo a hapticity shift following oxidation. Compound **3** was also characterized by its paramagnetic ^1H NMR spectrum which revealed broad singlets at 13.90 and 8.75 ppm. This data is also consistent with a three-fold symmetric solution structure. Further structural assignment was obtained by Evan's method which was

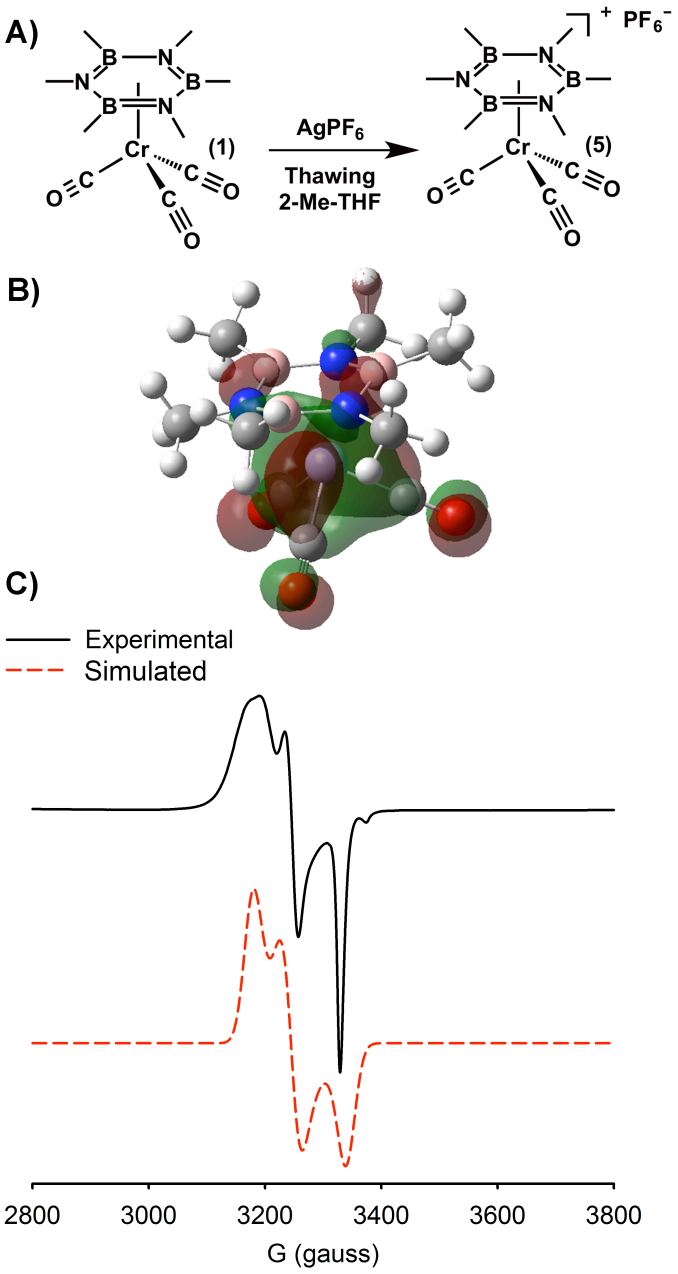

Figure 4-1. A) Synthetic scheme for oxidation of **1** to **5**. B) Calculated SOMO of **5**. C) Experimental (black) and simulated (red) X-band EPR spectrum of **2**.

used to determine μ_{eff} = 1.90 and N = 1.15, consistent with the predicted low-spin d^5 system. EPR spectroscopy (Figure 4-1C) was also obtained which revealed a simple rhombic spectrum (g_x = 2.0720, g_y = 2.0298, g_z = 1.9722) that does not show hyperfine coupling consistent with a primarily metal centered SOMO. This was confirmed by our calculated SOMO, which revealed that the unpaired electron exists primarily in a metal

non-bonding orbital (Figure 4-1B).

Surprisingly, **5** undergoes very little structural distortion (compared to **1**) following oxidation including only negligible changes in the structure and bonding of the borazine ring itself. However, an examination of the calculated thermodynamic hydricity reveals a significant increase (66 vs. 41 kcal/mol) in hydride affinity following oxidation (Scheme 4-1). Unfortunately, experimental confirmation of this trend was complicated by the high thermal sensitivity of **5** which could not be isolated as a pure compound. Treatment of **5** with $NaEt_3BH$ did yield a new paramagnetic product, however, the resultant species was not EPR active, and did not show any paramagnetic ^1H NMR resonances which precluded definitive characterization. Additionally, the use of weaker hydride sources such as $NaBH_4$ or $LiB(OAc)_3H$ resulted in displacement of the borazine ring rather than hydride transfer.

4.2.3 Protonation reactions of dearomatized hydride adducts

In addition to hydride delivery, we were interested in exploring reactions of our dearomatized borazine complexes with proton sources to yield a partially saturated 1,2-H_2-adduct. Our previous experimental studies suggested that the products obtained from these reactions were highly dependent on the proton source used, as well as the specific reaction conditions employed. In any case, the products formed were either too unstable to be isolated and fully characterized, or substituted cyclotriborazanes such as the previously reported $OAc^F{}_2Me_4B_3N_3Me_3D_3$ and $OAc^F{}_3Me_3B_3N_3Me_3D_3$ were obtained following treatment of $[(Me_4B_3N_3Me_3)Cr(CO)_3]MgBr$ or $Me_3B_3N_3Me_3$ with excess trifluoroacetic acid ($DOAc^F$). The former results from the trapping of the putative intermediate $(Me_4B_3N_3Me_3D)Cr(CO)_3$ wherein a borazine B=N bond has been reduced by the sequential addition of a Me^- nucleophile and a proton.[2] Additionally, the reaction of **2** with 1 eq. of $HOAc^F$ produced a probable 1,2-H_2-species that precipitates from solution and was too unstable for complete characterization (See section 3.2).

Given the challenges associated with studying such 1,2-H_2-intermediates due to their limited stability, the feasibility of these reactions was explored computationally. For these studies, we derived both the relative bascicity of the 2 and 4-position nitrogen

Scheme 4-2. Calculated pK_a values, and free energy of H_2 loss, for borazine hydride adducts **3** and **4**

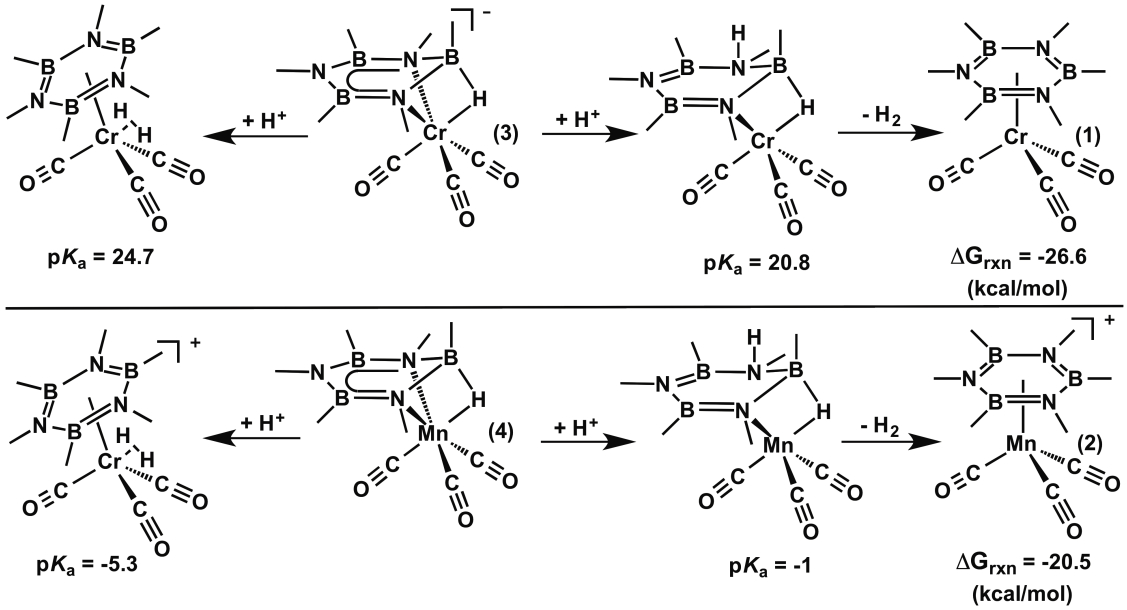

atoms as well as the hydride (Scheme 4-2). Additionally, the free energy of hydrogen elimination from the 1,2-H_2-adduct was calculated in order to assess its relative stability.

Not surprisingly, H_2 elimination is predicted to be favored by > 20 kcal/mol from both metal complexes. This is consistent with our experimental data which suggests that partially saturated borazine species are highly unstable. Interestingly though, the bascicity of both the hydride and the 2-position nitrogen atom are predicted to be closely matched (Δ_{pKa} = 4.3 for Mn and 4.1 for Cr). This is consistent with the experimental observations discussed in chapters 2 and 3 and suggests such intermediates may be transiently accessible, and could be intercepted in a catalytic regeneration scheme.

4.2.4 Single electron transfer to (2) and subsequent reactivity

As previously established, the discovery of low energy routes to the formation of boron hydrides is key to the success of metal-mediated borazine reduction. The substitution of chemical hydrides with hydrides generated from protons and electrons would therefore be a major advance if reduction could be carried out at modest operating potentials. As detailed in chapter 2, complex **2** displays two reductions at -1.38 and -1.88 V vs. $Fc^{0/+}$, the first of which is quasi-reversible. This work demonstrated that 2 eq. of $Na/C_{10}H_8$ and 1 eq. of $HOAc^F$ can be used to synthesize the complex

Scheme 4-3. Free energy of hydride reduction of **2** to **4** by 1 and 2 e^- reduction pathways

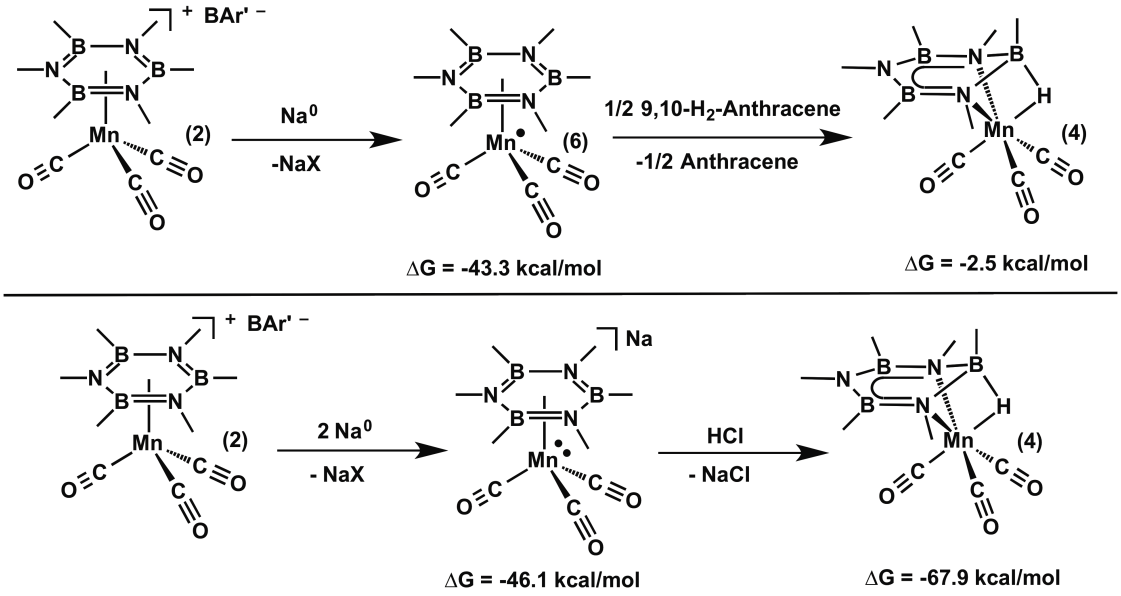

$(Me_3B_3N_3Me_3)(\mu\text{-H})Mn(CO)_3$ (**4**) from **2**. Although this dearomatized borazine hydride was obtained solely via the delivery of protons and electrons, we were intrigued to further explore the reversible 1 e^- reduction of **2** and whether that reduced species could participate in H-atom transfer reactions to afford the hydride **4** using lower energy terminal reductants. Computationally derived free energy values (Scheme 4-3) for both reaction pathways reveal that both the 1 e^- (-43.3 kcal/mol) and 2 e^- (-46.1 kcal/mol) reduction reactions are highly exergonic. However, the quenching step, either protonation of the 2 e^- reduced complex, or H-atom transfer to the 1 e^- reduced complex, showed significant differences in the calculated free energies. Protonation is favored by -67.9 kcal/mol, whereas the hypothesized H-atom transfer reaction was predicted to be approximately thermo-neutral (-2.5 kcal/mol), While this treatment does not constitute and explicit derivation of the activation energies associated with these two distinct pathways to **4**, the significant (c.a. 65.4 kcal/mol) difference in the energy released suggests that single electron reduction followed by H-atom transfer would provide a substantially lower energy pathway to borazine reduction.

To further explore this, we attempted the single electron reduction of complex **2** using Cp_2Co (-1.30 V vs. $Fc^{0/+}$)[8] which is sufficiently reducing to access the first redox couple observed in the CV for **2** (-1.19 V vs. $Fc^{0/+}$)[8] but not the second.

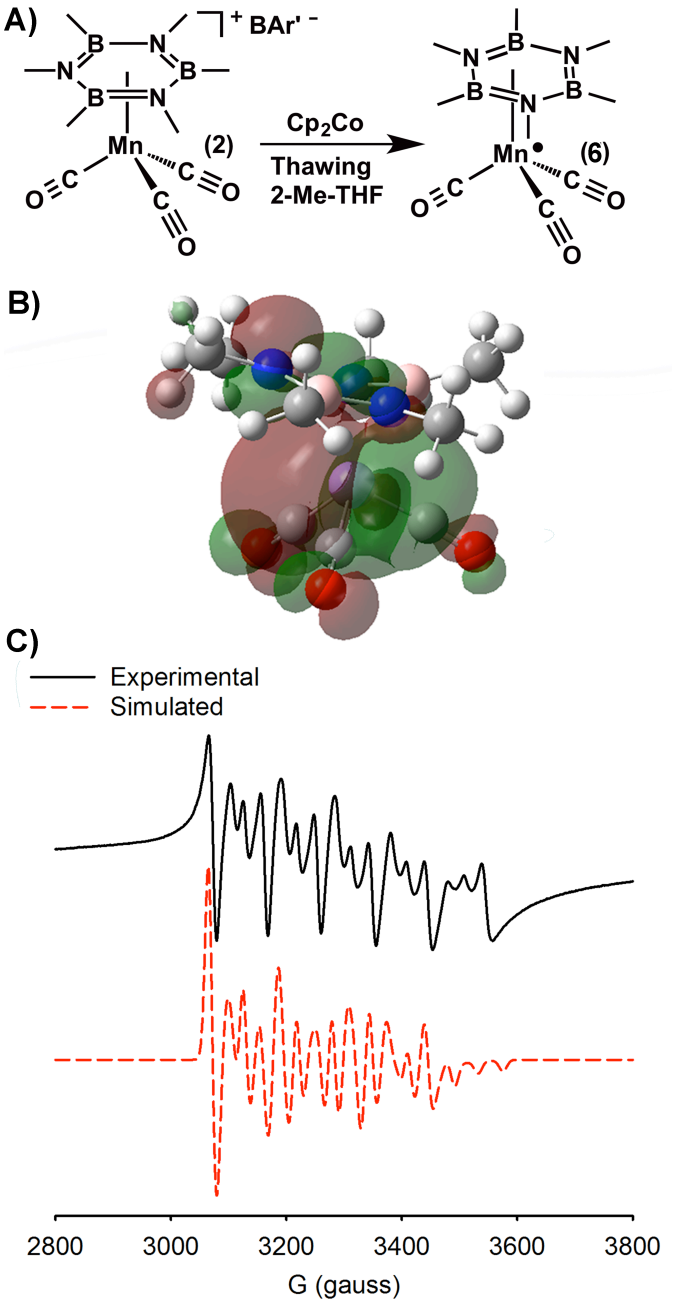

Figure 4-2. A) Synthetic scheme for the reduction of **2** to **6**. B) Calculated SOMO orbital of **6**. C) Experimental (black) and simulated (red) X-band EPR spectrum of **6**.

As predicted by our computations, reduction proceeded readily when 1 eq. of Cp_2Co was added to a frozen 2-Me-THF solution of **2** (Figure 4-2A). The resulting reduced complex (**6**) was characterized by EPR spectroscopy (Figure 4-2C), which revealed a rhombic spectrum (g_x = 2.0238, g_y = 2.0269, g_z = 1.9803) with hyperfine coupling

interactions to ^{55}Mn (A_{55Mn} = 169.7, 184.8, 223.8 mHz) and ^{14}N (A_{14N} = 107.8, 62.2, 119.1 mHz) nuclei. Further confirmation of single electron reduction was afforded by applying Evan's method to a solution containing **6** which revealed a μ_{eff} value of 1.92 and N = 1.17 unpaired electrons, consistent with an s = 1/2 system. IR spectroscopy was conducted on a solution containing **6**, and new ν_{CO} bands were observed at 2011 and 1944 and 1930 cm^{-1} consistent with a reduced metal species being present in solution featuring C_s symmetry. The reduced symmetry is likely the result of a hapticity shift from η^6 *to* η^4 following reduction. Unfortunately, this could not be verified by ^1H NMR as no signals were observed for complex **6**. Characterization by X-ray diffraction was also precluded by its thermal instability.[9] However, our calculations predicted a hapticity shift and the calculated SOMO (Figure 4-2B) is distributed between the MCO_3 fragment and the N-p-orbitals, consistent with the observed ^{14}N hyperfine coupling.

4.2.5 Anthraquinone mediated hydride transfer to (2)

With a means to generate reduced complex **6** in situ, we next turned our attention to developing conditions for affecting H-atom abstraction to synthesize hydride **4** by single electron reduction. Unfortunately, the addition of traditional H-atom donors such as 9,10-H_2-anthracene, toluene, and Bu_3SnH did not induce H-atom transfer to **6**. This was surprising as our calculations predicted that H-atom transfer from 9,10-H_2-anthracene is exergonic by 2.5 kcal/mol. However, the lack of reactivity can likely be explained by a combination of the limited thermal stability of **6** and a high kinetic barrier to H-atom transfer which favors decomposition over quenching to give **4**. To further explore this, attempting these reactions in a variety of solvents and screening alternative H-atom donors with lower bond dissociation free energies such as anhydrous TEMPO-H and $Mn(CO)_5H$ would be interesting future studies.

As an alternative to the direct quenching of **6** by H-atom transfer, we were intrigued by the possibility of adding a redox mediator which would assist in H-atom transfer from the reaction solvent allowing the reduction of **2** to **4** via the delivery of a single electron. Along these lines, we were intrigued by the extensive literature available on quinones and the redox reactions that they participate in.[10,11] Interestingly, quinones are known to readily abstract H-atoms from a variety of sources when reduced under conditions that

promote single electron transfer.[12-14] These reactions afford reduced hydroquinone salts, that contain hydridic O–H bonds.[15] Inspired by this, we hypothesized that Cp_2Co reduction of a suitable quinone could facilitate hydride transfer to **2** yielding **4** where the hydride is formed by the delivery of a single electron and a hydrogen atom.

Based on this hypothesis we examined the effect of added 9,10-anthraquinone (AQ) in the Cp_2Co reduction reaction discussed in section 4.2.4. AQ was selected because its corresponding hydroquinone salt (**7**) is a relatively strong hydride donor. Furthermore, our calculations determined that the **7** would be sufficiently hydridic (ΔG_{H-} = 37.2 kcal/mol) to react with **2** to form **4**. In agreement with our calculations, we were pleased to observe a 90% yield of the hydride **4** when a mixture of AQ and **2** (1:1) was treated with Cp_2Co (1 eq.) in thawing 2-Me-THF (Figure 4-3). We initially hypothesized a mechanism in which reduction of anthraquinone is the first step, followed by H-atom transfer to the resulting semi-quinone, and finally hydride transfer from **7** to **2**. However, addition of Cp_2Co to AQ in the absence of **2** did not produce a reaction. This can be explained by the identical (-1.30 vs. -1.21 V vs. $Fc^{0/+}$) reduction potential of Cp_2Co and AQ observed in DPV data collected in 2-Me-THF (0.05 M $^{n}Bu_4NBAr'$). However, when **2** is present in the solution, the anthraquinone wave is cathodically shifted ~400 mV, (Figure 4-3 and C-13) such that Cp_2Co is competent to reduce AQ to its corresponding semiquinone. It is likely that a solution interaction between **2** and AQ is responsible for lowering the AQ reduction overpotential, and in-situ IR spectroscopy would be an informative future study to examine this.

With evidence that **2** was facilitating electron transfer to AQ, we next attempted to experimentally verify that **7** was acting as the terminal hydride donor to reduce **2** to **4**. Evidence to that effect was afforded by generating this species in-situ via addition of $NaEt_3BH$ to AQ. Complete reaction was verified by solution-cell IR spectroscopy which revealed that the BH stretch of Et_3BH had completely disappeared following addition of AQ. This mixture was added to complex **2** and the hydride adduct **4** was afforded in 65% yield suggesting that **7** is indeed a competent hydride donor for **2**. Further evidence was provided by substitution of p-benzoquinone, whose hydroquinone salt is a much weaker hydride donor (ΔG_{H-} = 56.7 kcal/mol), in the Cp_2Co reduction reaction which yielded none of the desired product under identical conditions.

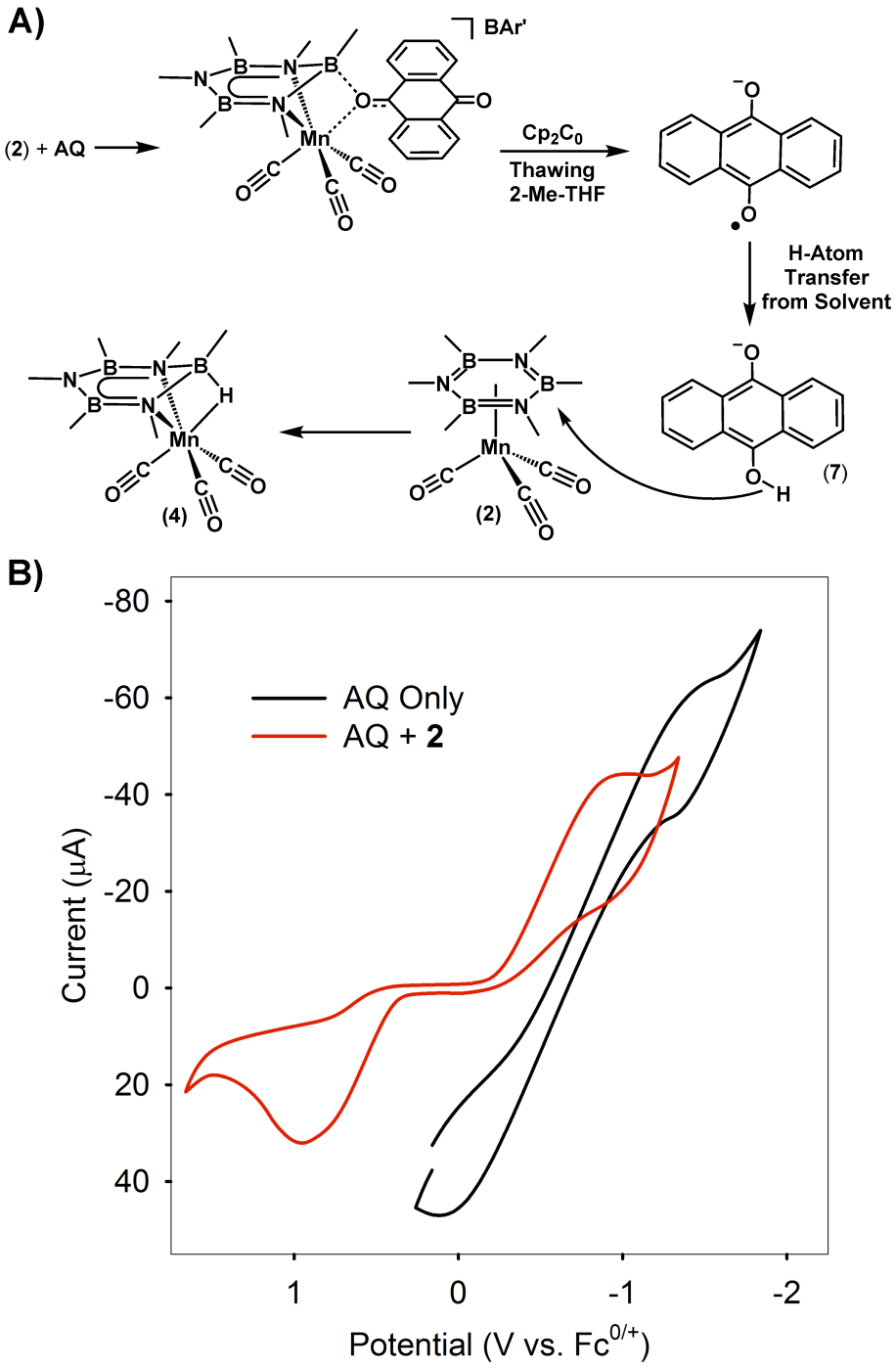

Figure 4-3. A) Proposed mechanism of AQ mediated hydride reduction of **2** to **4**. B) CV of solution containing AQ with (red) and without (black) added **2**, 0.05 M $^{n}Bu_4NBAr'$/2-Me-THF (100 mV/s).

4.2.6 Mechanism of anthraquinone mediated hydride transfer

Being confidant that **7** was ultimately responsible for hydride transfer to **2**, we next sought to determine the mechanism by which the active hydride forms. Notably,

hydroquinone species are accessible through both H-atom transfer and protonation pathways, so a series of experiments were conducted to differentiate these two mechanisms. Evidence for a single electron pathway was obtained by the addition of a second equivalent of Cp_2Co to the reaction which resulted in reduced (35%) yield Additionally, reactions carried out in the presence of the spin-trapping agent 5,5-Dimethyl-1-Pyrroline-N-Oxide (DMPO) showed a reduced (30%) yield and the presence of a new paramagnetic product. This species is observable by EPR spectroscopy (Figure C-12) as an S=1/2 rhombic spectrum (g_x = 1.9949, g_y = 1.9953, g_z = 1.9977). Although ^{13}C and ^{15}N hyperfine interactions are not observed, the absence of more pronounced ^{55}Mn coupling, and the relatively small shift in g-values as compared to the free electron value, suggests a primarily organic centered radical species consistent with a spin-trapped semiquinone.

We next explored whether the semiquione discussed above was indeed being quenched by H-atom transfer to form **7**. The substitution of C_6F_6 as the reaction solvent resulted in only trace amounts (< 10%) of **4**, suggesting that the solvent is likely the H-atom source. Furthermore, the addition of 2 eq. of H_2O to the reaction carried out in C_6F_6 also did not yield the desired product suggesting adventitious moisture does not play a role in the reaction. The reaction also proceeds readily (65% yield) when dichloromethane, a solvent with similar calculated C-H BDFE (86.4 kcal/mol vs. 81.7 kcal/mol for 2-Me-THF), is substituted as the reaction solvent, suggesting solvent

Scheme 4-4. Free energy of H-atom transfer to form **7** (top), and transfer of hydride from **7** to **2.**

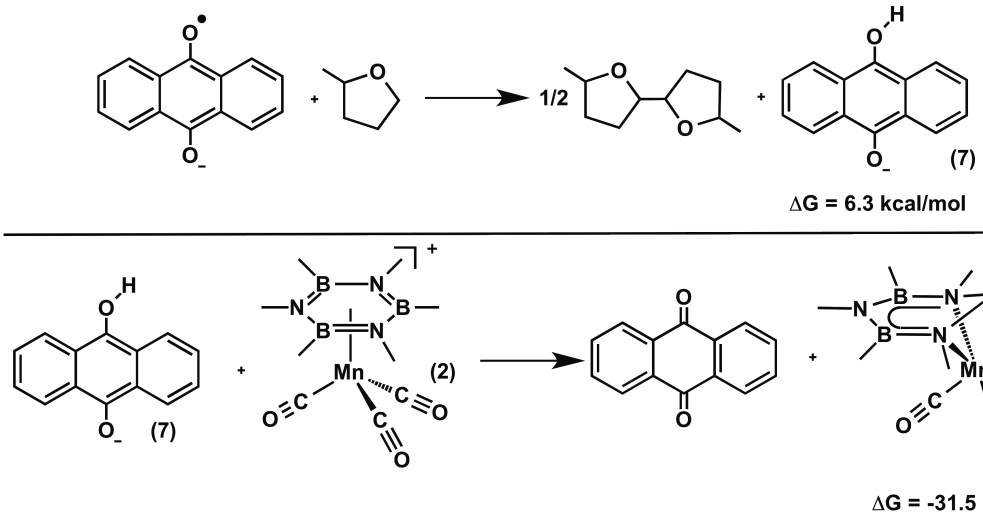

identity is not crucial to the reaction. Calculation of homolytic bond dissociation free energies (BDFE) showed the values for both **7** and **4,** 39.0 and 52.8 kcal/mol respectively, are significantly lower than that of 2-Me-THF (81.7 kcal/mol, Table C-4). However, the net reaction to reduce anthra-semiquinone to **7** is only 6.3 kcal/mol uphill (Scheme 4-4) and the reduction of **2** to **4**, using **7** as the hydride source, is favored by 31.5 kcal/mol. This results in a net-reaction free energy of -25.2 kcal/mol suggesting that the resulting products are sufficiently stable to drive the reaction forward and promote cleavage of the relatively strong solvent C-H bonds.

Verification of the H-atom source by isotopic labeling of the reaction solvent was also attempted, however, the results of this experiment were inconclusive due to inability to locate the M-H-B unit in the IR spectrum, as well as quadrapolar broadening which prevented visualization of the hydride by ^{1}H and ^{2}H NMR.[16] Attempts to isolate the product of this reaction and differentiate the M-H from the M-D species by EI-MS were complicated by strong overlapping signal associated with AQ. Another method that is typically used to provide evidence for an H-atom transfer mechanism is the observation of an appreciable rate enhancement in the presence of common H-atom donors (H-atom transfer reactions are typically faster when weak X-H bonds are present).[17] The Cp_2Co reduction of **2** with AQ, however, occurs rapidly near the thawing point of the solvent, which prevented kinetic analysis by many common techniques such as NMR or UV-Vis. However, in light of the results discussed in section 4.2.7, spectro-electrochemical techniques may provide insight as to the effect of added H-atom donors and would be an informative future study. Despite the challenges encountered with these mechanistic studies, it is clear that AQ mediates hydride transfer to **2** via the deliver of a 1 e^- reductant with a relatively mild reducing potential (-1.30 V vs. $Fc^{0/+}$) which is an important advance towards a comprehensive, low energy B=N, reduction method.

4.2.7 AQ mediated hydride reduction of 2 by applied potential

In an effort to further optimize 1 e^- pathways to boron hydrides we next sought to adapt AQ mediated redox chemistry to controlled potential electrolysis as this would constitute an important step towards developing future electro-catalytic B=N reduction

strategies. In this reaction, the over-potential required for B=N reduction is determined by the reduction potential of the metal. Therefore, appropriate tuning of the electronic environment would allow the reduction energy to be minimized to the point that it is near the thermodynamic potential for borazine reduction.

Demonstrating this reaction would provide further support for, and demonstrate the generality of, the anthraquinone mediated hydride transfer mechanism described in sections 4.2.5-4.2.6. The involvement of two electron pathways can be further ruled out if a potential is selected such that only the quasi-reversible 1 e^- reduction of **2** is accessible and a total current equivalent to 1 e^- is passed. Gratifyingly, when a solution of **2** and anthraquinone in 0.1 M Bu_4NPF_6 in DCM was held at an applied potential of –1.85 V vs. $Fc^{0/+}$ the hydride **4** was afforded in ~40% yield. Unfortunately, electrochemistry in $[^nBu_4N]PF_6$ was complicated by the fact that F-atom (or F^-) transfer was a competing side-reaction (40% yield). Samples analyzed following bulk electrolysis showed two tetrahedral boron atoms (9 and 6 ppm) in the ^{11}B NMR spectrum. The latter of which is consistent with the hydride, and the former was identified as the analogous fluoride product by comparison to the independently synthesized species resulting from the addition of a 1.0 M solution of $[^nBu_4N]F$ in THF to **2**. Additionally, this species was characterized by ESI-MS and a molecular ion peak was observed at M/z = 308 consistent with the fluoride reduced species ($-CH_3$).

In an effort to circumvent F-atom transfer, we next sought to carry out bulk electrolysis in a solvent-electrolyte system which does not contain fluorine atoms. Unfortunately, common electrolytes such as $[^nBu_4N]ClO_4$ and $[^nBu_4N]Cl$ displace borazine from the metal center, and many others are insoluble in solvents compatible with complex **2.** As an alternative, we turned to the $[^nBu_4N]^+$ salt of mono-carborane ($CB_{11}H_{12}^-$), as carborane electrolytes are known to be highly soluble in a variety of solvents, are non-nucleophillic, and possess a high electrochemical stability.[18-19] Gratifyingly, when bulk electrolysis was conducted in a 0.05 M solution of $[^nBu_4N][CB_{11}H_{12}]$ at -1.55 V (vs. $Fc^{0/+}$), **4** is obtained in 95% yield (Figure 4-4) based on integration of the ^{11}B NMR spectrum using $(TMSO)_3B$ as an internal standard (Figure C-7). Additionally, the solution-cell IR spectrum was collected and **4** was the only metal containing

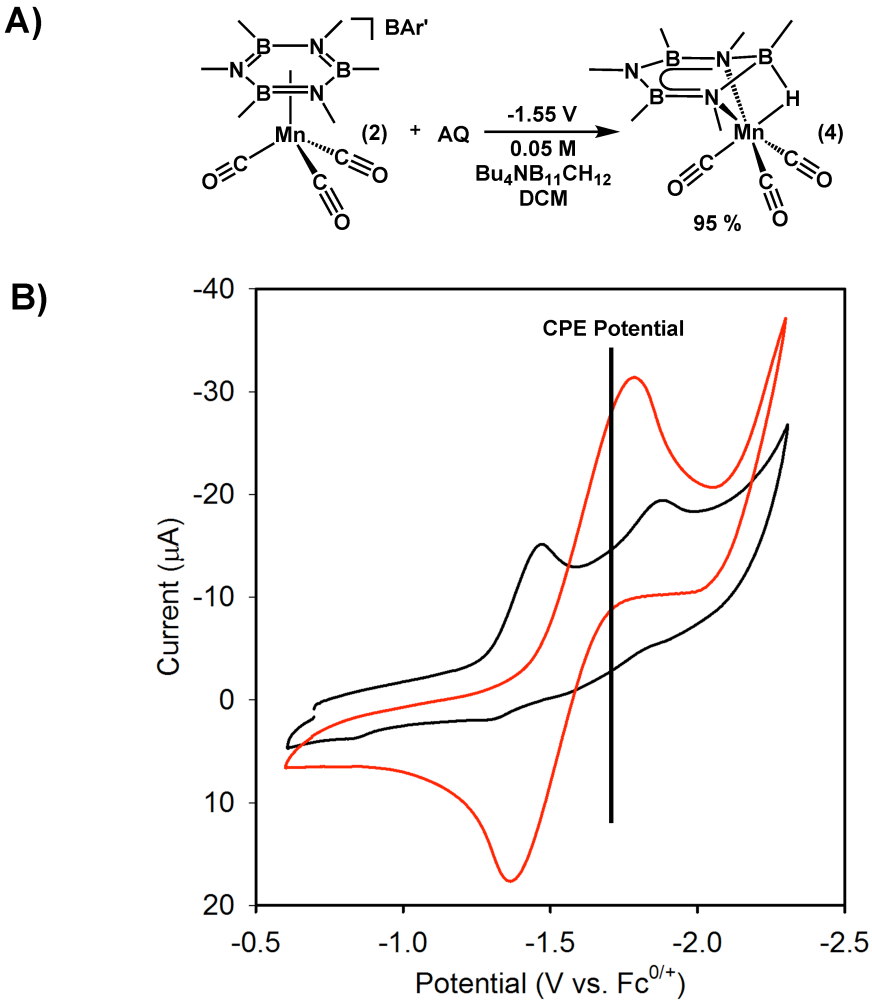

Figure 4-4 A) Synthetic scheme for the reduction of **2** to **4** by controlled potential electrolysis (CPE). B) Cyclic voltammetry of solutions containing **2** (black) or AQ (red) showing potential selected for CPE.

species observed in > 5% yield. In agreement with our chemical reductions, **4** was not observed when bulk electrolysis was conducted in the absence of 9,10-anthraquinone. This, considered in conjunction with the high (> 50%) yield of **4** after 1 e^- was delivered to the solution, provides further support for a general anthraquinone mediated H-atom transfer mechanism. Additionally, the hydride reduction of **2** by an applied potential lays the groundwork for future studies which will seek to develop further electrochemical transformations of coordinated B-N heterocycles.

4.3 Conclusion

Through a combination of computational and experimental studies, this chapter has built on the work outlined in chapters 2 and 3 to establish a more fundamental

understanding of how transition metal coordination can be used to facilitate the reduction of spent B–N fuels. Thermodyniamic hydricity values were computationally derived and found to correlate strongly with metal oxidation state. Additionally, odd-electron borazine complexes of Cr(I) and Mn(0) were generated and characterized, providing insight into the unique structure and bonding of metal-borazine complexes. Finally, the understanding of hydricity requirements for borazine dearomatization gained by our computations was used to uncover a unique hydride delivery mechanism which proceeds through a single electron reduction and H-atom transfer mediated by anthraquinone. This transformation was also carried out electrochemically, at modest potential (-1.55 V vs. $Fc^{0/+}$), establishing an important proof of concept for a future electrocatalytic B=N bond reduction sequence.

4.4 Experimental Details

Computational Details: All structures were fully optimized without symmetry constraints using either the M06-2X[20] or the B3LYP[21-24] functional as implemented in Gaussian 09,[25] using the 6-31G** basis set.[26,27] The ultrafine integration grid was employed in all calculations, which ensured the stability of the optimization procedure for the investigated molecules. Each stationary point was confirmed by a frequency calculation at the same level of theory to be a real local minimum on the potential energy surface without imaginary frequency. More accurate electronic energies were computed for the optimized geometries using the larger 6-311++G(d,p) basis set.[28,29] All reported free energies are for Et_2O solution at the standard state (T = 298 K, P = 1 atm, 1 mol/L concentration of all species in Et_2O) as modeled by a polarized continuum model.[30] The energy values given in the paper correspond to solvent-corrected Gibbs free energies that are based on B3LYP/6-311++G(d,p) electronic energies and all corrections calculated at the B3LYP/6-31G(d) level. All calculated pK_a values are for Et_2O solutions. Although no pK_a scales have been experimentally determined in diethyl ether, we chose to employ Et_3NH^+ as the anchor of our pK_a scale and assign it a pK_a value of 12.5. A value of 12.5 was chosen because Et_3NH^+ has been previously employed as an anchor (pK_a value of 12.5) for a structurally similar solvent, THF.[31,32] Initial optimizations employed the M06-2X functional as the included dispersion corrections have been shown to provide better estimation of main-group systems.[20,33,34]

Although computations employing the M06-2X functional better modeled the thermochemistry of borazine and hexamethylborazine, all computations reported within made use of the B3LYP functional, which was found to model the manganese and chromium complexes better than the M06-2X functional.

General Experimental Procedures: All experiments were conducted using standard Schlenk techniques or in a nitrogen filled glovebox. NMR spectra were recorded on Varian MR400, vnmrs 500, or vnmrs 700 MHz. spectrometers. ^{1}H spectra were referenced relative to the solvent resonance, and ^{11}B spectra were referenced indirectly based on the ^{1}H spectrum.[35] IR spectra were recorded on a Nicolet iS-10 spectrometer from Thermo Scientific in a KBr plate solution cell. X-band EPR spectra were recorded on a Bruker EMX ESR spectrometer equipped with a 4102-ST cavity. EPR simulations were conducted using the easy spin software package for MATLAB.[36] Mass spectra were collected by electron impact ionization on a VG 70-250-S magnetic sector, double-focusing mass spectrometer. The electron energy was set to 70 eV, and the source temperature was 240 ºC. Nominal mass spectra were obtained scanning the magnet from m/z 1000 to m/z 35 at 8 seconds per decade, using an external mass calibration. Evan's method was conducted using a coaxial NMR tube insert from Wilmad glass with benzene or dichloromethane added to samples as the diamagnetic reference compound. 9,10-anthraquinone and p-benzoquinone were obtained from Sigma Aldrich and recrystallized from ethyl-acetate before use. Cobaltocene (Cp_2Co) was purchased from Strem chemicals and used as received. $HCo(dmpe)_2$ was provided by Dr. M. Mock and was prepared by a previously reported procedure.[7] Cyclic voltammetry experiments were collected on a Pine Research Instrumentation WaveNow potentiostat. Experiments were conducted in a 0.05 M solution of tetrabutylammonium tetrakis[3,5-bis(trifluoromethyl)phenyl]borate ($^{n}Bu_4NBAr'$) in 2-Me-THF or 0.1 M tetrabutylammonium hexafluorophosphate ($^{n}Bu_4NPF_6$) in CH_2Cl_2. A glassy carbon working electrode and a platinum disk counter electrode were used and voltammograms referenced relative to ferrocene ($Fc^{0/+}$) using a silver wire pseudo reference electrode. Scan rate was 0.1 V/s unless otherwise specified. $E_{1/2}$ values were determined from the differential pulse voltammogram (DPV). Controlled potential electrolysis experiments were conducted using a 0.05 M solution of tetrabutylammonium carborane ($[^{n}Bu_4N][CB_{11}H_{12}]$) using a

carbon felt working electrode, Ni mesh counter electrode, and Ag/AgCl reference electrode. [^{n}Bu$_4$N][CB$_{11}$H$_{12}$] was prepared by reacting the commercially available Cs[CB$_{11}$H$_{12}$] with [^{n}Bu$_4$N]Cl in aqueous solution. The resulting precipitate was isolated by filtration and dried under vacuum at 100 ºC for 48 h. (Me$_3$B$_3$N$_3$Me$_3$)Cr(CO)$_3$ and [(Me$_3$B$_3$N$_3$Me$_3$)Mn(CO)$_3$]BAr' were synthesized by previously reported routes.[2,3] All solvents were passed through an S.G. Waters solvent purification system or dried and degassed by standard methods.[37] All other chemicals were purchased from commercial vendors and used as received. All filtrations were conducted using a pipet blocked with Whatman glass fiber filter paper.

Reaction of 1 with HCo(dmpe)$_2$ to afford 3. A solution of **1** (9.1 mg, 0.03 mmol) was prepared in 1 ml 2-Me-THF. The solution was frozen, and HCo(dmpe)$_2$ (9.1 mg, 0.03 mmol) was added. The mixture was thawed and shaken vigorously for 20 seconds, and then transferred to an NMR tube. The ^{11}B NMR spectrum (Figure C-1) was consistent with formation of **4** in 30% yield.

Preparation of Mn(μ-H)(Me$_3$B$_3$N$_3$Me$_3$)(CO)$_3$ (4) by Reduction with Cp$_2$Co and Aq. A solution containing **2** (16.7 mg 0.014 mmol) and 9,10-anthraquinone (3.0 mg, 0.014 mmol) in 1 ml 2-Me-THF was frozen in the glovebox cold-well inside a 20 ml scintillation vial. To the frozen solution is added solid Cp$_2$Co (2.7 mg 0.014 mmol). The mixture is then allowed to thaw and the capped vial vigorously shaken for 30 seconds. The solution was then warmed to room temperature and the yield (85 %) of the hydride **4** was determined by ^{11}B NMR (Figure C-2.) integration using the residual BAr' salt as an internal standard.[3] As previously noted, the spectroscopic properties of **4** are highly sensitive to the solution environment.[3] Slight differences in the ^{11}B NMR are observed from that previously reported (Figure C-3.), because of this, solution cell IR was also used to confirm the identity of the product (Figure C-8.).

Preparation of Mn(μ-H)(Me$_3$B$_3$N$_3$Me$_3$)(CO)$_3$ (4) by bulk electrolysis. A solution of **2** (57.2 mg, 0.049 mmol) and 9,10-anthraquinone (10.2 mg, 0.049 mmol) in 7 ml [^{n}Bu$_4$N]B$_{11}$CH$_{12}$ electrolyte solution (0.05 M in DCM) was prepared and placed in the working electrode chamber of a bulk electrolysis cell. The counter electrode chamber was filled with electrolyte solution and equipped with a nickel gauze electrode. Cyclic

voltammetry was recorded in the working electrode chamber (GC working electrode, Ag/AgCl reference electrode) and the potential for bulk electrolysis (-1.550 V vs. $Fc^{0/+}$) was selected to be coincident with first observed redox couple for anthraquinone (see Figure 4-4B). The cell was then equipped with a carbon felt working electrode and bulk electrolysis was conducted until a total charge of 4.07 C (1 e^- relative to Mn) was passed. Electrolysis was then stopped, and the solution from the working electrode chamber was removed. This solution was then characterized by ^{11}B NMR, and the total yield of the hydride was determined based on relative integration against a $B(OTMS)_3$ internal standard (16.6 µl, 0.049 mmol) added after electrolysis.

Preparation of $[Cr(Me_3B_3N_3Me_3)(CO)_3]PF_6$ (5). A solution of **1** (14.4 mg, .048 mmol) in 1 ml DCM was frozen in the glovebox coldwell inside a 20 ml scintillation vial. To the frozen solution was added $AgPF_6$ (12.1 mg, .048 mmol) dissolved in 1 ml in DCM. The mixture was then allowed to thaw until the solution turned dark (approximately 30 seconds), indicating the precipitation of Ag metal. The solution was then filtered as rapidly as possible to give a yellow solution of **5** that was characterized without further workup. Solutions of **5** were highly thermally sensitive and were stored either frozen or at -78 ºC to prevent thermal decomposition. EPR spectroscopy was conducted on samples prepared as described above but substituting 2-Me-THF as the reaction solvent. Wet1D NMR (699.8 MHz, CH_2Cl_2): δ 8.75 (s), 13.9 (s); IR (KBr Solution Cell): ν_{CO} 2057, 1980 cm^{-1}; X-Band EPR (77 K): g_x =2.0720 g_y = 2.0298 g_z = 1.9722 (Gauss); Evan's Method (CD_2Cl_2): Diamagnetic additive: CH_2Cl_2, Peak separation = 0.48 ppm, μ_{eff} = 1.90, N = 1.15.

Preparation of $Mn(Me_3B_3N_3Me_3)(CO)_3$ (6). A solution of **1** (20.0 mg, .017 mmol) in 0.75 ml 2-Me-THF was prepared and solution frozen in the glovebox coldwell inside a 20 ml scintillation vial. To the frozen solution was added solid Cp_2Co (3.6 mg, .017 mmol). The mixture was then allowed to thaw for 30 seconds with vigorous shaking. The red/orange solution was then refrozen to obtain a mixture containing $[Cp_2Co]BAr'$ and the reduced Mn complex **6** that was characterized without further workup. **6** proved to be highly thermally sensitive, thus, solutions of **6** were stored either frozen or at -78 ºC to prevent thermal decomposition. IR (KBr Solution Cell): ν_{CO} 2011, 1944, 1930 cm^{-1}; X-Band EPR (77 K) g_x = 2.0238 g_y = 2.0269 g_z = 1.9803 (Gauss), hyperfine coupling: ^{14}N

(107.8, 62.2, 119.1) ^{55}Mn (118, 50, 54) (mHz); Evan's Method (2-Me-THF): Diamagnetic additive: C_6H_6, Peak separation = 0.20 ppm, μ_{eff} = 1.92, N = 1.17.

4.5 References

1) Manuscript in preparation.

2) Carter, T. J.; Kampf, J. W.; Szymczak, N. K. *Angew. Chem. Int. ed.* **2012**, *51*, 13168.

3) Carter, T. J.; Wang, J. Y.; Szymczak, N. K. *Organometallics* **2014**, *33*, 1540.

4) All computational studies were conducted by Dr. Zachariah M. Heiden from Washington State University.

5) Andersson, M. P.; Uvdal, P. *J. Phys. Chem. A* **2005**, *109*, 2937.

6) Strong acids with nucleophillic anions (e.g. HCl) react readily with borazines through concerted addition. In our hands, Brookhart's acid (HBAr') and HCl:$AlCl_3$ did not produce a reaction with borazine suggesting that protonated ether (pK_a = -9.7) is not sufficiently acidic to react with borazine in the absence of a coordinating anion. To our knowledge, the only example of non-concerted borazine protonation was reported by Nöth and co-workers, who used the superacid HBr:$AlBr_3$ in non-polar solvent. See: Gemünd, B.; Günther, B.; Nöth, H. *ARKIVOC* **2008**, 136.

7) Mock, M. T.; Potter, R. G.; O'Hagan, M. J.; Camaioni, D. M.; Dougherty, W. G.; Kassel, W. S.; DuBois, D. L. *Inorg. Chem.* **2011**, *50*, 11914.

8) Measured in 0.05 M $^{n}Bu_4NBAr'$/2-Me-THF and reported based on peak current of DPV signal.

9) Slow decomposition was noted even when solutions of **6** were held at -78 ºC.

10) Song, N.; Gagliardi, C. J.; Binstead, R. A.; Zhang, M. T.; Thorp, H.; Meyer, T. J. *J. Am. Chem. Soc.* **2012**, *134*, 18538.

11) Guo, X.; Zipse, H.; Mayr, H. *J. Am. Chem. Soc.* **2014**, *136*, 13863.

12) Ci, X.; Silveira da Silva, R.; Nicodem, D.; Whitten, D. G. *J. Am. Chem. Soc.* **1989**, *111*, 1337.

13) Wurche, F.; Sicking, W.; Sustmann, R.; Klärner, F. G.; Rüchardt, C. *Chem. Eur. J.* **2004**, *10*, 2707.

14) Rüchardt, C.; Gerst, M.; Ebenhoch, J. *Angew. Chem. Int. ed.* **1997**, *36*, 1406.

15) Zhu, X.; Wang, C. *J. Org. Chem.* **2010**, *75*, 5037.

16) The bridging hydride is visible by ^{1}H NMR in the pure material, however, the proton NMR resonances of **4** are broadened in the presence of AQ.

17) Lewandowska-Andralojc, A.; Grills, D. C.; Zhang, J.; Bullock, R. M.; Miyazawa, A.; Kawanishi, Y.; Fujita, E. *J. Am. Chem. Soc.* **2014**, *136*, 3572.

18) Carter, T. J.; Mohtadi, R.; Arthur, T. S.; Mizuno, F.; Zhang, R.; Shirai, S.; Kampf, J. W. *Angew. Chem. Int. ed.* **2014**, *53*, 3173.

19) Johnson, J. W.; Thompson, A. H. *J. Electrochem. Soc.* **1981**, *128*, 932.

20) Zhao, Y.; Truhlar, D. G. *J. Chem. Theory Comput. J. Chem.* **2008**, *4*, 1849.

21) Becke, A. D. *J. Chem. Phys.* **1993**, *98*, 5648.

22) Lee, C.; Yang, W.; Parr, R. G. *Phys. Rev. B* **1988**, *37*, 785.

23) Vosko, S. H.; Wilk, L.; Nusair, M. *Can. J. Phys.* **1980**, *58*, 1200.

24) Stephens, P. J.; Devlin, F. J.; Chabalowski, C. F.; Frisch, M. J. *J. Phys. Chem.* **1994**, *98*, 11623.

25) Gaussian 09, Revision D.01, M. J. Frisch, G. W. Trucks, H. B. Schlegel, G. E. Scuseria, M. A. Robb, J. R. Cheeseman, G. Scalmani, V. Barone, B. Mennucci, G. A. Petersson, H. Nakatsuji, M. Caricato, X. Li, H. P. Hratchian, A. F. Izmaylov, J. Bloino, G. Zheng, J. L. Sonnenberg, M. Hada, M. Ehara, K. Toyota, R. Fukuda, J. Hasegawa, M. Ishida, T. Nakajima, Y. Honda, O. Kitao, H. Nakai, T. Vreven, J. A. Montgomery, Jr., J. E. Peralta, F. Ogliaro, M. Bearpark, J. J. Heyd, E. Brothers, K. N. Kudin, V. N. Staroverov, T. Keith, R. Kobayashi, J. Normand, K. Raghavachari, A. Rendell, J. C. Burant, S. S. Iyengar, J. Tomasi, M. Cossi, N. Rega, J. M. Millam, M. Klene, J. E. Knox, J. B. Cross, V. Bakken, C. Adamo, J. Jaramillo, R. Gomperts, R. E. Stratmann, O. Yazyev, A. J. Austin, R. Cammi, C. Pomelli, J. W. Ochterski, R. L. Martin, K. Morokuma, V. G. Zakrzewski, G. A. Voth, P. Salvador, J. J. Dannenberg, S. Dapprich, A. D. Daniels, O. Farkas, J. B. Foresman, J. V. Ortiz, J. Cioslowski, and D. J. Fox, Gaussian, Inc., Wallingford CT, 2013.

26) Dill, J. D.; Pople, J. A. *J. Chem. Phys.* **1975**, *62*, 2921.

27) Hehre, W. J.; Ditchfield, R.; Pople, J. A. *J. Chem. Phys.* **1972**, *56*, 2257.

28) Krishnan, R.; Binkley, J. S.; Seeger, R.; Pople, J. A. *J. Chem. Phys.* **1980**, *72*, 650.

29) Francl, M. M.; Pietro, W. J.; Hehre, W. J.; Binkley, J. S.; Gordon, M. S.; DeFrees, D. J.; Pople, J. A. *J. Chem. Phys.* **1982**, *77*, 3654.

30) Cossi, M.; Rega, N.; Scalmani, G.; Barone, V. *J. Comp. Chem.* **2003**, *24*, 669.

31) Abdur-Rashid, K.; Fong, T. P.; Greaves, B.; Gusev, D. G.; Hinman, J. G.; Landau, S. E.; Lough, A. J.; Morris, R. H. *J. Am. Chem. Soc.* **2000**, *122*, 9155.

32) Rodima, T.; Kaljurand, I.; Pihl, A.; Maemets, V.; Leito, I.; Koppel, I. *J. Org. Chem.* **2002**, *67*, 1873.

33) Zhao, Y.; Truhlar, D. G. *Theor. Chem. Acc.* **2008**, *120*, 215.

34) Goerigk, L.; Grimme, S. *Phys. Chem. Chem. Phys.* **2011**, *13*, 6670.

35) Harris, R. K.; Becker, E. D.; Menezes, S. M. C.; Goodfellow, R.; Granger, P. *Pure and Applied Chemistry* **2001**, *73*, 1795.

36) Stoll, S.; Schweiger, A. *J. Magn. Reson.* **2006**, *178*, 42.

37) Armarego, W. L. F.; Chai, C. L. L.; Knovel; ScienceDirect *Purification of laboratory chemicals*; Elsevier/Butterworth-Heinemann: Amsterdam ; Boston, 2009.

Chapter 5: Conclusions and Future Outlook

This thesis outlines a unique metal-mediated approach to the direct conversion of borazine ($H_3N_3B_3N_3H_3$) to cyclotriborazane ($H_6B_3N_3H_6$; CTB) which is a promising hydrogen storage material. The advantage of this approach is that the need for a separate digestion step prior to reduction is eliminated. This translates to a regeneration scheme for which the energy input can be as close as possible to the associated thermodynamic barrier for the net hydrogenation of borazine.

Chapter 2 explored the reactivity of one the only known transition metal borazine complexes (η^6-$Me_3B_3N_3Me_3$)$Cr(CO)_3$ (**1**) in an effort to establish the feasibility of metal-mediated B–N bond reduction. It was shown that coordination to $Cr(CO)_3$ facilitated unique reactivity of the borazine ring. The nucleophillic addition of hydride and methyl anions resulted in the isolation of dearomatized borazine complexes, the latter of which could be quenched by the addition of excess $DOAc^F$ to give a substituted CTB obtained by successful stepwise reduction of a borazine B=N bond. One major limitation of this work, however, was the high thermal sensitivity of the Cr-hydride ([Cr(μ-H)($Me_3B_3N_3Me_3$)$(CO)_3$]Li; **3**) which decomposed above -30 ºC.[1] Additionally, hydride delivery by chemical (or electrochemical) reduction could not be successfully studied due to the extremely rapid decomposition of **1** following the addition of reductant.

Chapter 3 extended this work to the isostructural and isoelectronic complex [(η^6-$Me_3B_3N_3Me_3$)$Mn(CO)_3$]BAr' (**2**). Reactivity analogous to the Cr system was observed, and dearomatized complexes resulting from Me^- or H^- addition could be isolated. Interestingly, the corresponding Mn-hydride (Mn(μ-H)($Me_3B_3N_3Me_3$)$(CO)_3$; **4**) was much more thermally robust than **3** and could tolerate storage at room temperature for several hours. Though the reactivity towards nucleophiles was similar, **2** offered a major advantage over **1** for studing borazine reduction. Complex **2** displayed two redox couples at -1.38 and -1.88 V vs. $Fc^{0/+}$, the first of which was reversible. Both of these oxidation states were chemically accessible and the former could be intercepted by the

addition of a proton source to successfully demonstrate hydride delivery by 2 e^- reduction and protonation.[2]

Chapter 4 used a combination of computational and experimental evidence to provide a deeper understanding of the results discussed in chapters 2 and 3. Thermodynamic hydricity and pK_a values were calculated for the metal borazine complexes discussed in the previous chapters, and this information was used to identify a much milder hydride source ($HCo(dmpe)_2$) that was competent to reduce **1** to its corresponding hydride **3**. Computational insight was also used to uncover a unique reaction pathway where 9,10-anthraquinone mediates reduction via H-atom transfer to **2** yielding **4**. This reaction was also carried out electrochemically by controlled potential electrolysis, which lays the foundation for future studies that will seek to extend this methodology to an electrocatalytic regeneration method. Finally, the feasibility of delivering a single proton equivalent to either **3** or **4** was examined. Interestingly, the bascicity of the hydride and ring nitrogen atoms are closely matched suggesting a 1,2-H_2 adduct via N-protonation may be possible. Unfortunately, these intermediates were also predicted to be highly unstable with H_2 elimination favored by > 20 kcal/mol. This is consistent with the experimental observation that these reactions proceed via decomposition of the dearomatized species. However, the observation of a probable 1,2-H_2-adduct when **4** is treated with 1 equivalent of $DOAc^F$, as well as the successful trapping of $OAc^F{}_2Me_4B_3N_3Me_3D_3$, suggests that these species exist as intermediates in solution, and could be intercepted under suitable conditions.

In light of the insight gained by these studies there are several additional research questions that, moving forward, must be explored before a the metal-mediated indirect hydrogenation of borazine can be realized as a viable regeneration scheme for spent B–N fuels. Although calculated free energies of hydrogenation suggest that the mechanistic knowledge gained in our previous studies on $Me_3B_3N_3Me_3$ is directly applicable to the reduction of natural borazine, the exploration of natural borazine coordination chemistry is a significant area for future research. Ideally, this strategy could be extended to natural borazine ($H_3N_3B_3H_3$) and its cross-linked derivative, polyborazylene, to increase the useable hydrogen content of the proposed hydrogen storage cycle. However, several challenges complicate the isolation of $H_3N_3B_3H_3$

analogues of **1** and **2**. $H_3N_3B_3H_3$ is highly volatile, which prevents successful application of the entrainment method developed be Werner and coworkers (see section 1.7).[3] Borazine is also susceptible to thermally induced cross-linking[4] which complicates application of the synthetic protocol described in chapter 3 to the synthesis of [(η^6-$H_3B_3N_3H_3$)$Mn(CO)_3$]BAr'. For instance, when a mixture of TlBAr', 10 $H_3B_3N_3H_3$, and $Mn(CO)_5Br$ is heated in dibutyl ether a new ^{11}B NMR resonance was observed at 25 ppm (see section D.4 route A). This was identified as a B-N crosslinked species, however, as a viscous oil could be isolated from the reaction mixture which displayed an identical ^{11}B NMR resonance and did not contain M-CO stretches in the IR spectrum.

As an alternative to heating, photolysis of metal carbonyl precursors such as $Mn(CO)_5Br$ and $Fe(CO)_5$ in the presence of $H_3B_3N_3H_3$ was attempted. These reactions either produced no reaction or induced B–N cross-linking to yield the same species observed in the thermal reaction (see section D.4 route B and section D.5). Finally, borazine ring exchange reactions were attempted by reacting **1** with excess borazine under a variety of conditions (see section D.3). Free $Me_3B_3N_3Me_3$ was observed in these reactions, however, no resonances consistent with $H_3B_3N_3H_3$ coordination were identified. Additionally, attempts to induce precipitation from these reactions only resulted in isolation of starting material. This can likely be explained by computations (carried out as an extension of the studies in chapter 4) which revealed a predicted a free energy for this reaction of 3.4 kcal/mol which can be used to predict an equilibrium constant of approximately $6*10^{-4}$.[5]

While obtaining a discreet complex of natural borazine would be the ideal scenario, the above experiments suggest that this may not be a realistic possibility. However, observing borazine coordination in solution (as an alternative to an isolable complex) is the main prerequisite for extending an electrocatalytic regeneration scheme to natural borazine. Along these lines, preliminary results obtained by treating a $Cr(CO)_3$ solvate with borazine reveal a new oxidative couple in the cyclic voltammagram whose peak current is correlated to added borazine concentration (Figure 5-1). Although attempts to isolate a new complex from this solution have been unsuccessful, these results suggest that an equilibrium population of bound borazine exists in solution. The ^{11}B NMR spectrum of this mixture did not reveal any new resonances that could be attributed to

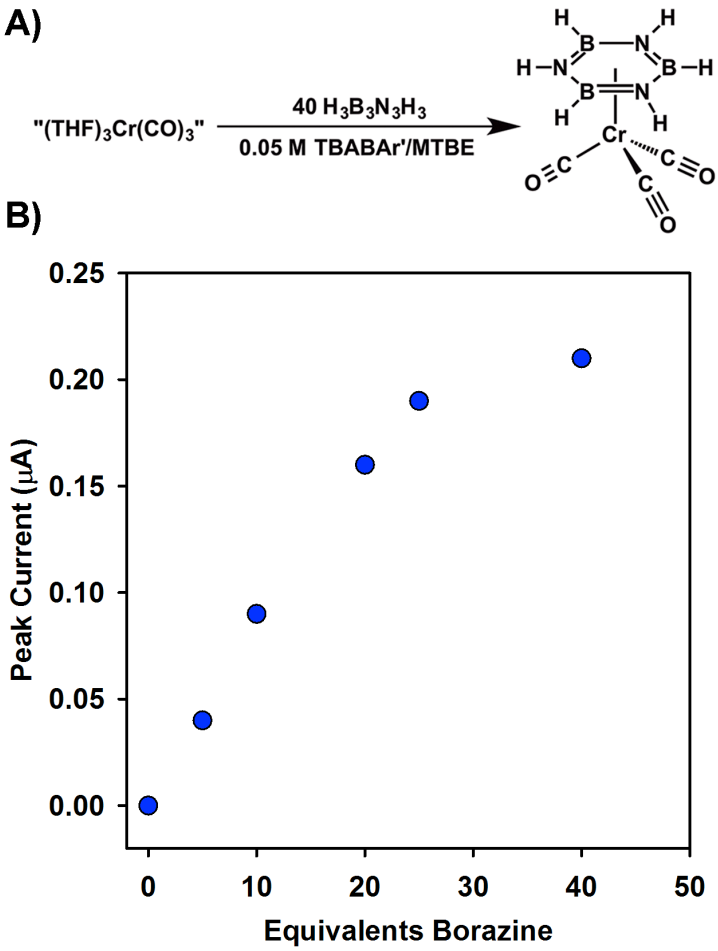

Figure 5-1. A) Synthetic scheme for titration of "$(THF)_3Cr(CO)_3$" (see appendix D section 2) with $H_3B_3N_3H_3$. B) Binding isotherm obtained by measuring normailized preak current of new oxidative wave at 0.25 V (vs. SCE) with respect to $H_3B_3N_3H_3$ concentration.

coordinated borazine, however, broadening due to rapid exchange is a likely explanation, as binding of natural borazine is expected to be very weak. Applying an alternative solution characterization method, with a shorter spectroscopic timescale than NMR, such as XANES, would therefore be an informative future study.

Though obtaining a coordination complex of natural borazine would be an impressive advance, it is not necessary to apply the results outlined in this thesis to hydrogen storage materials that would be useful in more limited applications. Indeed, if the reversible conversion of hexamethyl borazine to hexamethylcyclotriborazane could be realized, this would still constitute a hydrogen storage system with a capacity of 3.2 wt.% H_2. Additionally, these methods could easily be adapted for use on the materials proposed by Liu and coworkers which were discussed at the end of section 1.3.[6]

However, realizing successful metal-mediated regeneration of these B–N fuels requires the sequential reduction of multiple borazine B=N bonds, this remains unprecedented, and demonstration of a complete reduction cycle will therefore be instrumental in the future development of this methodology. Given that 1,2-H_2-borazines are predicted to be very unstable, step-wise stoichiometric reductions are unlikely to be successful. However, the kinetics of subsequent reductions in the vicinity of an electrode are likely to be rapid enough to allow these reactive intermediates to be intercepted.

As such, bulk electrolysis conducted on solutions of **1** or **2** in the presence of a proton source is a logical future direction. Unfortunately, proton reduction is the primary reaction observed when cyclic voltammetry is conducted on solutions of **1** or **2** with added proton sources. Additionally, bulk electrolysis conducted on an analogous solution of **2** did not yield any reduced borazine species. Given that hydride **4** can be readily synthesized by controlled potential electrolysis, the proton reduction background or potentially the instability of the 1,2-H_2-intermediate are the most likely explanation for the lack of desired reactivity. Determining which of these two detrimental side reactions is ultimately responsible for interfering with the bulk electrolysis will be key to assessing the viability of these metal complexes as electrocatalysts for the reduction of B–N spent fuels.

A promising approach to accomplish this is the use of novel electrode materials which feature a high proton reduction overpotential. Along these lines, we were intrigued by reports that hydrogen and fluorine terminated conductive diamond electrodes display very high proton reduction overpotentials with the latter possessing a 5 V potential window in aqueous solutions.[7] Unfortunately, only the non-surface terminated electrode is commercially available, and we were disappointed to find that the as-delivered electrode displayed comparable performance to a standard glassy carbon electrode when cyclic voltammetry was conducted on a solution of **2** with added $HOAc^F$ (Figure 5-2). Additionally, surface hydrogen or fluorine termination was not within the capabilities of facilities available at the University of Michigan. However, if an appropriately treated electrode could be obtained through collaboration with an external researcher or facility, the information gained by deconvoluting the reduction and protonation of **2** from the proton reduction background would prove invaluable for further

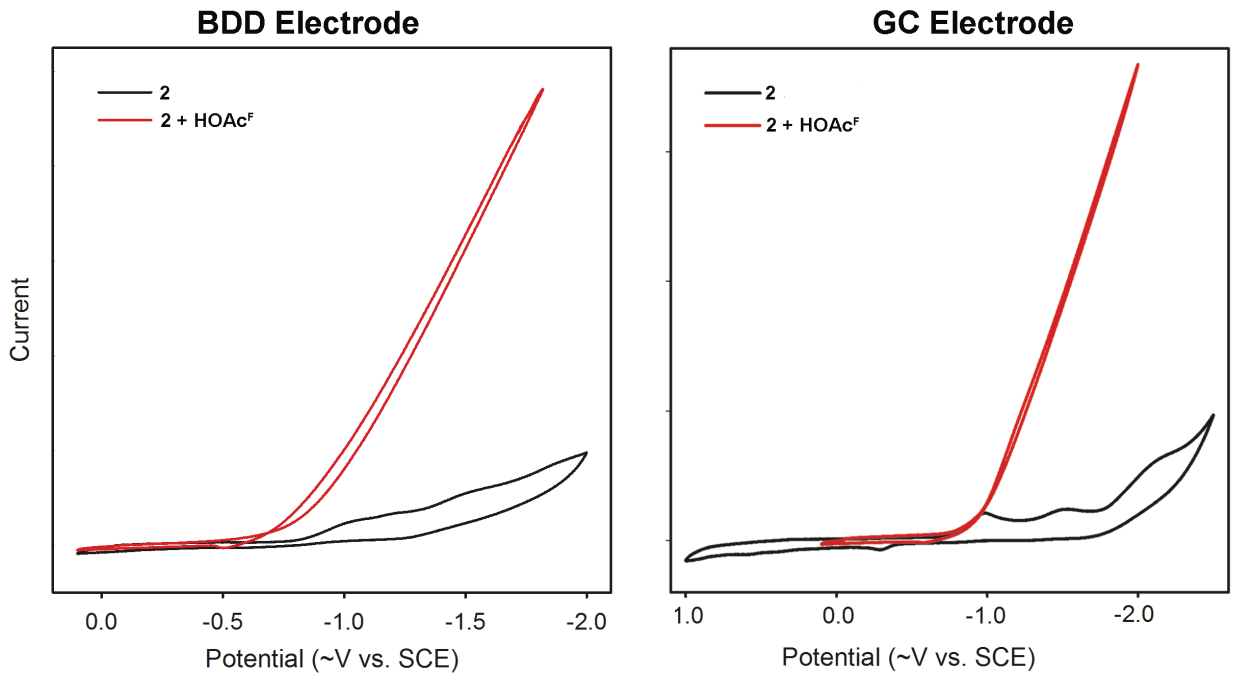

Figure 5-2. Cyclic voltammetry conducted on solutions of **2** and excess $HOAc^F$ using glassy carbon and boron doped diamond working electrodes, 0.1 M $^nBu_4NPF_6$/DCM.

extending this work to fully reducing borazines to CTBs.

This combined body of work conclusively demonstrates that metal coordination can be used as a strategy to activate borazines towards reductive transformations relevant to the regeneration of B–N hydrogen storage materials. The delivery of hydride equivalents to borazine by direct hydride addition, 2 e^- reduction and protonation, and 1 e^- reduction and H-atom transfer demonstrates the generality of this approach and constitutes and important advance as dearomatization by hydride addition is the thermodynamically most difficult step for borazine hydrogenation. Additionally, trapping of the putative intermediate ($(Me_4B_3N_3Me_3D)Cr(CO)_3$) to give the substituted CTB ($OAc^F{}_2Me_2B_3N_3Me_3D_3$), as well as the probable delivery of a single proton equivalent to **4** (see section 3.2), demonstrate that complete B=N bond reduction is feasible using this strategy. If future research is successful in demonstrating natural borazine coordination, and the reduction of multiple B=N bonds by applied potential, this work can be adapted to a general, low-energy, approach for the recycling of B–N spent fuels and would be a major contribution the field.

5.1 References

1) Carter, T. J.; Kampf, J. W.; Szymczak, N. K. *Angew. Chem. Int. ed.* **2012**, *51*, 13168.

2) Carter, T. J.; Wang, J. Y.; Szymczak, N. K. *Organometallics* **2014**, *33*, 1540.

3) Prinz, R.; Werner, H. *Angew. Chem. Int. ed.* **1967**, *6*, 91.

4) Wideman, T.; Fazen, P. J.; Lynch, A. T.; Su, K.; Remsen, E. E.; Sneddon, L. G.; Chen, T.; Paine, R. T. In *Inorganic Syntheses*; John Wiley & Sons, Inc.: 2007, p 232.

5) Calculations were prefromed by Professor Zachariah Heiden at Washington State University

6) Luo, W.; Campbell, P. G.; Zakharov, L. N.; Liu, S. Y. *J. Am. Chem. Soc.* **2011**, *133*, 19326.

7) Ferro, S.; De Battisti, A. *Anal. Chem.* **2003**, *75*, 7040.

Appendix A: Supporting Information Associated with Chapter 2

A.1 Additional Computational Information

Table A-1. Hydrogenation free energy values calculated using M06-2X and B3LYP functionals.

Compound	ΔG_{H-} for reaction with 3 H_2 (kcal/mol)	
	M06-2X	B3LYP
C_6H_6	-24.1	-13
$H_6B_3N_3$	40.8	27.8
$Me_3B_3N_3Me_3$	48.4	61.7

A.2 NMR Spectra

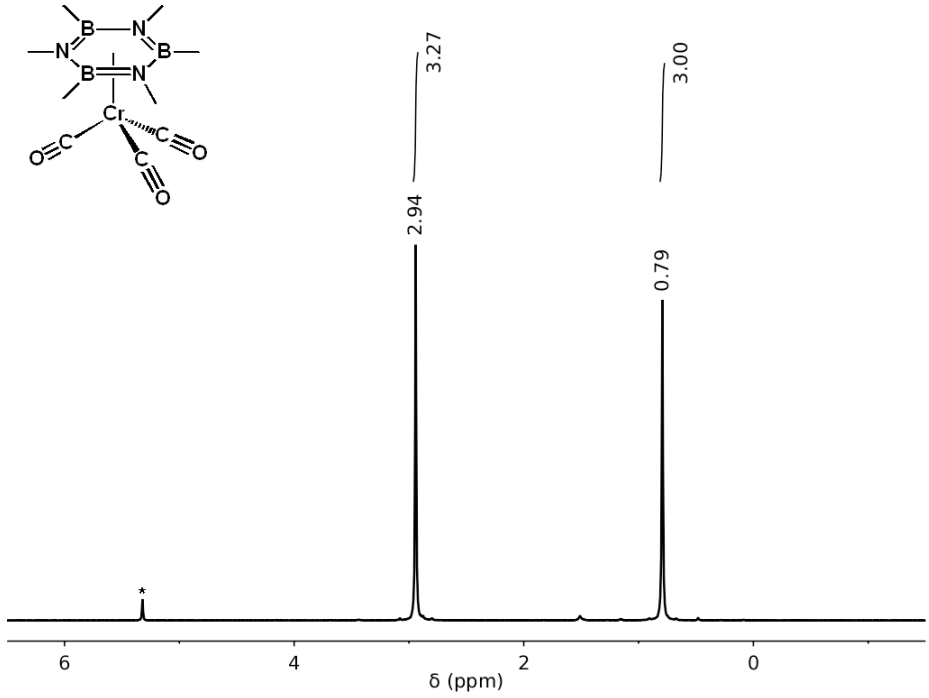

Figure A-1. ^{1}H NMR spectrum of **1**, 399.5 MHz, CD_2Cl_2.

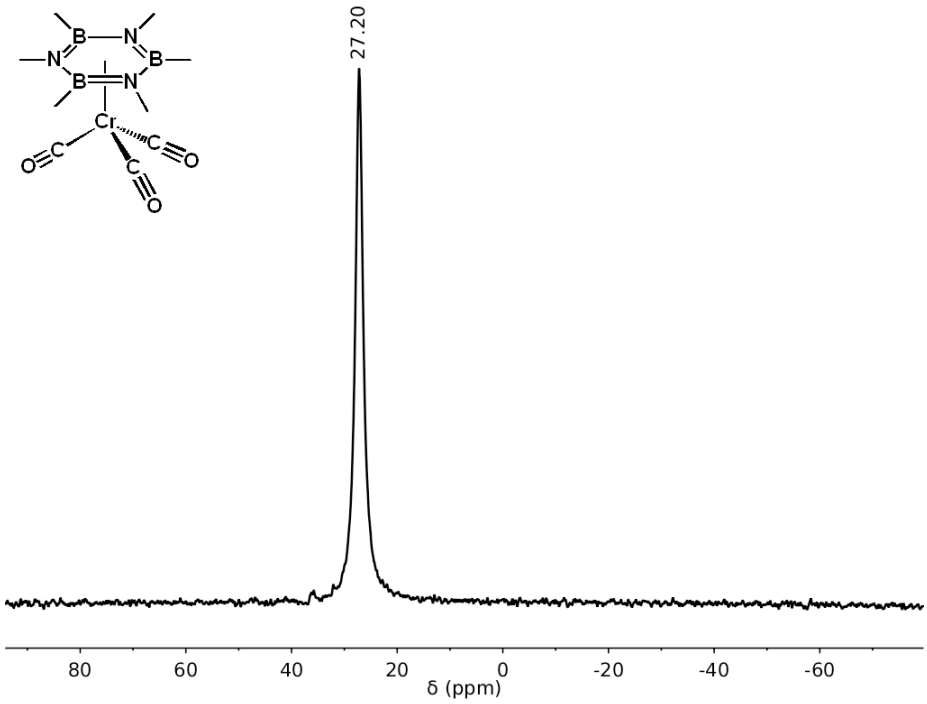

Figure A-2. ^{11}B NMR spectrum of **1**, 128.2 MHz, CD_2Cl_2.

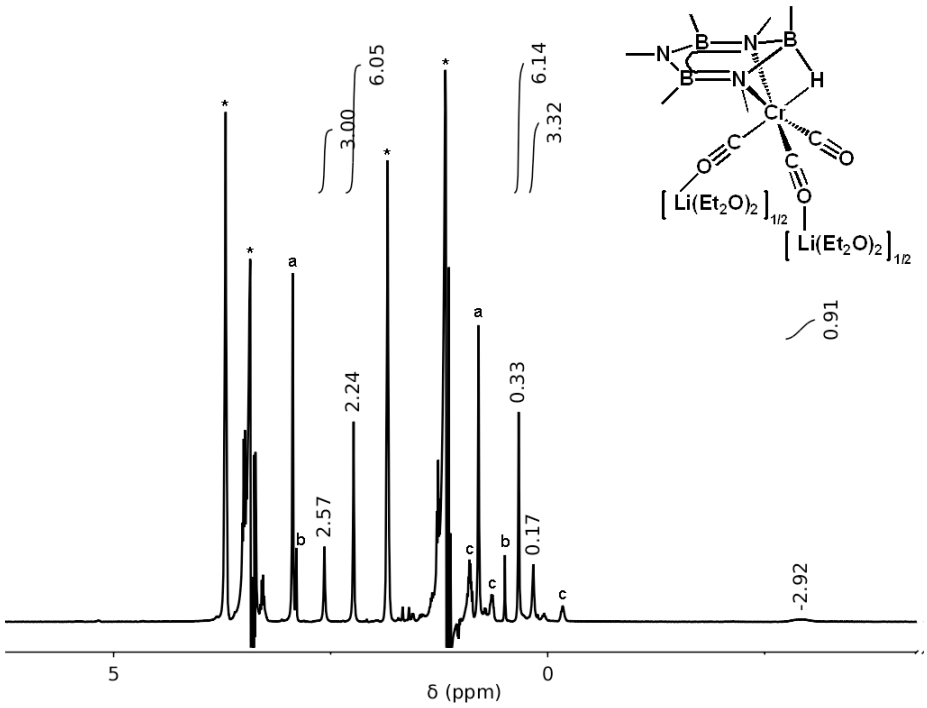

Figure A-3. Wet1D solvent supression ^1H NMR spectrum of reaction mixture containing **2**, 500.1 MHz, Diethyl ether. a) Unreacted 1 b) $Me_3B_3N_3Me_3$ c) Et_3B,[1] unreacted $LiEt_3BH$, and $LiEt_4B$ (impurity present in $LiEt_3BH$).

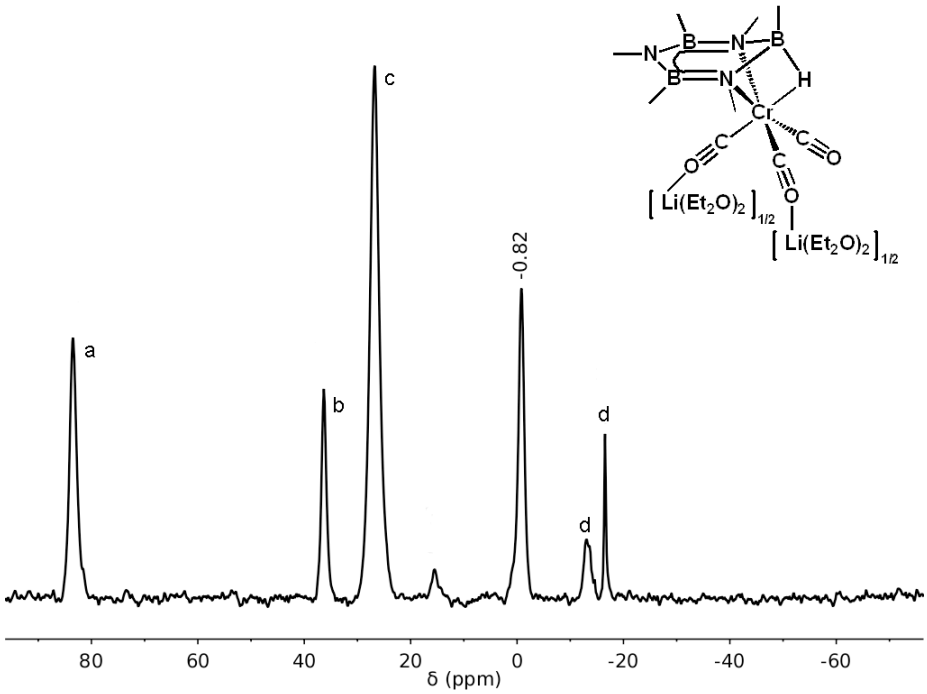

Figure A-4. ^{11}B NMR spectrum of reaction mixture containing **2**, 160.5 MHz, Diethyl ether. a) Et_3B[1] b) $Me_3B_3N_3Me_3$ c) Unreacted 1 d) Unreacted $LiEt_3BH$ and $LiEt_4B$ (impurity present in $LiEt_3BH$).

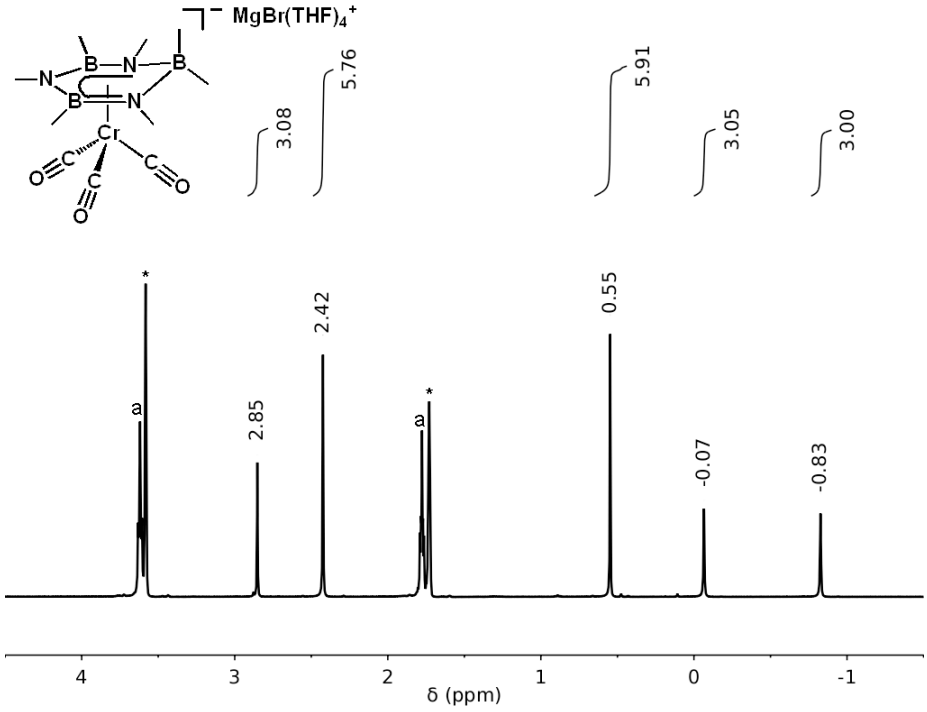

Figure A-5. ^1H NMR spectrum of **3**, 500.1 MHz, [D_8]THF. a) Protic THF associated with Mg^{2+} cation.

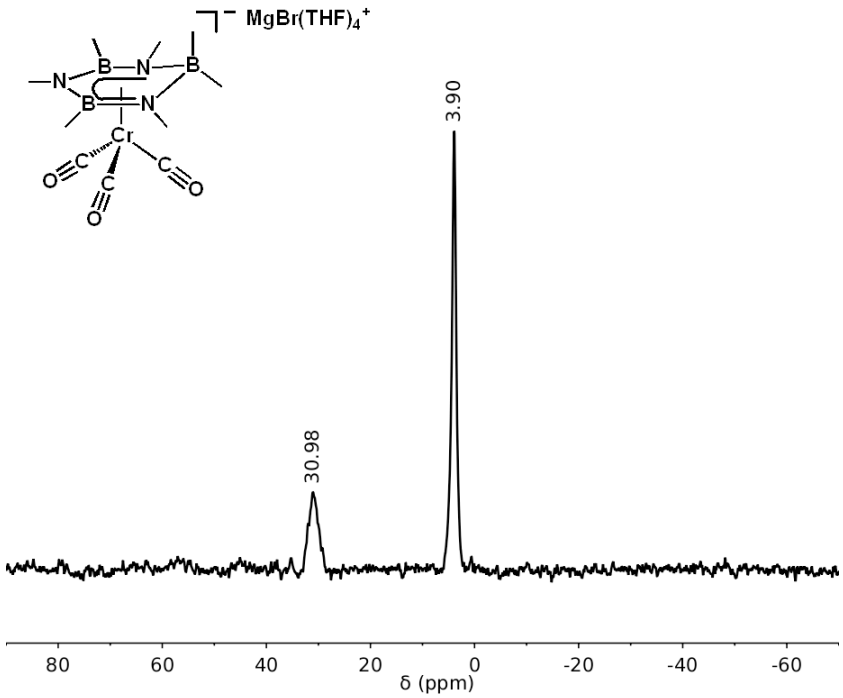

Figure A-6. ^{11}B NMR of **3**, 128.2 MHz, [D_8]THF.

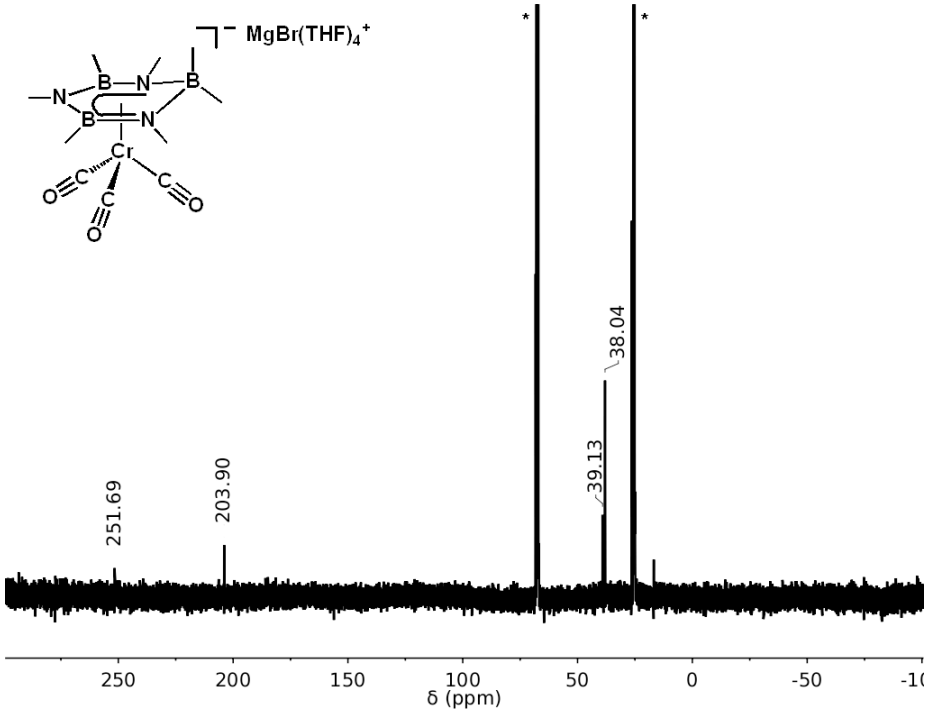

Figure A-7. ^{13}C NMR spectrum of **3**, 125.7 MHz, [D_8]THF.

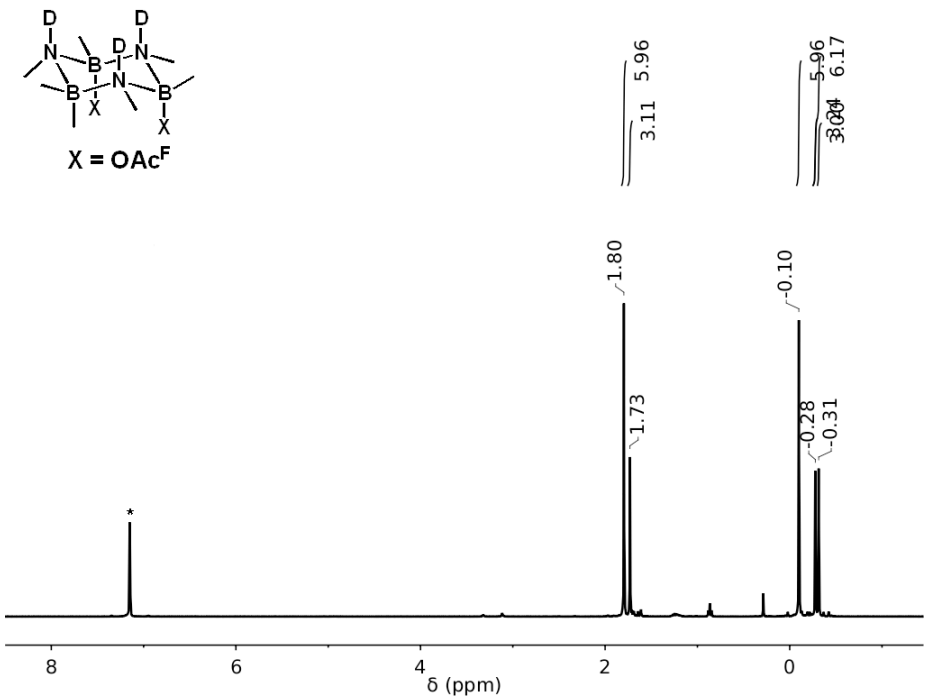

Figure A-8. ^{1}H NMR spectrum of **4**, 399.5 MHz, C_6D_6.

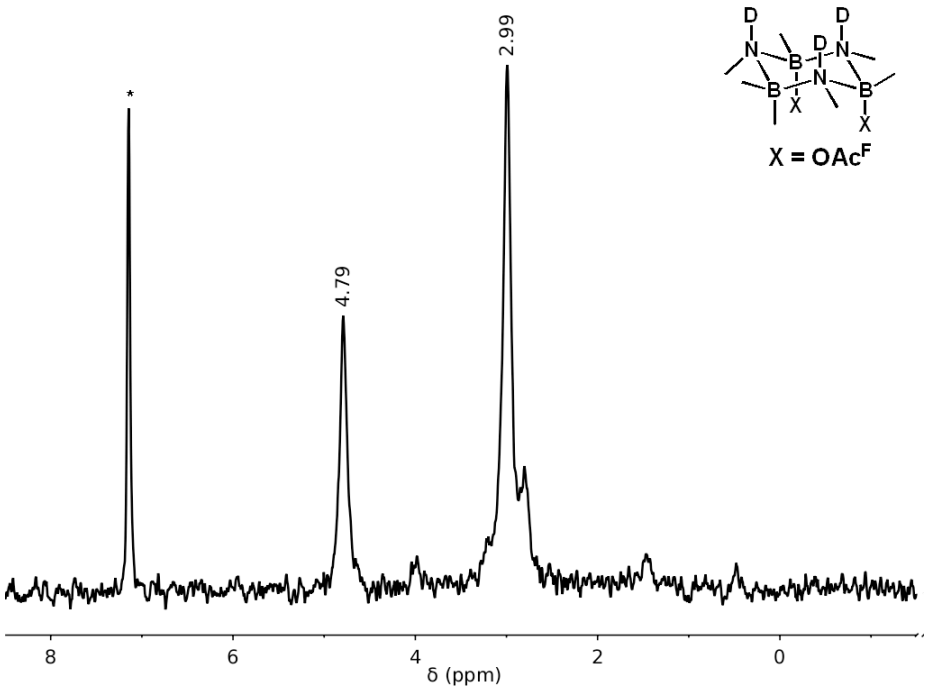

Figure A-9. ^{2}H NMR spectrum of **4**, 61.3 MHz, C_6D_6.

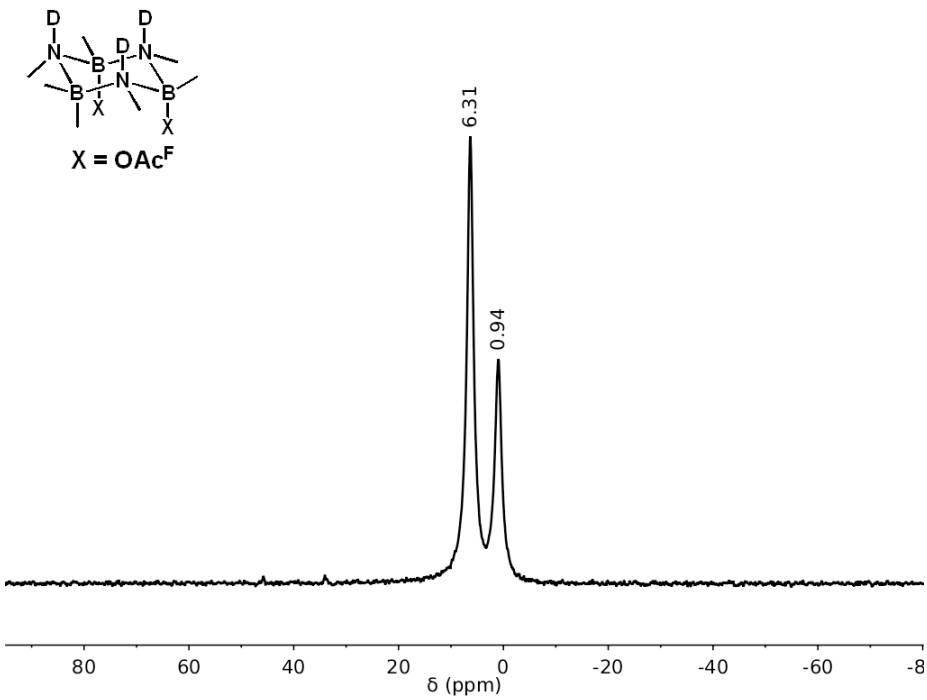

Figure A-10. ^{11}B NMR spectrum of **4**, 128.2 MHz, C_6D_6.

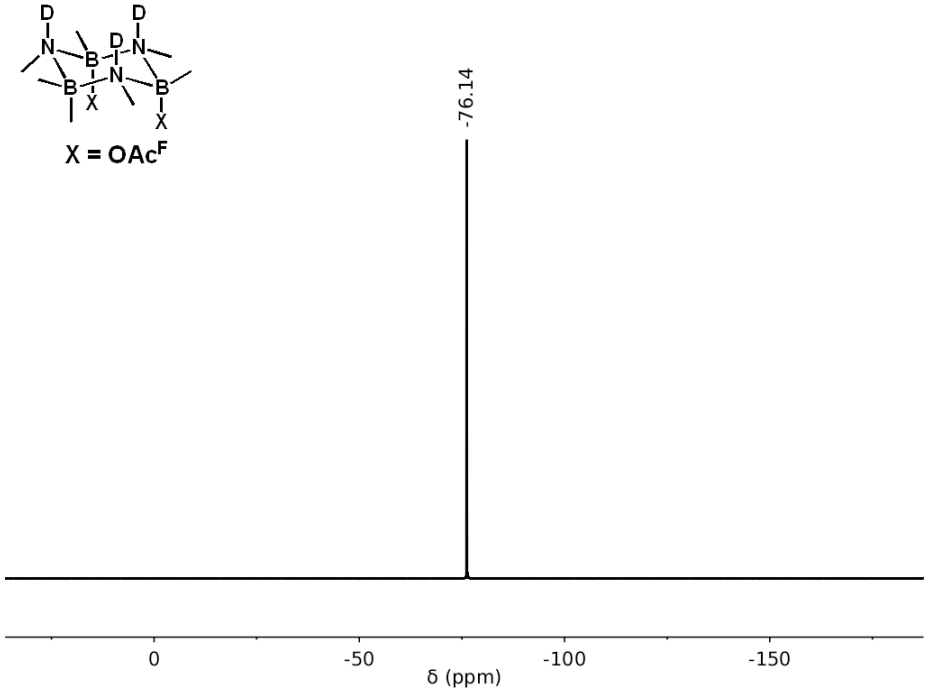

Figure A-11. ^{19}F NMR spectrum of **4**, 375.9 MHz, C_6D_6.

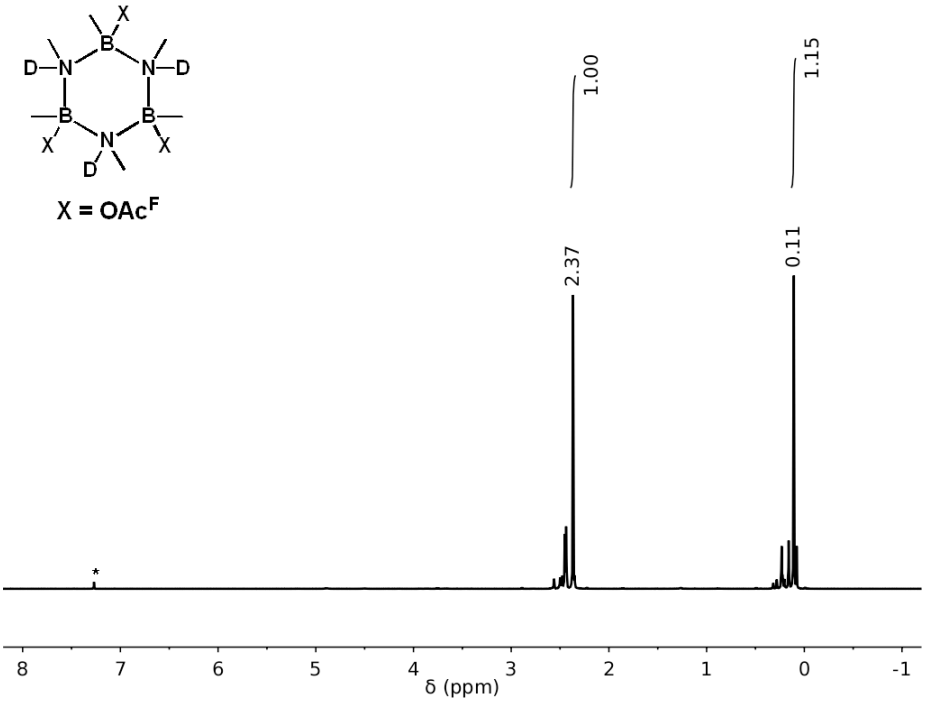

Figure A-12. ^{1}H NMR spectrum of **5** with major isomer labeled, 500.1 MHz, $CDCl_3$.

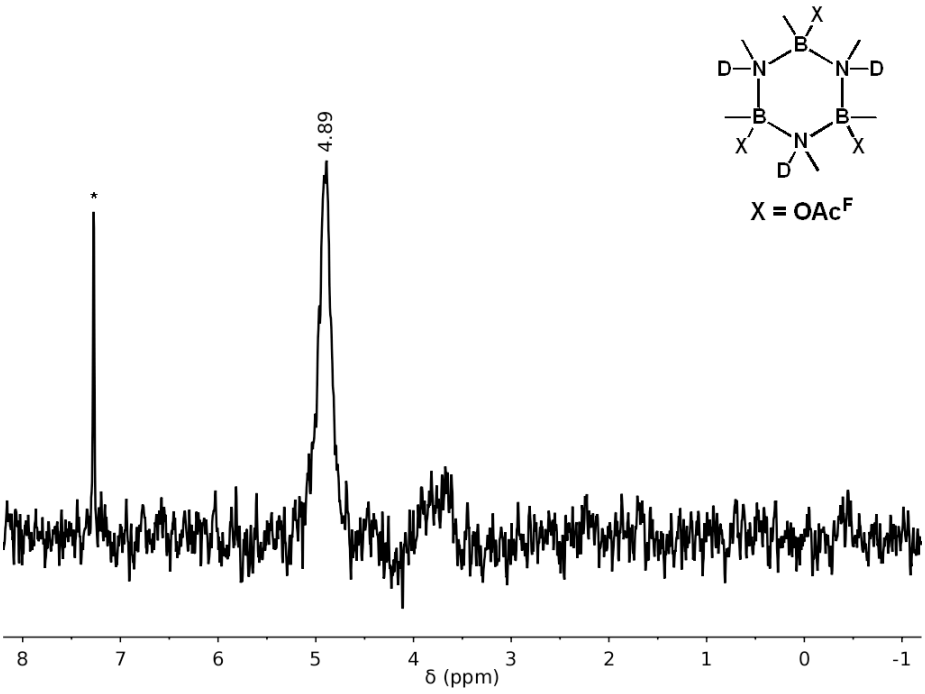

Figure A-13. ^{2}H NMR spectrum of **5**, 61.3 MHz, $CDCl_3$.

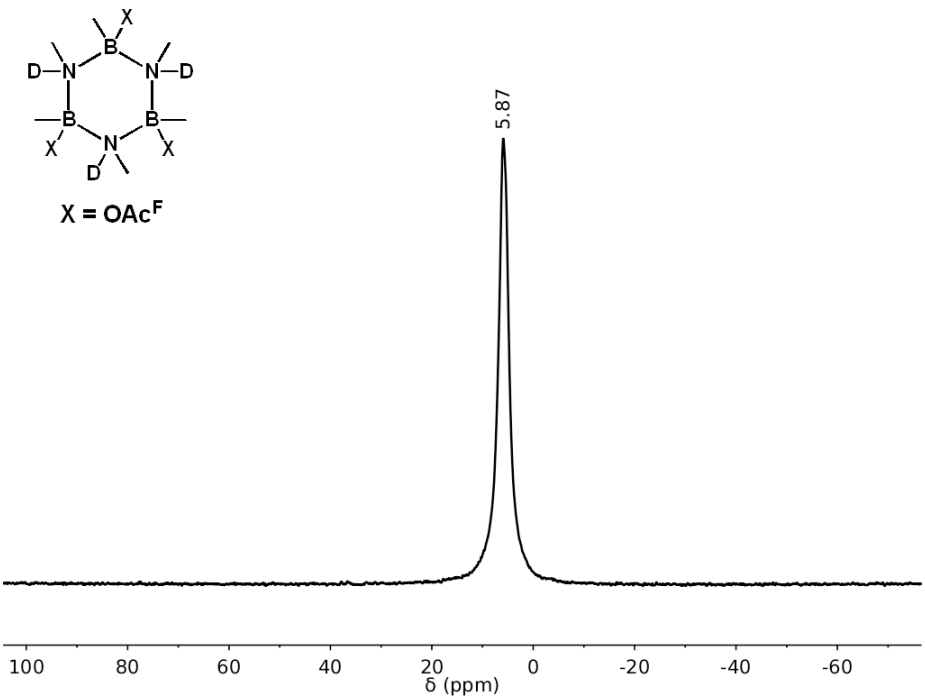

Figure A-14. ^{11}B NMR spectrum of **5**, 160.4 MHz, $CDCl_3$.

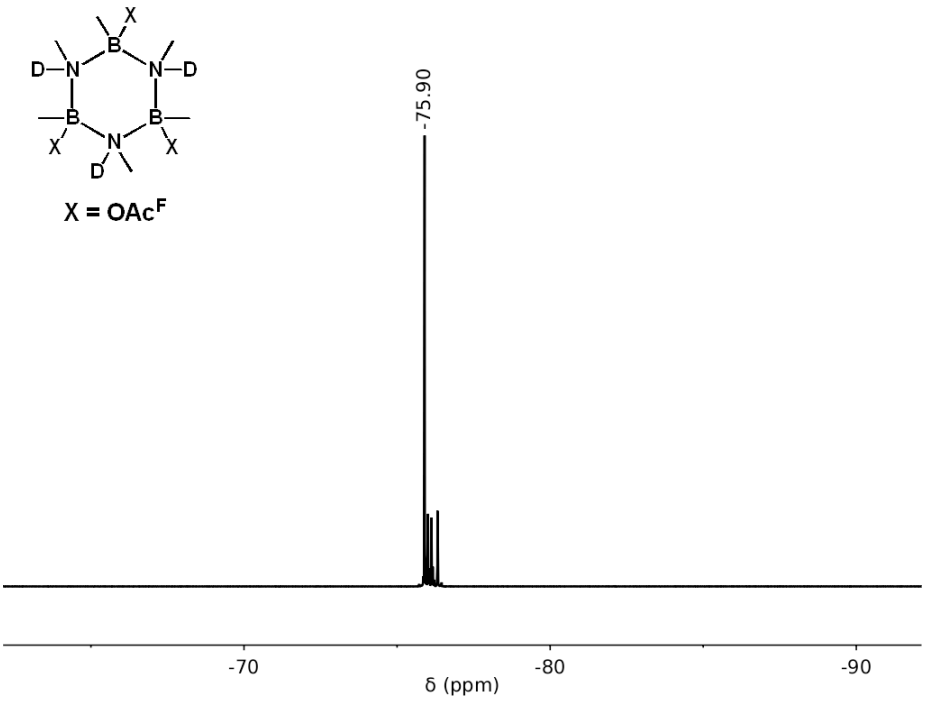

Figure A-15. ^{19}F NMR spectrum of **5** with major isomer labeled, 470.5 MHz, $CDCl_3$.

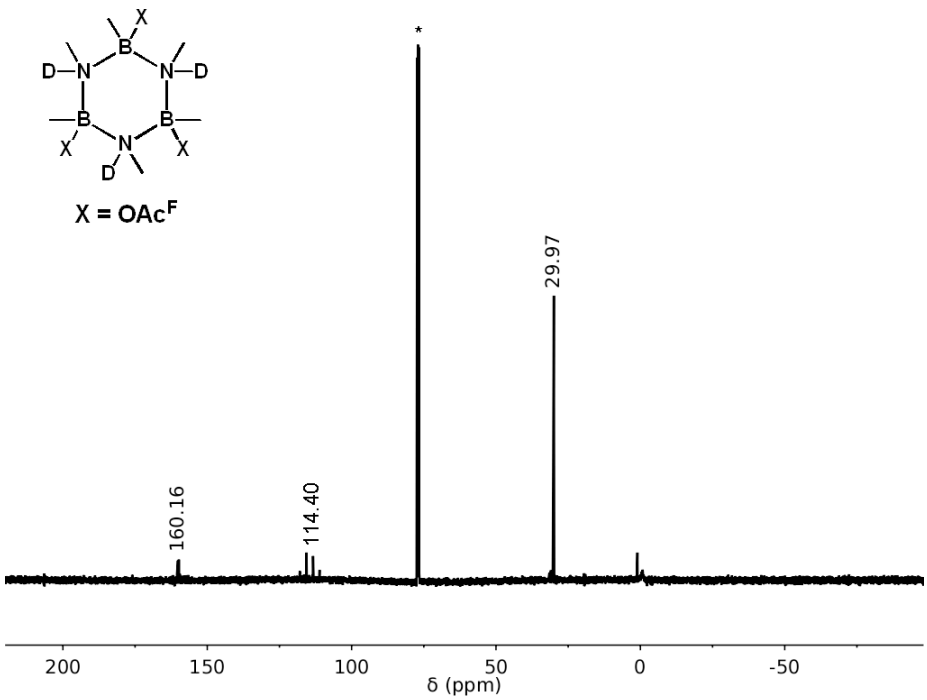

Figure A-16. ^{13}C NMR spectrum of **5**, 125.7 MHz, $CDCl_3$.

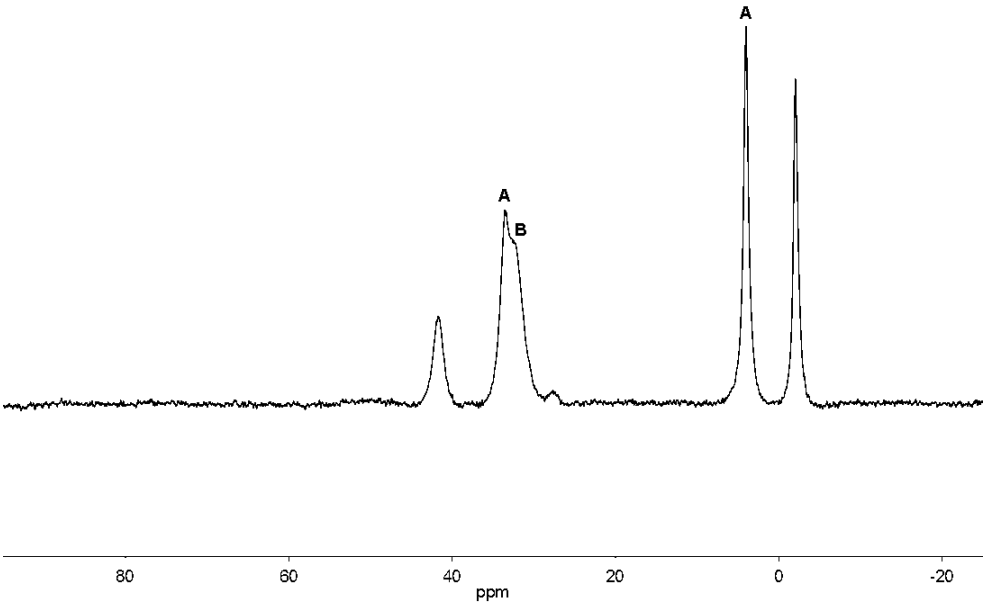

Figure A-17. ^{11}B NMR spectrum of solution following treatment of **3** with 50 equivalents TMSOTf, 160.4 MHz, DME. A) Unreacted **3**. B) Compound **1**.

A.3 IR Spectra

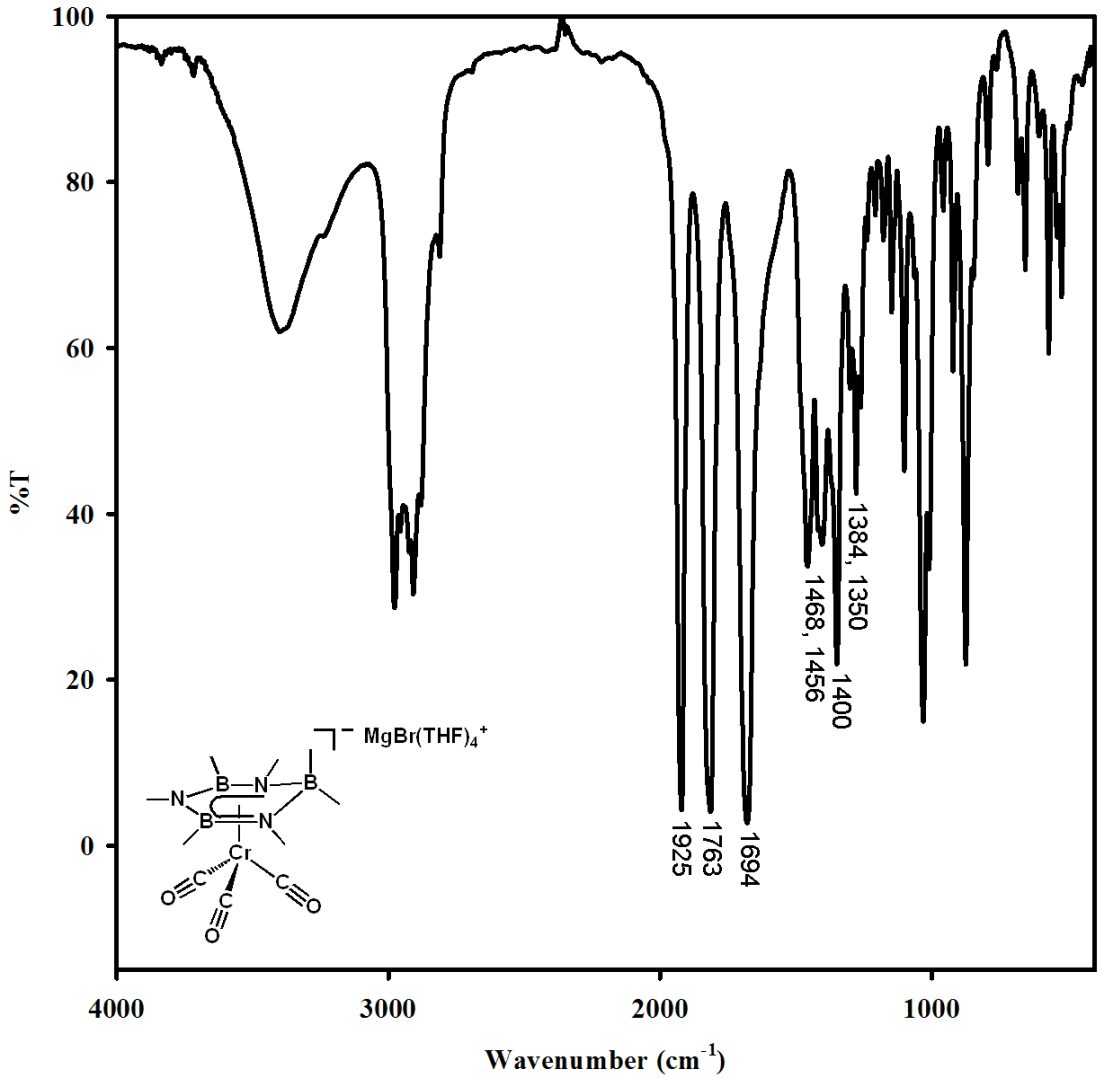

Figure A-18. IR spectrum of **3**, KBr pellet.

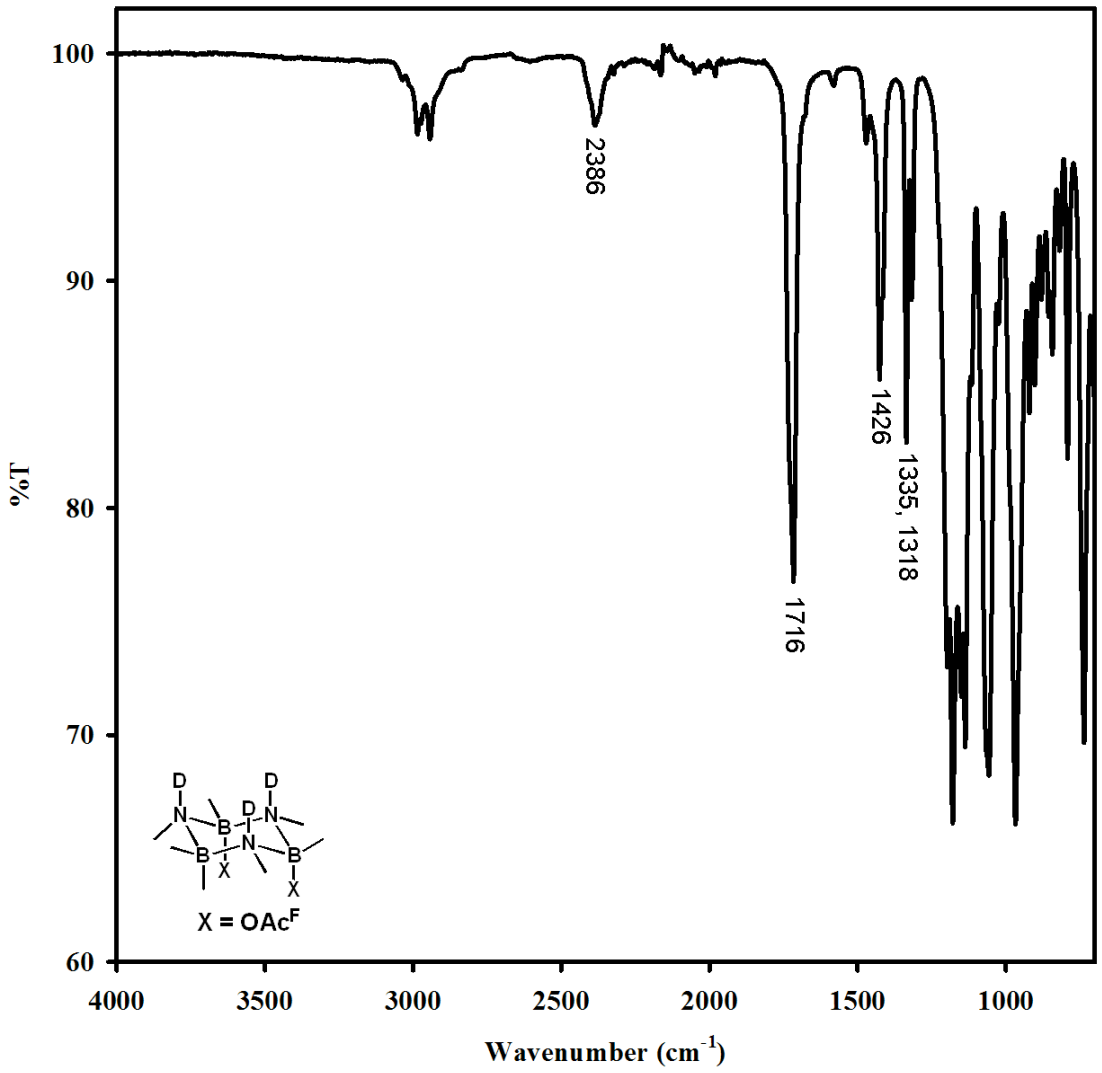

Figure A-19. IR spectrum of **4**, Diamond ATR accessory.

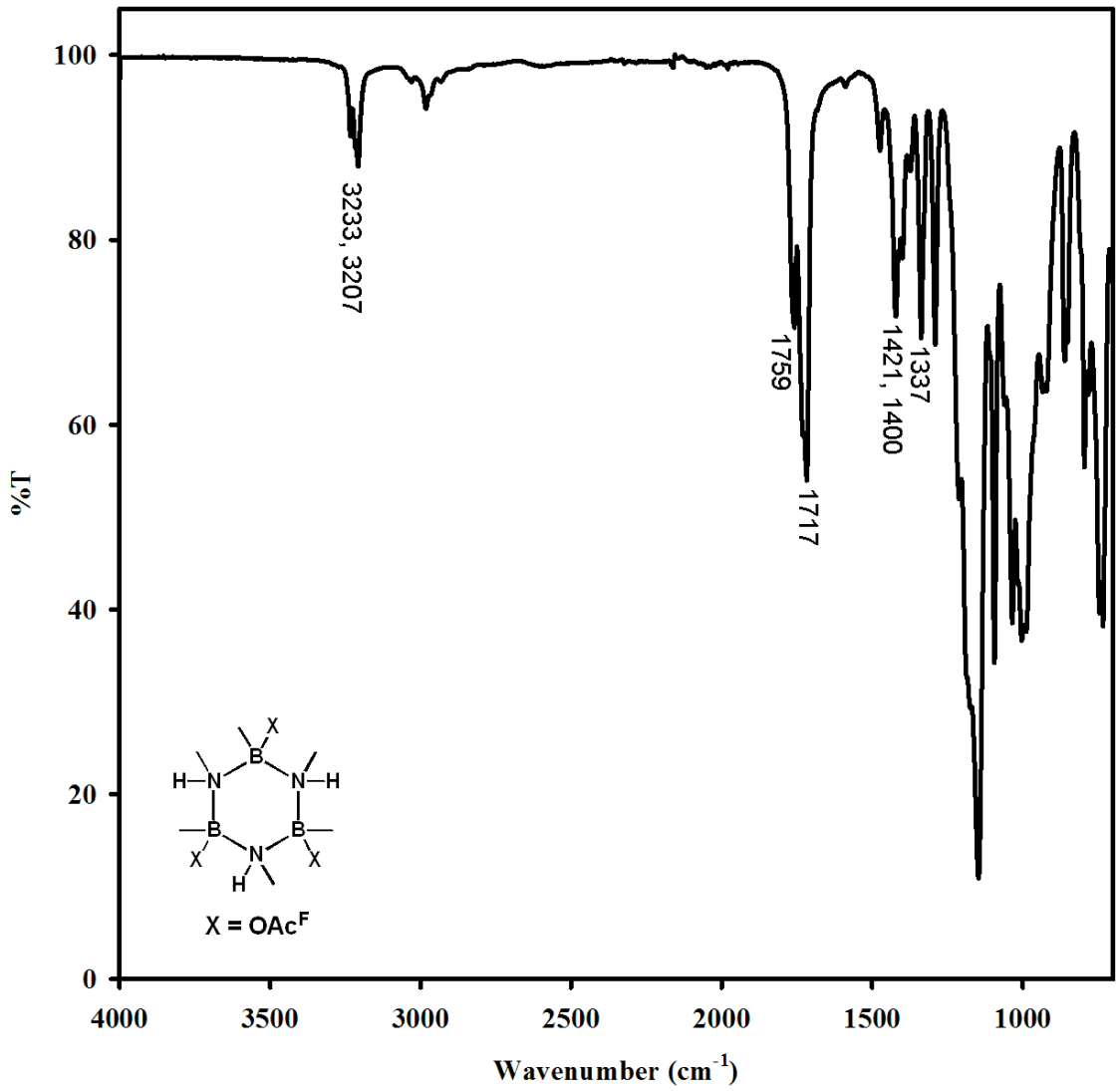

Figure A-20. IR spectrum of **5** (protic isotoplogue of **4**), Diamond ATR accessory.

A.4 Electrochemistry

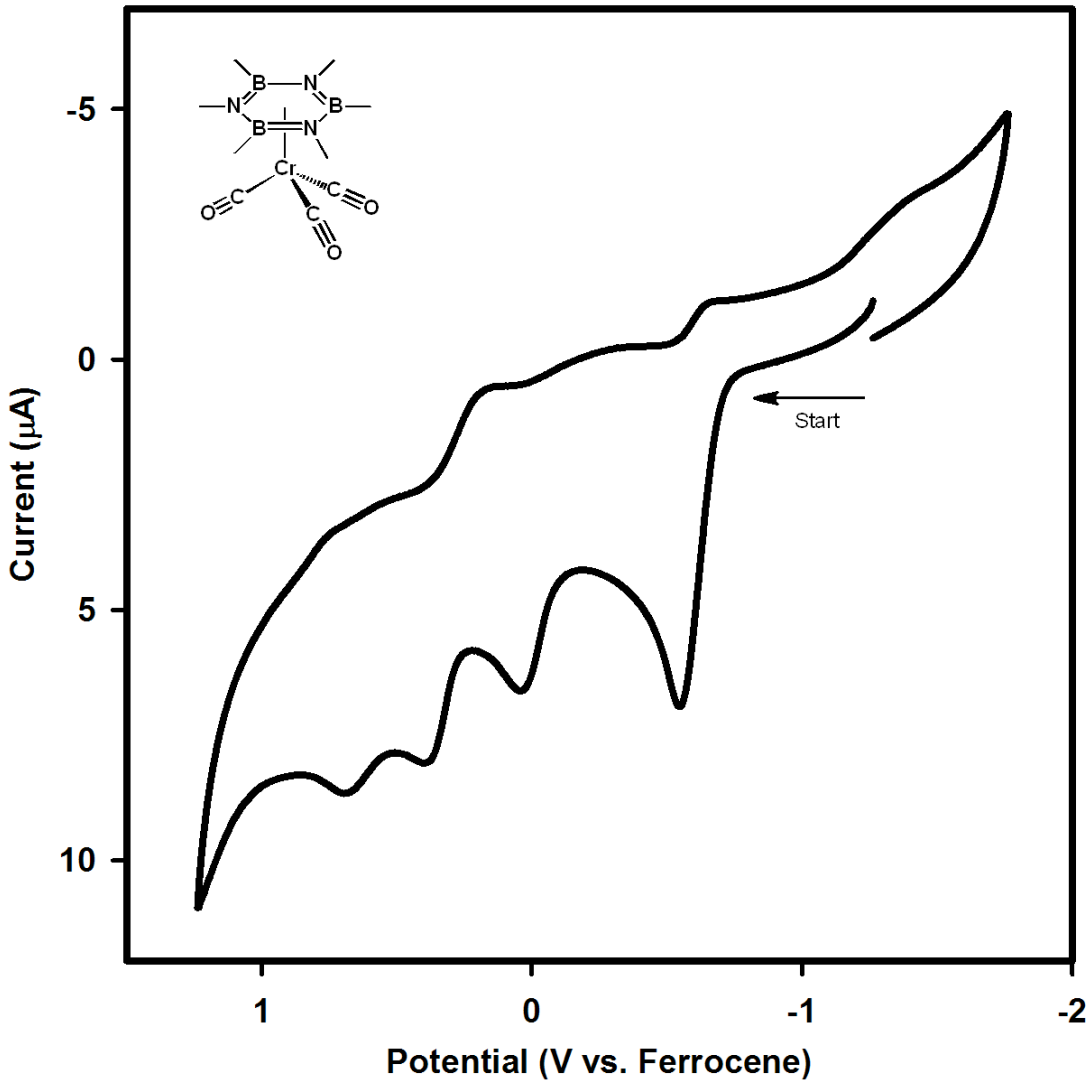

Figure A-21. Cyclic voltammagram of **1**, oxidative portion, 0.05 M $^{n}Bu_4NBAr'/Et_2O$.

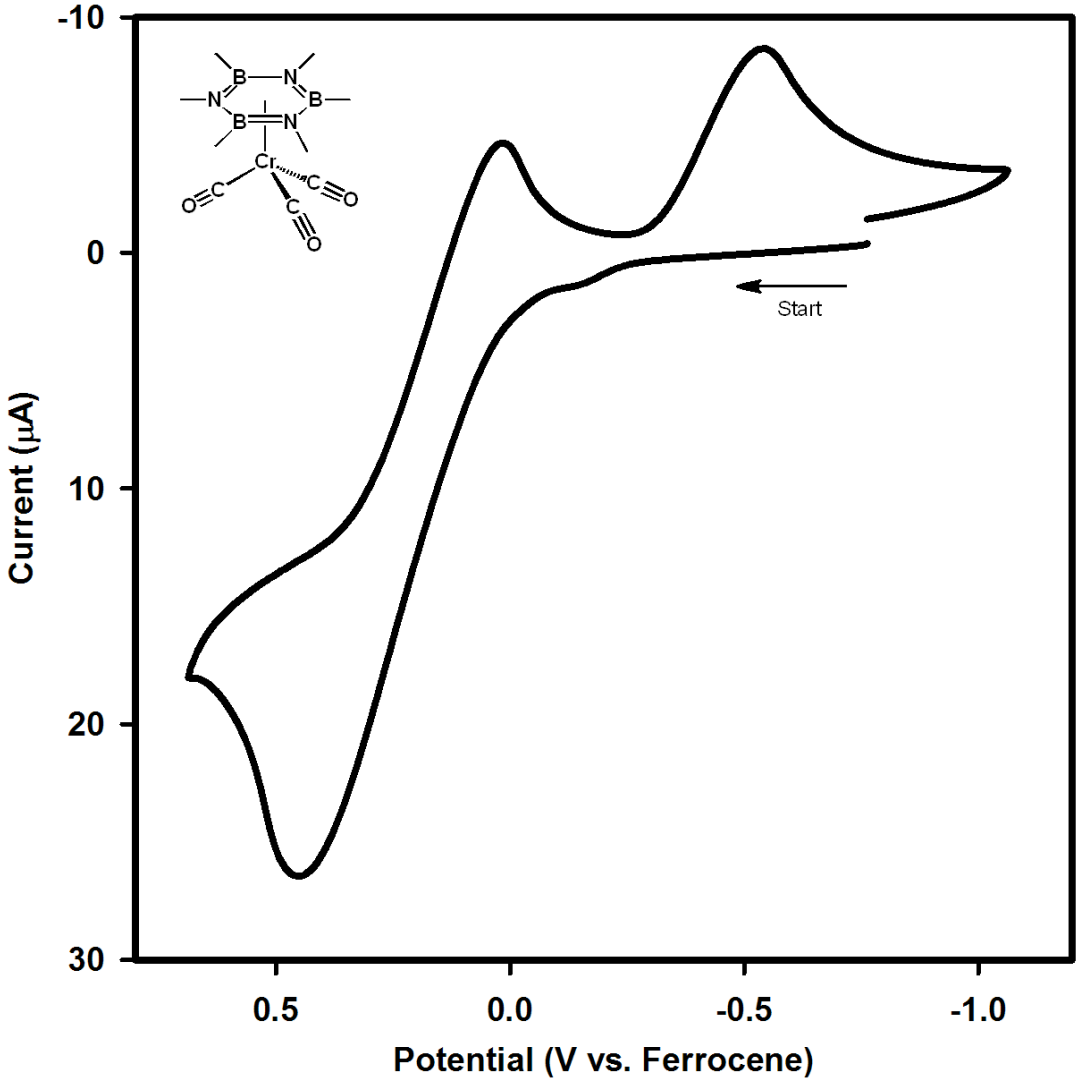

Figure A-22. Cyclic voltammagram of first oxidation of **1**, 0.05 M $^{n}Bu_4NBAr'/Et_2O$.

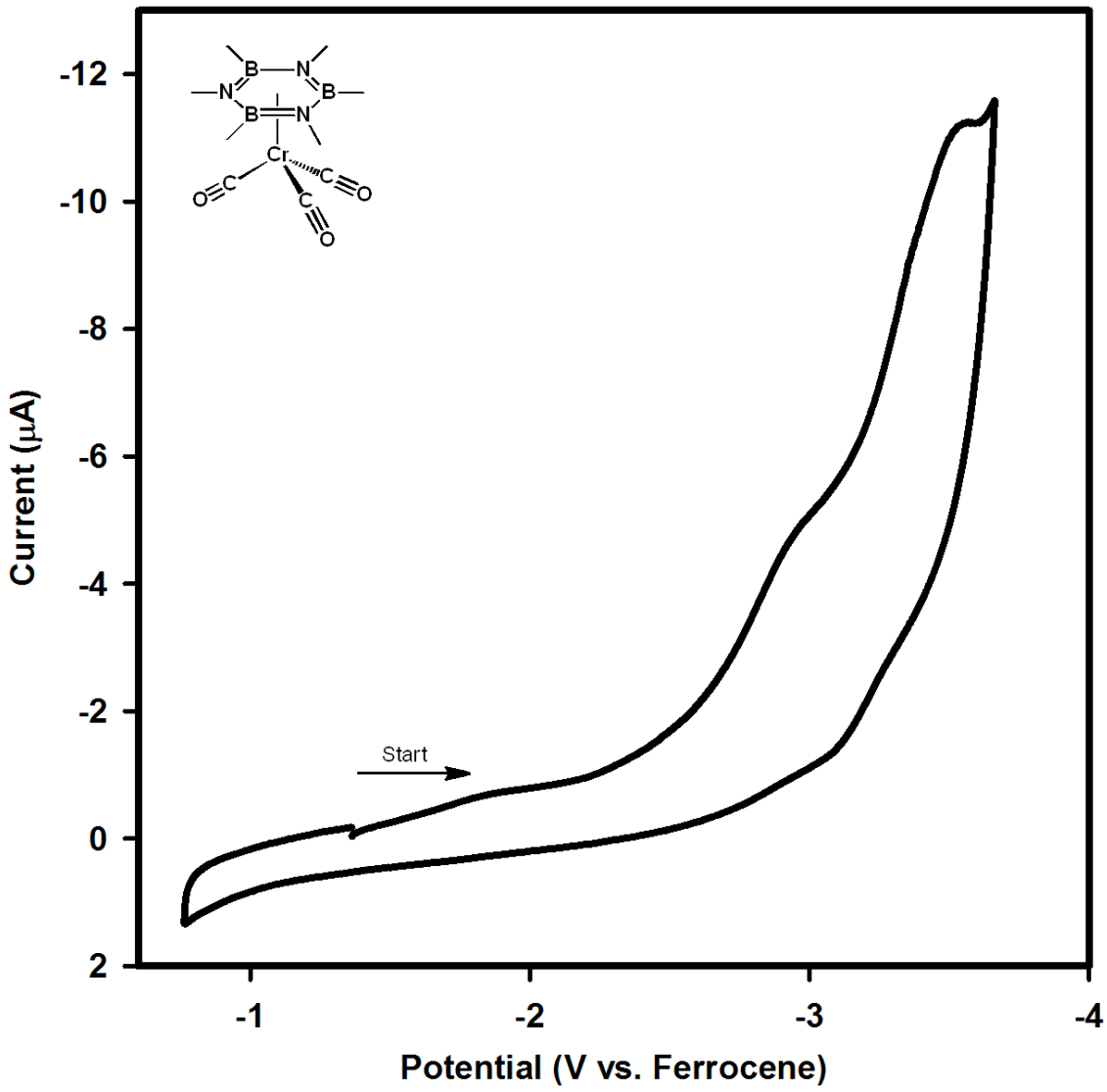

Figure A-23. Cyclic voltammagram of **1**, reductive portion, 0.05 V/s, 0.05 M $^{n}Bu_4NBAr'/Et_2O$.

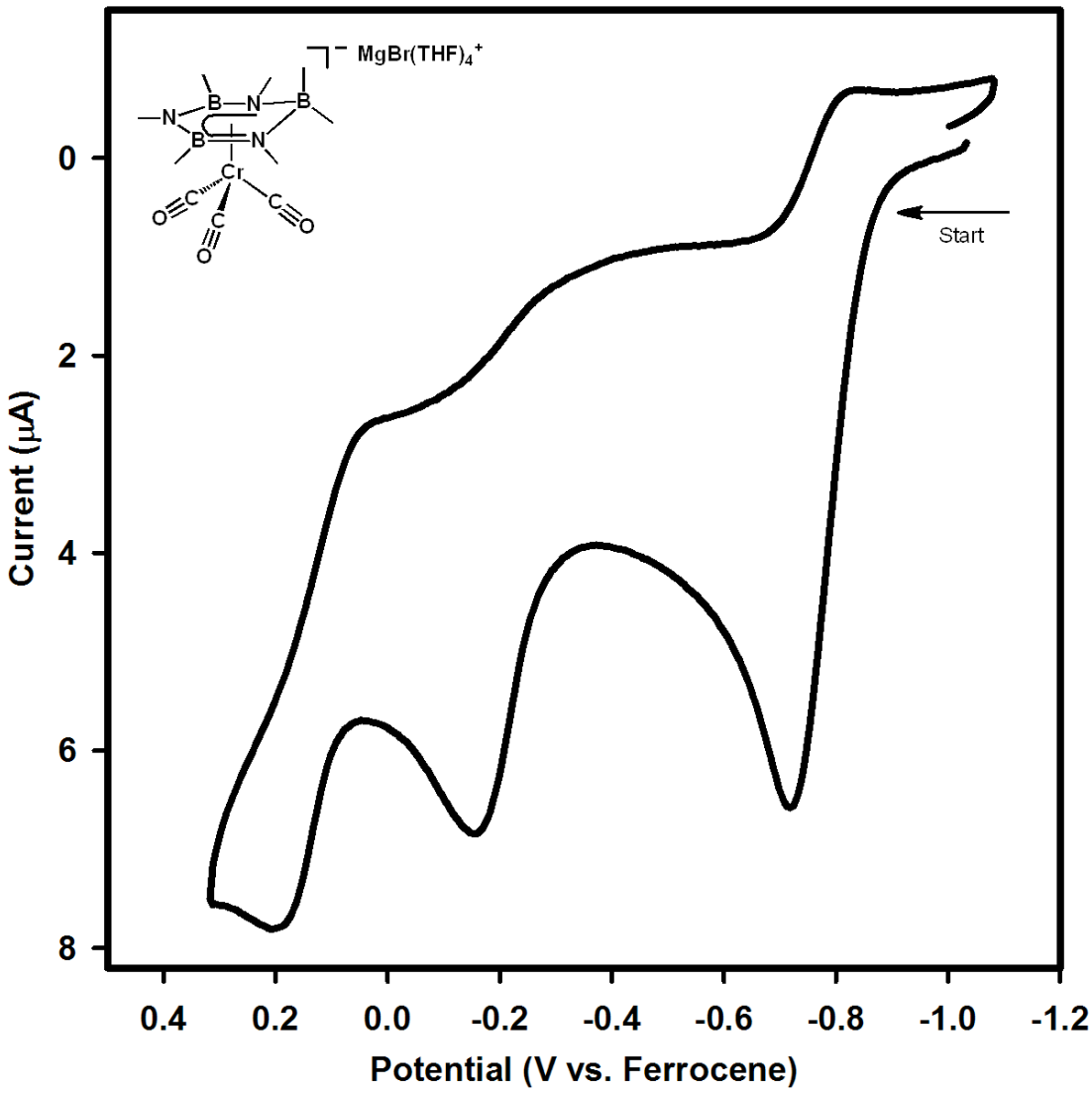

Figure A-24. Cyclic voltammagram of **2**, 0.05 M $^{n}Bu_4NBAr'$/1,2-dimethoxyethane.

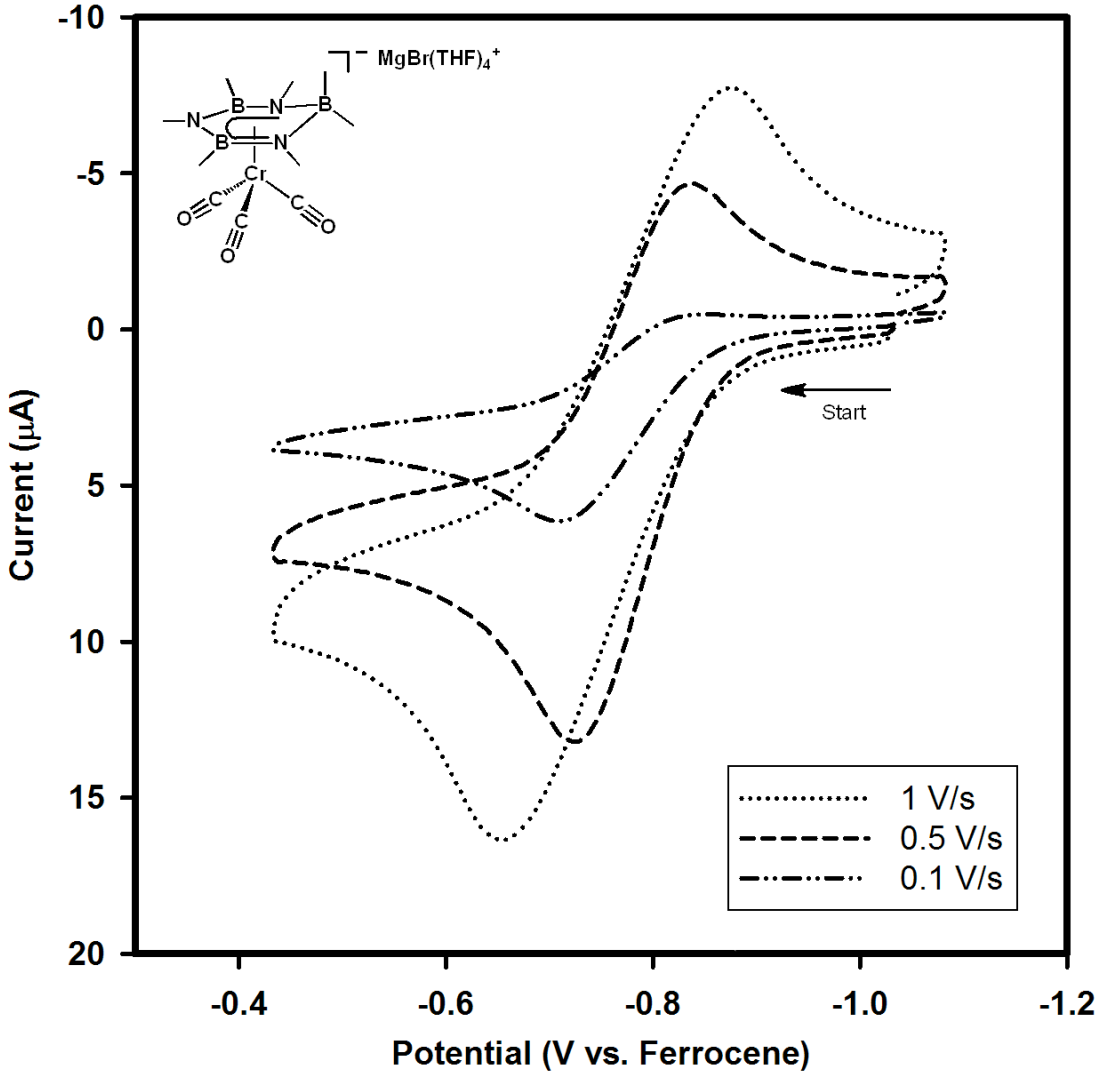

Figure A-25. Quasi-reversible oxidation of **2** at several scan rates, 0.05 M $^{n}Bu_4NBAr'$/1,2-dimethoxyethane

A.5 X-Ray Crystallographic Data

Structure Determination of 1: Orange needles of 1 were grown from a diethyl ether and pentane solution of the compound at –35 ºC. A crystal of dimensions 0.13 x 0.13 x 0.09 mm was mounted on a Rigaku AFC10K Saturn 944+ CCD-based X-ray diffractometer equipped with a low temperature device and Micromax-007HF Cu-target micro-focus rotating anode (λ = 1.54187 A) operated at 0.3 kW power (30 kV, 10 mA). The X-ray intensities were measured at 85(1) K with the detector placed at a distance 42.00 mm from the crystal. A total of 1014 images were collected with an oscillation width of 1.0° in ω. The exposure time was 15 sec. for the low angle images, 30 sec. for high angle. The integration of the data yielded a total of 21196 reflections to a maximum 2θ value of 136.48° of which 2654 were independent and 2477 were greater than 2σ(I). The final cell constants were based on the xyz centroids of 17109 reflections above 10σ(I). Analysis of the data showed negligible decay during data collection; the data were processed with CrystalClear 2.0[2] and corrected for absorption. The structure was solved and refined with the Bruker SHELXTL (version 2008/4) software package.[3] Refined formula: $C_9H_{18}B_3CrN_3O_3$, M_r = 300.69, Monoclinic, space group P2(1)/c, a = 8.6474(6), b = 25.7574(5), c = 7.1476(2) Å, α = 90, β = 114.412(8), γ = 90°, V = 1449.69(11) $Å^3$, Z = 4, ρ_{calcd} = 1.378 Mgm^{-3}, μ = 6.533 mm^{-1}, reflections collected: 21196, independent reflections: 2654 (Rint = 0.0674), Final R indicies [I > 2σ(I)]: R1 = 0.0401, wR2 = 0.1042, R indicies (all data): R1 = 0.0424, wR2 = 0.1066. The crystal was a pseudo-merohedral twin (1 0 1, 0 –1 0, 0 0 –1) and refined twin volume ratio 0.472(2). CIF file available under CCDC 895043.

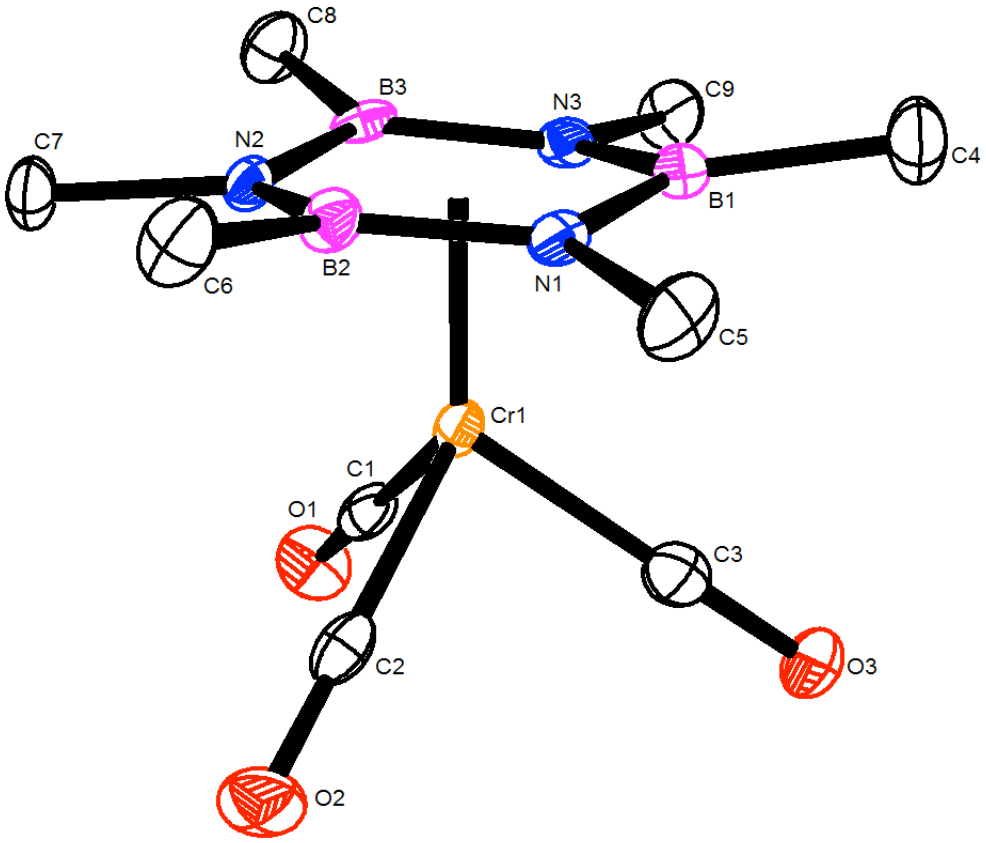

Figure A-26. Thermal ellipsoid plot of **1** shown at 50% probability. Hydrogens omitted for clarity.

Structure Determination of 2: Orange plates of 2 were grown from a diethyl ether and pentane solution of a reaction mixture containing the compound at –35 ºC. A crystal of dimensions 0.13 x 0.10 x 0.04 mm was mounted on a Rigaku AFC10K Saturn 944+ CCD-based X-ray diffractometer equipped with a low temperature device and Micromax-007HF Cu-target micro-focus rotating anode (λ = 1.54187 A) operated at 0.3 kW power (30 kV, 10 mA). The X-ray intensities were measured at 85(1) K with the detector placed at a distance 42.00 mm from the crystal. A total of 1493 images were collected with an oscillation width of 2.0° in ω. The exposure time was 20 sec. for the low angle images, 35 sec. for high angle. The integration of the data yielded a total of 26770 reflections to a maximum 2θ value of 136.40° of which 4605 were independent and 4303 were greater than 2σ(I). The final cell constants were based on the xyz centroids 14740 reflections above 10σ(I). Analysis of the data showed negligible decay during data collection; the data were processed with CrystalClear 2.0[2] and corrected for absorption. The structure was solved and refined with the Bruker SHELXTL (version 2008/4) software package.[3] Refined Formula: $C_{34}H_{78}B_6Cr_2Li_2N_6O_{10}$, M_r = 913.76, Triclinic, space group P1bar, a = 10.4686(2), b = 10.6651(2), c = 12.9445(9) Å, α = 70.204, β = 83.211, γ = 70.904°, V = 1284.96(10) $Å^3$, Z = 1, ρ_{calcd} = 1.181 Mgm^{-3}, μ = 3.895 mm^{-1}, reflections collected: 26770, independent reflections: 4605 (Rint = 0.0605), Final R indicies [I > 2σ(I)]: R1 = 0.0475, wR2 = 0.1172, R indicies (all data): R1 = 0.0500, wR2 = 0.1192. CIF file available under CCDC 895042.

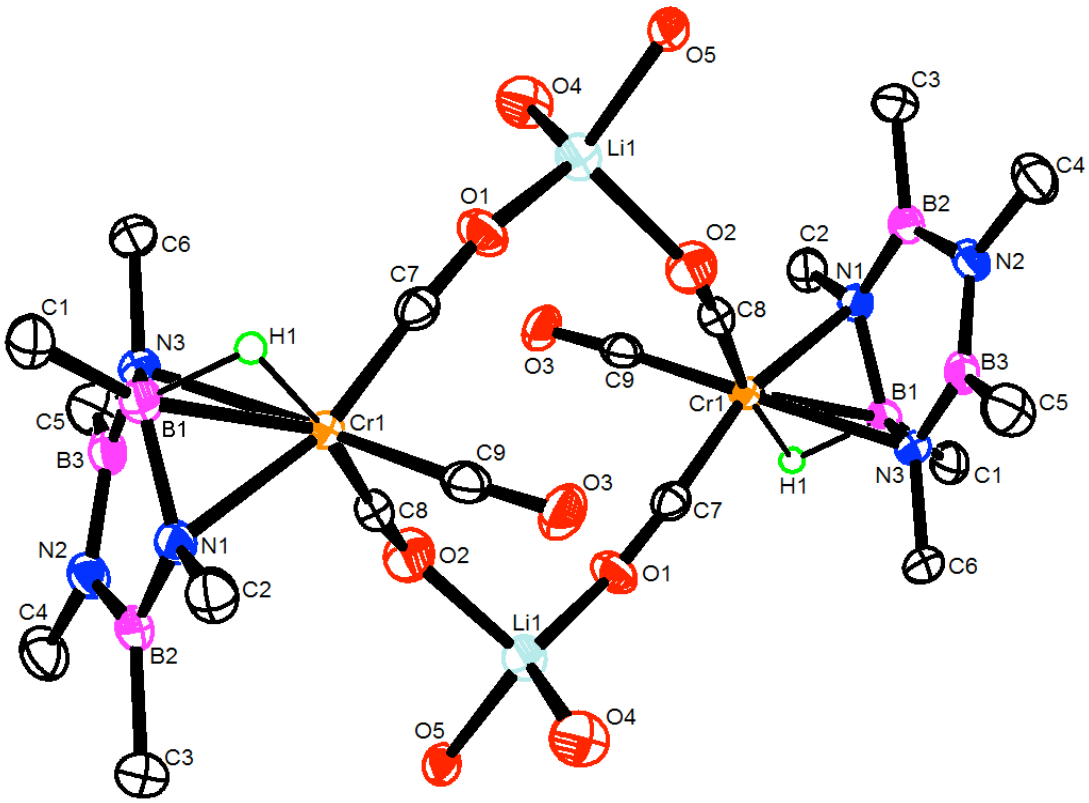

Figure A-27. Thermal ellipsoid plot of **2** shown at 50% probability. Hydrogens and carbons attached to diethyl ether solvent molecules (O4 and O5) have been omitted for clarity

Structure Determination of 3: Yellow plates of 3 were grown from a tetrahydrofuran/pentane solution of the compound at 24 ºC. A crystal of dimensions 0.14 x 0.13 x 0.12 mm was mounted on a Rigaku AFC10K Saturn 944+ CCD-based X-ray diffractometer equipped with a low temperature device and Micromax-007HF Cu-target micro-focus rotating anode (λ = 1.54187 A) operated at 1.2 kW power (40 kV, 30 mA). The X-ray intensities were measured at 85(1) K with the detector placed at a distance 42.00 mm from the crystal. A total of 3753 images were collected with an oscillation width of 1.0° in ω The exposure time was 1 sec. for the low angle images, 4 sec. for high angle. The integration of the data yielded a total of 91823 reflections to a maximum 2θ value of 136.46° of which 6464 were independent and 6153 were greater than 2σ(I). The final cell constants were based on the xyz centroids 61306 reflections above 10σ(I). Analysis of the data showed negligible decay during data collection; the data were processed with CrystalClear 2.0[2] and corrected for absorption. The structure was solved and refined with the Bruker SHELXTL (version 2008/4) software package.[3] Refined Formula:$C_{26}H_{53}B_3BrCrMgN_3O_7$, M_r = 708.36, Monoclinic, space group C2/c, a = 17.1605(3), b = 17.7737(3), c = 23.9599(17) Å, α = 90, β = 104.678(7), γ = 90°, V = 7096.4(5) $Å^3$, Z = 8, ρ_{calcd} = 1.331 Mgm^{-3}, μ = 4.510 mm^{-1}, reflections collected: 91823, independent reflections: 6464 (Rint = 0.0919), Final R indicies [I > 2σ(I)]: R1 = 0.0558, wR2 = 0.1416, R indicies (all data): R1 = 0.0572, wR2 = 0.1427. The borazine and tetrahydrofuran ligands show conformational disorder. CIF file available under CCDC 895044.

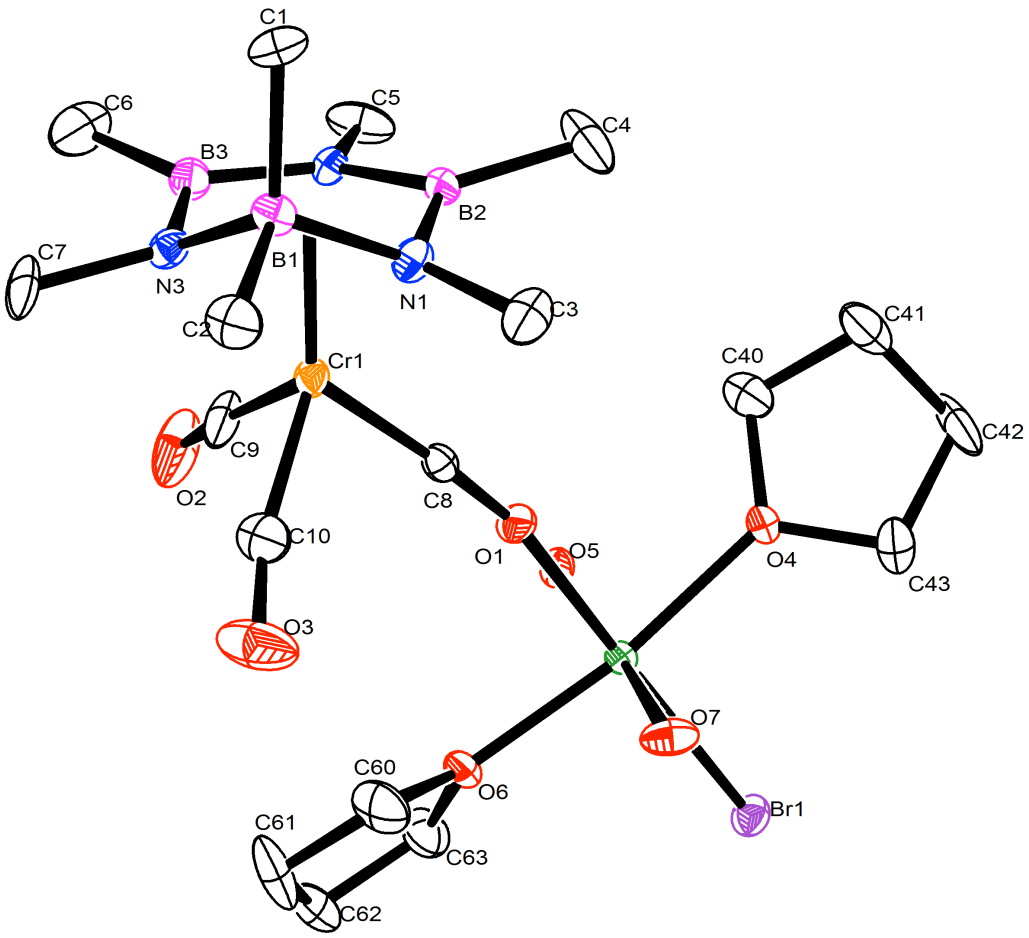

Figure A-28. Thermal ellipsoid plot of **3** shown at 50% probability. Two THF solvent molecules (containing O5 and O7) have been truncated for clarity. Also, hydrogens and alternative orientations of atoms exhibiting conformational disorder have removed.

Structure Determination of 4: Colorless plates of 4 were grown from a pentane solution of the compound at –35 ºC. A crystal of dimensions 0.14 x 0.10 x 0.10 mm was mounted on a Rigaku AFC10K Saturn 944+ CCD-based X-ray diffractometer equipped with a low temperature device and Micromax-007HF Cu-target micro-focus rotating anode (λ = 1.54187 A) operated at 0.2 kW power (20 kV, 10 mA). The X-ray intensities were measured at 85(1) K with the detector placed at a distance 42.00 mm from the crystal. A total of 3897 images were collected with an oscillation width of 1.0° in ω The exposure time was 4 sec. for the low angle images, 8 sec. for high angle. The integration of the data yielded a total of 22060 reflections to a maximum 2θ value of 136.44° of which 3372 were independent and 2904 were greater than 2σ(I). The final cell constants were based on the xyz centroids 12519 reflections above 10σ(I). Analysis of the data showed negligible decay during data collection; the data were processed with CrystalClear 2.0[2] and corrected for absorption. The structure was solved and refined with the Bruker SHELXTL (version 2008/4) software package.[3] Refined Formula: $C_{11}H_{21}B_3CrD_3F_6N_3O_4$, M_r = 411.78, Orthorhombic, space group Pbca, a = 16.7286(12), b = 12.9871(2), c = 16.9917(3) Å, α = 90, β = 90, γ = 90°, V = 3691.5(3) $Å^3$, Z = 8, ρ_{calcd} = 1.482 Mgm^{-3}, μ = 1.268 mm^{-1}, reflections collected: 22060, independent reflections: 3372 (Rint = 0.0518), Final R indicies [I > 2σ(I)]: R1 = 0.0479, wR2 = 0.1196, R indicies (all data): R1 = 0.0536, wR2 = 0.1241. The CF_3 substituents show conformational disorder. CIF file available under CCDC 895045.

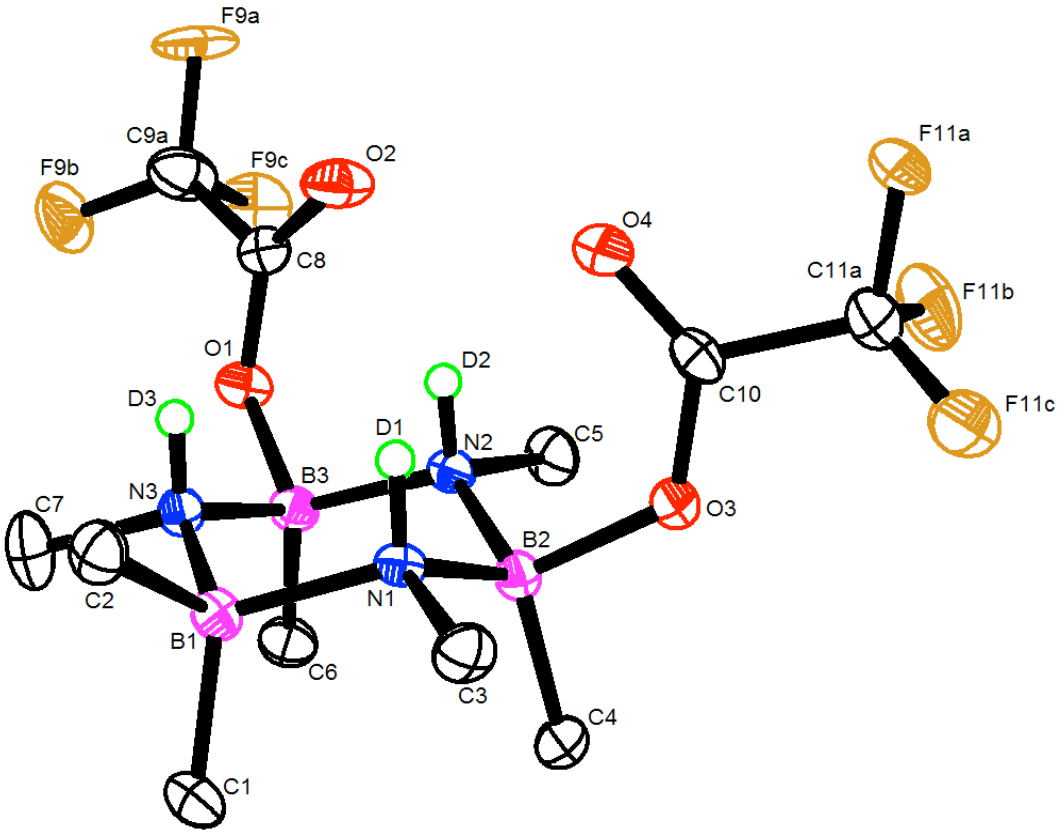

Figure A-29. Thermal ellipsoid plot of **4** shown at 50% probability. Hydrogens and alternative orientations of fluorine atoms exhibiting conformational disorder removed for clarity.

A.6 References

1) Chemical shift is also potentially consistent with Et3BH...BEt3.

2) CrystalClear Expert 2.0 r12, Rigaku Americas and Rigaku Corporation (2011), Rigaku Americas, 9009, TX, USA 77381-5209, Rigaku Tokyo, 196-866, Japan.

3) SHELXL, Bruker AXS: Madison WI, 1998.

Appendix B: Supporting Information Associated with Chapter 3

B.1 NMR Spectra

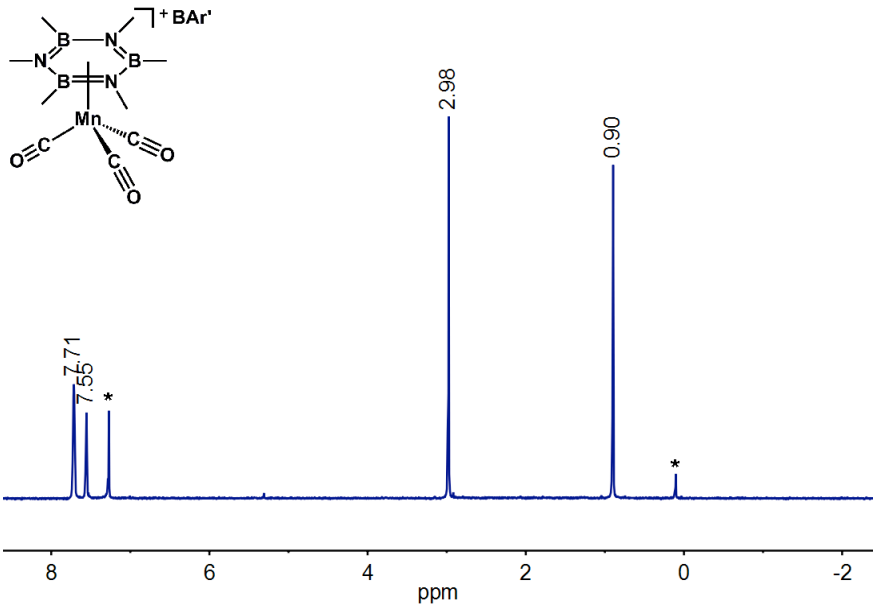

Figure B-1. ^{1}H NMR spectrum of **1**, 399.5 MHz, $CDCl_3$. * Residual $CHCl_3$ and TMS

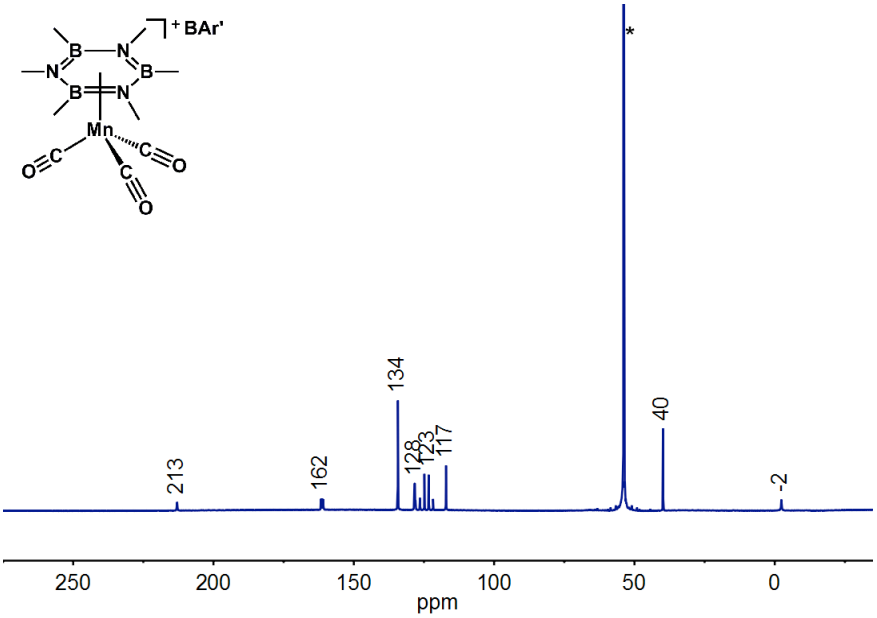

Figure B-2. ^{13}C NMR spectrum of **1**, 175.0 MHz, CH_2Cl_2, -30 ºC. *Solvent signal and solvent isotopologues.

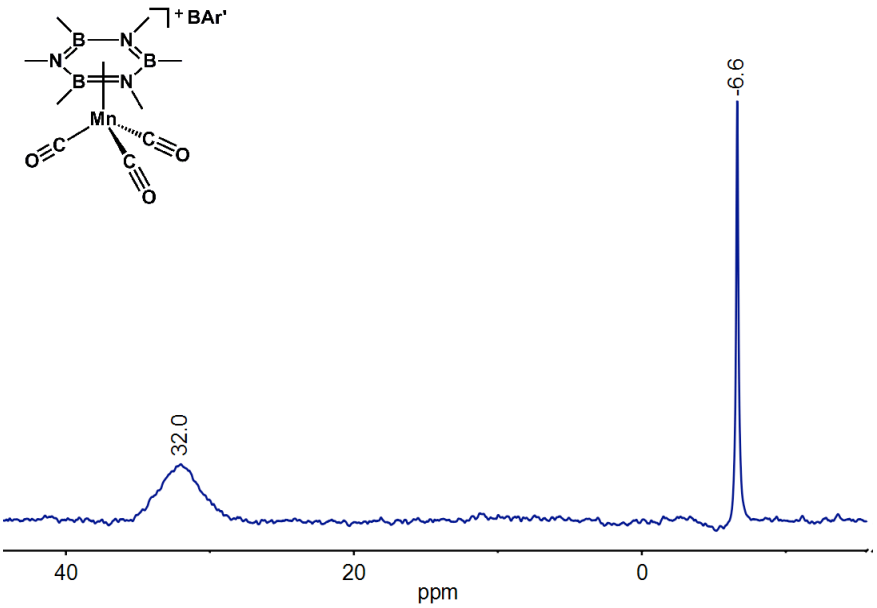

Figure B-3. ^{11}B NMR spectrum of **1**, 128.2 MHz, $CDCl_3$.

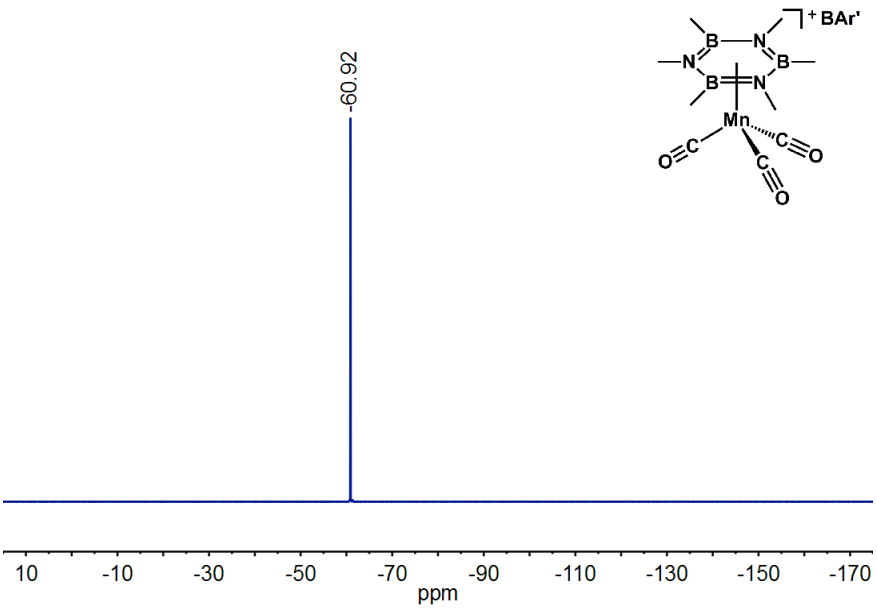

Figure B-4. ^{19}F NMR spectrum of **1**, 470.5 MHz, CD_2Cl_2.

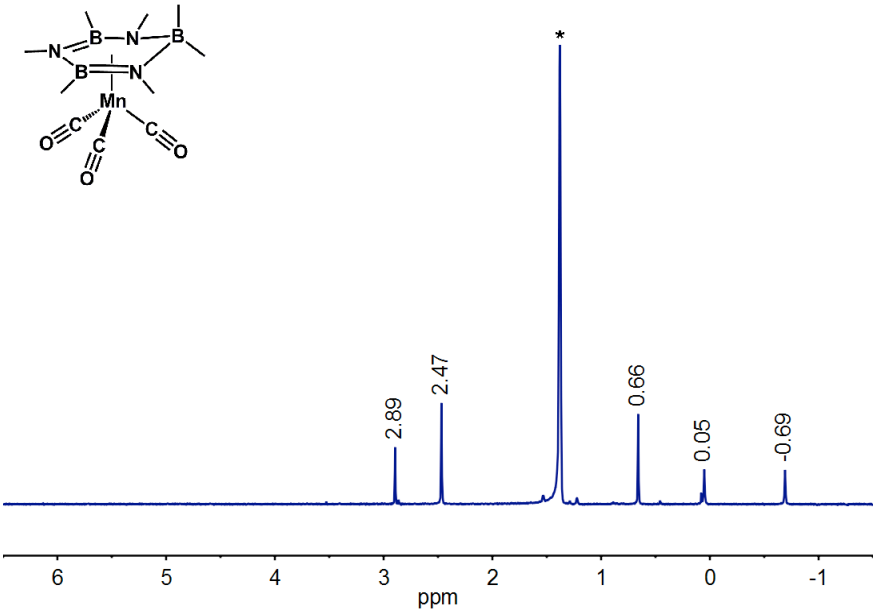

Figure B-5. ^{1}H NMR spectrum of **2**, 399.5 MHz, $[D_{12}]$cyclohexane. * Residual protic cyclohexane

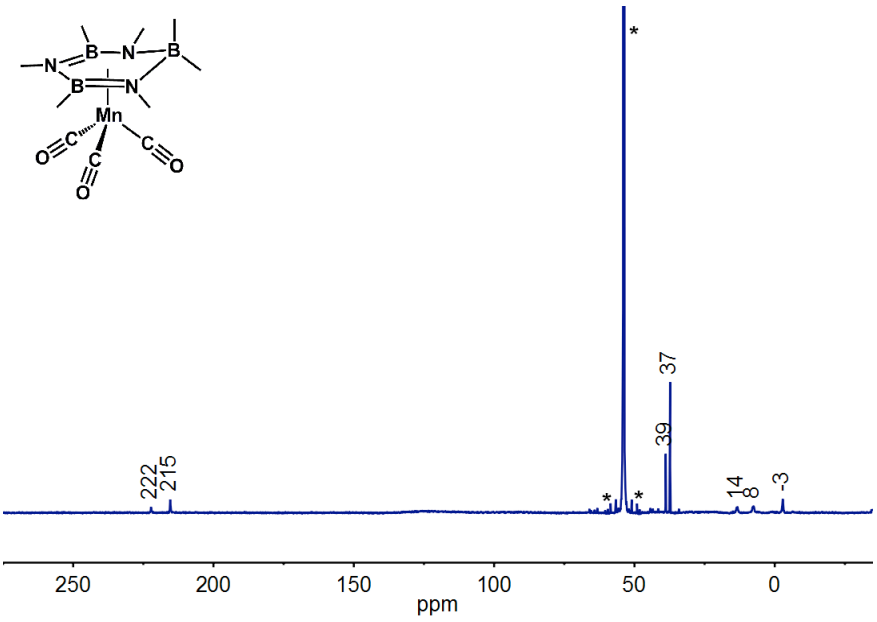

Figure B-6. ^{13}C NMR spectrum of **2**, 175.0 MHz, CH_2Cl_2, -30 ºC. *Solvent signal and solvent isotopologues.

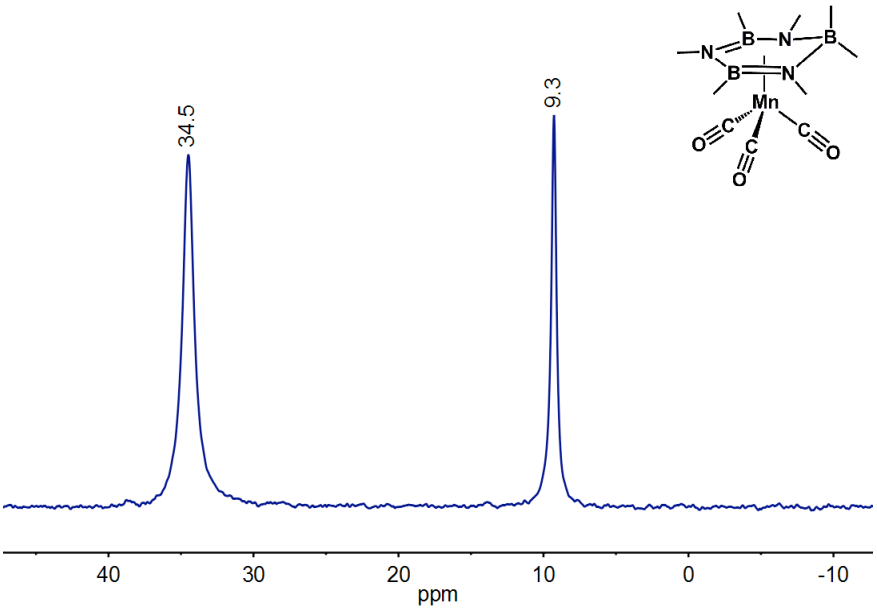

Figure B-7. ^{11}B NMR spectrum of **2**, 128.2 MHz, $[D_{12}]$cyclohexane.

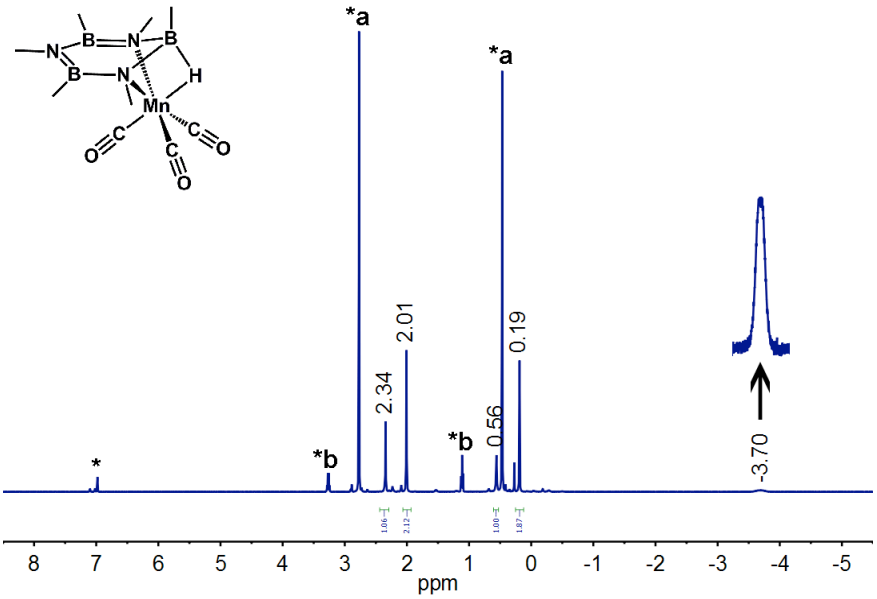

Figure B-8. ^{1}H NMR spectrum of sublimed **3**, 500.1 MHz, [D_8]toluene. * Redsidual protic toluene *a = Free $Me_3B_3N_3Me_3$ *b = Diethyl ether

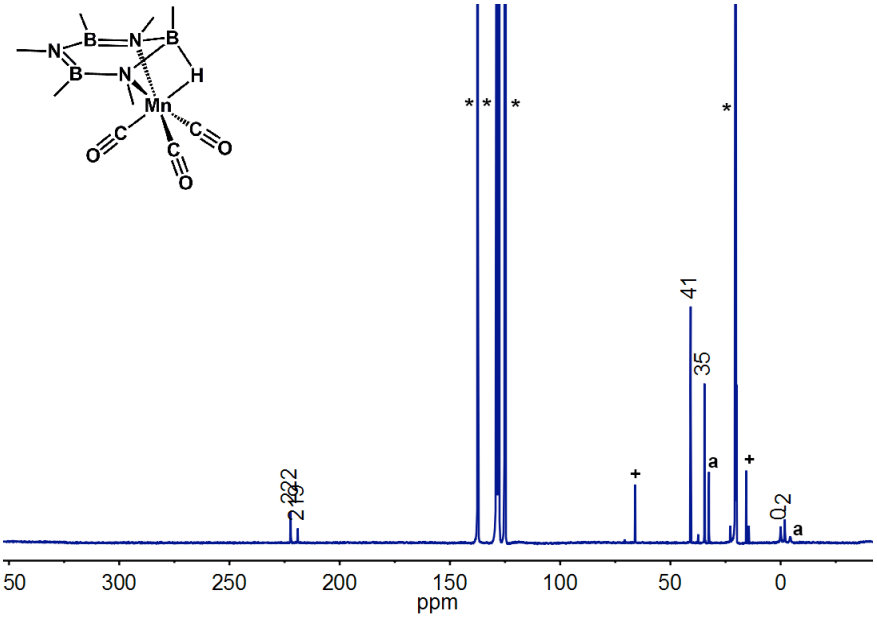

Figure B-9. ^{13}C NMR spectrum of **3**, 175.0 MHz, [D_8]Toluene, -30 ºC. *Solvent signal. $^{+}$Residual Et_2O. $^{a}Me_3B_3N_3Me_3$

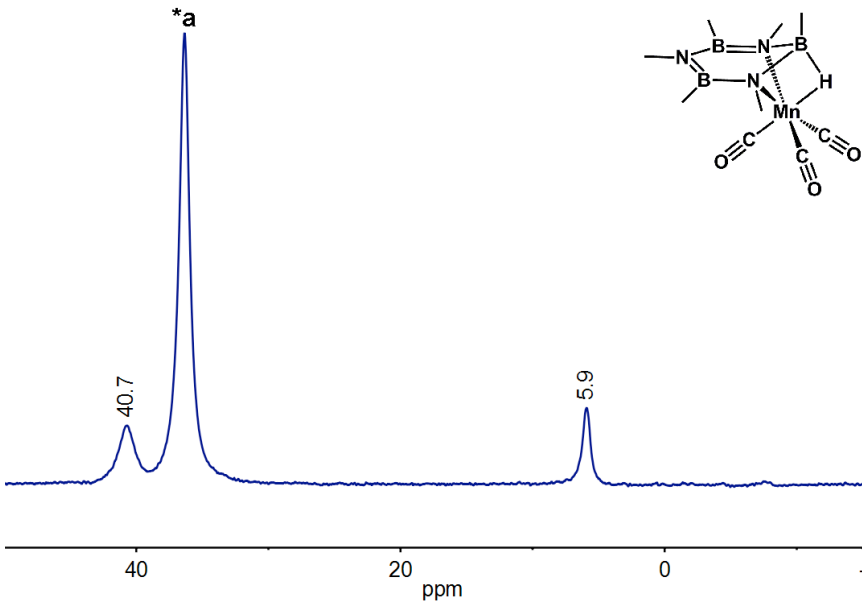

Figure B-10. ^{11}B NMR spectrum of sublimed **3**, 160.5 MHz, [D_8]Toluene. *a = Free $Me_3B_3N_3Me_3$

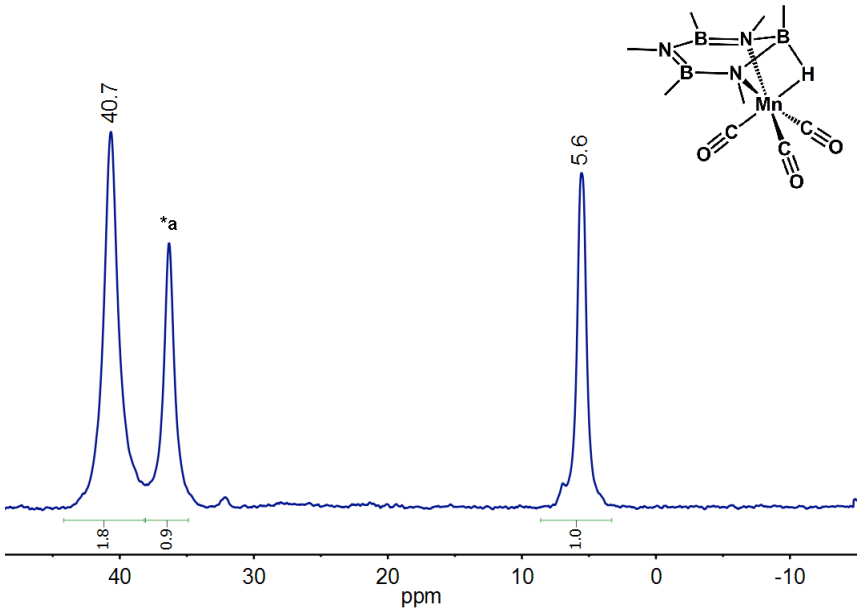

Figure B-11. ^{11}B NMR of **3** immediately following work-up, 128.2 MHz, Pentane. *a = Free $Me_3B_3N_3Me_3$

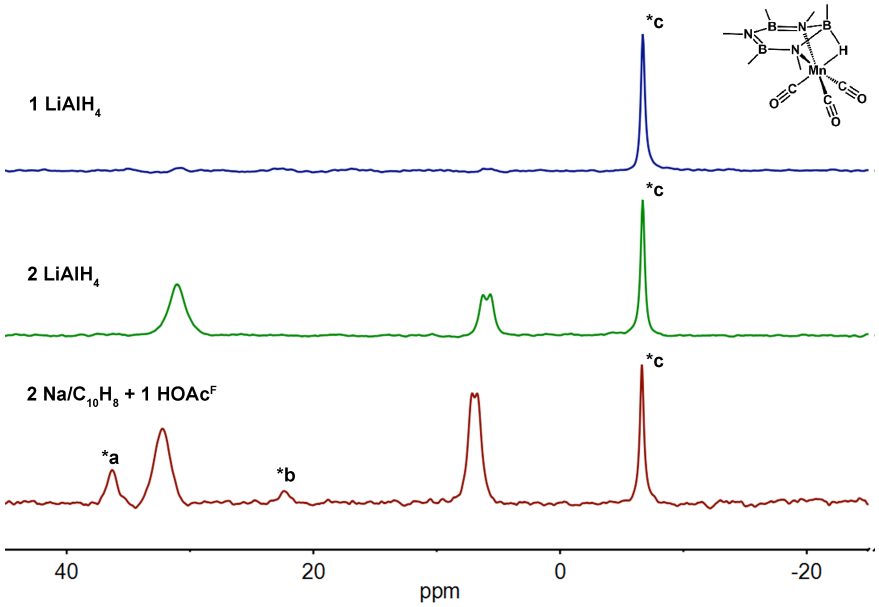

Figure B-12. Overlay of ^{11}B NMR spectra (-30 ºC) of **3** prepared under various reaction conditions. Top: Addition of 1 eq. $LiAlH_4$ to a frozen Et_2O solution of **1**. Middle: Addition of 2 eq. $LiAlH_4$ to a frozen Et_2O solution of **1**. Bottom: Addition of 2 eq. $Na/C_{10}H_8$ followed by 1 eq. $HOAc^F$ to a frozen Et_2O solution of **1**. *a = Free $Me_3B_3N_3Me_3$ *b = unidentified by-product (see caption for Figure 3-3) *c = Na or LiBAr'

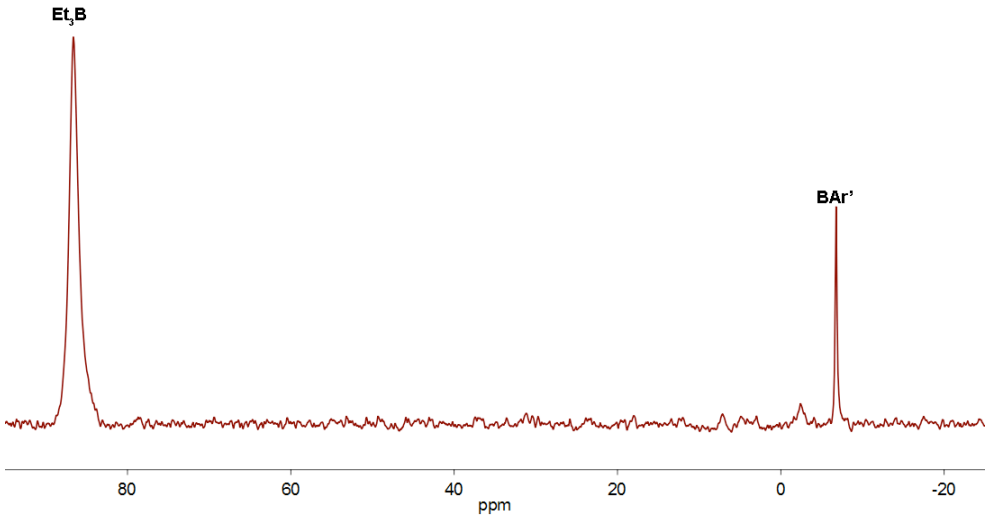

Figure B-13. ^{11}B NMR of solution of **3** following treatment with 1 $HOAc^F$, 128.2 MHz, $CDCl_3$.

B.2 IR Spectra

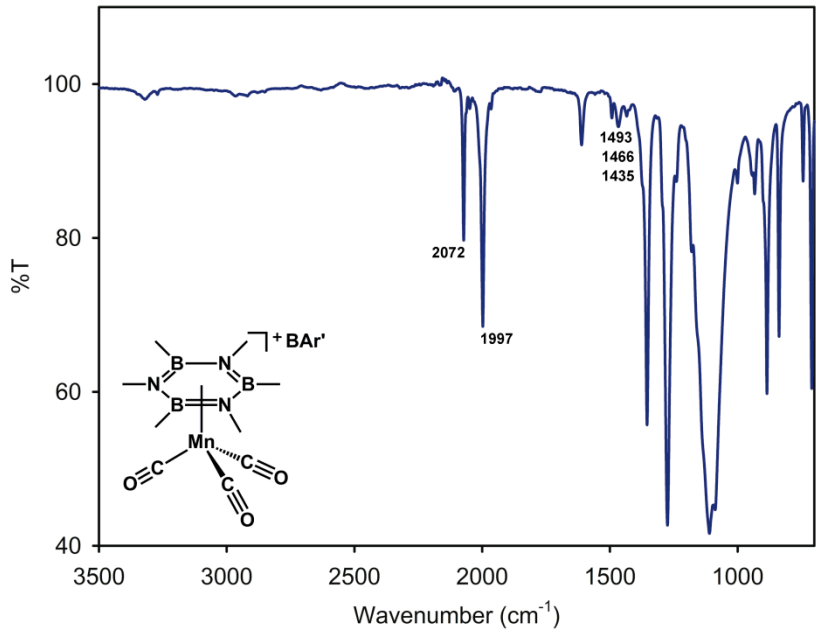

Figure B-14. IR spectrum of **1**, Diamond ATR accessory.

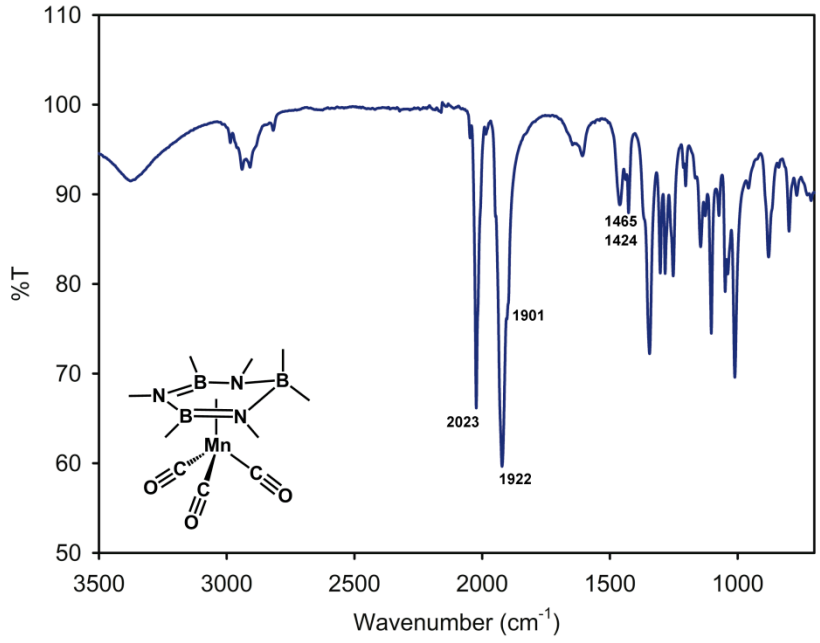

Figure B-15. IR spectrum of **2**, Diamond ATR accessory.

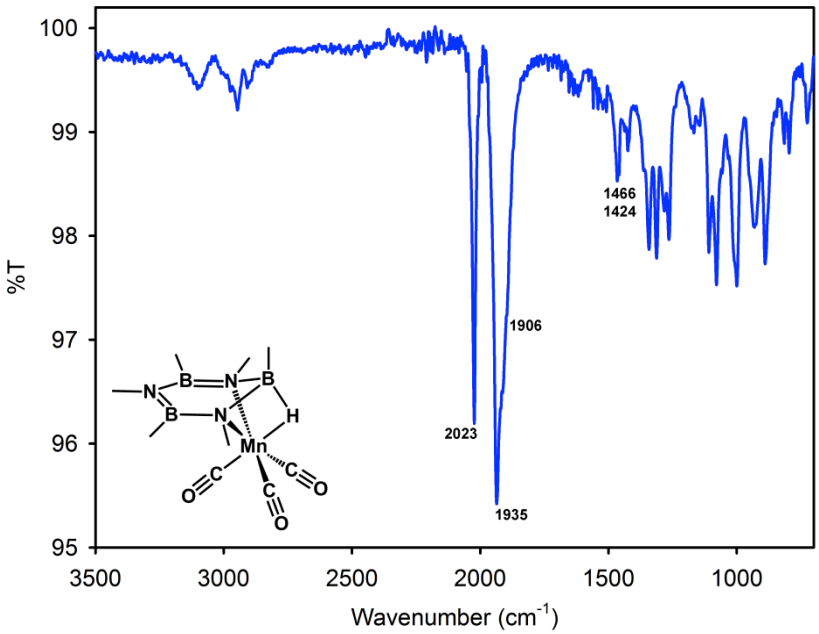

Figure B-16. IR spectrum of crystalline **3**, Diamond ATR accessory.

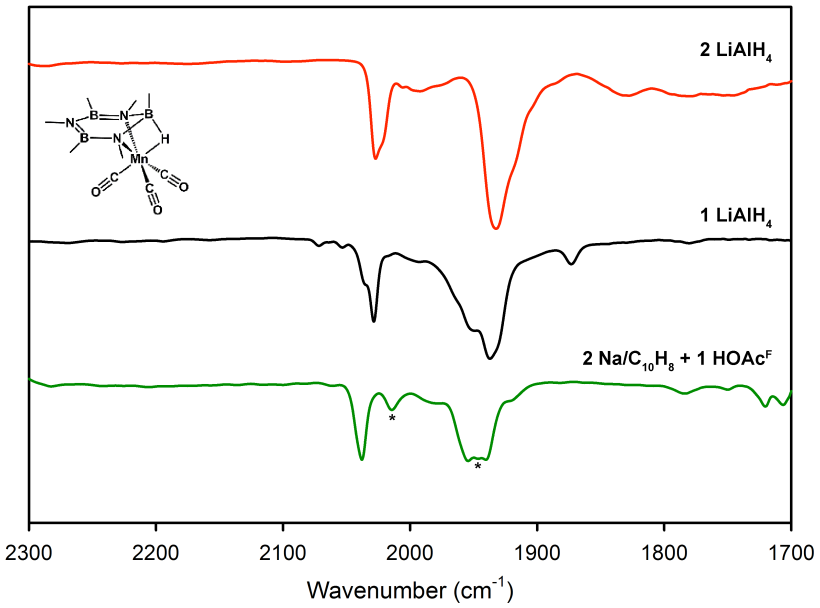

Figure B-17. Overlaid IR spectra of CO stretching region for **3** synthesized under various conditions, KBr plate solution cell. Top: Addition of 2 eq. $LiAlH_4$ to a frozen Et_2O solution of **1**. Middle: Addition of 1 eq. $LiAlH_4$ to a frozen Et_2O solution of **1**. Bottom: Addition of 2 eq. $Na/C_{10}H_8$ followed by 1 eq. $HOAc^F$ to a frozen Et_2O solution of **1**. * = (η^5-$C_{10}H_9$)(μ-H)$Mn(CO)_3$ formed by competitive displacement of $Me_3B_3N_3Me_3$ by naphthalene.[1]

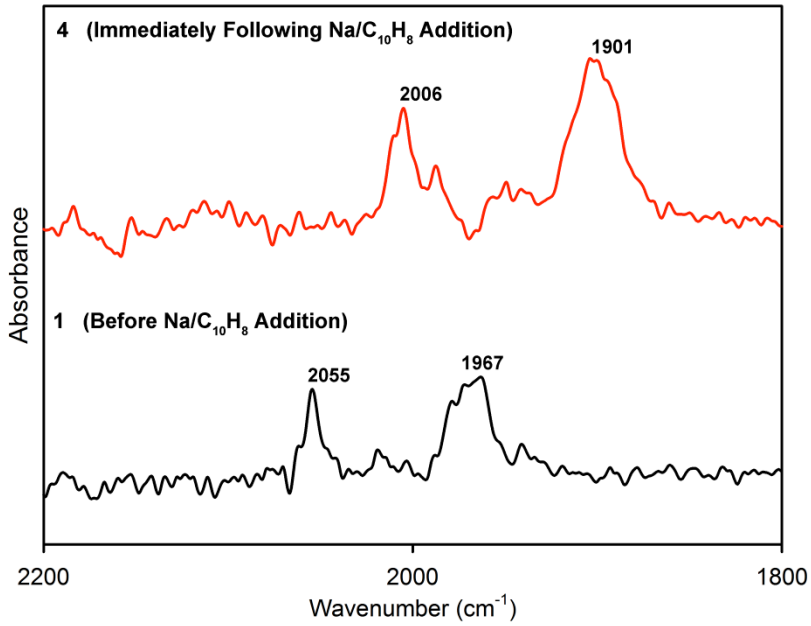

Figure B-18. In-situ IR spectra, Diamond tipped fiber optic probe. Bottom: Et_2O solution of **1**. Top: Solution immediately following addition of 2 eq. $Na/C_{10}H_8$ to form **4**.

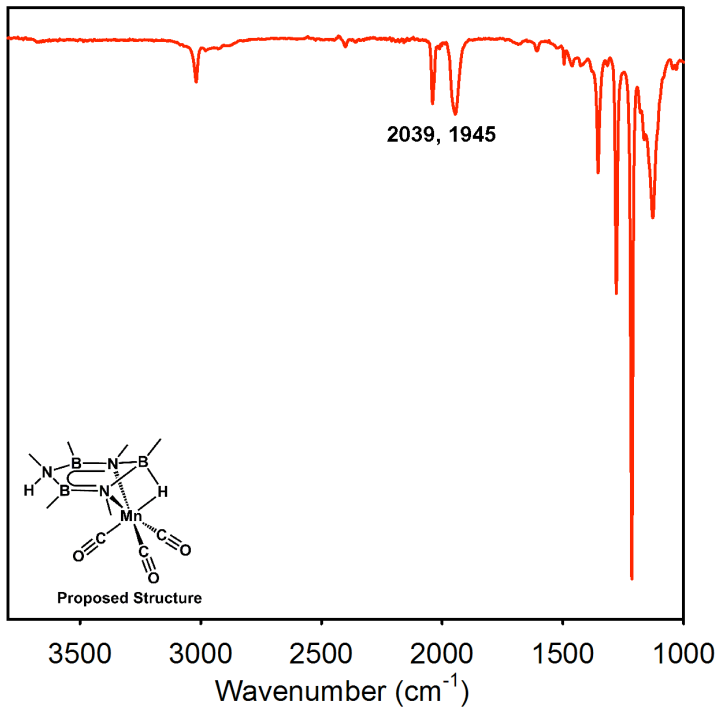

Figure B-19. IR spectrum of species resulting from reaction of **3** with 1 $HOAc^F$, diamond ATR accessory.

B.3 Mass Spectra

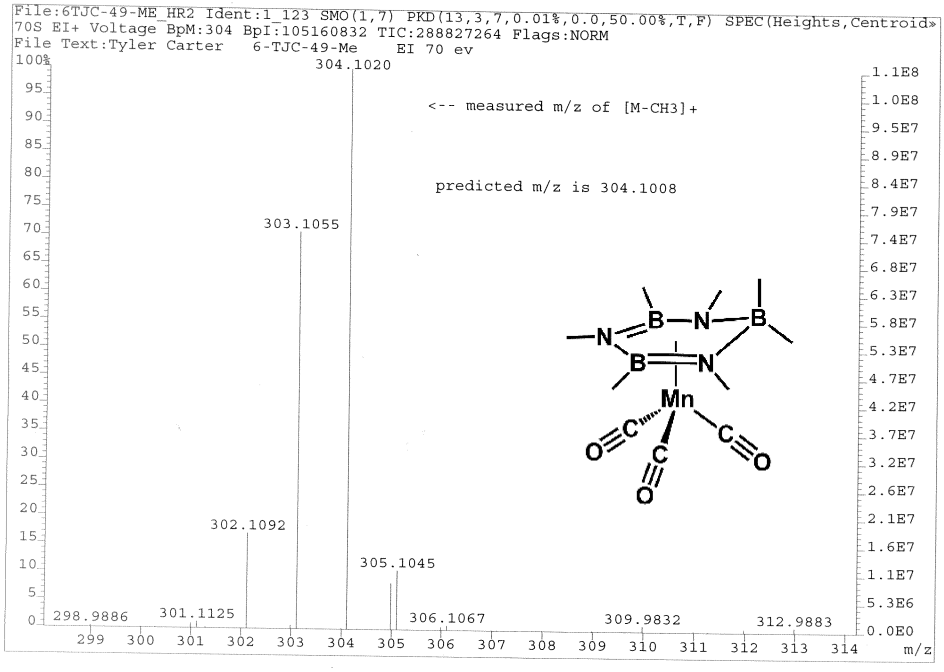

Figure B-20. HR-MS of **2** collected by EI ionization.

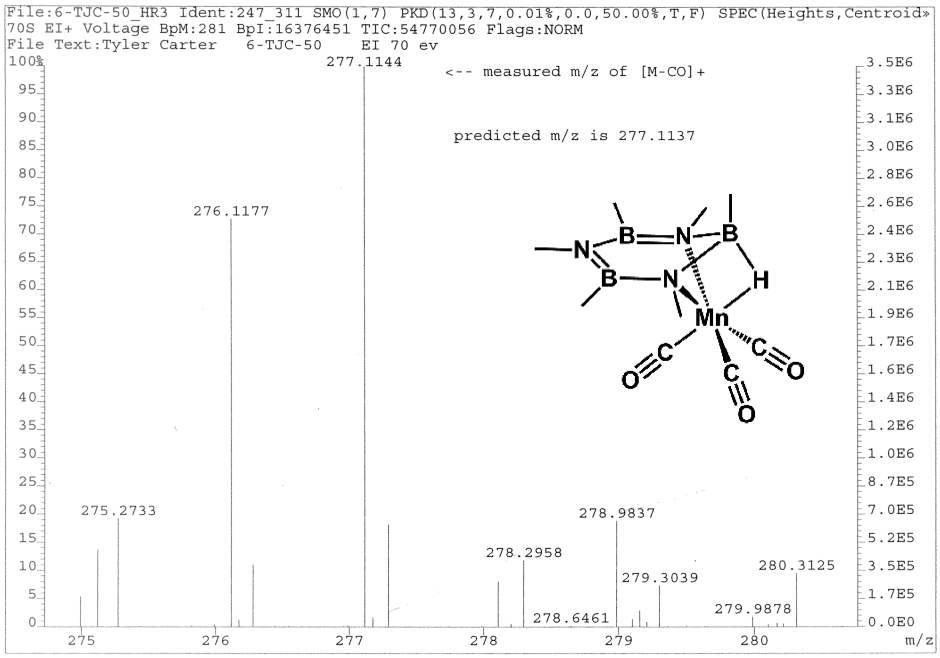

Figure B-21. HR-MS of **3** collected by EI ionization.

B.4 Electrochemistry

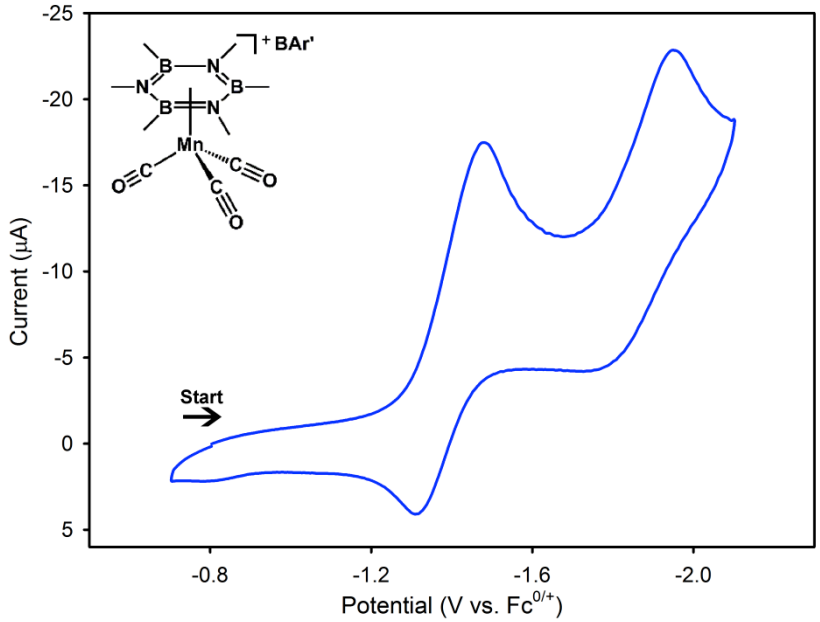

Figure B-22. Cyclic voltammogram of **1** in 0.1 M $^{n}Bu_4NPF_6$/DCM. (Scan Rate: 100 mV/s)

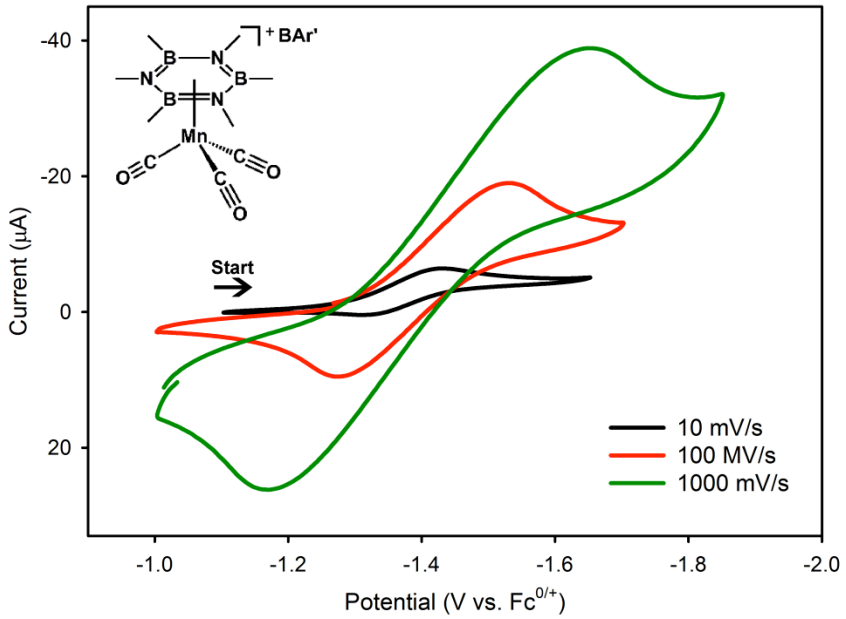

Figure B-23. Cyclic voltammogram showing first reduction of **1** at a variety of scan rates in 0.1 M $^{n}Bu_4NPF_6$/DCM.

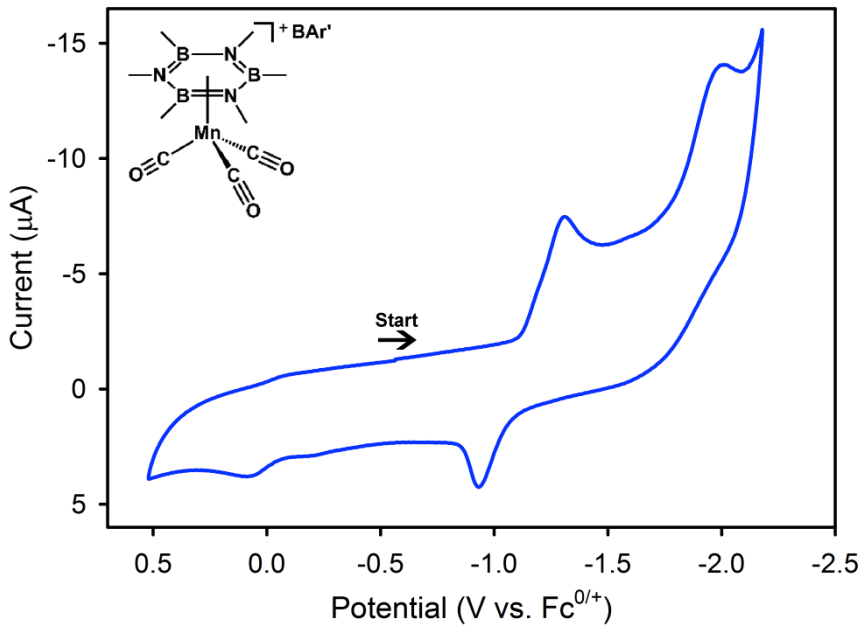

Figure B-24. Cyclic voltammogram of **1** in 0.1 M $^{n}Bu_4NBAr'/Et_2O$. (Scan Rate: 100 mV/s)

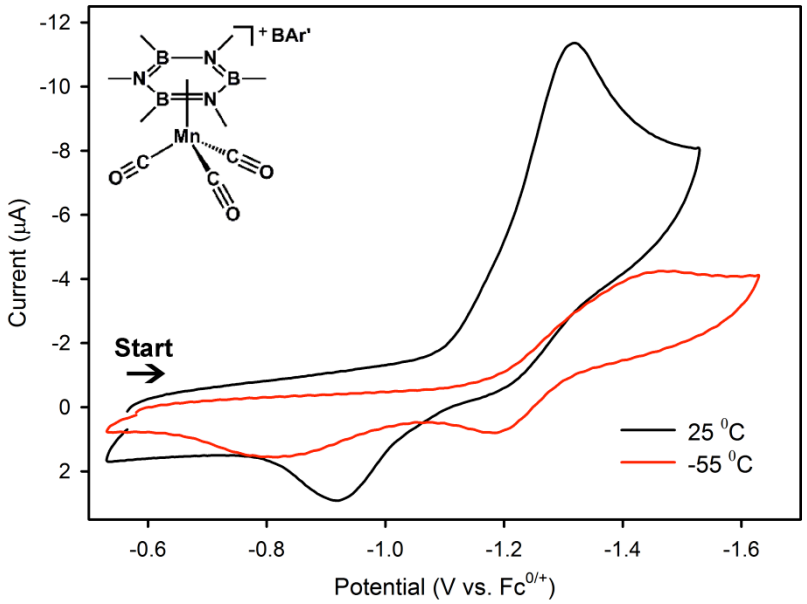

Figure B-25. Cyclic voltammogram of **1** in 0.1 M $^{n}Bu_4NBAr'/Et_2O$ at 25 ºC and -55 ºC. (Scan Rate: 100 mV/s).

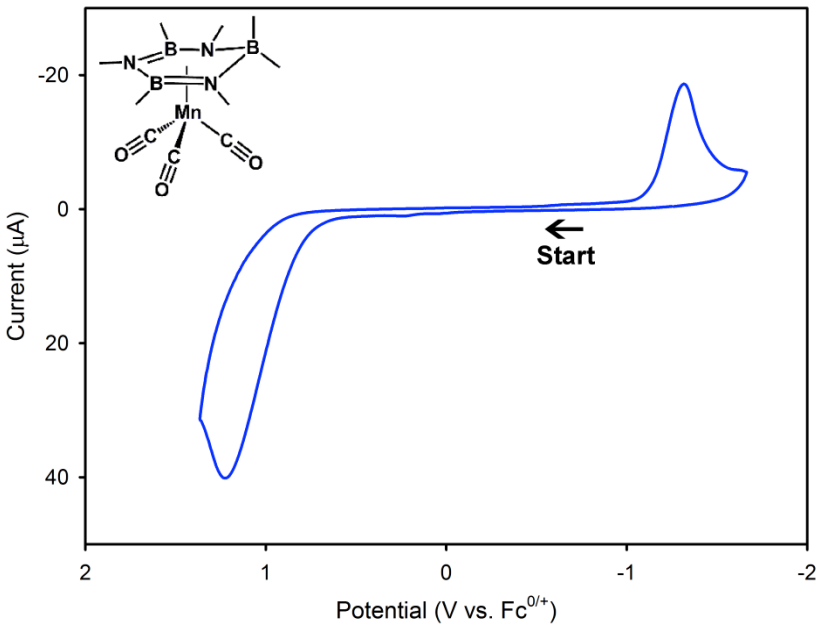

Figure B-26. Oxidation of **2** in 0.1 M $^{n}Bu_4NBAr'/Et_2O$ and associated return wave. (Scan Rate: 10 mV/s)

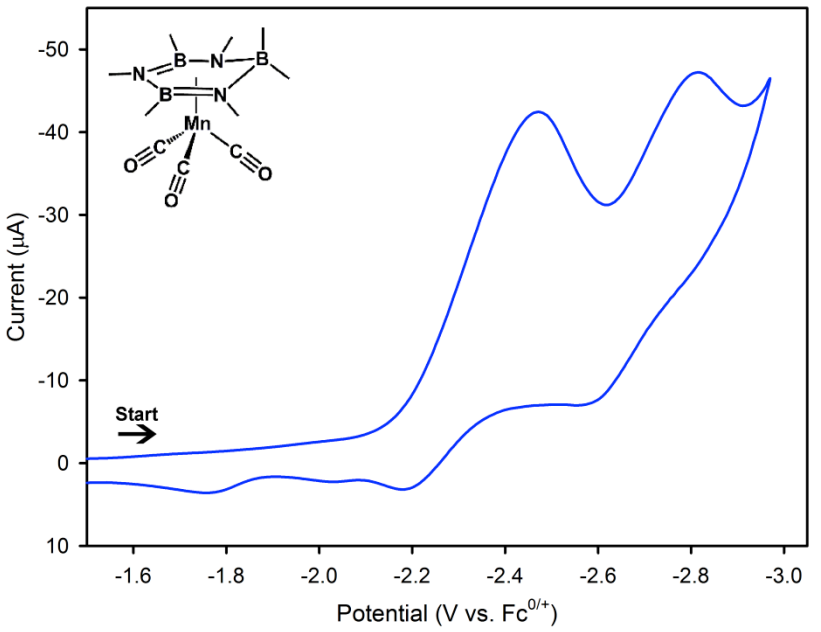

Figure B-27. Reductive electrochemistry of **2** in 0.1 M $^{n}Bu_4NBAr'/Et_2O$. (Scan Rate: 10 mV/s)

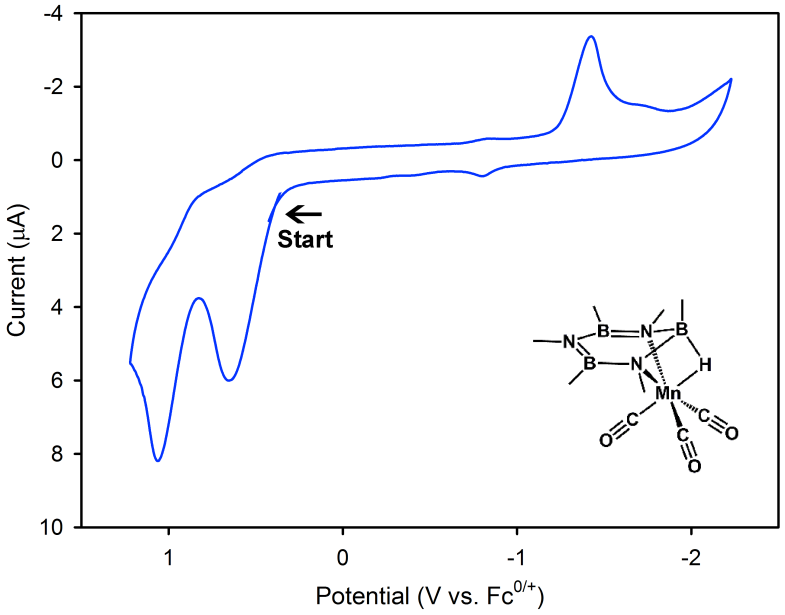

Figure B-28. Oxidative electrochemistry of **3** in 0.1 M $^{n}Bu_4NPF_6$/DCM. (Scan Rate: 10 mV/s) *As mentioned in the synthetic protocol, **3** is obtained with ~25 % free $Me_3B_3N_3Me_3$. Control experiments verify that $Me_3B_3N_3Me_3$ does not display any redox activity in the potential window shown.

B.5 X-Ray Crystallographic Data

Structure Determination of 1: Yellow needles of **1** were grown from a diethyl ether, DCM, and pentane solution (1:1:1) of the compound at –35 ºC. A crystal of dimensions 0.13 x 0.05 x 0.03 mm was mounted on a Rigaku AFC10K Saturn 944+ CCD-based X-ray diffractometer equipped with a low temperature device and Micromax-007HF Cu-target micro-focus rotating anode (λ = 1.54187 A) operated at 1.2 kW power (40 kV, 30 mA). The X-ray intensities were measured at 85(1) K with the detector placed at a distance 42.00 mm from the crystal. A total of 4296 images were collected with an oscillation width of 1.0° in ω. The exposure time was 2 s for the low angle images, and 8 s for high angle. The integration of the data yielded a total of 274740 reflections to a maximum 2θ value of 136.4° of which 8743 were independent and 7716 were greater than 2σ(I). Analysis of the data showed negligible decay during data collection; the data were processed with CrystalClear 2.0[2] and corrected for absorption. The structure was solved and refined with the SHELXL software package.[3] Refined formula: $C_{41}H_{30}B_4F_{24}MnN_3O_3$, M_r = 1166.86, Orthorhombic, space group PBCA, a = 18.6145(3), b = 18.8636(3), c = 27.1879(19) Å, α = 90, β = 90, γ = 90°, V = 9546.7(7) $Å^3$, Z = 8, ρ_{calcd} = 1.624 Mgm^{-3}, μ = 3.507 mm^{-1}, reflections collected: 274740, independent reflections: 8743 (Rint = 0.1052), Final R indicies [I > 2σ(I)]: R1 = 0.0670, wR2 = 0.1763, R indicies (all data): R1 = 0.0730, wR2 = 0.1810. Conformational disorder was observed in the CF_3 group containing C24. CIF file available under CCDC 975657.

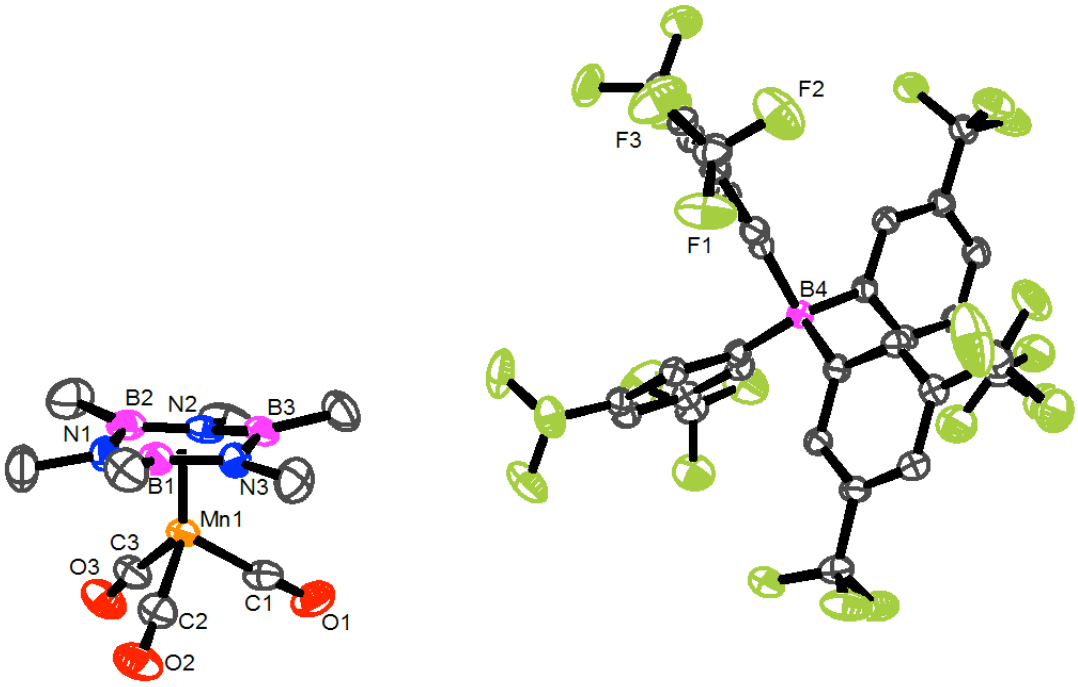

Figure B-29. Thermal ellipsoid plot of **1** shown at 50% probability. Hydrogens, and representations of CF_3 disorder, omitted for clarity.

Structure Determination of 2: Yellow plates of **2** were grown from a pentane solution of a reaction mixture containing the compound held at –35 ºC. Crystals were taken from the walls of the scintillation vial above the level of the solvent. A crystal of dimensions 0.12 x 0.02 x 0.02 mm was mounted on a Rigaku AFC10K Saturn 944+ CCD-based X-ray diffractometer equipped with a low temperature device and Micromax-007HF Cu-target micro-focus rotating anode (λ = 1.54187 A) operated at 1.2 kW power (40 kV, 30 mA). The X-ray intensities were measured at 85(1) K with the detector placed at a distance 42.00 mm from the crystal. A total of 4102 images were collected with an oscillation width of 1.0° in ω. The exposure time was 2 s for the low angle images, and 10 s for high angle. The integration of the data yielded a total of 88378 reflections to a maximum 2θ value of 136.4° of which 5652 were independent and 4915 were greater than 2σ(I). Analysis of the data showed negligible decay during data collection; the data were processed with CrystalClear 2.0[2] and corrected for absorption. The structure was solved and refined with the SHELXL software package.[3] Refined Formula: $C_{10}H_{21}B_3MnN_3O_3$, M_r = 318.67, Triclinic, space group P-1, a = 7.3606(3), b = 14.9688(12), c = 15.5742(8) Å, α = 113.175(7), β = 90.433(4), γ = 90.646(3)°, V = 1577.23(3) $Å^3$, Z = 4, ρ_{calcd} = 1.342 Mgm^{-3}, μ = 6.865 mm^{-1}, reflections collected: 88378, independent reflections: 5652 (Rint = 0.1178), Final R indicies [I > 2σ(I)]: R1 = 0.0677, wR2 = 0.1955, R indicies (all data): R1 = 0.0745, wR2 = 0.2066. CIF file available under CCDC 975658.

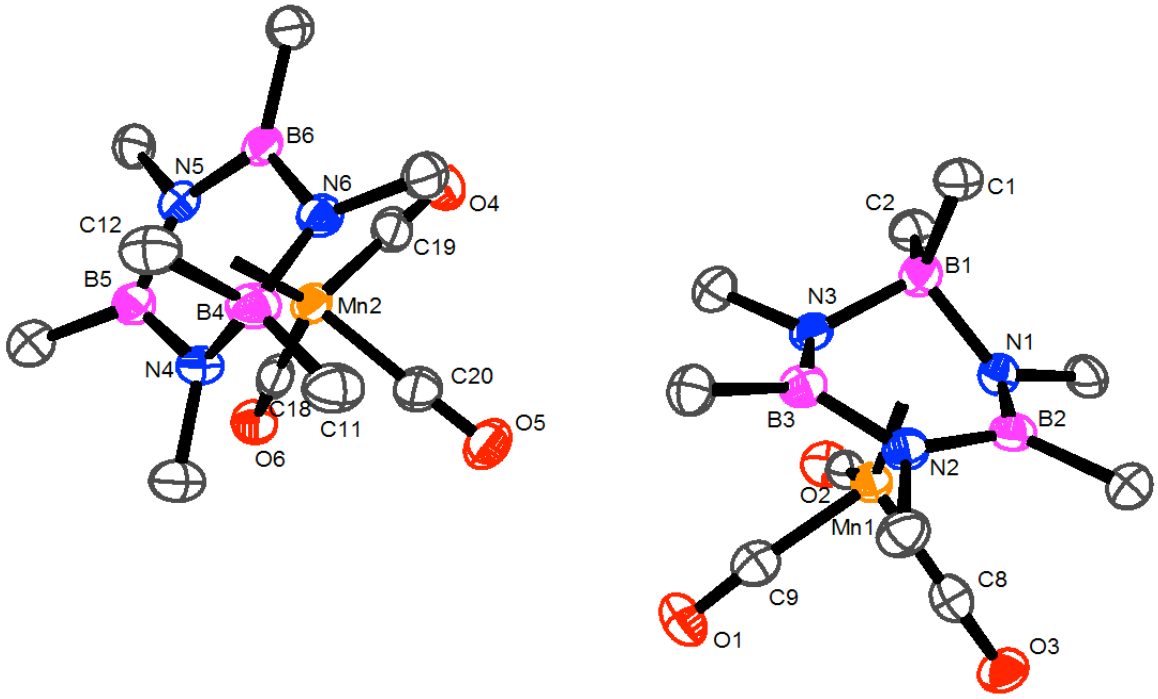

Figure B-30. Thermal ellipsoid plot of **2** shown at 50% probability. Hydrogens have been omitted for clarity.

Structure Determination of 3: Yellow plates of **3** were grown from a pentane solution of a reaction mixture containing the compound held at –35 ºC. Crystals were taken from the walls of the scintillation vial above the level of the solvent. A crystal of dimensions 0.20 x 0.16 x 0.05 mm was mounted on a Rigaku AFC10K Saturn 944+ CCD-based X-ray diffractometer equipped with a low temperature device and Micromax-007HF Cu-target micro-focus rotating anode (λ = 1.54187 A) operated at 1.2 kW power (40 kV, 30 mA). The X-ray intensities were measured at 85(1) K with the detector placed at a distance 42.00 mm from the crystal. A total of 4151 images were collected with an oscillation width of 1.0° in ω The exposure time was 3 s for the low angle images, and 15 s for high angle. The integration of the data yielded a total of 43158 reflections to a maximum 2θ value of 136.4° of which 2738 were independent and 2641 were greater than 2σ(I). Analysis of the data showed negligible decay during data collection; the data were processed with CrystalClear 2.0[2] and corrected for absorption. The structure was solved and refined with the SHELXL software package.[3] Refined Formula:$C_9H_{19}B_3MnN_3O_3$, M_r = 304.64, Monoclinic, space group P(2)1/n, a = 8.9006(2), b = 14.2192(3), c = 12.3119(9) Å, α = 90, β = 106.407(7), γ = 90°, V = 1494.74(12) Å^3, Z = 4, ρ_{calcd} = 1.354 Mgm^{-3}, μ = 7.219 mm^{-1}, reflections collected: 43158, independent reflections: 2738 (Rint = 0.0992), Final R indicies [I > 2σ(I)]: R1 = 0.0513, wR2 = 0.1459, R indicies (all data): R1 = 0.0520, wR2 = 0.1467. CIF file available under CCDC 975659.

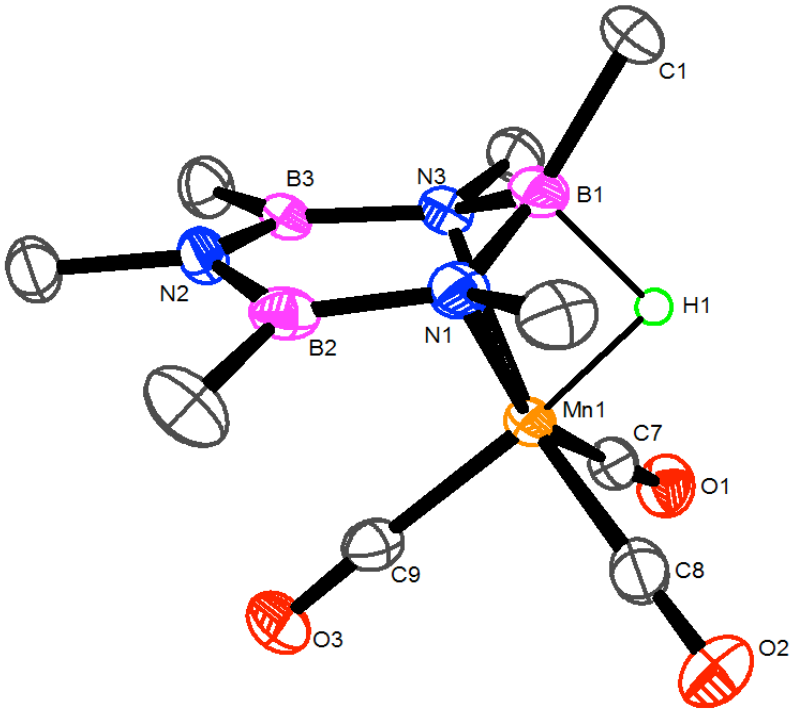

Figure B-31. Thermal ellipsoid plot of **3** shown at 50% probability. Hydrogen atoms, with the exception of the bridging hydride, were omitted for clarity.

B.6 References

1) Thompson, R. L.; Lee, S.; Rheingold, A. L.; Cooper, N. J. *Organometallics* **1991**, *10*, 1657.

2) CrystalClear Expert 2.0 r12, Rigaku Americas and Rigaku Corporation (2011), Rigaku Americas, 9009, TX, USA 77381-5209, Rigaku Tokyo, 196-866, Japan.

3) SHELXL, Bruker AXS: Madison WI, 1998.

Appendix C: Supporting Information Associated with Chapter 4

C.1 Additional Computational Information

Table C-1. Experimental and calculated (0.96 correction factor applied; see section 4.2.1) carbonyl stretching frequencies for M-$Me_3B_3N_3Me_3$ complexes.

Compound	V_{co} Experimental			V_{co} Calculated		
1	1951	1844		1957	1860	1857
2	2072	1997		2069	2002	2001
3				1898	1784	1783
4	2023	1935	1906	2016	1929	1929
5	2057	1980		2064	1995	1989
6	2011	1944	1930	2046	1926	1902
$[Mn(Me_3B_3N_3Me_3)(CO)_3]Na$	2006	1901		1912	1827	1818

Table C-2. Experimental and calculated redox potentials for M-$Me_3B_3N_3Me_3$ complexes.

Complex	$E_{1/2}$ Experimental	$E_{1/2}$ Calculated
4	0.6	0.12
5	-0.59	-0.61
6	-1.38	-1.49
$[Mn(Me_3B_3N_3Me_3)(CO)_3]Na$	-1.88	-3.29

Table C-3. Calculated pK_a values of borazines, and M-$Me_3B_3N_3Me_3$ complexes

Complex	pK_a (of conjugate acid)
$H_3B_3N_3H_3$	-15.4
$Me_3B_3N_3Me_3$	-4.3
1	-17
2	-47.7
3 (at N1)	20.8
3 (at H^-)	24.7
4 (at N1)	-1
4 (at H^-)	-5.3
$[Mn(Me_3B_3N_3Me_3)(CO)_3]Na$	49.8

Table C-4. Calculated BDFE values for **4**, hydroquinone species, and reaction solvnent.

Compound	BDFE (kcal/mol)
4	52.8
7	39.0
9,10-H_2-AQ	52.9
CH_2Cl_2	86.4
2-Me-THF	81.7

Table C-5. Calculated thermodynamic hydricity of $Me_3B_3N_3Me_3$ and M-$Me_3B_3N_3Me_3$ hydride adducts

Complex	ΔG_{H-}
$(H_4B_3N_3H_3)^-$	9.2
$(HMe_3B_3N_3Me_3)^-$	4
3	41.1
4	68.7
$Cr^I(\mu\text{-}H)(Me_3B_3N_3Me_3)(CO)_3$	66.1
7	37.2
4-hydroxyphenolate	56.7

C.2 NMR Spectra

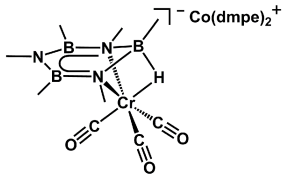

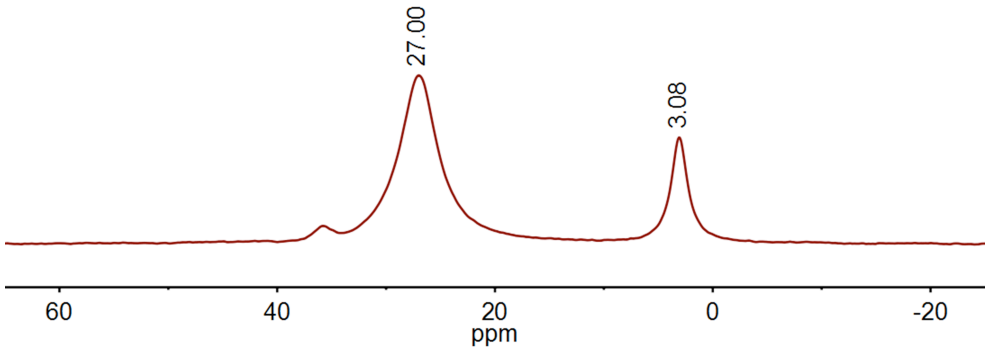

Figure C-1. ^{11}B NMR spectrum of **3** from reaction of **1** with $HCo(dmpe)_2$, 160.4 MHz, 2-Me-THF, -30 ºC.

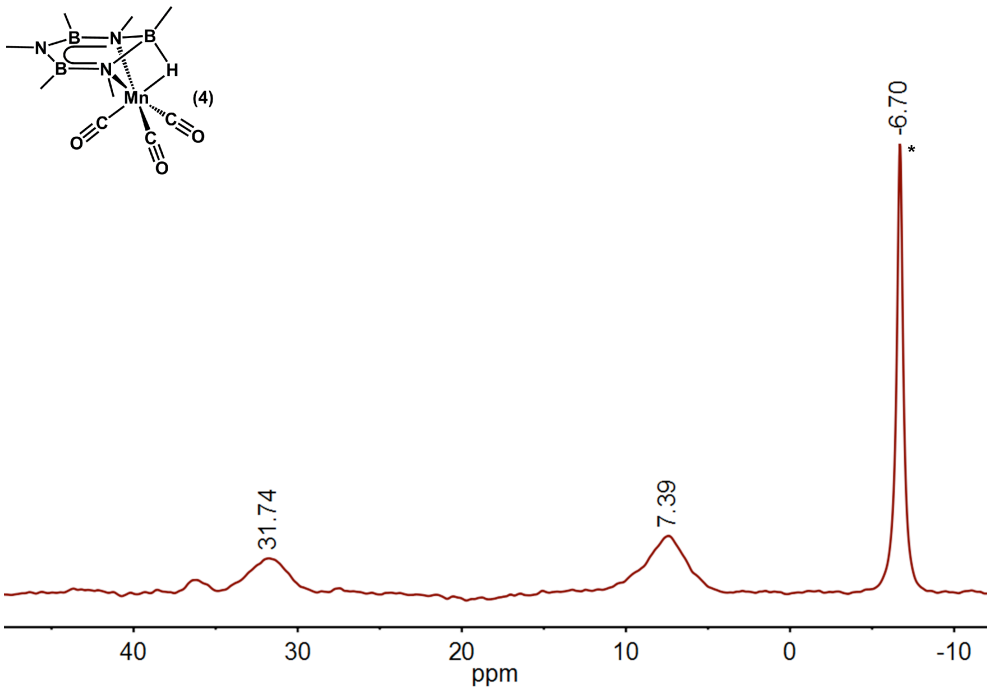

Figure C-2. ^{11}B NMR spectrum of **4** synthesized by reaction of **2** with Cp_2Co and 9,10-anthraquinone, 128.2 MHz, 2-Me-THF. * Residual BAr' salt used as internal integration standard.

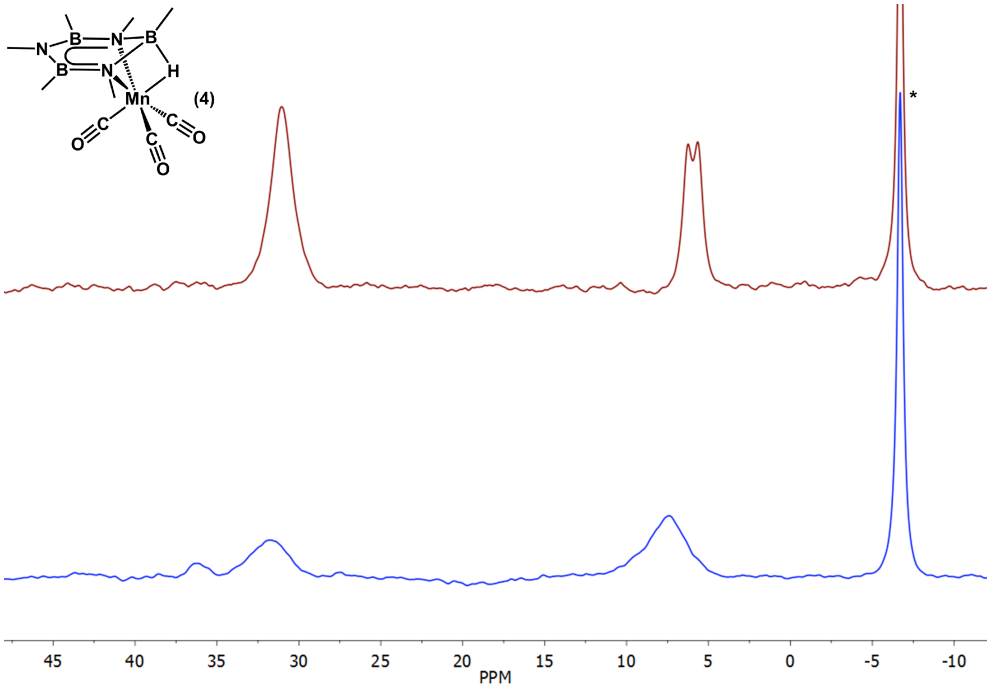

Figure C-3. Overlaid ^{11}B NMR spectra of **4** synthesized by $NaEt_3BH$ addition (Top) and addition of Cp_2Co and 9,10-anthraquinone (Bottom). . * Residual BAr' salt used as internal integration standard.

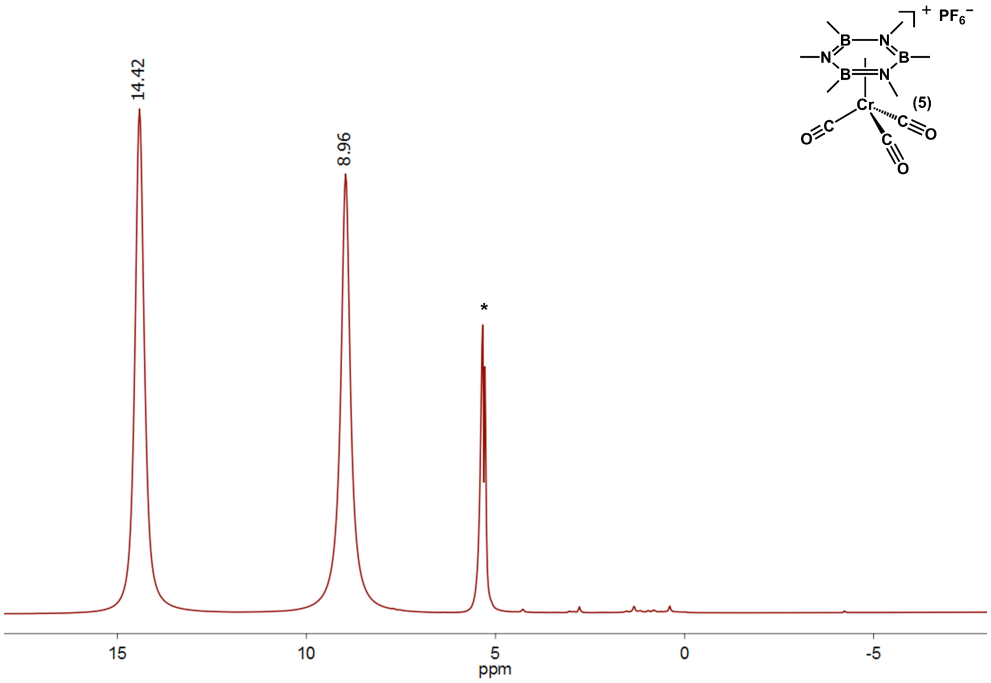

Figure C-4. ^{1}H NMR spectrum of solution containing **5**, 399.5 MHz, CH_2Cl_2.

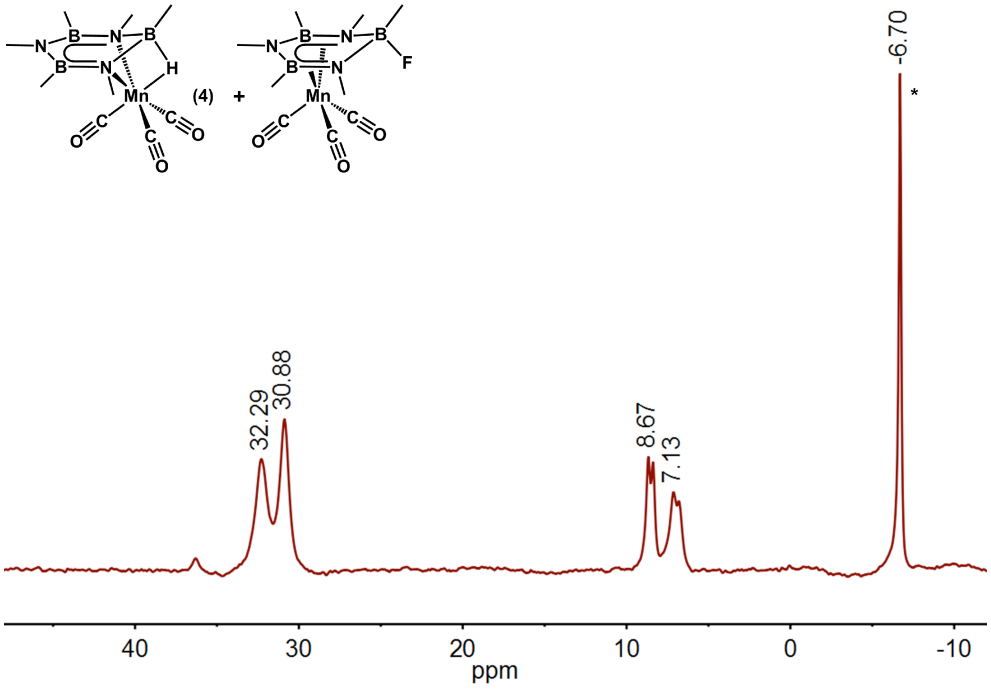

Figure C-5. ^{11}B NMR spectrum of solution containing **4** and $(FMe_3B_3N_3Me_3)Cr(CO)_3$ following controlled potential electrolysis, 128.2 MHz, 0.1 M $^{n}Bu_4NPF_6/CH_2Cl_2$. . * Residual BAr' salt used as internal integration standard.

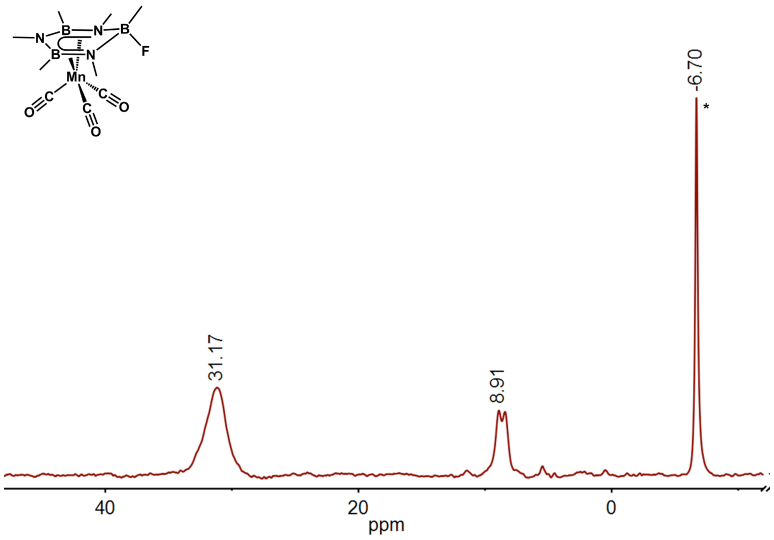

Figure C-6. ^{11}B NMR spectrum of $(FMe_3B_3N_3Me_3)Cr(CO)_3$ synthesized by addition of $^{n}Bu_4NF$ to **2**, 128.2 MHz, CH_2Cl_2. . * Residual BAr' salt.

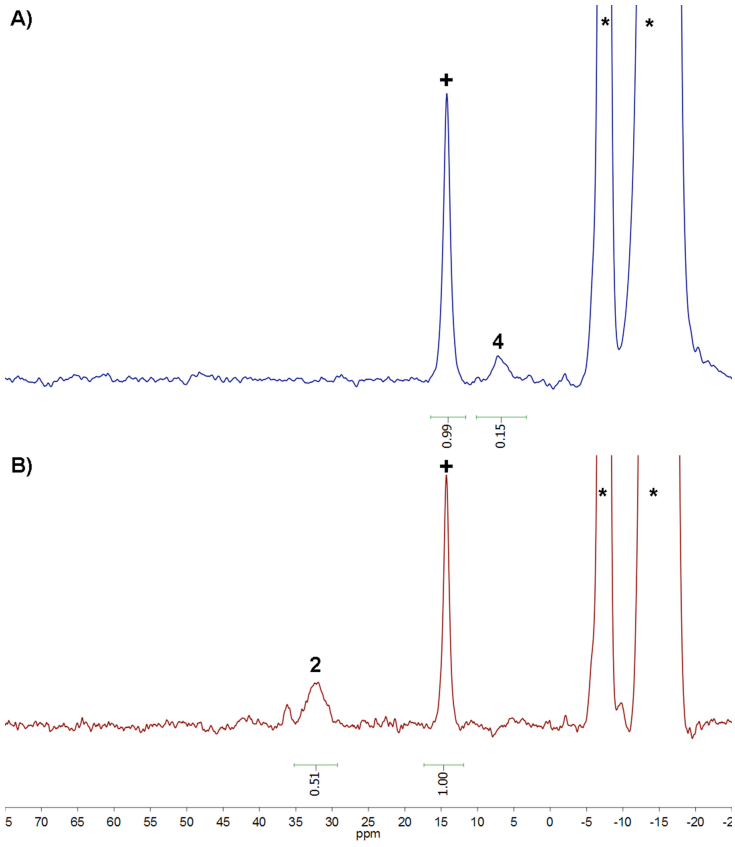

Figure C-7. ^{11}B NMR spectrum of solution following controlled potential electrolysis of **2** and 9,10-anthraquinone with carborane electrolyte, $^{+}(TMSO)_3B$ added as internal standard, 500.1 MHz, 0.05 M $[^{n}Bu_4N][CB_{11}H_{12}]/CH_2Cl_2$.

C.3 IR Spectra

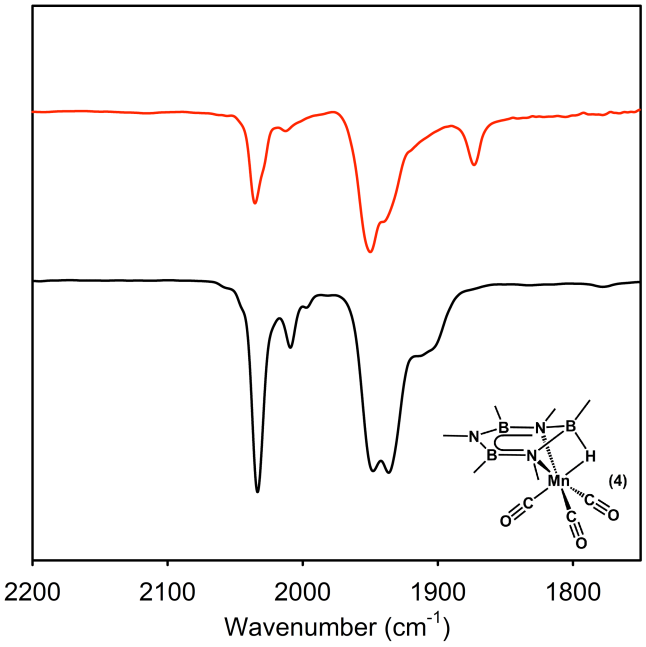

Figure C-8. Overlayed solution-cell IR spectrum of **4** synthesized by $NaEt_3BH$ addition (Top, Et_2O solution) and addition of Cp_2Co and 9,10-anthraquinone (Bottom, 2-Me-THF solution), KBr plate solution cell.

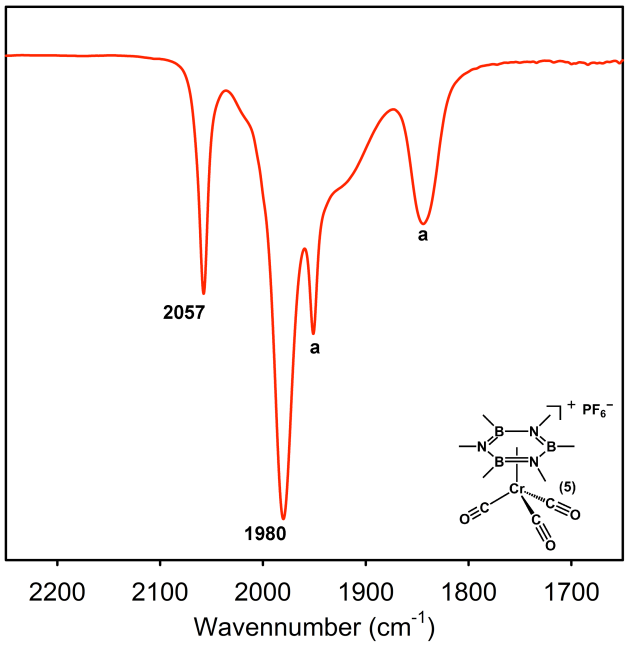

Figure C-9. IR spectrum of DCM solution containing **5**, KBr plate solution cell. a) Unreacted **1**.

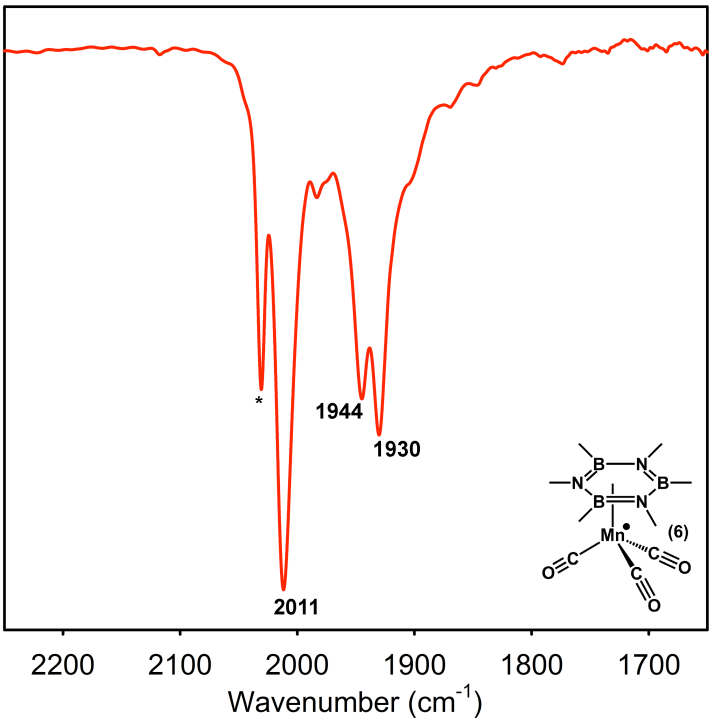

Figure C-10. IR spectrum of solution containing **6**, KBr solution cell, 2-Me-THF solution. *Unidentified by-product.

C.4 Mass Spectra

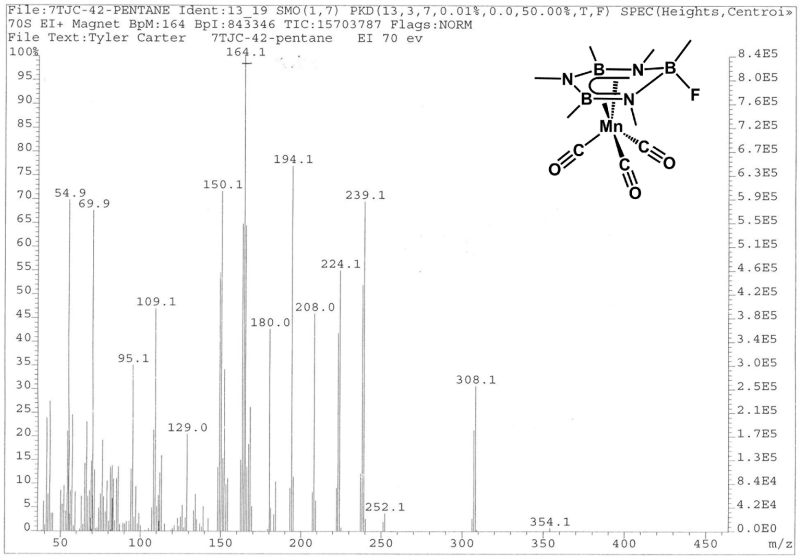

Figure C-11. MS of F-atom transfer product collected by EI ionization.

C.5 EPR Spectra

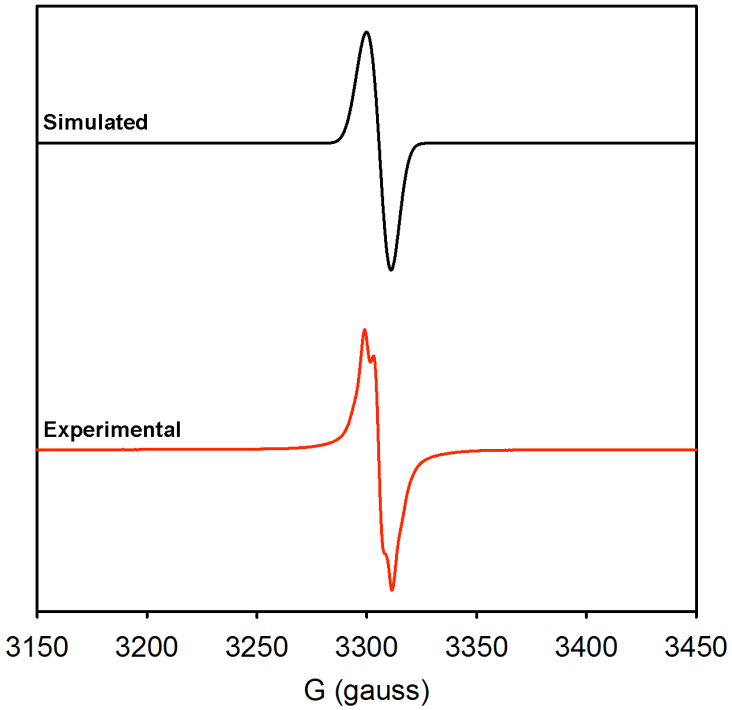

Figure C-12. Experimental (bottom) and simulated (top) X-Band EPR spectrum of DMPO-trapped semiquinone radical, 2-Me-THF, 77 K.

C.6 Electrochemistry

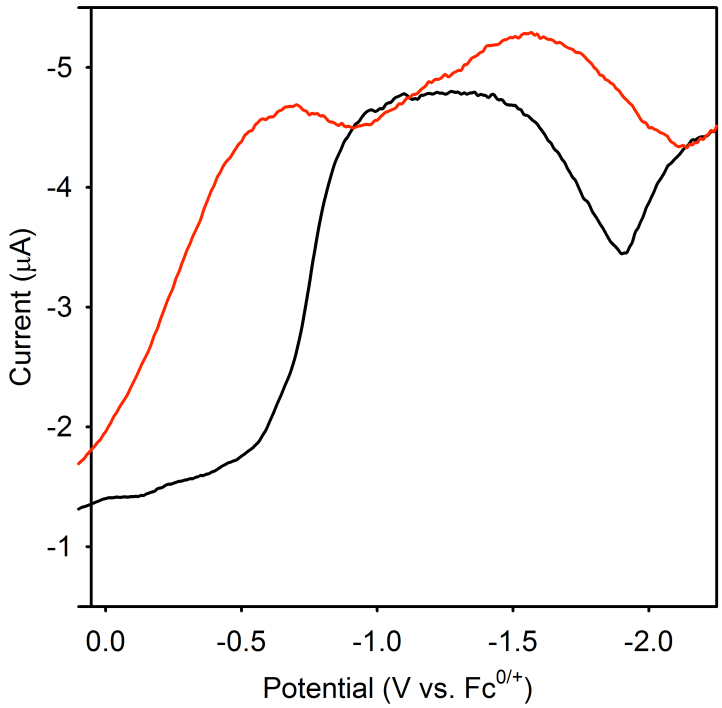

Figure C-13. DPV of AQ solution with (red) and without (black) added **2**, 0.05 M $^{n}Bu_4NBAr'$/2-Me-THF

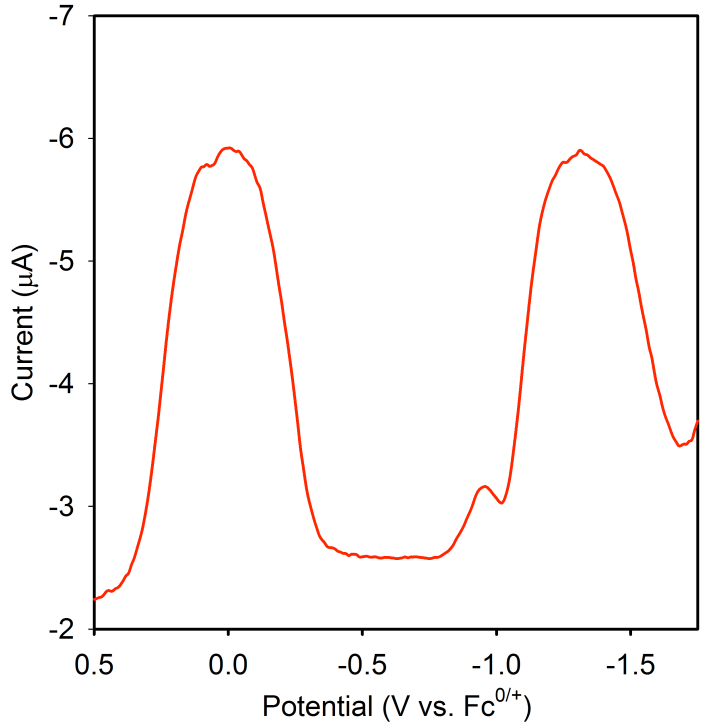

Figure C-14. DPV of solution containing Fc and Cp_2Co, 0.05 M $^{n}Bu_4NBAr'$/2-Me-THF.

Appendix D: Supporting Information Associated with Chapter 5

D.1 General Experimental Details

All experiments were conducted using standard Schlenk techniques or in a nitrogen filled glovebox. NMR spectra were recorded on Varian MR400, vnmrs 500, or vnmrs 700 MHz. spectrometers. ^{1}H NMR were referenced relative to the protio solvent resonance, and ^{11}B spectra were referenced indirectly based on the ^{1}H spectrum.[1] IR Spectra were recorded on a Nicolet iS-10 spectrometer from Thermo Scientific in a KBr plate solution cell or on a diamond attenuated total reflectance (ATR) accessory. Cyclic voltammetry experiments were collected on a Pine Research Instrumentation WaveNow potentiostat. Experiments were conducted in a 0.05 M solution of tetrabutylammonium tetrakis[3,5-bis(trifluoromethyl)phenyl]borate ($^{n}Bu_4NBAr'$) in metyl tert-butyl ether (MTBE). A glassy carbon working electrode and a platinum disk wire counter-electrode were used and voltammograms referenced relative to ferrocene ($Fc^{0/+}$) using a silver wire pseudo reference electrode. Potentials are reported as E_{Pc} values. Scan rate was 0.1 V s^{-1}. $^{n}Bu_4NBAr'$ was synthesized using a modified version of the procedure reported by Kobayashi and coworkers[2] for the synthesis of tetraethylammonium tetrakis[3,5-bis(trifluoromethyl)phenyl]borate. Tetrabutylammonium chloride was used in place of tetraethylammonium iodide, and extraction with ether followed by drying over $MgSO_4$ was used in-lieu of column chromatography. Sodium tetrakis[3,5-bis(trifluoromethyl)phenyl]borate, borazine ($H_3B_3N_3H_3$), hexamethylborazine ($Me_3B_3N_3Me_3$), (η^6-$Me_3B_3N_3Me_3$)$Cr(CO)_3$, and $Cr(CO)_3(CH_3CN)_3$ were synthesized by previously reported routes.[3-6] Diethyl ether, pentane, and tetrahydrofuran were ordered from Fisher Scientific and passed through an S.G. Waters solvent purification system. 1,4-dioxane was distilled from sodium and degassed prior to use. All other solvent were purchased from commercial vendors and dried and degassed by standard methods.[7] All other chemicals were from commercial vendors and used as received.

D.2 Titration of $(MeCN)_3Cr(CO)_3$ with $H_3B_3N_3H_3$

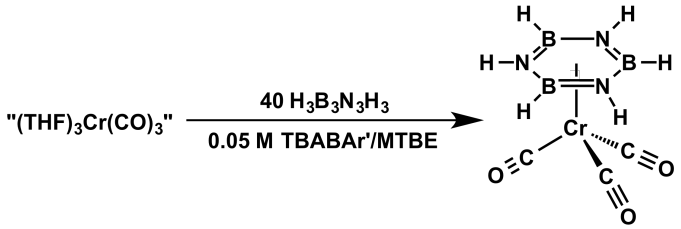

A solution of $MeCN_3Cr(CO)_3$ (1.3 mg, 0.005 mmol) was prepared in 2 ml THF. The solvent was then removed under vacuum and the residue was dissolved in 5 ml of 0.05 M solution of $^{n}Bu_4NBAr'$ in MTBE. Cyclic voltammetry was conducted using a glassy carbon working electrode, Pt wire counter electrode, and Ag/AgOTf reference electrode. The solution was scanned from -1.0 to 1.7 V (vs. SCE) as $H_3B_3N_3H_3$ was added in 5-10 molar equivalent increments. The oxidative couple for the Cr-solvate was seen to decrease, and a new event at -0.3 V appeared and reached saturation after 40 equivalents of $H_3B_3N_3H_3$ was added. ^{11}B NMR conducted on a solution containing 40 equivalents of borazine and "$THF_3Cr(CO)_3$" did not show any new peaks.

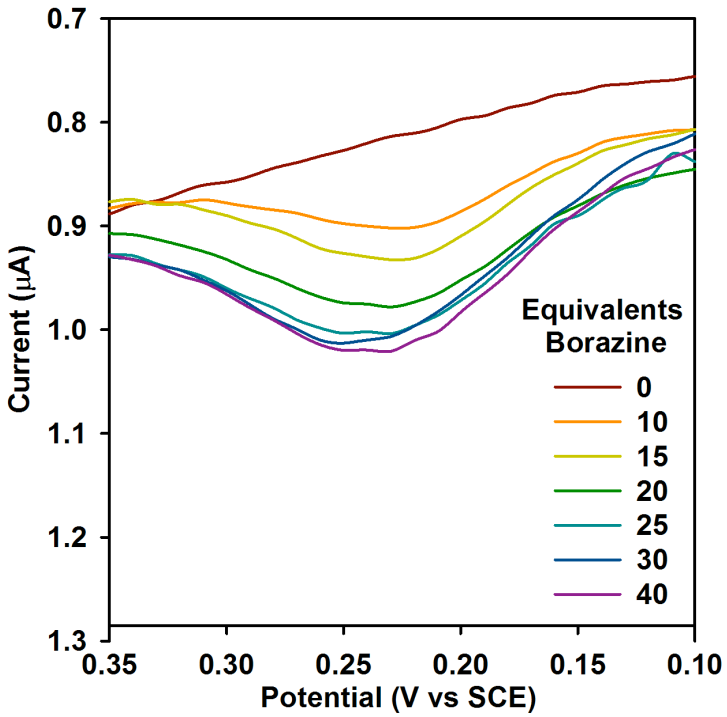

Figure D-1. Cyclic voltammetry data collected for experiment D.2.

D.3 Reaction of $Me_3B_3N_3Cr(CO)_3$ with $H_3B_3N_3H_3$

Route A: Attempted ring-exchange by precipitation from pentane

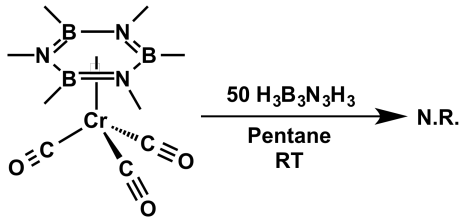

A suspension of (η^6-$Me_3B_3N_3Me_3$)$Cr(CO)_3$ (24.1 mg, 0.080 mmol) in 5 ml pentane was prepared in a 20 ml scintillation vial. To this was added $H_3B_3N_3H_3$ (100 µl, 1.06 mmol). The solution was capped and stirred at room temperature for 18 h. A yellow solution with a yellow precipitate was obtained. A sample of the filtrate was collected for NMR analysis, and only free borazine was observed in solution. The precipitate was collected for IR analysis, and only starting material, (η^6-$Me_3B_3N_3Me_3$)$Cr(CO)_3$, was observed.

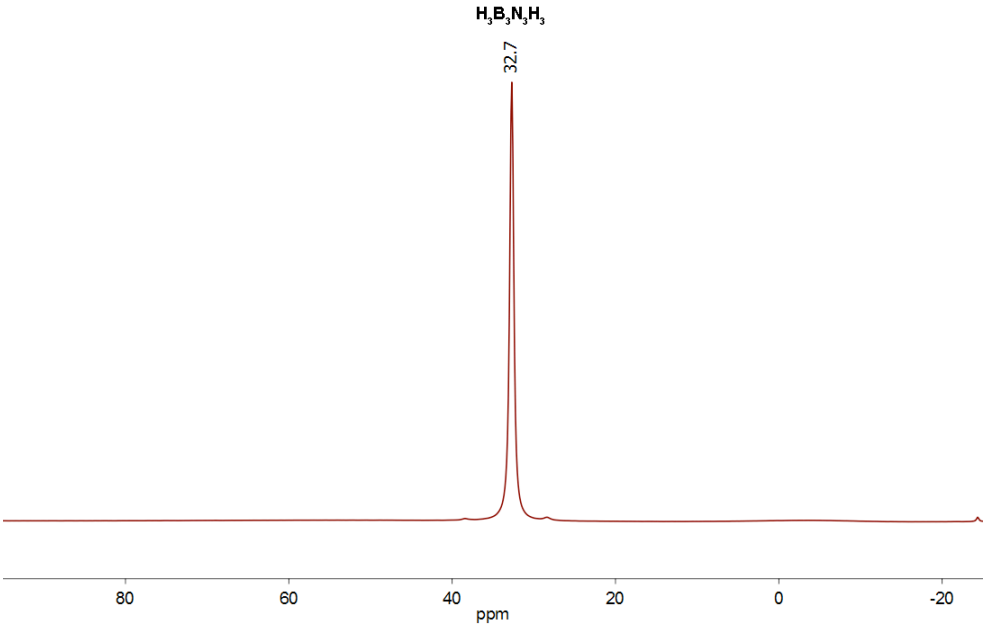

Figure D-2. $^{11}B\{^1H\}$ NMR spectrum of solution from experiment D.3 route A, 128.2 MHz, Pentane.

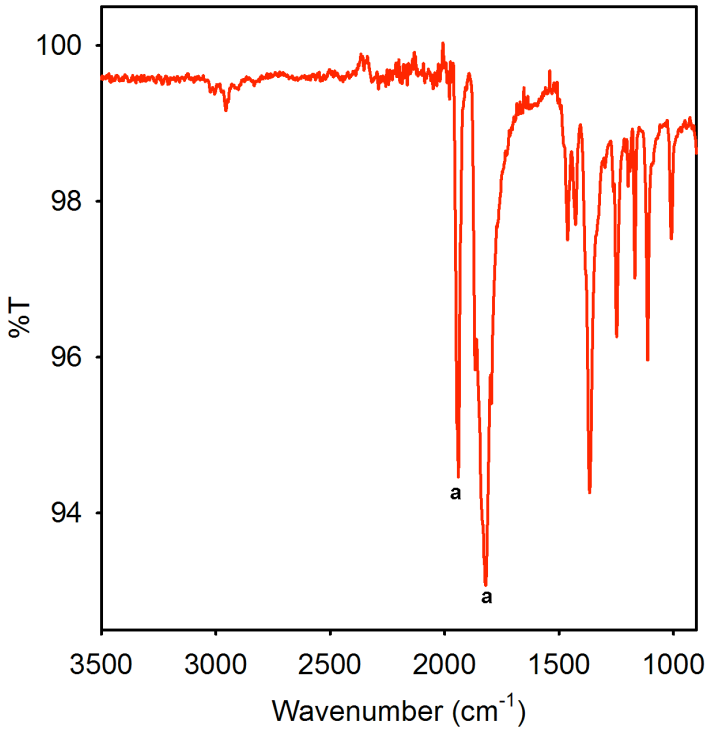

Figure D-3. IR spectrum of precipitate obtained from experiment D.3 route A, diamond ATR accessory. a) Unreacted (η^6-$Me_3B_3N_3Me_3$)$Cr(CO)_3$.

Route B: Attempted ring-exchange in neat borazine

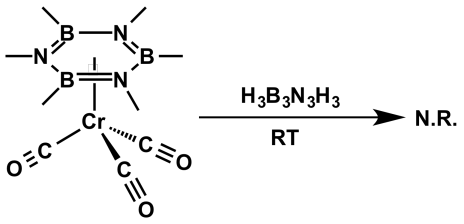

(η^6-$Me_3B_3N_3Me_3$)$Cr(CO)_3$ (15.2 mg, 0.051 mmol) was dissolved in $H_3B_3N_3H_3$ (600 µl, 6.4 mmol). The solution was placed in a J-Young NMR tube and allowed to stand at room temperature for 18 h. An orange solution was obtained. The sample was subjected to NMR analysis, and only $H_3B_3N_3H_3$ was observed in solution. The sample was layered with pentane and a yellow precipitate resulted. The precipitate was collected for ATR-IR analysis. Only (η^6-$Me_3B_3N_3Me_3$)$Cr(CO)_3$, was observed.

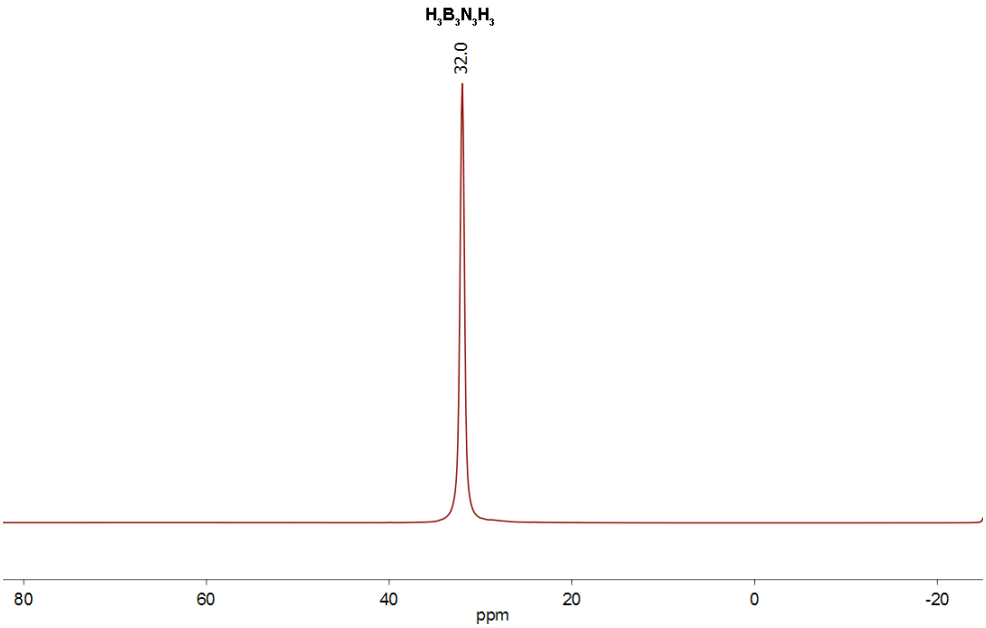

Figure D-4. $^{11}B\{^1H\}$ NMR spectrum of solution from experiment D.3 route B, 128.2 MHz, $H_3B_3N_3H_3$.

Route C: Attempted ring-exchange driven by heating

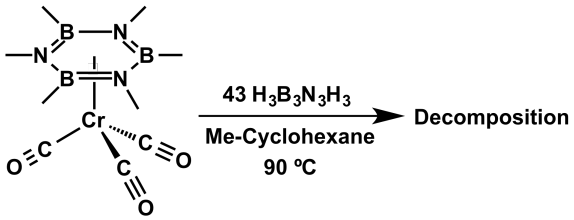

(η^6-$Me_3B_3N_3Me_3$)$Cr(CO)_3$ (35.0 mg, 0.12 mmol) was suspended in 12 ml Me-Cyclohexane and placed in a 20 ml scintillation vial. To this was added $H_3B_3N_3H_3$ (500 µl, 5.1 mmol). The solution was heated at 90 °C for 2 hours. An dark brown solution was obtained. The sample was subjected to NMR analysis, and free $H_3B_3N_3H_3$ and $Me_3B_3N_3Me_3$ was observed in solution.

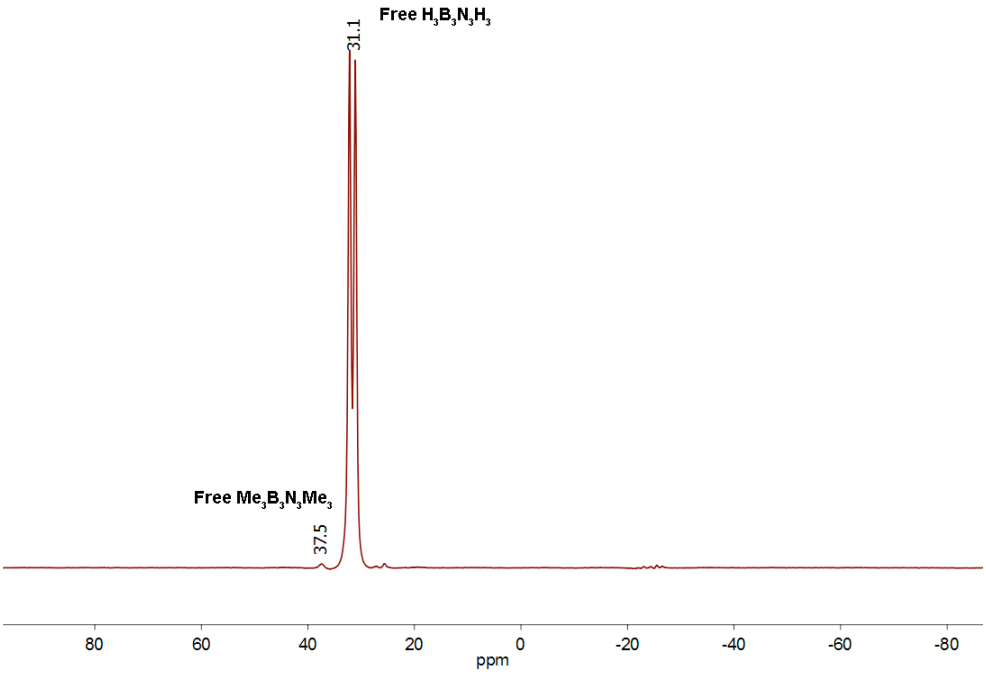

Figure D-5. ^{11}B NMR of solution from experiment D.3 route C, 128.2 MHz, $H_3B_3N_3H_3$.

D.4 Reaction of $Mn(CO)_5Br$ with $H_3B_3N_3H_3$ and TlBAr'

Route A: Attempted CO labilization by heating

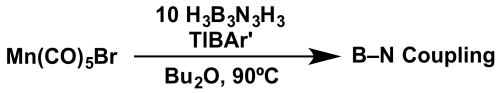

$Mn(CO)_5Br$ (36 mg, 0.13 mmol), TlBAr' (140 mg, 0.13 mmol) and $H_3B_3N_3H_3$ (100 µl, 1.06 mmol) were dissolved in 3 ml Bu_2O and the solution placed in a 20 ml scintillation vial. The solution was then heated to 90 ºC for 30 min, and sampled for NMR analysis. The crude ^{11}B NMR showed free $H_3B_3N_3H_3$, BAr', and new peaks at 32 and 25 ppm. The solution-cell IR spectrum of the crude mixture showed new ν_{CO} stretches at 2050 and 2010 cm^{-1}. However, a control reaction conducted without $H_3B_3N_3H_3$ gave rise to a mixture with identical ν_{CO} bands present, suggesting the ^{11}B NMR peaks observed are a result of B–N cross-linking.

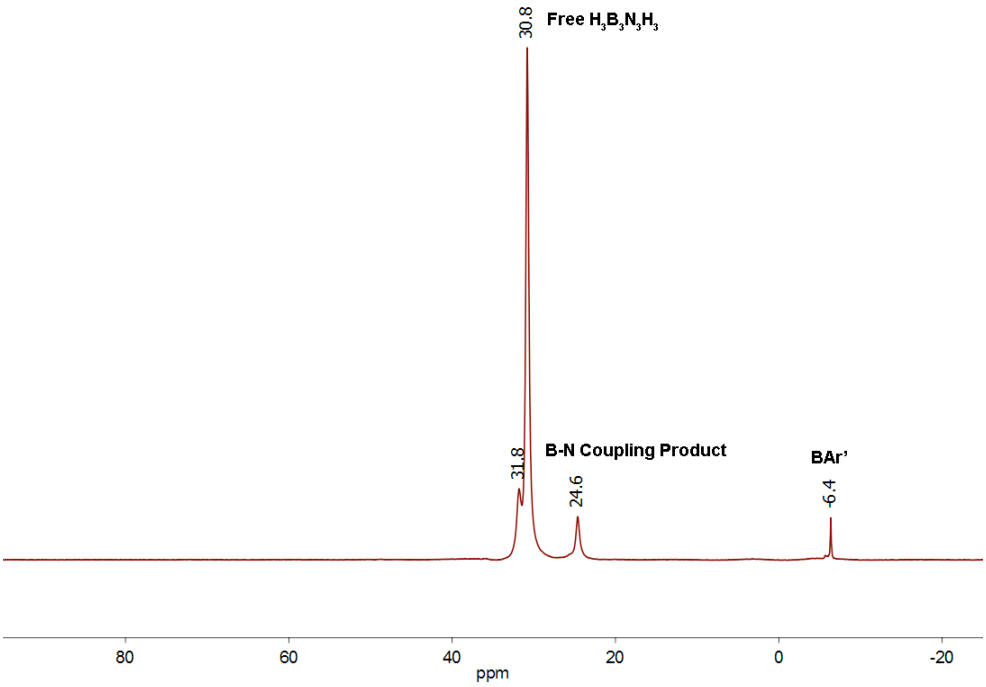

Figure D-6. $^{11}B\{^1H\}$ NMR spectrum of solution resulting from experiment D.4 route A, 128.2 MHz, Bu_2O.

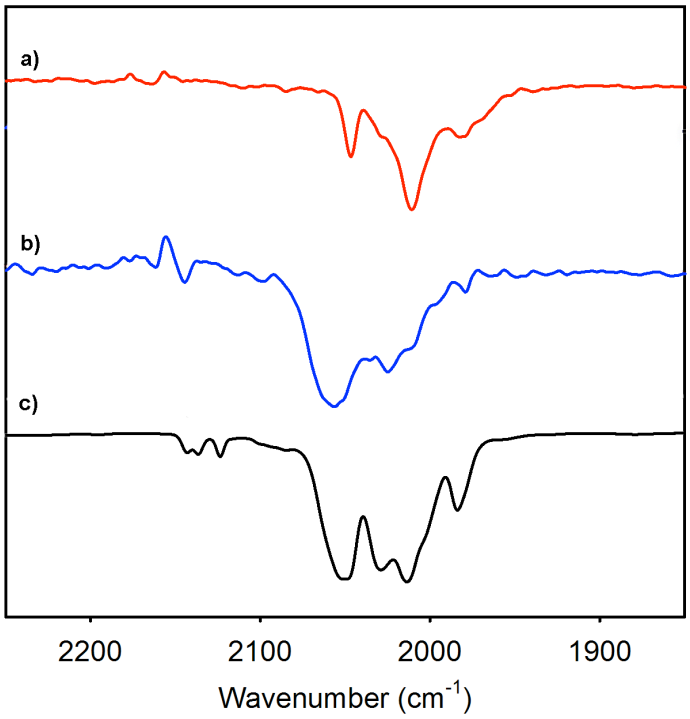

Figure D-7. KBr plate solution-cell IR spectra of isolated solids from Experiment D.4 route A (a) and B (b) and control reaction conducted via route A in the absence of $H_3B_3N_3H_3$ (c).

Route B: Attempted CO labilization by UV irradiation

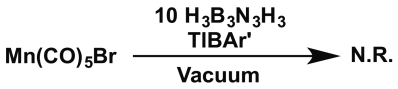

$Mn(CO)_5Br$ (56.7 mg, 0.20 mmol), TlBAr' (220 mg, 0.20 mmol, 1 eq.) and $H_3B_3N_3H_3$ (200 µl, 2.1 mmol, 10.5 eq.) were dissolved in 0.5 ml DCM and the solution placed in a J-Young NMR tube. The solution was was frozen and the atmosphere removed. The sample was then subjected to broadband UV-irradiation for 30 minutes at room temperture. The crude ^{11}B NMR showed only free $H_3B_3N_3H_3$, and BAr'. The solvent was then removed and the resulting solid was analyzed by ATR-IR which showed similar CO stretches to route A.

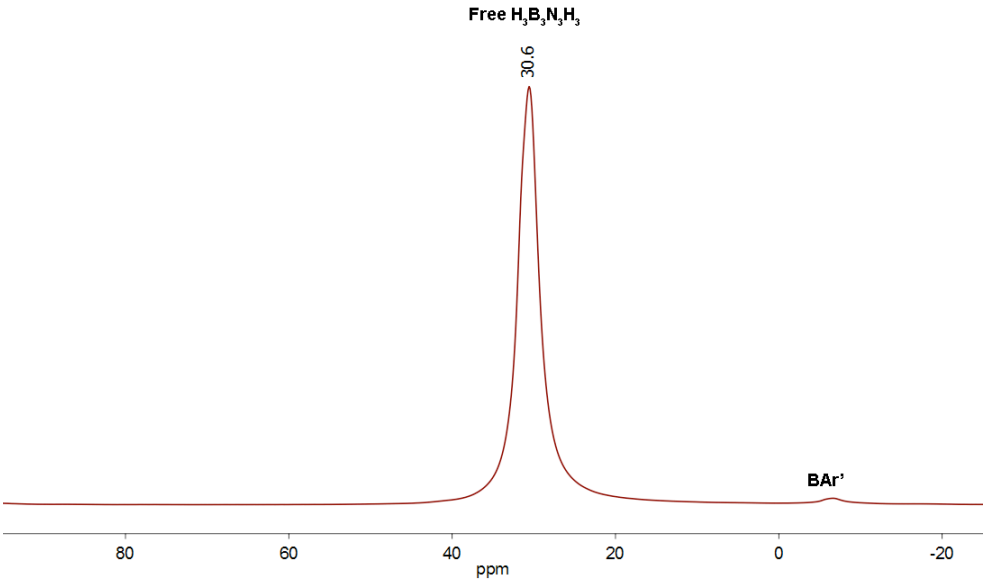

Figure D-8. $^{11}B\{^1H\}$ NMR spectrum of solution resulting from experiment D.4 route B, 160.4 MHz, CH_2Cl_2.

Route C: Attempted CO labilization by evacuation

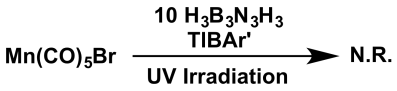

$Mn(CO)_5Br$ (25.8 mg, 0.094 mmol), TlBAr' (100 mg, 0.094 mmol) and $H_3B_3N_3H_3$ (50 µl, 0.53 mmol, 5.6 eq.) were dissolved in 0.75 ml Bu_2O and the solution placed in a J-Young NMR tube. The solution was then subjected to 14 sequential freeze-pump-thaw cycles. The crude ^{11}B NMR showed only free $H_3B_3N_3H_3$, BAr' and the B-N coupling product observed in route A.

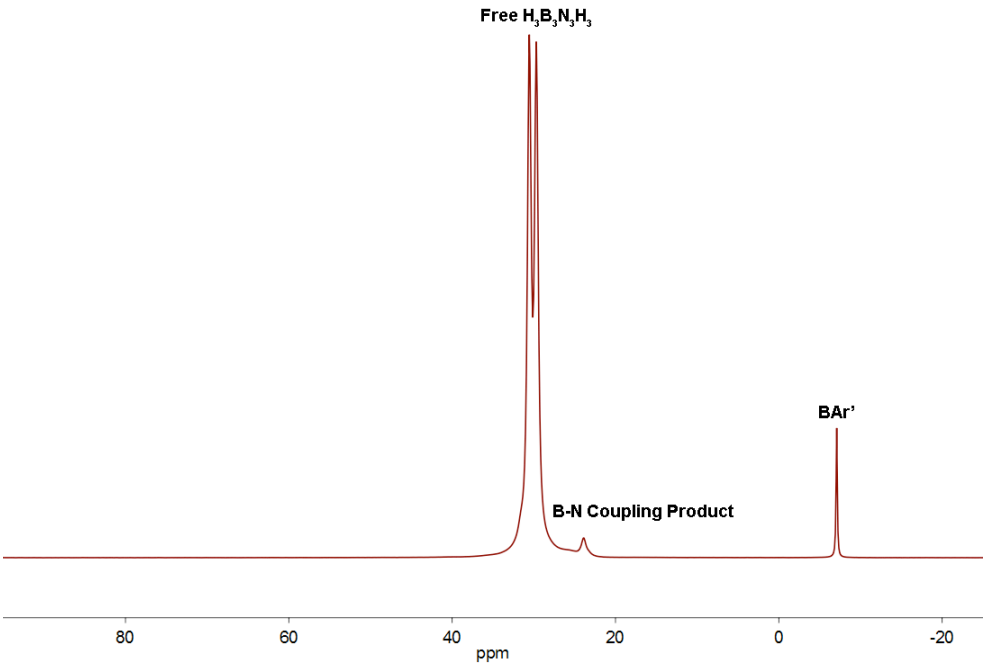

Figure D-9. ^{11}B NMR spectrum of solution resulting from experiment D.4 route C, 160.4 MHz, Bu_2O.

D.5 Reaction of $Fe(CO)_5$ with $H_3B_3N_3H_3$

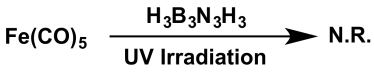

$Fe(CO)_5$ (50 µl, 0.37 mmol) was dissolved in $H_3B_3N_3H_3$ (400 µl, 3.18 mmol) in a quartz tube. The solution was then subjected to broadband UV irradiation for 5 h and vigorous gas evolution was observed. The solvent was then removed under vacuum and the residue extracted with 1 ml dichloromethane. The resulting solution was then analyzed by ^{11}B NMR and a complex mixture of products was observed.

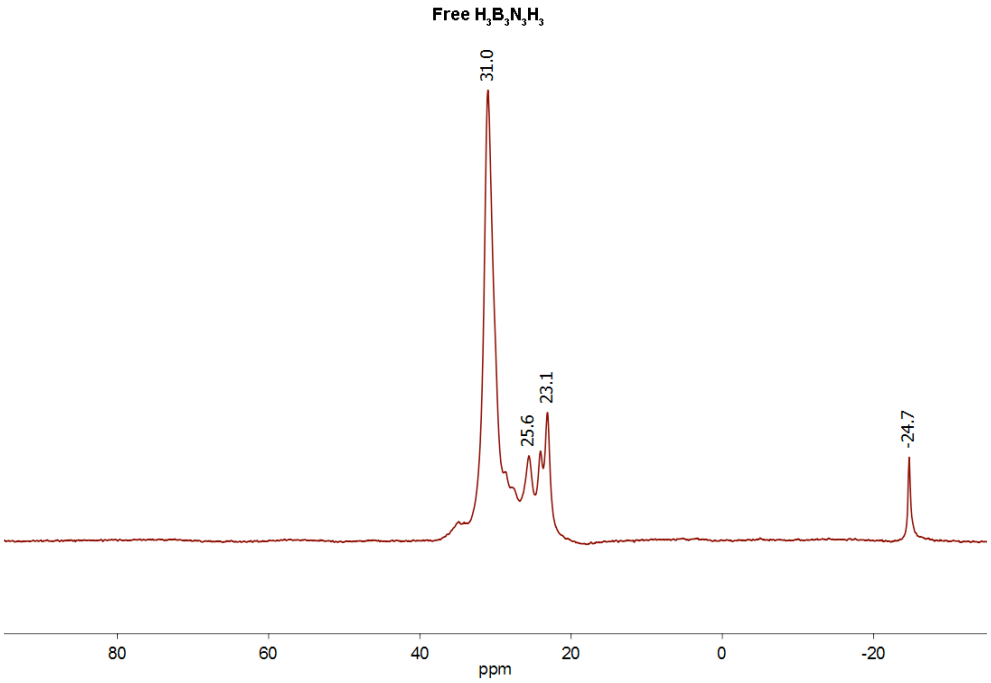

Figure D-10. $^{11}B\{^1H\}$ NMR of solution resulting from experiment D.5, 128.2 MHz, CH_2Cl_2.

D.6 Reaction of $FeBr_2$ with $H_3B_3N_3H_3$ TlBAr' and dmpe

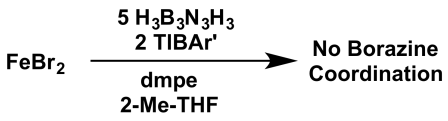

A solution of $FeBr_2$ (25.7 mg, 0.12 mmol), TlBAr' (254 mg, 0.24 mmol), dimethylphosphinoehtane (20 µl, 0.12 mmol), and $H_3B_3N_3H_3$ (60 µl (0.57 mmol) in 30 ml 2-Me-THF was prepared in a 20 ml scintillation vial. The mixture was heated at 50 ºC for 18 h and sampled for NMR analysis. The ^{11}B NMR of the crude mixture showed free $H_3B_3N_3H_3$, BAr', and the B-N coupling product observed in experiment 1 routes A-C.

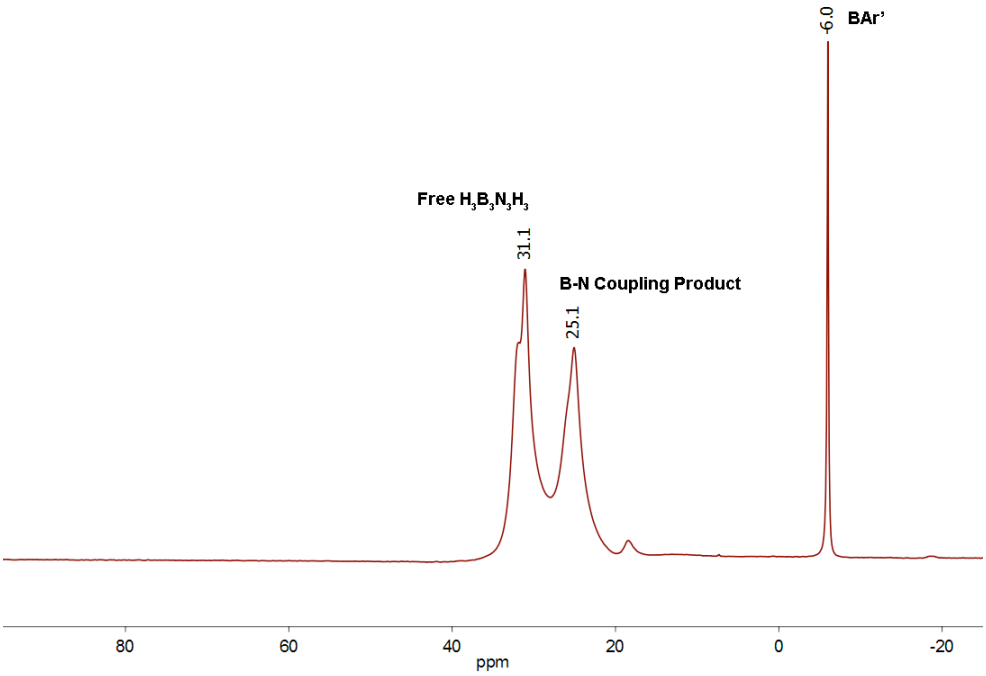

Figure D-11. ^{11}B NMR spectrum of solution resulting from experiment D.6, 128.2 MHz, 2-Me-THF.

D.7 References

1) Harris, R. K.; Becker, E. D.; Menezes, S. M. C.; Goodfellow, R.; Granger, P. *Pure and Applied Chemistry* **2001**, *73*, 1795.

2) Nishida, H.; Takada, N.; Yoshimura, M.; Sonoda, T.; Kobayashi, H. *Bull Chem. Soc. Japan* **1984**, *57*, 2600.

3) Bonham, J.; Drago, R. S.; Spielvogel, B. F.; Phillips, J. A.; Payet, C. R. In *Inorganic Syntheses*; John Wiley & Sons, Inc.: 2007, p 8.

4) Brookhart, M.; Grant, B.; Volpe, A. F. *Organometallics* **1992**, *11*, 3920.

5) Ross, B. L.; Grasselli, J. G.; Ritchey, W. M.; Kaesz, H. D. *Inorg. Chem.* **1963**, *2*, 1023.

6) Wideman, T.; Fazen, P. J.; Lynch, A. T.; Su, K.; Remsen, E. E.; Sneddon, L. G.; Chen, T.; Paine, R. T. In *Inorganic Syntheses*; John Wiley & Sons, Inc.: 2007, p 232.

7) Armarego, W. L. F.; Chai, C. L. L.; Knovel; ScienceDirect *Purification of laboratory chemicals*; Elsevier/Butterworth-Heinemann: Amsterdam ; Boston, 2009.